biomedicines

Special Issue Reprint

Advances in Cancer Biology and Experimental Anticancer Therapies (2nd Edition)

Edited by
Letizia Polito and Ewa Gajda

mdpi.com/journal/biomedicines

MDPI

Advances in Cancer Biology and Experimental Anticancer Therapies (2nd Edition)

Advances in Cancer Biology and Experimental Anticancer Therapies (2nd Edition)

Guest Editors

Letizia Polito
Ewa Gajda

MDPI

Basel • Beijing • Wuhan • Barcelona • Belgrade • Novi Sad • Cluj • Manchester

Guest Editors

Letizia Polito
Department of Medical and Surgical Sciences
University of Bologna
Bologna
Italy

Ewa Gajda
Department of Cell Biology and Immunology
Centre of Postgraduate Medical Education
Warsaw
Poland

Editorial Office
MDPI AG
Grosspeteranlage 5
4052 Basel, Switzerland

This is a reprint of the Special Issue, published open access by the journal *Biomedicines* (ISSN 2227-9059), freely accessible at: http://www.mdpi.com.

For citation purposes, cite each article independently as indicated on the article page online and as indicated below:

Lastname, A.A.; Lastname, B.B. Article Title. *Journal Name* **Year**, *Volume Number*, Page Range.

ISBN 978-3-7258-8727-9 (Hbk)
ISBN 978-3-7258-8728-6 (PDF)
https://doi.org/10.3390/books978-3-7258-8728-6

© 2026 by the authors. Articles in this reprint are Open Access and distributed under the Creative Commons Attribution (CC BY) license. The reprint as a whole is distributed by MDPI under the terms and conditions of the Creative Commons Attribution-NonCommercial-NoDerivs (CC BY-NC-ND) license (https://creativecommons.org/licenses/by-nc-nd/4.0/).

Contents

Letizia Polito and Ewa Gajda
Advances in Cancer Biology and Experimental Anticancer Therapies (2nd Edition)
Reprinted from: *Biomedicines* **2025**, *13*, 3055, https://doi.org/10.3390/biomedicines13123055 . . **1**

Huan Han, Hanwen Su, Zhihua Lv, Chengliang Zhu and Jingtao Huang
Identifying MTHFD1 and LGALS4 as Potential Therapeutic Targets in Prostate Cancer Through Multi-Omics Mendelian Randomization Analysis
Reprinted from: *Biomedicines* **2025**, *13*, 185, https://doi.org/10.3390/biomedicines13010185 . . . **4**

Janiah Alimudin, Zeynep Betts and Asuman Deveci Ozkan
Natural Compounds and Histone Deacetylase Inhibitors: A Combined Approach Against mCRPC Cells
Reprinted from: *Biomedicines* **2025**, *13*, 296, https://doi.org/10.3390/biomedicines13020296 . . . **22**

Shijun Jiang, Fengjuan Fan, Qun Li, Liping Zuo, Aoshuang Xu and Chunyan Sun
Therapeutic Target Discovery for Multiple Myeloma: Identifying Druggable Genes via Mendelian Randomization
Reprinted from: *Biomedicines* **2025**, *13*, 885, https://doi.org/10.3390/biomedicines13040885 . . . **36**

Ola M. Al-Sanabra, Luay F. Abu-Qatouseh, Mohammad I. A. Ahmad, Mutaz Jamal Al-Khreisat and Majd M. Alsaleh
Diminishing Hepcidin via Reducing *IL-6*/STAT3 Pathway by Utilizing Ferulic Acid: An In Vitro Study
Reprinted from: *Biomedicines* **2025**, *13*, 923, https://doi.org/10.3390/biomedicines13040923 . . . **63**

Stephen Mathew, Roslin Jose George, Alexsis Garcia, Sheila Powers, Subhash Aryal and W. Paul Bowman
Altered Expression of NK Receptors in Racially/Ethnically Diverse and Risk-of-Relapse Pediatric Acute Lymphoblastic Leukemia Patients
Reprinted from: *Biomedicines* **2025**, *13*, 1412, https://doi.org/10.3390/biomedicines13061412 . . **74**

Jialu Ma, Caleb McQuay, John Talburt, Amit K. Tiwari and Mary Qu Yang
Single-Cell Transcriptomic Analysis Unveils Key Regulators and Signaling Pathways in Lung Adenocarcinoma Progression
Reprinted from: *Biomedicines* **2025**, *13*, 1606, https://doi.org/10.3390/biomedicines13071606 . . **89**

Pei-I Lin, Yu-Cheng Lee, I-Hung Chen and Hsien-Hui Chung
Pharmacological Modulation of Mutant *TP53* with Oncotargets Against Esophageal Cancer and Therapy Resistance
Reprinted from: *Biomedicines* **2025**, *13*, 450, https://doi.org/10.3390/biomedicines13020450 . . . **111**

Alireza Tojjari, Sepideh Razi, Osama M. Younis, Ramez M. Odat, Ibrahim Halil Sahin and Anwaar Saeed
Chemoimmunotherapy in Advanced Biliary Tract Cancers: A Meta-Analysis of Clinical Outcomes
Reprinted from: *Biomedicines* **2025**, *13*, 2099, https://doi.org/10.3390/biomedicines13092099 . . **123**

biomedicines

MDPI

Editorial

Advances in Cancer Biology and Experimental Anticancer Therapies (2nd Edition)

Letizia Polito [1,*] and Ewa Gajda [2]

[1] Department of Medical and Surgical Sciences-DIMEC, General Pathology Section, Alma Mater Studiorum, University of Bologna, 40126 Bologna, Italy
[2] Department of Cell Biology and Immunology, Centre of Postgraduate Medical Education, 01-813 Warsaw, Poland; ewa.gajda@cmkp.edu.pl
* Correspondence: letizia.polito@unibo.it

Following the invitation from *Biomedicines*, we launched a second edition of the Special Issue "Advances in Cancer Biology and Experimental Anticancer Therapies", as we believe it is truly important to continue focusing on advances in cancer biology and experimental antitumor therapies. Indeed, although chemotherapy, surgery, and radiotherapy remain the most commonly available cancer treatments, their use has shown numerous limitations, despite their demonstrated antitumor efficacy. The major limitations include the lack of selectivity for tumor cells, the development of drug resistance, and the risk of secondary tumor formation. Consequently, the study and development of alternative targeted therapies, such as immunotherapy and nanotherapy, have been extensively explored to find therapies with greater specificity for transformed cells and lower nonspecific toxicity. Therefore, it is essential to intensify studies on the molecular mechanisms of carcinogenesis and to develop new strategies for diagnosing and combating tumors.

This Special Issue includes eight manuscripts, among which there are six high-quality research articles, one review and one meta-analysis article, published from 2024 to 2025.

Acute lymphoblastic leukemia (ALL) is the most common cancer in children; however, racial and ethnic disparities persist in both the incidence and treatment outcome of ALL. Children of African descent have a significantly lower incidence of ALL compared to European Americans, while the disease is most common in Hispanic Americans [1]. The study by Mathew et al. investigated immune cell receptor expression across racial/ethnic populations and examined risk factors for relapse that could potentially influence outcomes in pediatric ALL. The authors proposed that altered expression of immune receptors in racially/ethnically and risk-stratified groups may provide insight into T cell- and NK cell-mediated immune surveillance against pediatric ALL [2].

Although several new therapeutic approaches have improved clinical outcomes in multiple myeloma, the majority of patients eventually experience disease relapse [3]. To address this, the study by Jiang et al., utilizing Mendelian randomization analysis, identified nine druggable genes, including Orosomucoid 1 and Oviductal Glycoprotein 1. The efficacy of two agonists of these molecules (pregnenolone for Orosomucoid 1 and irinotecan for Oviductal Glycoprotein 1) in suppressing myeloma cell growth suggests the potential application of these two molecules for clinical treatment of multiple myeloma [4].

In the study of Han et al. several druggable genes were evaluated for their association with prostate adenocarcinoma risk. The genes *MTHFD1* and *LGALS4* were identified as promising therapeutic targets for prostate adenocarcinoma, with evidence provided at multiomics levels. *LGALS4* was predominantly expressed in malignant cells and was correlated with enhanced immune checkpoint pathways and immunotherapy resistance.

In contrast, *MTHFD1* was expressed in both tumor and microenvironmental cells and was associated with poor survival [5].

Single-cell RNA sequencing (scRNA-seq) technology has led to an exponential increase in the number of personalized data analyses in cancer patients. The clinical information obtained from single-cell analysis is crucial for exploring biomarkers of disease progression or treatment response and for guiding precise clinical decision-making for patients with malignant tumors [6]. Ma et al. carried out an integrative analysis of scRNA-seq data from lung adenocarcinoma patients. The results revealed that epithelial cells from stage IV tumors exhibited a distinct transcriptional profile compared to earlier stages. Several signaling pathways enriched in stage-specific crosstalk, including Wnt, PTN, and PDGF pathways, were identified, suggesting they may play critical roles in lung adenocarcinoma progression [7].

Hepcidin, a peptide synthesized by hepatocytes, is a crucial factor in systemic iron homeostasis of the organism. Since iron is essential for the highly active neoplastic cells, the induction of hepcidin has been implicated in the pathogenesis of anemia in patients with inflammatory and neoplastic diseases. It is well known that the IL-6/STAT3 signaling pathway is important for the transcriptional regulation of hepcidin [8]. Ferulic acid (FA) is an important active component of many traditional medicines that has a variety of biological activities, especially concerning oxidative stress and inflammation [9,10]. In the study by Al-Sanabra et al., the addition of FA to HepG2 cells significantly decreased the secretion levels of IL-6/STAT3 and hepcidin compared to the cells treated with LPS alone. The authors suggest that FA may be a potential therapeutic agent against hypoferremia and anemia resulting from dysregulated hepcidin levels in inflammatory and oncological diseases [11].

Sodium butyrate is a histone deacetylase inhibitor considered a promising anticancer drug for several types of cancer. It can inhibit the progression of prostate cancer, suppressing proliferation and inducing apoptosis [12]. Rutin is an antioxidant flavonoid found in many plants that has demonstrated antitumor activity in several cancer models [13]. The study by Alimudin et al. evaluated the effects of sodium butyrate and rutin combination therapy on metastatic castration-resistant prostate cancer cells. Enhanced apoptotic induction and elevated ROS levels were observed in combination-treated cells, alongside notable changes in cellular and nuclear morphology and mRNA expression [14].

The review by Lin et al. describes and summarizes some interesting oncotargets involved in the metabolic modulation of esophageal cancer, providing useful information for developing therapeutic strategies aimed at overcoming therapy resistance [15].

Tojjari et al. conducted a comprehensive meta-analysis of the clinical outcomes of chemoimmunotherapy in advanced biliary tract cancer [16]. The results demonstrated that chemoimmunotherapy significantly improved both overall survival and progression-free survival compared to chemotherapy alone in advanced biliary carcinoma, supporting the idea of chemoimmunotherapy as a first-line treatment strategy.

In conclusion, the findings from this Special Issue highlight the multifaceted potential of novel cancer therapy strategies that simultaneously target multiple cancer characteristics and improve conventional treatments.

Author Contributions: Writing—original draft preparation, L.P., writing—review and editing, L.P. and E.G. All authors have read and agreed to the published version of the manuscript.

Funding: This paper was supported by RFO fund (Ricerca Fondamentale Orientata) for selected topics from the Alma Mater Studiorum, University of Bologna, by the Pallotti Legacies for Cancer and by the National Science Centre in Poland (grant No. 2021/41/N/NZ5/04408).

Conflicts of Interest: The authors declare no conflicts of interest.

References

1. Lim, J.Y.; Bhatia, S.; Robison, L.L.; Yang, J.J. Genomics of racial and ethnic disparities in childhood acute lymphoblastic leukemia. *Cancer* **2014**, *120*, 955–962. [CrossRef] [PubMed]
2. Mathew, S.; George, R.J.; Garcia, A.; Powers, S.; Aryal, S.; Bowman, W.P. Altered Expression of NK Receptors in Racially/Ethnically Diverse and Risk-of-Relapse Pediatric Acute Lymphoblastic Leukemia Patients. *Biomedicines* **2025**, *13*, 1412. [CrossRef] [PubMed]
3. Yadav, R.; Chaudary, J.K.; Bisht, K.; Dhamija, P.; Chaudhary, P.K.; Nath, U.K.; Jain, N. Multiple myeloma: Insights into underlying mechanisms, advances in diagnostic and therapeutic modalities. *Semin. Oncol.* **2025**, *52*, 152390. [CrossRef] [PubMed]
4. Jiang, S.; Fan, F.; Li, Q.; Zuo, L.; Xu, A.; Sun, C. Therapeutic Target Discovery for Multiple Myeloma: Identifying Druggable Genes via Mendelian Randomization. *Biomedicines* **2025**, *13*, 885. [CrossRef] [PubMed]
5. Han, H.; Su, H.; Lv, Z.; Zhu, C.; Huang, J. Identifying MTHFD1 and LGALS4 as Potential Therapeutic Targets in Prostate Cancer Through Multi-Omics Mendelian Randomization Analysis. *Biomedicines* **2025**, *13*, 185. [CrossRef] [PubMed]
6. Jia, Q.; Chu, H.; Jin, Z.; Long, H.; Zhu, B. High-throughput single-cell sequencing in cancer research. *Signal Transduct. Target. Ther.* **2022**, *7*, 145. [CrossRef] [PubMed]
7. Ma, J.; McQuay, C.; Talburt, J.; Tiwari, A.K.; Yang, M.Q. Single-Cell Transcriptomic Analysis Unveils Key Regulators and Signaling Pathways in Lung Adenocarcinoma Progression. *Biomedicines* **2025**, *13*, 1606. [CrossRef] [PubMed]
8. Wrighting, D.M.; Andrews, N.C. Interleukin-6 induces hepcidin expression through STAT3. *Blood* **2006**, *108*, 3204–3209. [CrossRef] [PubMed]
9. Li, D.; Rui, Y.X.; Guo, S.D.; Luan, F.; Liu, R.; Zeng, N. Ferulic acid: A review of its pharmacology, pharmacokinetics and derivatives. *Life Sci.* **2021**, *284*, 119921. [CrossRef] [PubMed]
10. Salehi, B.; Azzini, E.; Zucca, P.; Maria Varoni, E.; V Anil Kumar, N.; Dini, L.; Panzarini, E.; Rajkovic, J.; Valere Tsouh Fokou, P.; Peluso, I.; et al. Plant-Derived Bioactives and Oxidative Stress-Related Disorders: A Key Trend towards Healthy Aging and Longevity Promotion. *Appl. Sci.* **2020**, *10*, 947. [CrossRef]
11. Al-Sanabra, O.M.; Abu-Qatouseh, L.F.; Ahmad, M.I.A.; Al-Khreisat, M.J.; Alsaleh, M.M. Diminishing Hepcidin via Reducing *IL-6*/STAT3 Pathway by Utilizing Ferulic Acid: An In Vitro Study. *Biomedicines* **2025**, *13*, 923. [CrossRef] [PubMed]
12. Mu, D.; Gao, Z.; Guo, H.; Zhou, G.; Sun, B. Sodium butyrate induces growth inhibition and apoptosis in human prostate cancer DU145 cells by up-regulation of the expression of annexin A1. *PLoS ONE* **2013**, *8*, e74922. [CrossRef] [PubMed]
13. Satari, A.; Ghasemi, S.; Habtemariam, S.; Asgharian, S.; Lorigooini, Z. Rutin: A Flavonoid as an Effective Sensitizer for Anticancer Therapy; Insights into Multifaceted Mechanisms and Applicability for Combination Therapy. *Evid. Based Complement. Altern. Med.* **2021**, *2021*, 9913179. [CrossRef] [PubMed]
14. Alimudin, J.; Betts, Z.; Ozkan, A.D. Natural Compounds and Histone Deacetylase Inhibitors: A Combined Approach Against mCRPC Cells. *Biomedicines* **2025**, *13*, 296. [CrossRef] [PubMed]
15. Lin, P.-I.; Lee, Y.-C.; Chen, I.-H.; Chung, H.-H. Pharmacological Modulation of Mutant *TP53* with Oncotargets Against Esophageal Cancer and Therapy Resistance. *Biomedicines* **2025**, *13*, 450. [CrossRef] [PubMed]
16. Tojjari, A.; Razi, S.; Younis, O.M.; Odat, R.M.; Sahin, I.H.; Saeed, A. Chemoimmunotherapy in Advanced Biliary Tract Cancers: A Meta-Analysis of Clinical Outcomes. *Biomedicines* **2025**, *13*, 2099. [CrossRef] [PubMed]

Disclaimer/Publisher's Note: The statements, opinions and data contained in all publications are solely those of the individual author(s) and contributor(s) and not of MDPI and/or the editor(s). MDPI and/or the editor(s) disclaim responsibility for any injury to people or property resulting from any ideas, methods, instructions or products referred to in the content.

biomedicines

MDPI

Article

Identifying MTHFD1 and LGALS4 as Potential Therapeutic Targets in Prostate Cancer Through Multi-Omics Mendelian Randomization Analysis

Huan Han †, Hanwen Su †, Zhihua Lv, Chengliang Zhu * and Jingtao Huang *

Department of Clinical Laboratory, Institute of Translational Medicine, Renmin Hospital of Wuhan University, Wuhan 430060, Hubei, China; hh940622@whu.edu.cn (H.H.); hanwensu@whu.edu.cn (H.S.); lzh2007@whu.edu.cn (Z.L.)

* Correspondence: xinchengzhu@163.com (C.Z.); jthuang@whu.edu.cn (J.H.)

† These authors contributed equally to this work.

Abstract: Background: Prostate cancer remains one of the leading causes of cancer-related mortality in men worldwide. The treatment of it is currently based on surgical removal, radiotherapy, and hormone therapy. It is crucial to improve therapeutic prospects for the diagnosis and treatment of prostate cancer via drug target screening. **Methods:** We integrated eQTL data from the eQTLGen Consortium and pQTL data from UK Biobank Proteome Plasma Proteins (UKB-PPP) and deCODE health datasets. MR analyses (SMR, heterogeneity in dependent instruments (HEIDI), IVW, Wald ratio, weighted median, and MR-Egger) were used to screen candidate genes associated with prostate adenocarcinoma (PRAD) risk. Candidate genes were further verified through TCGA-based gene expression profile, survival analysis, and immune microenvironment evaluations. TIDE analysis was utilized to investigate gene immunotherapy response. Single-cell RNA sequencing data from the GSE176031 dataset were used to investigate the gene expression patterns. The Drug Bank, Therapeutic Target Database and Drug Signatures Database were utilized to predict targeted drugs for candidate genes. **Results:** MTHFD1 and LGALS4 were identified as promising therapeutic targets for PRAD, with evidence provided at multi-omics levels. LGALS4 was predominantly expressed in malignant cells and was correlated with enhanced immune checkpoint pathways, increased TIDE scores, and immunotherapy resistance. In contrast, MTHFD1was expressed in both tumor and microenvironmental cells and was associated with poor survival. Drug target prediction suggested that there are no currently approved drugs specifically targeting MTHFD1 and LGALS4. **Conclusions:** Our study identified MTHFD1 and LGALS4 as potential preventive targets for PRAD. However, future experiments are warranted to assess the utility and effectiveness of these candidate proteins.

Keywords: prostate cancer; drug target; LGALS4; MTHFD1; Mendelian randomization

1. Introduction

Prostate cancer is one of the most common malignancies of men worldwide. In 2018, there were approximately 1.3 million new cases of PCa and 307,000 deaths [1]. Although progress has been made through early detection by means of prostate-specific antigen (PSA) screening and therapeutic interventions, around 10% of patients develop metastatic disease, leading to a higher chance of PCa-related death [2,3]. Current treatment options for metastatic prostate cancer (mPCa) include androgen deprivation therapy (ADT),

prostatectomy, radiotherapy, and immunotherapy. ADT remains the primary therapeutic approach for mPCa. However, 30–50% of patients who receive ADT eventually develop castration-resistant prostate cancer (CRPC). Moreover, ADT is linked to an increased risk of cardiovascular disease [4,5]. Additional agents, such as docetaxel, abiraterone, apalutamide, and enzalutamide, have demonstrated significant clinical efficacy in improving metastasis survival. However, they are also associated with a number of unique side effects, limiting their clinical application in certain patients [6–8]. Sipuleucel-T remains the only FDA-approved immunotherapy for prostate cancer of any indication to date. However, Sipuleucel-T should not be used in patients with metastatic disease to sites other than bone and lymph nodes because patients with visceral disease were excluded from the Sipuleucel-T trial [8]. In addition, the heterogeneity of prostate cancer (PCa), characterized by diverse genetic, proteomic, and transcriptomic landscapes, plays a critical role in tumor development, and complicates the establishment of universally effective treatment strategies. This complexity underscores the imperative for personalized medicine approaches to effectively manage and treat PCa [9,10]. Understanding the genetic and proteomic alterations contributing to PCa susceptibility and therapeutic resistance is critical to discovering new biomarkers and developing targeted therapies, accordingly [11].

Genome-wide association studies (GWAS) have been instrumental in identifying genetic variants associated with an elevated risk of PCa. However, GWAS findings frequently pinpoint loci that are non-coding or reside within regions harboring multiple genes, thereby posing significant challenges in accurately identifying causal genes and elucidating their biological mechanisms [12]. To address these limitations, expression quantitative trait loci (eQTL) analyses have been employed to link genetic variants with gene expression levels, facilitating the identification of genes whose altered expression may contribute to disease etiology [13]. Additionally, protein quantitative trait loci (pQTL) analyses extend this framework by associating genetic variants with protein abundance, thereby providing a more direct assessment of the functional implications of genetic variation [14].

Mendelian randomization (MR) provides a powerful approach for establishing causal relationships between genetic variants and disease outcomes by using these variants as instrumental variables [15]. Unlike traditional observational studies, MR effectively reduces the influence of confounding factors and prevents reverse causation, thereby enhancing the reliability of causal inferences. By integrating eQTL and pQTL data with GWAS through MR and summary-based Mendelian randomization (SMR) analyses, we can more accurately identify causal genes with significant therapeutic potential [16]. This comprehensive strategy not only elucidates the genetic architecture of PCa but also highlights druggable targets that may be exploited for targeted therapeutic interventions.

The tumor microenvironment (TME) plays a pivotal role in the progression, metastasis, and therapeutic response of PCa [17]. Within the TME, immune cells, such as T lymphocytes, macrophages, and myeloid-derived suppressor cells, interact dynamically with cancer cells, influencing tumor growth and facilitating immune evasion [17]. Notably, immune checkpoints, including PD-1/PD-L1 and CTLA-4, have emerged as critical regulators of immune responses in cancer, presenting promising targets for immunotherapeutic interventions. These checkpoints not only facilitate immune escape mechanisms but also serve as promising targets for immunotherapy, with checkpoint inhibitors showing success in certain cancer types. Additionally, the TME encompasses non-immune components, including fibroblasts, endothelial cells, and extracellular matrix elements, which collectively contribute to tumor progression and resistance to therapy. A deeper understanding of the cellular and molecular interactions within the TME is essential for identifying novel therapeutic targets and improving treatment strategies for PCa [18].

In this study, we developed a comprehensive analytical framework to systematically identify and validate druggable genes associated with PCa. By integrating GWAS, eQTL, and pQTL data, we employed MR and SMR analyses to identify causal genes linked to PCa risk. Subsequent validation in independent datasets, combined with clinical expression and survival analyses using The Cancer Genome Atlas (TCGA), enabled us to assess the prognostic significance and immune-related associations of the identified genes. Additionally, we utilized single-cell RNA sequencing (scRNA-seq) data to elucidate the cellular context of gene expression within the TME and conducted drug prediction models and molecular docking simulations to explore the therapeutic potential of the top candidate genes. This integrative approach not only uncovers novel genetic determinants of PCa but also establishes a translational pathway toward the development of targeted therapies and precision medicine strategies.

2. Materials and Methods

2.1. Study Design

This study developed a comprehensive analytical framework, as shown in Figure 1, to systematically identify and validate druggable genes associated with PRAD. First, eQTL data from the eQTLGen Consortium were used as instrumental variables in the MR analysis to identify potential causal genes. This was followed by an SMR analysis and HEIDI tests that assessed the causal roles of these genes in PRAD.

These findings were further validated at a second stage using the pQTL data obtained from the UK Biobank Proteome Plasma Proteins (UKB-PPP) and deCODE health studies. Sensitivity analyses were stringently performed to ensure the robustness of the results.

To further investigate the clinical relevance, gene expression profiles, prognostic significance, and immune-related associations, an analysis using the TCGA database was performed. Colocalization analyses were conducted to assess whether the causal variants arose from shared or distinct genomic regions. Drug prediction models and molecular docking simulations were finally performed and gave useful insights into the therapeutic potential of identified targets and broader perspectives for the targeted treatments of PRAD.

2.2. Exposure Data

We curated the eQTL data from the eQTLGen Consortium (https://eqtlgen.org/ (accessed on 4 October 2024)) [19], including 16,989 cis-eQTL genes identified by a genetic analysis of 31,684 blood samples from healthy individuals of European ancestry. To study the genetic architecture of plasma protein abundance and its relation to disease, we integrated data from two large-scale GWAS: the UKB-PPP and the deCODE health study. The UKB-PPP used the Olink platform to analyze blood plasma from 54,219 UK Biobank participants and derived important genetic associations with the levels of 2923 proteins [20]. The deCODE health study similarly utilized the high-throughput SomaScan platform to quantify 4907 aptamers associated with plasma protein levels in a cohort of 35,559 Icelandic individuals [21].

For our analysis, we specifically selected index cis-pQTLs as instrumental variables, focusing on those that met genome-wide significance thresholds ($p < 5 \times 10^{-8}$). These were restricted to cis-pQTLs falling within 1 Mb of the gene encoding the respective protein. We estimated LD for our instrumental variables using data from the European panel of the 1000 Genomes Project. Moreover, colocalization analyses were performed only for proteins with index cis-pQTLs from the UKB-PPP dataset in order to further strengthen the robustness of our findings.

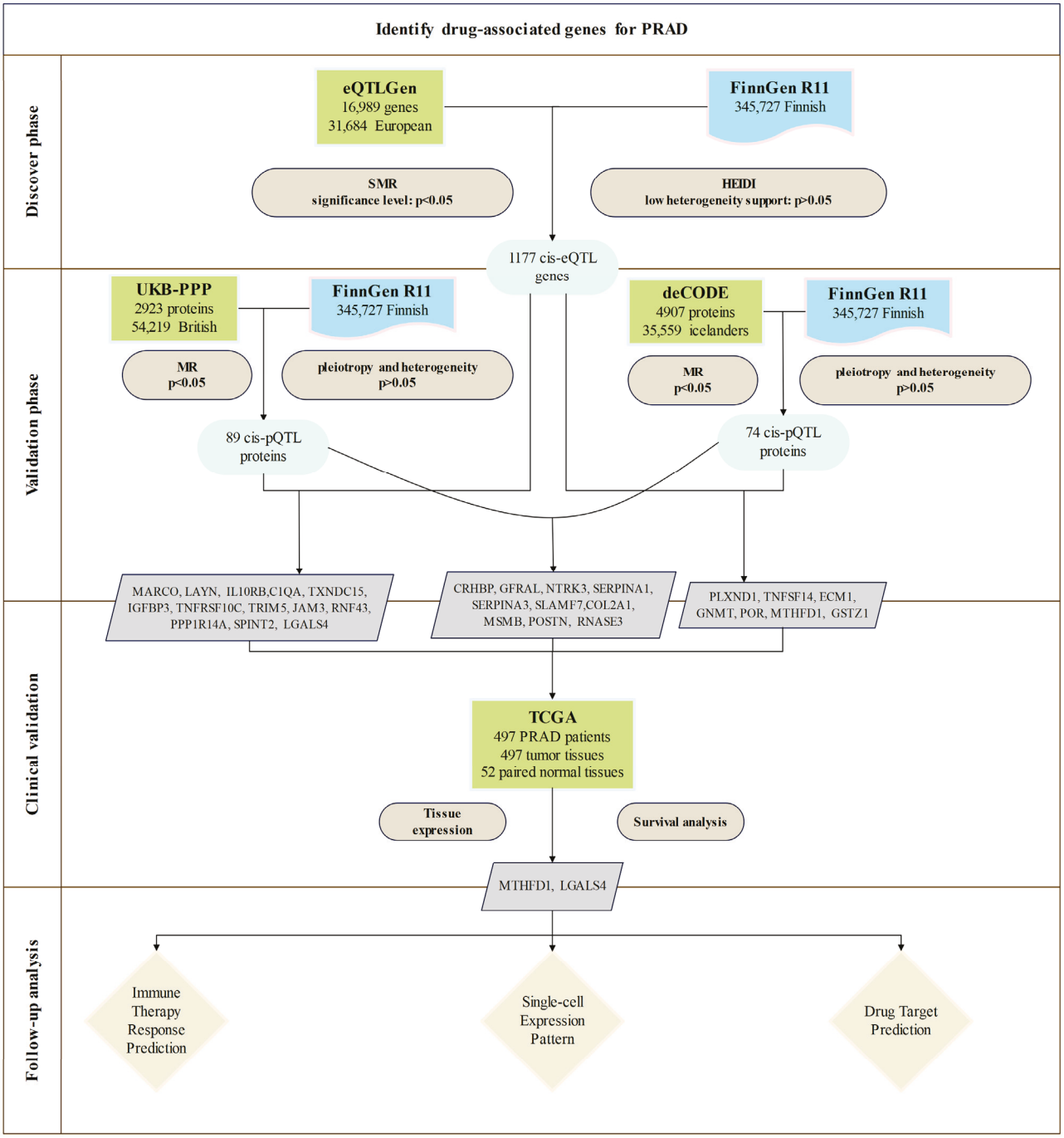

Figure 1. Overview of the study design.

2.3. Outcome Data

The PRAD cohort dataset utilized in this study was obtained from FinnGen Release 11, which was made publicly available in June 2024 and can be accessed at https://www.finngen.fi/ (accessed on 4 October 2024) [22]. This dataset includes 17,258 cases of PCa and 143,624 control individuals.

2.4. SMR Analysis and HEIDI Test

SMR and HEIDI methods integrate GWAS and eQTL summary data to differentiate between pleiotropy and linkage [23]. In the SMR analysis, associations between genetic variation and gene expression were identified by the use of summary statistics from both; significant associations were defined at $p < 0.05$. The HEIDI test was further used to

determine if the SMR association was due to either pleiotropy (a single variant affecting multiple traits), or linkage (closely linked variants affecting different traits). A significant HEIDI result ($p < 0.05$) indicates pleiotropy. Together, these methods provide strong evidence for causal links between PCa and gene expression.

2.5. Mendelian Randomization Analysis

In this study, the MR analysis was performed using the "TwoSampleMR (version 0.5.8)" R package. To ensure the validity and robustness of our instrumental variables (IVs), we followed a rigorous approach. First, we selected genetic variants with an F-statistic $\geq$10 to confirm their strength as instruments. We then prioritized variants with low linkage disequilibrium (LD; $r^2 < 0.1$) based on the European 1000 Genomes reference panel, ensuring IV independence [24]. To avoid reverse causation, we applied Steiger filtering to exclude SNPs with greater variance in the outcome than the exposure [25].

For genes with multiple IVs, we used the following four complementary methods: inverse-variance weighted (IVW); Wald ratios; weighted median; and MR-Egger. IVW, chosen as the primary method due to its statistical power, assumes that all IVs are valid [26]. In addition, the Wald ratio was used to assess individual SNPs [27], while the weighted median method remained reliable even with up to 50% invalid instruments [28]. MR-Egger, which accounts for pleiotropy, included an intercept term to estimate average pleiotropic effects and the slope for causal effects [29].

We also used some statistical tests to further assess horizontal pleiotropy and heterogeneity. We also tested for heterogeneity using Cochran's Q test and evaluated horizontal pleiotropy with MR-Egger regression intercepts and the MR-PRESSO method, which identifies directional pleiotropy [30].

2.6. Clinical Expression and Survival Analysis

Gene expression data and corresponding clinical information for PRAD were retrieved from the TCGA database (https://portal.gdc.cancer.gov (accessed on 4 October 2024)). Both count and TPM data were downloaded using R (version 4.3.0), with TPM values normalized via log2(TPM + 1) transformation. After excluding incomplete RNA sequencing and clinical data, 554 samples were included in the analysis.

Gene expression was assessed using the Kruskal–Wallis (KW) non-parametric test on count data. Kaplan–Meier (KM) survival analysis compared survival between two groups, with statistical significance determined by the log-rank test. KM curves, *p*-values, and hazard ratios (HR) with 95% confidence intervals (CI) were calculated using log-rank and univariate Cox regression. All analyses were conducted in R, with $p < 0.05$ considered significant.

2.7. Immune Scoring and Immune Checkpoint Analysis

To investigate the relationship between gene expression and the immune microenvironment in PRAD, RNA sequencing data were log2(TPM + 1) transformed. After excluding incomplete samples, 498 cases were analyzed and divided into high- and low-expression groups based on MTHFD1 and LGALS4 expression (249 cases each). Immune scores for each group were calculated using the ESTIMATE algorithm, which assesses stromal, immune, and total scores. The expression of immune checkpoint genes, such as ITPRIPL1, SIGLEC15, TIGIT, CD274, HAVCR2, PDCD1, CTLA4, LAG3, and PDCD1LG2, was compared between the groups. Statistical analyses were performed in R, with differences evaluated using the Wilcoxon rank-sum test ($p < 0.05$ considered significant).

2.8. Analysis of MTHFD1 and LGALS4 Expression in PRAD

Single-cell RNA sequencing data from the GEO database (GSE176031) were used to investigate the transcriptional profiles of MTHFD1 and LGALS4 in PRAD. scRNA-seq data, in .h5 format, together with annotation files, were obtained from the TISCH database (http://tisch.comp-genomics.org/ (accessed on 4 October 2024)). Data were processed with MAESTRO and Seurat for quality control, normalization, scaling, and clustering. t-SNE (t-distributed stochastic neighbor embedding) re-clustering identified cell types, which were annotated using marker genes. The expressions of MTHFD1 and LGALS4 were evaluated in tumor, stromal, and immune cells, and were represented using violin plots and heatmaps.

2.9. Drug Target Prediction

Potential drugs targeting MTHFD1 and LGALS4 were identified using two drug target prediction platforms: DrugBank (https://go.drugbank.com/ (accessed on 5 October 2024)) and the Therapeutic Target Database (TTD, https://db.idrblab.net/ttd/ (accessed on 5 October 2024)). These resources provided comprehensive details, including approved drugs, agents in clinical trials, and experimental compounds, along with their drug IDs, mechanisms of action, and current development stages.

Meanwhile, MTHFD1 and LGALS4 were submitted to the Drug Signatures Database (DSigDB, http://dsigdb.tanlab.org/DSigDBv1.0/ (accessed on 5 October 2024)) to identify potential protein–drug interactions. DSigDB contains 22,527 gene sets and 17,389 compounds linked to 19,531 genes, aiding the discovery of connections between drugs, chemicals, and target genes [31]. MTHFD1 and LGALS4 were also uploaded to the Enrichr tool (https://maayanlab.cloud/Enrichr/ (accessed on 5 October 2024)) to predict potential drug candidates targeting these genes [32].

3. Results

3.1. Discovery of Potential cis-eQTL Genes and PRAD

We integrated data from the eQTLGen Consortium, UKB-PPP, and deCODE datasets to identify genes significant at both RNA and protein levels. In the discovery phase, we identified 16,989 cis-eQTL genes from eQTLGen, validated by 1974 cis-pQTL proteins from UKB-PPP, and 1703 from deCODE.

We found the following gene overlaps between the datasets: 851 genes between eQTLGen and UKB-PPP; 654 genes between eQTLGen and deCODE; 241 genes between UKB-PPP and deCODE; and 644 genes overlapping across the three datasets of SMR, UKB-PPP, and deCODE.

For PRAD patients (17,258 cases, 143,624 controls from FinnGen), SMR and HEIDI analyses identified 1177 cis-eQTL genes associated with PRAD risk that passed the SMR test criteria ($p < 0.05$) and the HEIDI test criteria ($p > 0.05$) (Figure 1, Table S1).

3.2. MR Analysis of pQTLs in Validation Phase

To examine the causal effects of candidate genes on PRAD at the protein level, we used cis-pQTL protein data from the UKB-PPP and deCODE databases. Because of missing gene data, only 26 genes from the discovery phase were included in the MR analysis.

In the validation phase, we found that C1QA, MARCO, TXNDC15, IGFBP3, TNFRSF10C, TRIM5, LAYN, JAM3, RNF43, PPP1R14A, SPINT2, LGALS4, TOR1AIP1, AGER, CILP, CEACAM21, and IL10RB were significantly associated with PRAD risk. MARCO, LAYN, and IL10RB were linked to reduced PRAD risk, while C1QA, TXNDC15, IGFBP3, TNFRSF10C, TRIM5, JAM3, RNF43, PPP1R14A, SPINT2, and LGALS4 were associated with increased risk (Figure 2, Table S2).

Exposure	Outcome	No.of SNP	Method	OR(95% CI)	*P*
C1QA	PRAD	4	IVW	1.08 (1.00 to 1.16)	0.050
MARCO	PRAD	3	IVW	0.87 (0.79 to 0.96)	0.004
TXNDC15	PRAD	6	IVW	1.04 (1.01 to 1.08)	0.012
IGFBP3	PRAD	6	IVW	1.17 (1.06 to 1.29)	0.002
TNFRSF10C	PRAD	4	IVW	1.13 (1.04 to 1.24)	0.006
TRIM5	PRAD	3	IVW	1.09 (1.01 to 1.19)	0.030
LAYN	PRAD	3	IVW	0.92 (0.84 to 1.00)	0.049
JAM3	PRAD	3	IVW	1.34 (1.11 to 1.63)	0.003
RNF43	PRAD	2	IVW	1.32 (1.08 to 1.62)	0.008
PPP1R14A	PRAD	4	IVW	1.36 (1.18 to 1.58)	0.000
SPINT2	PRAD	3	IVW	1.38 (1.21 to 1.57)	0.000
LGALS4	PRAD	3	IVW	1.36 (1.06 to 1.74)	0.015
TOR1AIP1	PRAD	3	IVW	0.94 (0.88 to 0.99)	0.022
AGER	PRAD	2	IVW	1.22 (1.03 to 1.44)	0.023
CILP	PRAD	2	IVW	0.89 (0.82 to 0.97)	0.010
CEACAM21	PRAD	16	IVW	0.93 (0.90 to 0.95)	0.000
IL10RB	PRAD	6	IVW	0.94 (0.90 to 0.99)	0.013

P<0.05 was considered statistically signnificant

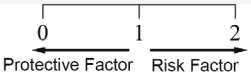

Figure 2. Forest plots illustrating the results of the validation stage for 17 essential genes in UK Biobank Proteome Plasma Proteins (UKB-PPP). OR: odds ratio, 95% CI: 95% confidence intervals; PRAD: prostate adenocarcinoma, SNP: single-nucleotide polymorphisms, IVW: inverse-variance weighted.

The direction of effect for these 13 proteins was consistent with the SMR results, showing no evidence of heterogeneity or pleiotropy (Table S3). Steiger filtering also confirmed the causal relationship (Table S4). Four proteins—TOR1AIP1, AGER, CILP, and CEACAM21—were excluded due to inconsistent effects between the discovery and replication phases.

The deCODE database analysis identified PLXND1 and TNFSF14 as genes linked to a reduced risk of PRAD (Figure 3, Table S5), while NEGR1, REG4, ECM1, GNMT, POR, MTHFD1, and GSTZ1 were associated with increased PRAD risk. The effects of PLXND1, TNFSF14, ECM1, GNMT, POR, MTHFD1, and GSTZ1 were consistent with the SMR results, showing no heterogeneity or pleiotropy in both proteins across four analytical methods (Tables S6 and S7). However, NEGR1 and REG4 were excluded due to inconsistencies between the discovery and replication phases.

Exposure	Outcome	No.of SNP	Method	OR(95% CI)	*P*
PLXND1	PRAD	4	IVW	0.85 (0.74 to 0.97)	0.018
TNFSF14	PRAD	3	IVW	0.82 (0.70 to 0.96)	0.016
NEGR1	PRAD	6	IVW	0.71 (0.59 to 0.84)	0.000
REG4	PRAD	6	IVW	0.81 (0.70 to 0.93)	0.003
ECM1	PRAD	4	IVW	1.07 (1.01 to 1.13)	0.022
GNMT	PRAD	3	IVW	1.12 (1.01 to 1.26)	0.039
POR	PRAD	3	IVW	1.19 (1.04 to 1.35)	0.011
MTHFD1	PRAD	3	IVW	1.38 (1.12 to 1.72)	0.003
GSTZ1	PRAD	2	IVW	1.05 (1.01 to 1.08)	0.016

P<0.05 was considered statistically signnificant

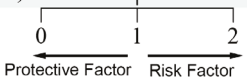

Figure 3. Forest plots illustrating the results of the validation stage for nine essential genes in deCODE.

Then, using cis-pQTL data in UKB-PPP and deCODE, the MR analysis identified CRHBP, GFRAL, NTRK3, SERPINA1, SERPINA3, and SLAMF7 as being associated with increased PRAD risk, whereas COL2A1, MSMB, POSTN, and RNASE3 were associated with reduced PRAD risk (Figure 4, Table S8).

Exposure	Outcome	No.of SNP	Method	OR(95% CI)	*P*
$CRHBP_{UKB-PPP}$	PRAD	5	IVW	1.09 (1.03 to 1.14)	0.002
$CRHBP_{deCODE}$	PRAD	6	IVW	1.10 (1.02 to 1.20)	0.018
$GFRAL_{UKB-PPP}$	PRAD	6	IVW	1.07 (1.01 to 1.13)	0.019
$GFRAL_{deCODE}$	PRAD	3	IVW	1.13 (1.01 to 1.27)	0.040
$NTRK3_{UKB-PPP}$	PRAD	3	IVW	1.13 (1.01 to 1.25)	0.029
$NTRK3_{deCODE}$	PRAD	5	IVW	1.13 (1.01 to 1.27)	0.036
$SERPINA1_{UKB-PPP}$	PRAD	2	IVW	1.20 (1.02 to 1.40)	0.027
$SERPINA1_{deCODE}$	PRAD	6	IVW	1.08 (1.00 to 1.15)	0.036
$SERPINA3_{UKB-PPP}$	PRAD	6	IVW	1.13 (1.06 to 1.22)	0.001
$SERPINA3_{deCODE}$	PRAD	5	IVW	1.13 (1.03 to 1.25)	0.011
$SLAMF7_{UKB-PPP}$	PRAD	5	IVW	1.05 (1.00 to 1.10)	0.041
$SLAMF7_{deCODE}$	PRAD	7	IVW	1.09 (1.02 to 1.15)	0.006
$COL2A1_{UKB-PPP}$	PRAD	4	IVW	0.95 (0.91 to 1.00)	0.036
$COL2A1_{deCODE}$	PRAD	5	IVW	0.93 (0.88 to 0.99)	0.031
$MSMB_{UKB-PPP}$	PRAD	4	IVW	0.78 (0.70 to 0.87)	0.000
$MSMB_{deCODE}$	PRAD	5	IVW	0.80 (0.74 to 0.88)	0.000
$POSTN_{UKB-PPP}$	PRAD	3	IVW	0.90 (0.82 to 0.99)	0.032
$POSTN_{deCODE}$	PRAD	4	IVW	0.89 (0.80 to 0.99)	0.027
$RNASE3_{UKB-PPP}$	PRAD	4	IVW	0.88 (0.80 to 0.98)	0.019
$RNASE3_{deCODE}$	PRAD	6	IVW	0.92 (0.86 to 0.99)	0.022

P<0.05 was considered statistically signnificant

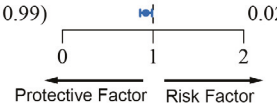

Figure 4. Forest plots illustrating the results of the validation stage for 10 essential genes in both UKB-PPP and deCODE.

3.3. Clinical Expression and Survival Analysis

Using RNA sequencing data from TCGA for PRAD, we validated the previously identified candidate drug-associated genes for PRAD. Figure 5 shows the significant differential expression between the tumor and paired-normal tissues. Specifically, RNF43 ($p = 2.9 \times 10^{-4}$), IL10RB ($p = 1.4 \times 10^{-3}$), GSTZ1 ($p = 3.0 \times 10^{-5}$), COL2A1 ($p = 0.011$), SERPINA3 ($p = 2.6 \times 10^{-3}$),SPINT2 ($p = 0.035$), TRIM ($p = 0.035$), GNMT ($p = 0.037$) and MTHFD1 ($p = 2.7 \times 10^{-6}$) were upregulated in tumor samples compared to their normal counterparts, while IGFBP3 ($p = 1.2 \times 10^{-3}$), TNFRSF10C ($p = 4.3 \times 10^{-5}$), LAYN ($p = 7.3 \times 10^{-8}$), JAM3 ($p = 4.7 \times 10^{-7}$), PPP1R14A ($p = 1.4 \times 10^{-9}$), LGALS4 ($p = 5.8 \times 10^{-6}$), ECM1 ($p = 2.6 \times 10^{-3}$), CRHBP ($p = 8.1 \times 10^{-5}$), MSMB ($p = 0.011$), NTRK3 ($p = 2.3 \times 10^{-3}$) and RNASE3 ($p = 6.6 \times 10^{-5}$) were downregulated.

Due to low mortality, only a few genes were linked to overall survival (OS). TNFRSF10C (HR (95% CI) = 0.19 (0.055–0.66), $p = 3.91 \times 10^{-3}$) and CRHBP (HR (95% CI) = 0.24 (0.067–0.85), $p = 1.64 \times 10^{-2}$) were linked to good OS, while LGALS4 (HR (95% CI) = 5.56 (1.20–25.86), $p = 1.40 \times 10^{-2}$), IL10RB (HR (95% CI) = 5.94 (1.28–27.57), $p = 9.84 \times 10^{-3}$), MTHFD1 (HR (95% CI) = 6.55 (1.76–24.45), $p = 1.26 \times 10^{-3}$), and POSTN (HR (95% CI) = 3.85 (1.00–14.76), $p = 3.52 \times 10^{-2}$) were associated with poor overall survival (Figure 6).

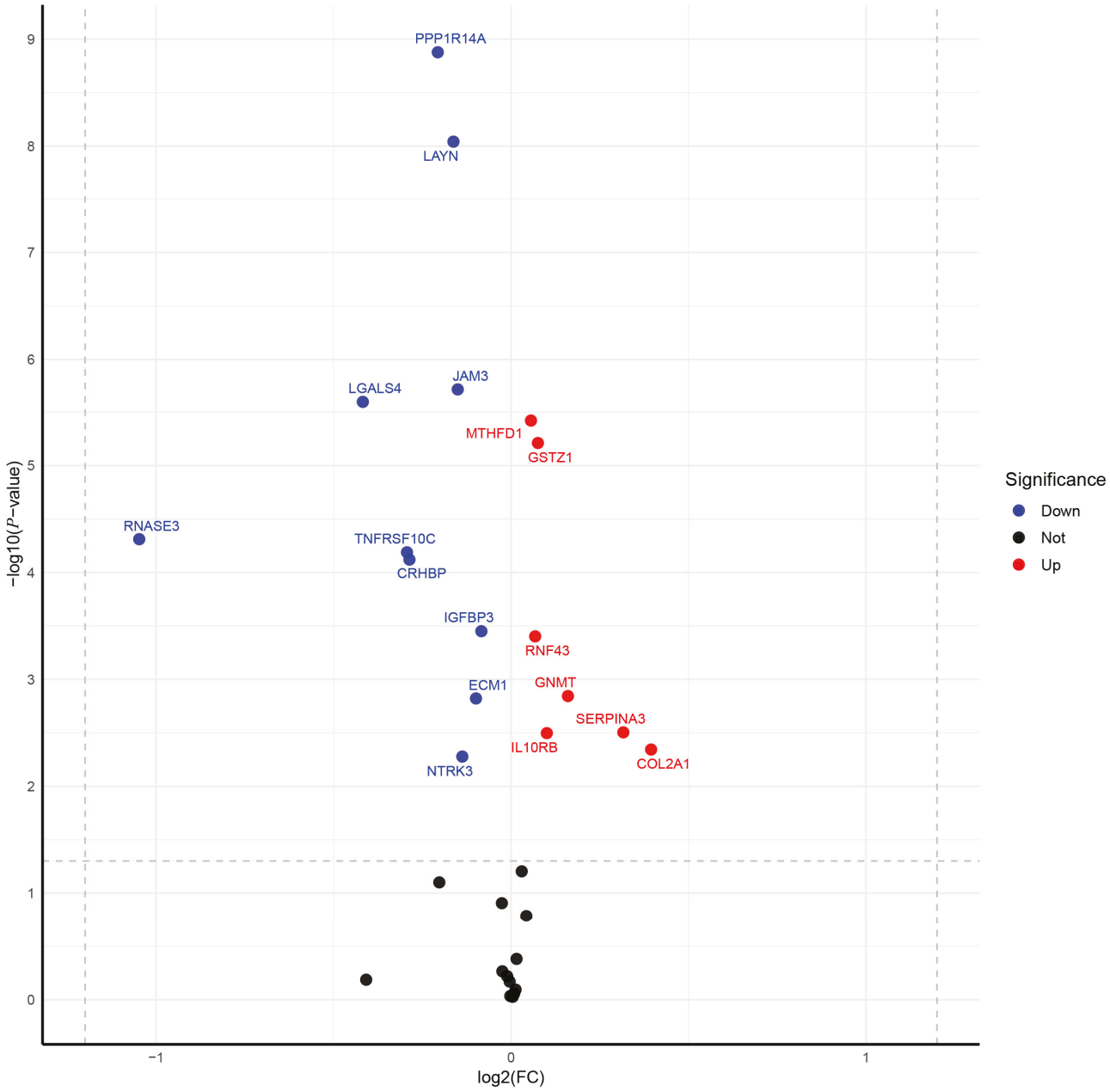

Figure 5. The expression of 30 essential genes between PRAD and paired-normal tissues. The volcano plot illustrates the differential gene expression analysis of 52 paired prostate cancer tissues compared to adjacent non-cancerous tissues. The x-axis represents the log2 fold change (log2FC) in gene expression, where positive values indicate upregulated genes in cancer tissues, and negative values indicate downregulated genes. The y-axis shows the −log10 (*p*-value), indicating the statistical significance of the differential expression. Significant genes are highlighted based on their fold change and *p*-value thresholds. Genes upregulated in prostate cancer are marked in red, while downregulated genes are marked in blue. Non-significant genes are displayed in black.

Thus, based on the survival analysis of the TCGA database, all genes except MTHFD1 and LGALS4 were excluded due to inconsistencies in the directionality of their effects.

3.4. Potential Immune Therapy Response Prediction

The TIDE (tumor immune dysfunction and exclusion) analysis revealed a strong association of MTHFD1 and LGALS4 expression with immunotherapy outcomes in PRAD. Specifically, higher LGALS4 expression was associated with higher TIDE scores (Figure 7A,

$p < 0.001$), reflecting higher immune dysfunction and exclusion, and thus a poorer response to immune checkpoint therapies. In contrast, high expression of MTHFD1 was associated with lower TIDE scores (Figure 7B, $p < 0.01$), suggesting a different role in the tumor microenvironment. These findings highlight LGALS4 as a potential biomarker of poor immunotherapy response in PRAD.

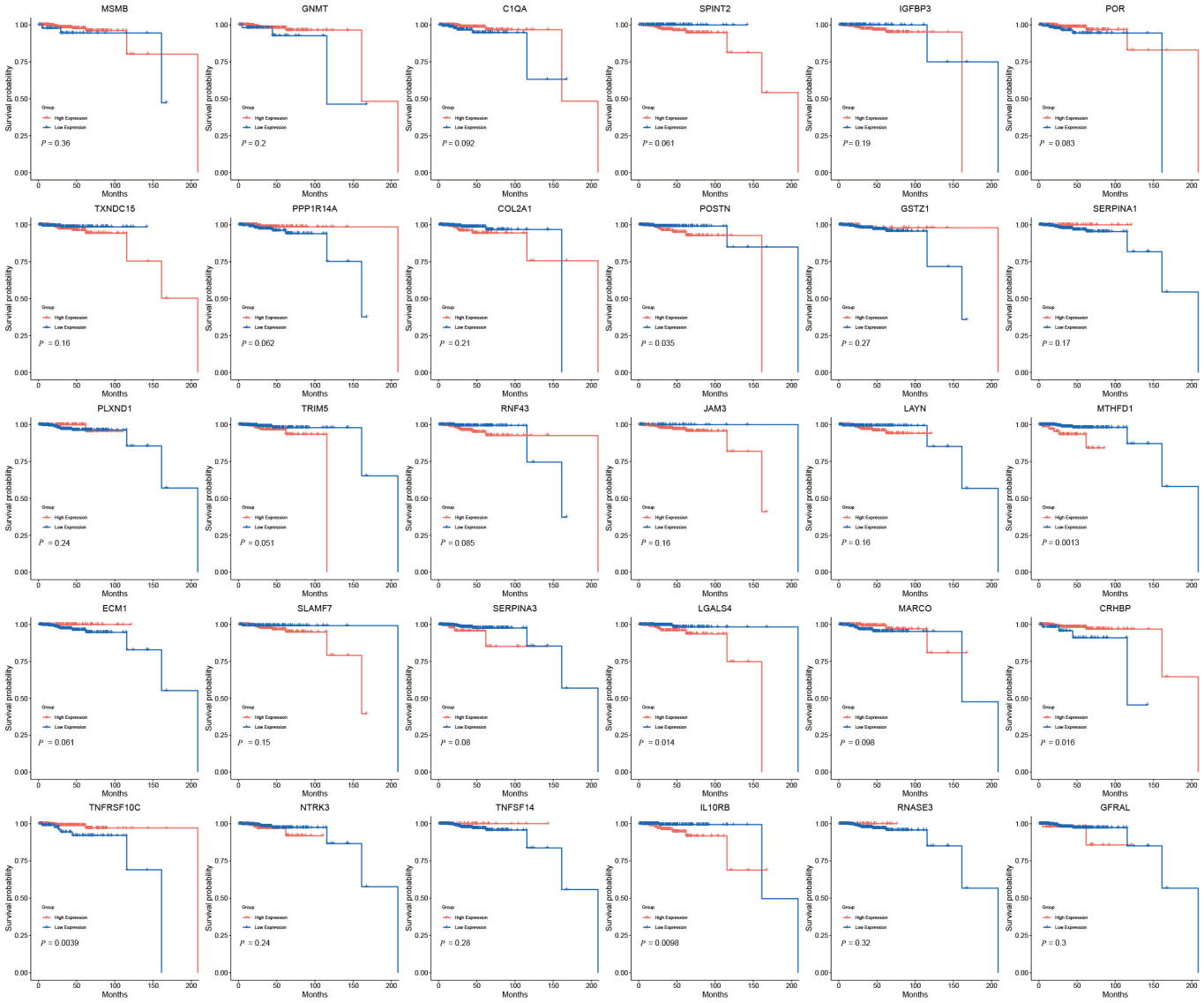

Figure 6. The survival analysis of 30 essential genes in PRAD patients. The KM survival curve distribution of different sample groups in the TCGA dataset, with log-rank tests conducted between groups.

Moreover, high LGALS4 expression was accompanied by increased immune checkpoint genes such as CD274 (PD-L1), CTLA4, HAVCR2 (TIM-3), ITPRIPL1, LAG3, PDCD1 (PD-1), PDCD1LG2 (PD-L2), SIGLEC15, and TIGIT (Figure 7C, $p < 0.01$ for all). MTHFD1 expression was related to high levels of PD-L2 and SIGLEC15 (Figure 7D). The upregulation of these immune checkpoint pathways may thus be indicative of the creation of an immunosuppressive tumor microenvironment that can foster mechanisms of immune evasion.

The elevated expression of LGALS4 therefore impairs immunotherapy response and facilitates the immune escape of PRAD by enhancing the signals of immune checkpoints.

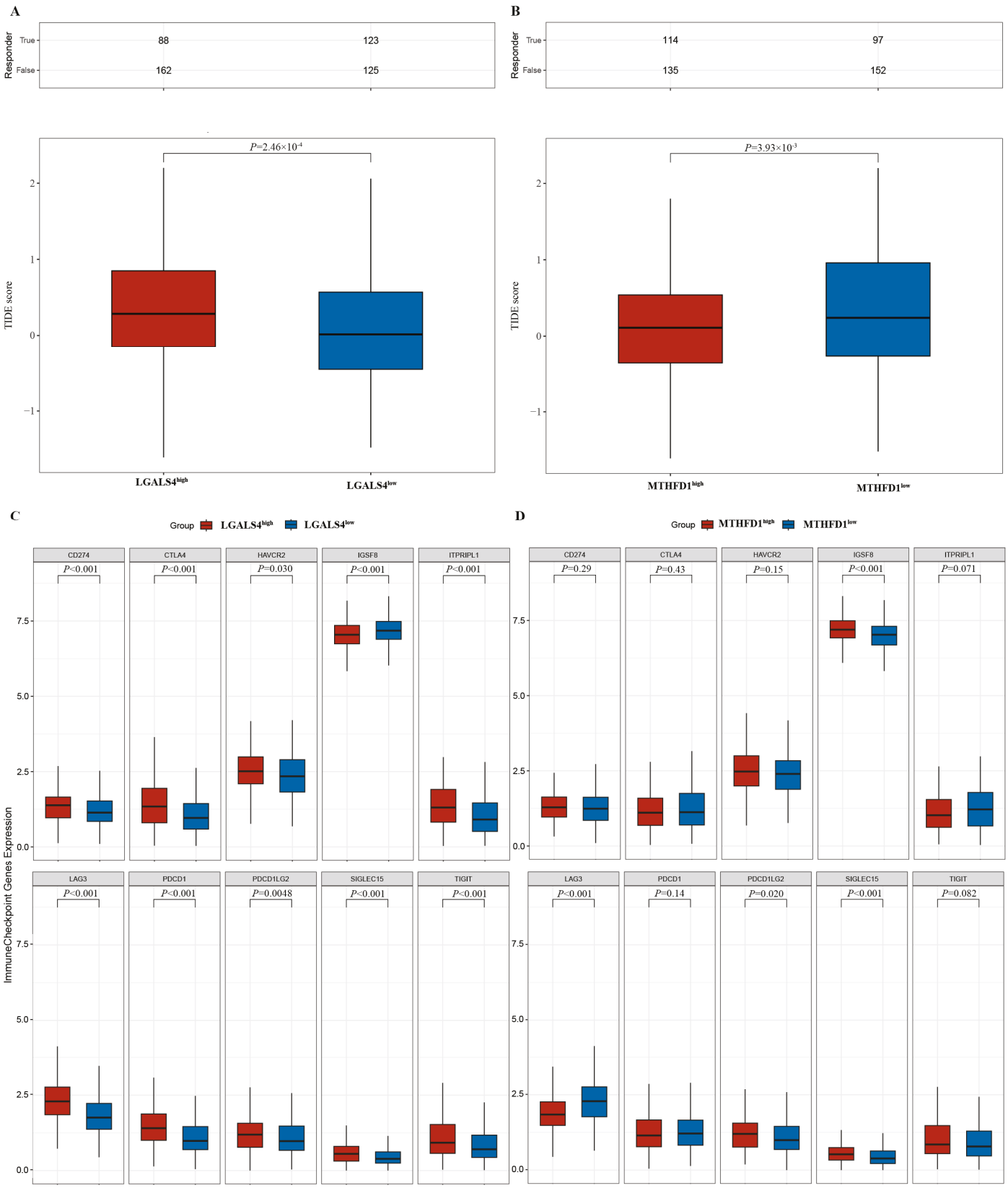

Figure 7. The potential immune therapy response prediction of LGALS4 and MTHFD1: (**A**) TIDE scores of immune response in LGALS4-high and LGALS4-low groups in the prediction results; (**B**) TIDE scores of immune response in MTHFD1-high and MTHFD1-low groups in the prediction results; (**C**) the distribution of immune checkpoint gene expression in LGALS4-high and LGALS4-low groups; and (**D**) the distribution of immune checkpoint gene expression in MTHFD1-high and MTHFD1-low groups. The significance was tested with the Wilcoxon test.

3.5. Expression Patterns of MTHFD1 and LGALS4 in PRAD

Single-cell RNA sequencing (scRNA-seq) data from the GSE176031 dataset further illuminated these distinct expression patterns within the tumor microenvironment. LGALS4 demonstrates significantly elevated expression levels in malignant cells compared to other cell populations such as fibroblasts, T regulatory (Treg) cells, and epithelial cells (Figure 8A). The preferential expression in malignant cells suggests that LGALS4 may play a critical role in tumorigenesis and cancer cell-specific metabolic or signaling pathways. In contrast, the expression of MTHFD1 is more heterogeneous, with notable enrichment in mast cells, malignant cells, and macrophage/monocyte populations. This suggests the multifaceted role of MTHFD1 in cancer cell metabolism and the tumor microenvironment (Figure 8B).

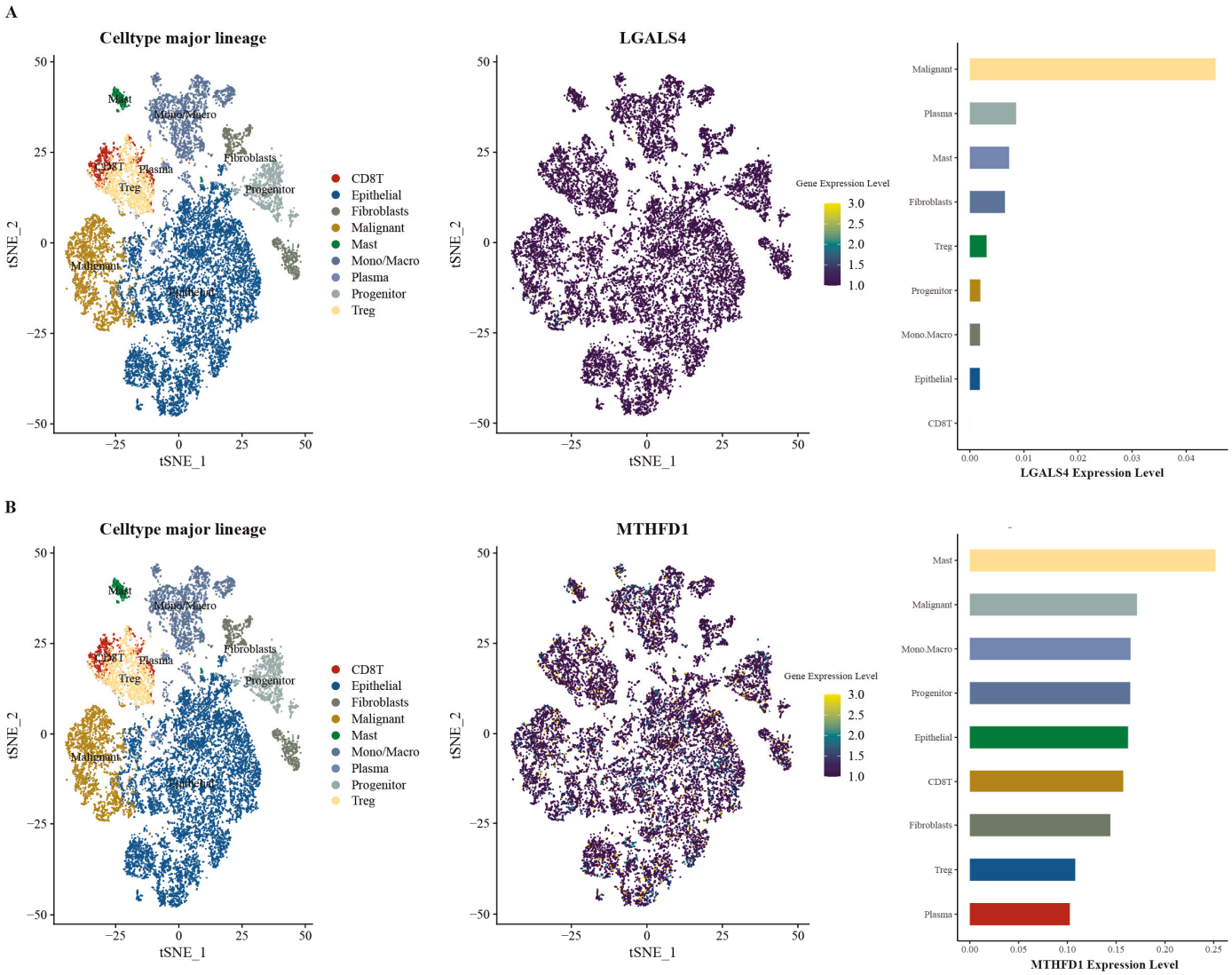

Figure 8. The single-cell expression of LGALS4 and MTHFD1 in PRAD: (**A**) the left is the t-SNE plot of single-cell clustering, where different colors represent different types of cells; the middle is the expression distribution of LGALS4 in different cells; and the right is the LGALS4 expression abundance in different cells. (**B**) the left is the t-SNE plot of single-cell clustering, where different colors represent different types of cells; the middle is the expression distribution of MTHFD1 in different cells; and the right is the MTHFD1 expression abundance in different cells.

Together, the distinct expression patterns of LGALS4 and MTHFD1 highlight their potential as biomarkers or therapeutic targets in PRAD. LGALS4's association with malignant cells may reflect its role in tumor-specific pathways, while MTHFD1's broader expres-

sion suggests its involvement in both cancer cell proliferation and microenvironmental interactions.

3.6. Drug Target Prediction of MTHFD1 and LGALS4

An analysis of the DrugBank and TTD (Therapeutic Target Database) databases revealed that there are no currently approved drugs specifically targeting MTHFD1 and LGALS4. Meanwhile, using the DSigDB drug database on Enrichr, etoposide, 1-(5-deoxypentofuranosyl)-5-fluoropyrimidine-2,4(1h,3h)-dione, capecitabine, and lactose are the candida drugs associated with LGALS4. The drugs associated with MTHFD1 are choline, choline hydroxide, dl-methionine, folic acid, methotrexate, dihydroergocristine, zinc sulfate, and alprostadil (Table 1).

Table 1. Candidate drugs predicted using DSigDB.

Term	*p* Value	Odds Ratio	Combined Score	Genes
etoposide BOSS	0.003	688.6	4000.6	LGALS4
1-(5-deoxypentofuranosyl)-5-fluoropyrimidine-2,4(1h,3h)-dione CTD 00001171	0.005	399.0	2106.4	LGALS4
choline CTD 00005662	0.005	399.0	2106.4	MTHFD1
capecitabine CTD 00003557	0.006	362.6	1880.6	LGALS4
lactose BOSS	0.010	197.0	903.8	LGALS4
choline hydroxide BOSS	0.011	185.9	842.3	MTHFD1
dl-methionine BOSS	0.017	119.5	489.4	MTHFD1
folic acid BOSS	0.018	110.1	442.2	MTHFD1
methotrexate BOSS	0.018	109.5	439.1	MTHFD1
dihydroergocristine HL60 DOWN	0.019	103.7	410.4	MTHFD1
zinc sulfate CTD 00007264	0.028	68.9	245.2	MTHFD1
paclitaxel CTD 00007144	0.049	39.6	119.8	LGALS4
alprostadil HL60 DOWN	0.049	39.1	117.6	MTHFD1

4. Discussion

In the past decade, androgen deprivation therapy (ADT) remains the gold standard treatment for metastatic prostate cancer [33]. However, the majority of patients eventually develop castration-resistant prostate cancer (CRPC) [34]. With the advancement of molecular sequencing techniques, the emergence of biomarker-driven treatments offers a novel option for precision medicine for prostate cancer [35]. Our study suggested a significant correlation between the upregulation of MTHFD1 and LGALS4 and an increased risk of prostate cancer. Accordingly, the results emphasize the possibility of MTHFD1 and LGALS4 inhibitors as therapeutic interventions for mitigating PRAD risk.

Galectins are a family of soluble proteins that are involved in many physiological functions such as immune responses and cell migration, autophagy, and signaling [36–38]. LGALS4, a member of galectins, contains two carbohydrate recognition domains within the same peptide chain, with a high affinity for β-galactoside residues [39].

Previous studies have demonstrated that the expression of galectin-4 varies across different types and stages of cancer. The levels of galectin-2, -4, and -8 in blood were significantly elevated in patients with colon and breast cancers, particularly in those with metastases [40,41]. Tsai et al. demonstrated that LGALS4 was increased in clinical samples of prostate cancer and was correlated with tumor progression, poor survival, and cancer recurrence. Western blotting further revealed that LGALS4 activated the expression of pERK, pAkt, fibronectin, and Twist1, and lowered the expression of E-cadherin [42]. These results suggest that LGALS4 may play an important role in driving tumorigenesis and

metastasis through the process of epithelial–mesenchymal transition (EMT). Moreover, LGALS4 was shown to induce apoptosis in T cells by binding CD3ε/δ and driving immune evasion in pancreatic cancer [43]. Notably, as a natural ligand for galactoglucan lectin-4, MUC1 induced EMT at the post-transcriptional level by modulating the expression of miRNAs in pancreatic cancer. Hypo-glycosylated forms of MUC1 have been shown to accumulate within cells, thereby initiating tumorigenic processes [44,45]. In summary, the available evidence supports the notion that LGALS4 is a potential therapeutic target in tumorigenesis and cancer progression.

Our results indicate that LGALS4 is predominantly expressed in malignant cells and is correlated with immunotherapy resistance and enhanced immune checkpoint pathways. Immune checkpoint inhibitors (ICIs) are monoclonal antibodies against immune checkpoint molecules that have shown remarkable efficacy in treating patients with a variety of cancers [46]. It has been demonstrated that CTLA4 and PD-1, along with its ligand PD-L1, have demonstrated significant therapeutic efficacy in cancers, including non-small cell lung cancer, metastatic melanoma, and bladder cancer [47]. Moreover, our results suggest that LGALS4 may be involved in immune evasion, a mechanism that contributes to resistance to both immunotherapy and androgen deprivation therapy. Therefore, targeting LGALS4 could improve the efficacy of ICIs and ATD in prostate cancer, especially in metastatic or castration-resistant cases.

MTHFD1 has three distinct enzymatic activities (5,10-methylenetetrahydrofolate dehydrogenase, 5,10-methenyltetrahydrofolate cyclohydrolase, 10-formyltetrahydrofolate synthetase), which played a significant role in the development of different types of cancers [48–51]. Research suggests that the overexpression of MTHFD1 in hepatocellular carcinoma was associated with poorer survival and recurrence [52]. The published data confirmed that the knockdown of MTHFD1 inhibited the proliferation, migration, and induced apoptosis of neuroblastoma (NB) cells. In addition, the study also suggested that MTHFD1 was upregulated in MYCN-amplified NB and correlated with the poor prognosis of NB patients [53]. In colorectal cancer (CRC), MTHFD1 regulated autophagic processes to facilitate tumor growth and metastasis through the PI3K–AKT–mTOR signaling pathway [54]. Furthermore, the expression level of MTHFD1 was associated with survival time, tumor size, TNM stage, histologic grade, and metastasis in non-small cell lung cancer and that MTHFD1 expression in tumor tissues and cells was significantly elevated compared to adjacent normal tissues and cells [55]. A current study found that MTHFD1 levels were not only associated with prognosis after CRT treatment of small cell lung cancer patients, but could also discriminate SCLC from both lung squamous cell carcinoma (LUSC) and lung adenocarcinoma (LUAD) [56]. Additionally, MTHFD1 may form a nuclear complex with the phosphatase and tensin homologue deleted on chromosome 10 (PENT) to assist dTMP synthesis in human prostate cancer cell lines that may have implications for targeting nuclear-excluded PTEN prostate cancer cells with antifolate drugs [57]. These findings emphasize the possibility of MTHFD1 as a potential therapeutic target for PRAD.

Our research has shown that MTHFD1 is widely expressed in malignant prostate cancer cells, mast cells, and macrophages. MTHFD1 is a key enzyme in single-carbon metabolism, involved in crucial processes such as methylation, nucleotide synthesis and amino acid metabolism [58–60]. Therefore, MTHFD1 inhibition may increase the sensitivity of PCa cells to chemotherapeutic agents, such as docetaxel, by disrupting the nucleotide and amino acid pathways essential for tumor growth. In addition, mast cells and macrophages play a key role in immune escape from tumors; MTHFD1 may alter the immune response in the tumor microenvironment by modulating the metabolism of these immune cells. In combination with ICIs, MTHFD1 inhibitors may help to restore immune cell recognition of, and attack on, tumors, thereby improving the efficacy of immunotherapy.

In summary, the targeting of LGALS4 or MTHFD, in combination with ADT, chemotherapy, and immunotherapy, could offer a novel approach to treating prostate cancer, particularly in cases where resistance to current therapies limits clinical efficacy.

There are numerous strengths in this study. Sensitivity analyses and reverse Mendelian randomization were utilized to confirm the robustness and reliability of the results. SMR and HEIDI tests were conducted for the elimination of horizontal pleiotropy. The TCGA database was used for further validation. Our study also has some limitations. First, MR analysis offers information on potential causal correlations, but its assumptions might not be entirely consistent with actual clinical trial conditions. Second, the primary data were obtained from European populations, which may hinder the extrapolation of our findings to diverse populations.

5. Conclusions

Our study identified MTHFD1 and LGALS4 as potential preventive targets for PRAD. LGALS4 may play a critical role in tumor-specific pathways, while MTHFD1 may be involved in both cancer cell proliferation and microenvironmental interactions. However, clinical trials are critical to ultimately assess the efficacy and safety of potential drug targets.

Supplementary Materials: The following supporting information can be downloaded at: https://www.mdpi.com/article/10.3390/biomedicines13010185/s1. Table S1. The positive genetic variations of eQTLs utilized in the discovery phase; Table S2. The positive UKB-PPP pQTLs utilized in the validation phase; Table S3. The heterogeneity and pleiotropy analysis in the significance results of MR analysis of UKB-PPP cis-pQTLs and PRAD; Table S4. The instrumental variables in MR analysis of UKB-PPP cis-pQTLs on PRAD; Table S5. The positive deCODE pQTLs utilized in the validation phase; Table S6. The heterogeneity and pleiotropy analysis in the significance results of MR analysis of deCODE cis-pQTLs and PRAD; Table S7. The instrumental variables in MR analysis of deCODE cis-pQTLs on PRAD; Table S8. The positive UKB-PPP and deCODE pQTLs utilized in the validation phase.

Author Contributions: Conceptualization, H.H. and J.H.; methodology, H.H.; software, Z.L.; validation, H.S. and H.H.; formal analysis, H.S.; investigation, Z.L.; resources, J.H.; data curation, H.H.; writing—original draft preparation, H.H.; writing—review and editing, H.S. and C.Z.; visualization, Z.L.; su-pervision, C.Z.; project administration, J.H.; funding acquisition, J.H. All authors have read and agreed to the published version of the manuscript.

Funding: This work was supported by the National Key R&D Program of China (2023YFC2308405), the National Natural Science Foundation of China (82372232, 81902141), the Natural Science Foundation of Hubei Province (2022CFB127), and the Interdisciplinary Innovative Talents Foundation from Renmin Hospital of Wuhan University (JCRCFZ-2022-023).

Institutional Review Board Statement: The study was conducted in accordance with the Declaration of Helsinki and approved by the Ethics Committee of the Renmin Hospital of Wuhan University (WDRY2019-K080) on 12 September 2024.

Informed Consent Statement: Not applicable.

Data Availability Statement: Data are provided within the manuscript or in the Supplementary Information Files.

Acknowledgments: Thanks to all the contributors and participants.

Conflicts of Interest: The authors declare no conflicts of interest.

References

1. Rawla, P. Epidemiology of Prostate Cancer. *World J. Oncol.* **2019**, *10*, 63–89. [CrossRef] [PubMed]

2. Kohaar, I.; Petrovics, G.; Srivastava, S. A Rich Array of Prostate Cancer Molecular Biomarkers: Opportunities and Challenges. *Int. J. Mol. Sci.* **2019**, *20*, 1813. [CrossRef] [PubMed]
3. Pierre-Victor, D.; Parnes, H.L.; Andriole, G.L.; Pinsky, P.F. Prostate Cancer Incidence and Mortality Following a Negative Biopsy in a Population Undergoing PSA Screening. *Urology* **2021**, *155*, 62–69. [CrossRef]
4. DE Nunzio, C.; Fiori, C.; Fusco, F.; Gregori, A.; Pagliarulo, V.; Alongi, F. Androgen Deprivation Therapy and Cardiovascular Risk in Prostate Cancer. *Minerva Urol. Nephrol.* **2022**, *74*, 508–517. [CrossRef]
5. Cheng, H.H.; Lin, D.W.; Yu, E.Y. Advanced Clinical States in Prostate Cancer. *Urol. Clin. N. Am.* **2012**, *39*, 561–571. [CrossRef]
6. Atiq, M.; Chandran, E.; Karzai, F.; Madan, R.A.; Aragon-Ching, J.B. Emerging Treatment Options for Prostate Cancer. *Expert. Rev. Anticancer Ther.* **2023**, *23*, 625–631. [CrossRef]
7. Adamaki, M.; Zoumpourlis, V. Prostate Cancer Biomarkers: From Diagnosis to Prognosis and Precision-Guided Therapeutics. *Pharmacol. Ther.* **2021**, *228*, 107932. [CrossRef]
8. Swami, U.; McFarland, T.R.; Nussenzveig, R.; Agarwal, N. Advanced Prostate Cancer: Treatment Advances and Future Directions. *Trends Cancer* **2020**, *6*, 702–715. [CrossRef]
9. Sekhoacha, M.; Riet, K.; Motloung, P.; Gumenku, L.; Adegoke, A.; Mashele, S. Prostate Cancer Review: Genetics, Diagnosis, Treatment Options, and Alternative Approaches. *Molecules* **2022**, *27*, 5730. [CrossRef]
10. Deluce, J.E.; Cardenas, L.; Lalani, A.-K.; Maleki Vareki, S.; Fernandes, R. Emerging Biomarker-Guided Therapies in Prostate Cancer. *Curr. Oncol.* **2022**, *29*, 5054–5076. [CrossRef]
11. Haffner, M.C.; Zwart, W.; Roudier, M.P.; True, L.D.; Nelson, W.G.; Epstein, J.I.; De Marzo, A.M.; Nelson, P.S.; Yegnasubramanian, S. Genomic and Phenotypic Heterogeneity in Prostate Cancer. *Nat. Rev. Urol.* **2021**, *18*, 79–92. [CrossRef] [PubMed]
12. Farashi, S.; Kryza, T.; Clements, J.; Batra, J. Post-GWAS in Prostate Cancer: From Genetic Association to Biological Contribution. *Nat. Rev. Cancer* **2019**, *19*, 46–59. [CrossRef] [PubMed]
13. Lee, C. Towards the Genetic Architecture of Complex Gene Expression Traits: Challenges and Prospects for eQTL Mapping in Humans. *Genes* **2022**, *13*, 235. [CrossRef] [PubMed]
14. Suhre, K.; McCarthy, M.I.; Schwenk, J.M. Genetics Meets Proteomics: Perspectives for Large Population-Based Studies. *Nat. Rev. Genet.* **2021**, *22*, 19–37. [CrossRef]
15. Emdin, C.A.; Khera, A.V.; Kathiresan, S. Mendelian Randomization. *JAMA* **2017**, *318*, 1925–1926. [CrossRef]
16. Wu, Y.; Zeng, J.; Zhang, F.; Zhu, Z.; Qi, T.; Zheng, Z.; Lloyd-Jones, L.R.; Marioni, R.E.; Martin, N.G.; Montgomery, G.W.; et al. Integrative Analysis of Omics Summary Data Reveals Putative Mechanisms Underlying Complex Traits. *Nat. Commun.* **2018**, *9*, 918. [CrossRef]
17. Hansen, S.B.; Unal, B.; Kuzu, O.F.; Saatcioglu, F. Immunological Facets of Prostate Cancer and the Potential of Immune Checkpoint Inhibition in Disease Management. *Theranostics* **2024**, *14*, 6913–6934. [CrossRef]
18. Graham, M.K.; Wang, R.; Chikarmane, R.; Abel, B.; Vaghasia, A.; Gupta, A.; Zheng, Q.; Hicks, J.; Sysa-Shah, P.; Pan, X.; et al. Convergent Alterations in the Tumor Microenvironment of MYC-Driven Human and Murine Prostate Cancer. *Nat. Commun.* **2024**, *15*, 7414. [CrossRef]
19. Võsa, U.; Claringbould, A.; Westra, H.-J.; Bonder, M.J.; Deelen, P.; Zeng, B.; Kirsten, H.; Saha, A.; Kreuzhuber, R.; Yazar, S.; et al. Large-Scale Cis- and Trans-eQTL Analyses Identify Thousands of Genetic Loci and Polygenic Scores That Regulate Blood Gene Expression. *Nat. Genet.* **2021**, *53*, 1300–1310. [CrossRef]
20. Sun, B.B.; Chiou, J.; Traylor, M.; Benner, C.; Hsu, Y.-H.; Richardson, T.G.; Surendran, P.; Mahajan, A.; Robins, C.; Vasquez-Grinnell, S.G.; et al. Plasma Proteomic Associations with Genetics and Health in the UK Biobank. *Nature* **2023**, *622*, 329–338. [CrossRef]
21. Ferkingstad, E.; Sulem, P.; Atlason, B.A.; Sveinbjornsson, G.; Magnusson, M.I.; Styrmisdottir, E.L.; Gunnarsdottir, K.; Helgason, A.; Oddsson, A.; Halldorsson, B.V.; et al. Large-Scale Integration of the Plasma Proteome with Genetics and Disease. *Nat. Genet.* **2021**, *53*, 1712–1721. [CrossRef] [PubMed]
22. Kurki, M.I.; Karjalainen, J.; Palta, P.; Sipilä, T.P.; Kristiansson, K.; Donner, K.M.; Reeve, M.P.; Laivuori, H.; Aavikko, M.; Kaunisto, M.A.; et al. FinnGen Provides Genetic Insights from a Well-Phenotyped Isolated Population. *Nature* **2023**, *613*, 508–518. [CrossRef] [PubMed]
23. Zhu, Z.; Zhang, F.; Hu, H.; Bakshi, A.; Robinson, M.R.; Powell, J.E.; Montgomery, G.W.; Goddard, M.E.; Wray, N.R.; Visscher, P.M.; et al. Integration of Summary Data from GWAS and eQTL Studies Predicts Complex Trait Gene Targets. *Nat. Genet.* **2016**, *48*, 481–487. [CrossRef] [PubMed]
24. 1000 Genomes Project Consortium; Abecasis, G.R.; Auton, A.; Brooks, L.D.; DePristo, M.A.; Durbin, R.M.; Handsaker, R.E.; Kang, H.M.; Marth, G.T.; McVean, G.A. An Integrated Map of Genetic Variation from 1092 Human Genomes. *Nature* **2012**, *491*, 56–65. [CrossRef]
25. Davey Smith, G.; Hemani, G. Mendelian Randomization: Genetic Anchors for Causal Inference in Epidemiological Studies. *Hum. Mol. Genet.* **2014**, *23*, R89–R98. [CrossRef]
26. Burgess, S.; Butterworth, A.; Thompson, S.G. Mendelian Randomization Analysis with Multiple Genetic Variants Using Summarized Data. *Genet. Epidemiol.* **2013**, *37*, 658–665. [CrossRef]

27. Hartwig, F.P.; Davey Smith, G.; Bowden, J. Robust Inference in Summary Data Mendelian Randomization via the Zero Modal Pleiotropy Assumption. *Int. J. Epidemiol.* **2017**, *46*, 1985–1998. [CrossRef]
28. Bowden, J.; Davey Smith, G.; Haycock, P.C.; Burgess, S. Consistent Estimation in Mendelian Randomization with Some Invalid Instruments Using a Weighted Median Estimator. *Genet. Epidemiol.* **2016**, *40*, 304–314. [CrossRef]
29. Bowden, J.; Davey Smith, G.; Burgess, S. Mendelian Randomization with Invalid Instruments: Effect Estimation and Bias Detection through Egger Regression. *Int. J. Epidemiol.* **2015**, *44*, 512–525. [CrossRef]
30. Verbanck, M.; Chen, C.-Y.; Neale, B.; Do, R. Detection of Widespread Horizontal Pleiotropy in Causal Relationships Inferred from Mendelian Randomization between Complex Traits and Diseases. *Nat. Genet.* **2018**, *50*, 693–698. [CrossRef]
31. Yoo, M.; Shin, J.; Kim, J.; Ryall, K.A.; Lee, K.; Lee, S.; Jeon, M.; Kang, J.; Tan, A.C. DSigDB: Drug Signatures Database for Gene Set Analysis. *Bioinformatics* **2015**, *31*, 3069–3071. [CrossRef] [PubMed]
32. Kuleshov, M.V.; Jones, M.R.; Rouillard, A.D.; Fernandez, N.F.; Duan, Q.; Wang, Z.; Koplev, S.; Jenkins, S.L.; Jagodnik, K.M.; Lachmann, A.; et al. Enrichr: A Comprehensive Gene Set Enrichment Analysis Web Server 2016 Update. *Nucleic Acids Res.* **2016**, *44*, W90–W97. [CrossRef] [PubMed]
33. Sparasci, D.; Napoli, I.; Rossi, L.; Pereira-Mestre, R.; Manconi, M.; Treglia, G.; Marandino, L.; Ottaviano, M.; Turco, F.; Mangan, D.; et al. Prostate Cancer and Sleep Disorders: A Systematic Review. *Cancers* **2022**, *14*, 1784. [CrossRef] [PubMed]
34. Henríquez, I.; Roach, M.; Morgan, T.M.; Bossi, A.; Gómez, J.A.; Abuchaibe, O.; Couñago, F. Current and Emerging Therapies for Metastatic Castration-Resistant Prostate Cancer (mCRPC). *Biomedicines* **2021**, *9*, 1247. [CrossRef]
35. Mizuno, K.; Beltran, H. Future Directions for Precision Oncology in Prostate Cancer. *Prostate* **2022**, *82* (Suppl. S1), S86–S96. [CrossRef]
36. Kapetanakis, N.-I.; Busson, P. Galectins as Pivotal Components in Oncogenesis and Immune Exclusion in Human Malignancies. *Front. Immunol.* **2023**, *14*, 1145268. [CrossRef]
37. Johannes, L.; Jacob, R.; Leffler, H. Galectins at a Glance. *J. Cell Sci.* **2018**, *131*, jcs208884. [CrossRef]
38. Liu, F.-T.; Stowell, S.R. The Role of Galectins in Immunity and Infection. *Nat. Rev. Immunol.* **2023**, *23*, 479–494. [CrossRef]
39. Cao, Z.-Q.; Guo, X.-L. The Role of Galectin-4 in Physiology and Diseases. *Protein Cell* **2016**, *7*, 314–324. [CrossRef]
40. Barrow, H.; Guo, X.; Wandall, H.H.; Pedersen, J.W.; Fu, B.; Zhao, Q.; Chen, C.; Rhodes, J.M.; Yu, L.-G. Serum Galectin-2, -4, and -8 Are Greatly Increased in Colon and Breast Cancer Patients and Promote Cancer Cell Adhesion to Blood Vascular Endothelium. *Clin. Cancer Res.* **2011**, *17*, 7035–7046. [CrossRef]
41. Chen, C.; Duckworth, C.A.; Fu, B.; Pritchard, D.M.; Rhodes, J.M.; Yu, L.-G. Circulating Galectins -2, -4 and -8 in Cancer Patients Make Important Contributions to the Increased Circulation of Several Cytokines and Chemokines That Promote Angiogenesis and Metastasis. *Br. J. Cancer* **2014**, *110*, 741–752. [CrossRef] [PubMed]
42. Tsai, C.-H.; Tzeng, S.-F.; Chao, T.-K.; Tsai, C.-Y.; Yang, Y.-C.; Lee, M.-T.; Hwang, J.-J.; Chou, Y.-C.; Tsai, M.-H.; Cha, T.-L.; et al. Metastatic Progression of Prostate Cancer Is Mediated by Autonomous Binding of Galectin-4-O-Glycan to Cancer Cells. *Cancer Res.* **2016**, *76*, 5756–5767. [CrossRef] [PubMed]
43. Lidström, T.; Cumming, J.; Gaur, R.; Frängsmyr, L.; Pateras, I.S.; Mickert, M.J.; Franklin, O.; Forsell, M.N.E.; Arnberg, N.; Dongre, M.; et al. Extracellular Galectin 4 Drives Immune Evasion and Promotes T-Cell Apoptosis in Pancreatic Cancer. *Cancer Immunol. Res.* **2023**, *11*, 72–92. [CrossRef] [PubMed]
44. Qing, L.; Li, Q.; Dong, Z. MUC1: An Emerging Target in Cancer Treatment and Diagnosis. *Bull. Cancer* **2022**, *109*, 1202–1216. [CrossRef]
45. Nath, S.; Mukherjee, P. MUC1: A Multifaceted Oncoprotein with a Key Role in Cancer Progression. *Trends Mol. Med.* **2014**, *20*, 332–342. [CrossRef]
46. Tang, Q.; Chen, Y.; Li, X.; Long, S.; Shi, Y.; Yu, Y.; Wu, W.; Han, L.; Wang, S. The Role of PD-1/PD-L1 and Application of Immune-Checkpoint Inhibitors in Human Cancers. *Front. Immunol.* **2022**, *13*, 964442. [CrossRef]
47. Ott, P.A.; Hu-Lieskovan, S.; Chmielowski, B.; Govindan, R.; Naing, A.; Bhardwaj, N.; Margolin, K.; Awad, M.M.; Hellmann, M.D.; Lin, J.J.; et al. A Phase Ib Trial of Personalized Neoantigen Therapy Plus Anti-PD-1 in Patients with Advanced Melanoma, Non-Small Cell Lung Cancer, or Bladder Cancer. *Cell* **2020**, *183*, 347–362.e24. [CrossRef]
48. Meng, Q.; Lu, Y.-X.; Wei, C.; Wang, Z.-X.; Lin, J.-F.; Liao, K.; Luo, X.-J.; Yu, K.; Han, Y.; Li, J.-J.; et al. Arginine Methylation of MTHFD1 by PRMT5 Enhances Anoikis Resistance and Cancer Metastasis. *Oncogene* **2022**, *41*, 3912–3924. [CrossRef]
49. Green, A.C.; Marttila, P.; Kiweler, N.; Chalkiadaki, C.; Wiita, E.; Cookson, V.; Lesur, A.; Eiden, K.; Bernardin, F.; Vallin, K.S.A.; et al. Formate Overflow Drives Toxic Folate Trapping in MTHFD1 Inhibited Cancer Cells. *Nat. Metab.* **2023**, *5*, 642–659. [CrossRef]
50. He, D.; Yu, Z.; Liu, S.; Dai, H.; Xu, Q.; Li, F. Methylenetetrahydrofolate Dehydrogenase 1 (MTHFD1) Is Underexpressed in Clear Cell Renal Cell Carcinoma Tissue and Transfection and Overexpression in Caki-1 Cells Inhibits Cell Proliferation and Increases Apoptosis. *Med. Sci. Monit.* **2018**, *24*, 8391–8400. [CrossRef]
51. Zheng, B.S.; Wang, S.D.; Zhang, J.Y.; Ge, C.G. Expression, Prognostic Value, and Immune Infiltration of MTHFD Family in Bladder Cancer. *Curr. Cancer Drug Targets* **2024**, *24*, 178–191. [CrossRef] [PubMed]

52. Yu, H.; Wang, H.; Xu, H.-R.; Zhang, Y.-C.; Yu, X.-B.; Wu, M.-C.; Jin, G.-Z.; Cong, W.-M. Overexpression of MTHFD1 in Hepatocellular Carcinoma Predicts Poorer Survival and Recurrence. *Future Oncol.* **2019**, *15*, 1771–1780. [CrossRef] [PubMed]
53. Guan, J.; Li, M.; Wang, Y.; Zhang, Y.; Que, Y.; Lu, S.; Wang, J.; Zhu, J.; Huang, J.; Zhen, Z.; et al. MTHFD1 Regulates the NADPH Redox Homeostasis in MYCN-Amplified Neuroblastoma. *Cell Death Dis.* **2024**, *15*, 124. [CrossRef]
54. Li, Z.; Ke, H.; Cai, J.; Ye, S.; Huang, J.; Zhang, C.; Yuan, M.; Lan, P.; Wu, X. MTHFD1 Regulates Autophagy to Promote Growth and Metastasis in Colorectal Cancer via the PI3K-AKT-mTOR Signaling Pathway. *Cancer Med.* **2024**, *13*, e70267. [CrossRef]
55. Ding, K.; Jiang, J.; Chen, L.; Xu, X. Methylenetetrahydrofolate Dehydrogenase 1 Silencing Expedites the Apoptosis of Non-Small Cell Lung Cancer Cells via Modulating DNA Methylation. *Med. Sci. Monit.* **2018**, *24*, 7499–7507. [CrossRef]
56. Hao, Y.; Lu, R.; Guo, Y.; Bao, P. Specific Association of MTHFD1 Expressions with Small Cell Lung Cancer Development and Chemoradiotherapy Outcome. *Saudi Med. J.* **2024**, *45*, 783–790. [CrossRef]
57. Loh, Z.N.; Wang, M.-E.; Wan, C.; Asara, J.M.; Ji, Z.; Chen, M. Nuclear PTEN Regulates Thymidylate Biosynthesis in Human Prostate Cancer Cell Lines. *Metabolites* **2023**, *13*, 939. [CrossRef]
58. Ducker, G.S.; Rabinowitz, J.D. One-Carbon Metabolism in Health and Disease. *Cell Metab.* **2017**, *25*, 27–42. [CrossRef]
59. MacFarlane, A.J.; Perry, C.A.; Girnary, H.H.; Gao, D.; Allen, R.H.; Stabler, S.P.; Shane, B.; Stover, P.J. Mthfd1 Is an Essential Gene in Mice and Alters Biomarkers of Impaired One-Carbon Metabolism. *J. Biol. Chem.* **2009**, *284*, 1533–1539. [CrossRef]
60. Field, M.S.; Kamynina, E.; Agunloye, O.C.; Liebenthal, R.P.; Lamarre, S.G.; Brosnan, M.E.; Brosnan, J.T.; Stover, P.J. Nuclear Enrichment of Folate Cofactors and Methylenetetrahydrofolate Dehydrogenase 1 (MTHFD1) Protect de Novo Thymidylate Biosynthesis during Folate Deficiency. *J. Biol. Chem.* **2014**, *289*, 29642–29650. [CrossRef]

Disclaimer/Publisher's Note: The statements, opinions and data contained in all publications are solely those of the individual author(s) and contributor(s) and not of MDPI and/or the editor(s). MDPI and/or the editor(s) disclaim responsibility for any injury to people or property resulting from any ideas, methods, instructions or products referred to in the content.

biomedicines

MDPI

Article

Natural Compounds and Histone Deacetylase Inhibitors: A Combined Approach Against mCRPC Cells

Janiah Alimudin [1], Zeynep Betts [2,3] and Asuman Deveci Ozkan [4,*]

[1] Department of Biology, Institute of Science, Kocaeli University, Kocaeli 41001, Türkiye; jenayiah18@gmail.com
[2] Manchester Institute of Biotechnology, Faculty of Science and Engineering, University of Manchester, Menchester M1 7DN, UK; duman.zeynep@gmail.com
[3] Department of Biology, Faculty of Science and Art, Kocaeli University, Kocaeli 41001, Türkiye
[4] Department of Medical Biology, Faculty of Medicine, Sakarya University, Sakarya 54290, Türkiye
* Correspondence: deveci@sakarya.edu.tr; Tel.: +90-2642954297

Abstract: Background: Sodium butyrate (NaBu), a short-chain fatty acid, modulates global gene expression through histone deacetylase (HDAC) inhibition, suppressing proliferation and inducing apoptosis in various cancers. Rutin (RUT), a polyphenolic flavonoid found in many plants, exhibits notable anticancer properties. Combining chemotherapeutic agents with natural polyphenols represents a promising strategy for cancer therapy. This study aims to evaluate, for the first time, the potential effects of NaBu and RUT combination therapy on metastatic castration-resistant prostate cancer (mCRPC) cells. **Methods**: PC-3 cells were treated with varying concentrations of NaBu, RUT, and their combinations. Cell viability was assessed using the WST-1 assay. Based on combination index values, selected treatments were further analyzed for apoptosis (Annexin V assay), intracellular reactive oxygen species (ROS) production, mRNA expression levels, and changes in cell and nuclear morphology. **Results**: The combined treatment of NaBu and RUT significantly reduced cell viability compared to individual treatments. Enhanced apoptotic induction and elevated ROS levels were observed in combination-treated cells, alongside notable changes in cellular and nuclear morphology and mRNA expression levels. **Conclusions**: NaBu and RUT combination therapy exhibits a synergistic anticancer effect in mCRPC cells by inhibiting cell viability, inducing apoptosis, and increasing ROS production. These findings suggest a promising therapeutic approach that warrants further investigation to elucidate the underlying molecular mechanisms and assess its potential in preclinical and clinical settings.

Keywords: prostate cancer; rutin; sodium butyrate; combination effect; apoptosis

1. Introduction

Prostate cancer (PCa), currently the second leading cause of cancer-related mortality in males within industrialized nations, has seen an increase in incidence over recent years [1]. Metastatic castration-resistant prostate cancer (mCRPC) is characterized by disease progression despite testosterone deprivation or surgical castration. This progression is driven by the persistence of androgen receptors (AR) and the activation of the androgen axis [2,3]. The complexity of cellular mechanisms involved in PCa development poses significant challenges for treatment [4]. To mitigate the side effects of current PCa therapies, alternative strategies are being explored, including the use of various bioactive compounds either as standalone treatments or in combination with chemotherapeutic agents [5,6].

Histone deacetylase (HDAC) enzymes, which regulate the acetylation and deacetylation of histone proteins, have emerged as promising therapeutic targets [7]. Sodium butyrate (NaBu), a short-chain fatty acid, acts as an HDAC inhibitor, influencing chromatin remodeling, altering global gene expression, reducing cell proliferation, and inducing apoptosis at low concentrations. It has shown potential as an anticancer agent in various cancer cell types [8,9]. Rutin (RUT), a polyphenolic antioxidant abundant in foods such as green tea and apples, has demonstrated a range of biological effects, including anti-carcinogenic, neuroprotective, anti-proliferative, anti-inflammatory, and anti-oxidative properties by inhibiting lipid peroxidation [10]. Additionally, RUT has been shown to induce apoptosis in various cancer cell lines [11,12].

The synergistic interaction between natural polyphenols and chemotherapeutic agents can enhance cancer treatment efficacy by inhibiting cell proliferation and promoting apoptosis [13]. Moreover, combination therapies involving herbal compounds have been reported to reduce drug resistance and mitigate chemotherapy-related complications [12]. Clinical studies have demonstrated that flavonoids administered alongside chemotherapeutic agents improve tumor suppression and patient survival outcomes [14].

The combination of natural polyphenols with chemotherapeutic drugs holds great promise as a strategy for cancer treatment. Natural agents, may reduce the likelihood of the severe side effects commonly associated with synthetic chemotherapeutic agents, thereby offering a more tolerable treatment option for patients. By focusing on the synergistic potential of sodium butyrate and rutin, we can develop a more effective, multi-pronged approach to cancer treatment that enhances therapeutic outcomes, improves patient tolerance, and offers the potential for use in combination with conventional chemotherapy regimens. This dual-target strategy may provide significant advantages in overcoming resistance mechanisms, reducing side effects, and improving overall treatment efficacy. Therefore, this study aims to investigate, for the first time, the combined therapeutic effects of RUT and NaBu on mCRPC PC-3 cells. To achieve this, PC-3 cells were treated with RUT, NaBu, and their combination, and various parameters were assessed, including Annexin V levels, intracellular reactive oxygen species (ROS), mRNA and protein expression levels, as well as cell and nuclear morphology.

2. Materials and Methods

2.1. Cell Culture

In this study, the PC-3 cell line was used as a model for mCRPC cells, while human umbilical vein endothelial cells (HUVEC) were employed to evaluate the cytotoxicity of the combined treatments specifically. Both cell lines were commercially obtained from the American Type Culture Collection (ATCC, Manassas, VA, USA). PC-3 cells were cultured in RPMI-1640 medium (Sigma Aldrich, St. Louis, MO, USA), while HUVEC cells were grown in Dulbecco's Modified Eagle's Medium (DMEM). The culture media for both of the cell lines were supplemented with 10% heat-inactivated fetal bovine serum (FBS) and 1% penicillin–streptomycin solution (Sigma Aldrich, St. Louis, MO, USA). The cells were maintained in a humidified incubator (Thermo Fisher Scientific, Waltham, MA, USA) set to 37 °C with 5% CO_2.

2.2. Cell Viability Assay

In this study, NaBu and RUT will be administered to cells both separately and in combination. The use of these two compounds, derived from natural sources, offers a versatile approach to address key challenges in cancer treatment, such as inhibiting cancer cell proliferation and promoting apoptosis. When combined, NaBu and RUT may exert synergistic effects on cancer cells by targeting multiple cellular pathways involved in tumor

progression [13]. NaBu's epigenetic modulation and ability to induce cell cycle arrest complement RUT's ability to disrupt key survival and proliferation signals, amplifying their individual anticancer properties [7,10]. Stock solutions of RUT (Tokyo Chemical Industry, Tokyo, Japan) and NaBu (Sigma Aldrich, USA) were prepared according to the manufacturers' instructions. PC-3 and HUVEC cells were treated with varying concentrations of RUT (0–1000 μM) and NaBu (0–10 mM), either individually or in combination, to assess cell viability using the WST-1 assay. For the assay, 96-well plates were seeded with approximately 2×10^4 cells per well of PC-3 and HUVEC cells. The cells were exposed to RUT, NaBu, or their combinations at different concentrations for 24 and 48 h. Following the incubation period, WST-1 reagent (Biovision, CA, USA) was added to each well, and the plates were incubated at 37 °C for 30 min. Cell viability was then measured using a microplate reader at 450 nm (Chromate, Shijiazhuang, China). Each experiment was performed in triplicate for both cell lines. The most effective combination concentrations of RUT and NaBu, along with the optimal exposure time, were determined by calculating the combination index (CI) and drug reduction index (DRI) values. HUVEC cells were used only in the viability assay.

2.3. Enzyme-Linked Immunosorbent Assay (ELISA)

Annexin A5 (ANXA5) is a 36 kDa protein that interacts with phospholipids in a calcium-dependent manner, with phosphatidylserine (PS) being its preferred binding partner. ANXA5 serves as a valuable tool for identifying apoptotic cells due to its ability to bind PS [15]. To evaluate the apoptotic effects of RUT and NaBu, both individually and in combination, an ELISA assay was conducted to quantify ANXA5 levels in only PC-3 cells. PC-3 cells (5×10^4 cells/well) were seeded into a 96-well plate and treated with RUT (500 and 750 μM), NaBu (1 and 2.5 mM), or their combinations for 48 h. Additionally, a control group was established, cultured under the same conditions but without the addition of RUT, NaBu, or their combination. After the incubation period, cell culture supernatants were collected from each treatment group and analyzed using the Human Annexin V ELISA Kit (Abexxa, Cambridge, UK) following the manufacturer's instructions. The results obtained were compared with this control group, which received no treatment, and were analyzed statistically.

2.4. ROS Measurement

To assess the impact of RUT and NaBu, both individually and in combination, on intracellular ROS levels, a cellular ROS assay was conducted. PC-3 cells (4×10^6 cells/well) were seeded into a 96-well plate and treated with RUT (500 and 750 μM), NaBu (1 and 2.5 mM), or their combinations for 48 h. Additionally, a control group was established, cultured under the same conditions but without the addition of RUT, NaBu, or their combination. Following the incubation period, intracellular ROS levels were measured using the DCFDA/H2DCFDA-Cellular ROS Assay Kit (Abcam, Cambridge, UK) in accordance with the manufacturer's instructions. The results obtained were compared with this control group, which received no treatment, and were analyzed statistically.

2.5. Cell and Nuclear Morphology Observation

To assess changes in cell and nuclear morphology following the treatment with RUT and NaBu, both individually and in combination, Acridine Orange (AO) and 4′,6-Diamidino-2-phenylindole dihydrochloride (DAPI) staining was performed. PC-3 cells (4×10^5 cells/well) were cultured in a 6-well plate with slides and treated with the most effective combined concentrations of RUT (500 and 750 μM) and NaBu (1 and 2.5 mM) for 48 h. Additionally, a control group was established, cultured under the same conditions but without the addition of RUT, NaBu, or their combination. After the incubation period, the

cells were fixed with 4% paraformaldehyde solution for 30 min. The fixed cells were stained with AO (100 mg/mL, Sigma Aldrich, USA) for 30 min and with DAPI (Sigma Aldrich, USA) for 5 min. The cells were then washed three times with phosphate-buffered saline, and the slides were examined under a fluorescence microscope (Olympus, Tokyo, Japan). The results obtained were compared with this control group, which received no treatment.

2.6. Real Time-Polymerase Chain Reaction (RT-PCR) Analysis

To evaluate the effect of RUT and NaBu, individually and in combination, on the mRNA expression levels of *Bax*, *Bcl-2*, and *SOD* genes, RT-PCR analysis was conducted. PC-3 cells (4×10^6 cells/well) were cultured in T25 flasks and treated with RUT (500 and 750 μM) and/or NaBu (1 and 2.5 mM) for 48 h. Additionally, a control group was established, cultured under the same conditions but without the addition of RUT, NaBu, or their combination. Following the incubation period, RNA isolation was performed using the Xtrazol solution (Hölzel, Cologne, Germany) according to the manufacturer's protocol. RNA concentrations were quantified by measuring the absorbance at 260 nm using a spectrophotometer (Nanodrop, Thermo Fisher Scientific, USA). A total of 2 μg of RNA was reverse-transcribed into cDNA using the Tetro cDNA Synthesis Kit (Meridian Bioscience, Cincy, OH, USA). RT-PCR analysis was performed with a CFX Connect Real-Time PCR Detection System (Bio-Rad, Hercules, CA, USA) to assess the mRNA expression levels of *Bax*, *Bcl-2*, and *SOD*. *ACTB* (Beta-actin; Santa Cruz Biotechnology, Dallas, TX, USA) was used as the reference gene for the normalization of target gene expression. Each experiment was conducted in triplicate to ensure reproducibility.

2.7. Statistical Analysis

The statistical software GraphPad Prism V9.0 and SPSS 22.0 were used and $p < 0.05$ was considered statistically significant. A one-way ANOVA analysis with variance Tukey's test was used for multiple comparisons. Web-based software https://www.qiagen.com/tr/shop/genes-andpathways/data-analysis-center-overviewpage/other-real-time-pcrprobes-orprimersdataanalysis-center/, (accessed on 20 May 2022) was used to determine the differences in the mRNA expression levels that vary depending on dose and time. Two-way repetitive measurements were performed with ANOVA analysis to determine the best combination concentrations. Additionally, the Calcusyn software V2.0 (Biosoft, Inc., Orlando, FL, USA) was used to determine the relationship between RUT and NaBu and the combination index (CI) values.

3. Results

3.1. The Cytotoxicity of RUT and NaBu Treatment in PC-3 Cells

To identify the most effective concentrations and exposure times for RUT and NaBu, a WST-1 assay was conducted (Figure 1). The results revealed that RUT exhibited a dose- and time-dependent cytotoxic effect on PC-3 cells, as shown in Figure 1a. Specifically, a treatment with higher concentrations of RUT (500, 750, and 1000 μM) reduced PC-3 cell viability by 48.47%, 26.92%, and 29.48%, respectively, after 48 h (Figure 1a, Table 1, $p < 0.001$). Similarly, NaBu treatment (1, 2.5, 5, and 10 mM) also decreased cell viability in a dose-dependent manner, with reductions of 65.58%, 52.34%, 48.15%, and 39.86%, respectively, after 48 h (Figure 1b, Table 1, $p < 0.001$). Based on these results, RUT concentrations of 500 and 750 μM, along with NaBu concentrations of 1, 2.5, 5, and 10 mM, were selected for combination treatment analysis over a 48 h period.

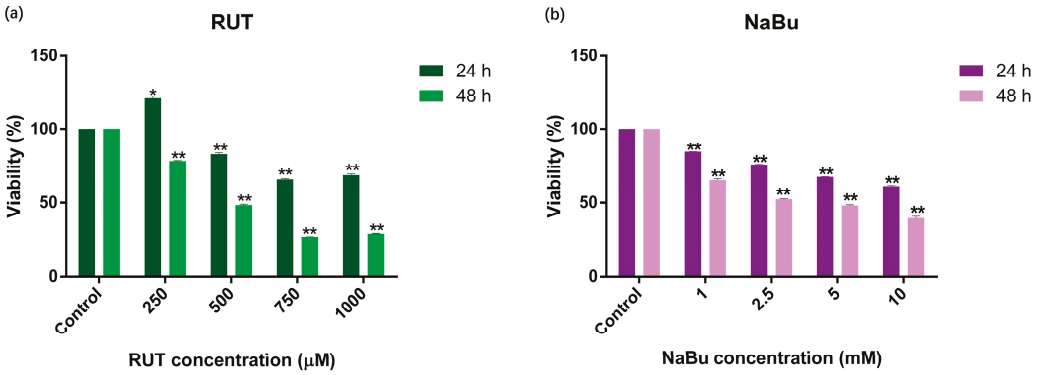

Figure 1. The viability rate of PC-3 prostate cancer cells after treatment with RUT or NaBu. (**a**) PC-3 cells were treated with RUT at concentrations of 250, 500, 750, or 1000 μM for 24 and 48 h. (**b**) PC-3 cells were treated with NaBu at concentrations of 1, 2.5, 5, or 10 mM for 24 and 48 h. Cell viability was determined using the WST-1 assay. Data are presented as the mean ± SD (n = 3) and are representative of experiments performed in triplicate. Statistical significance is indicated (* $p < 0.05$, **: Statistically significant, $p \leq 0.001$).

Table 1. The statistical analysis results of PC-3 cell viability after treatment with RUT or NaBu. A two-way ANOVA analysis with Tukey's multiple comparisons test was used for multiple comparisons. Statistical significance is denoted as ** $p < 0.001$.

RUT (μM)	Mean Difference	95% CI of Difference	Summary	Adjusted *p* Value
24 h				
Control vs. 250	−21.06	−23.14 to −18.98	**	<0.0001
Control vs. 500	16.97	14.89 to 19.05	**	<0.0001
Control vs. 750	34.02	31.95 to 36,10	**	<0.0001
Control vs. 1000	31.15	29.07 to 33.23	**	<0.0001
48 h				
Control vs. 250	21.59	19.51 to 23.67	**	<0.0001
Control vs. 500	51.53	49.45 to 53.61	**	<0.0001
Control vs. 750	73.07	70.99 to 75.15	**	<0.0001
Control vs. 1000	70.52	68.44 to 72.60	**	<0.0001
NaBu (mM)				
24 h				
Control vs. 1	15.35	13.83 to 16.87	**	<0.0001
Control vs. 2.5	23.96	22.44 to 25.48	**	<0.0001
Control vs. 5	32.34	30.82 to 33.86	**	<0.0001
Control vs. 10	38.87	37.35 to 40.39	**	<0.0001
48 h				
Control vs. 1	34.42	32.90 to 35.94	**	<0.0001
Control vs. 2.5	47.66	46.13 to 49.18	**	<0.0001
Control vs. 5	51.84	50.32 to 53.37	**	<0.0001
Control vs. 10	60.14	58.62 to 61.66	**	<0.0001

CI: confidence intervals.

3.2. The Effect of a Combined Treatment of RUT with NaBu on Cytotoxicity, Apoptosis, and Intracellular ROS Generation

To determine the most effective combined concentrations of RUT and NaBu, WST-1 analysis was performed (Figure 2). The combination of RUT and NaBu significantly reduced PC-3 cell viability compared to either treatment alone after 48 h (Table 2, $p < 0.001$). Specifically, the combinations of 500 μM RUT + 1 mM NaBu, 500 μM RUT + 2.5 mM NaBu,

750 μM RUT + 1 mM NaBu, and 750 μM RUT + 2.5 mM NaBu decreased PC-3 cell viability to 47.29%, 58.42%, 27.93%, and 38.33%, respectively (Table 2, $p < 0.001$), which were more effective than NaBu alone (65.52% and 52.34% for 1 and 2.5 mM NaBu, respectively) (Figure 2a). Notably, the RUT and NaBu combination treatments minimized NaBu's cytotoxic effects on HUVEC cells, showing no significant toxicity (Table 2, Figure 2b, $p < 0.001$). Moreover, the combination treatments demonstrated significant synergism (CI < 1) at lower concentrations in PC-3 cells, making them substantially more effective than RUT or NaBu alone (Tables 3 and 4). As a result, the combinations of 500 and 750 μM RUT with 1 and 2.5 mM NaBu for 48 h were selected for subsequent experiments in PC-3 cells.

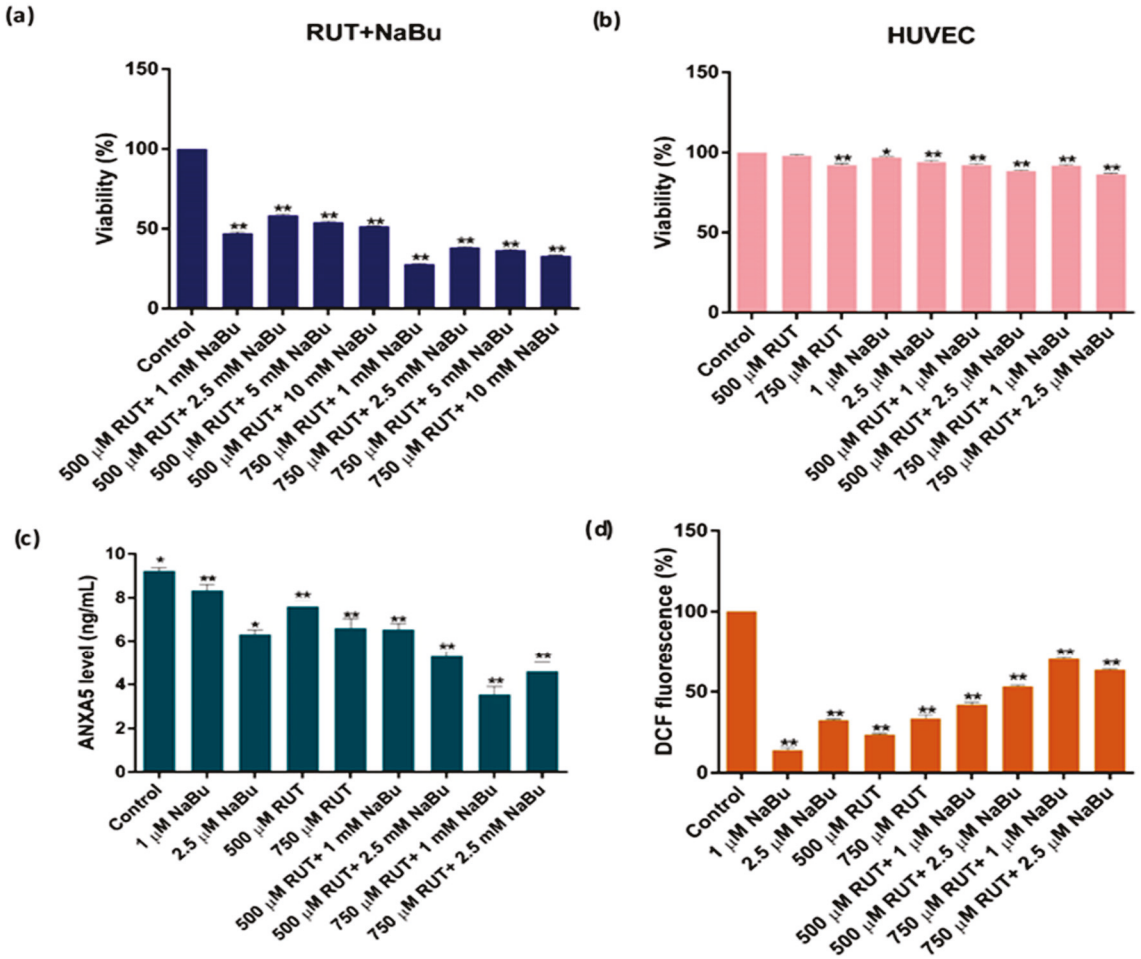

Figure 2. The effect of the combination treatment of RUT with NaBu on cell viability, apoptosis, and intracellular ROS generation. Cells were treated with RUT (500 and 750 μM) and/or NaBu (1, 2.5, 5, and 10 mM) for 48 h. (**a**) PC-3 and (**b**) HUVEC cell viability was assessed using the WST-1 assay. (**c**) Apoptosis was measured using the ANXA5 V ELISA assay. (**d**) Intracellular ROS generation was evaluated using the H2DCFDA assay, with fluorescence intensity indicating ROS levels. Data are presented as the mean ± SD (n = 3) and are representative of experiments performed in triplicate. Statistical significance is denoted as * $p < 0.05$ and ** $p < 0.001$.

The effects of RUT and NaBu combination treatments on apoptosis and intracellular ROS generation in PC-3 cells were assessed using ELISA and ROS analysis (Table 5, Figure 2c,d). The results revealed that the combination treatments significantly reduced free ANXA5 protein levels compared to individual treatments (Table 5, $p < 0.001$, Figure 2c). Similarly, RUT and NaBu combination treatments increased intracellular ROS levels more than either treatment alone (Table 5, $p < 0.001$, Figure 2d). Among the combinations, 750 μM RUT + 1 mM NaBu was the most effective in inducing both apoptosis and ROS production in PC-3 cells.

Table 2. The statistical analysis results of PC-3 and HUVEC cell viability after combination treatment with RUT and NaBu. A two-way ANOVA analysis with Dunnett's multiple comparisons test was used for multiple comparisons. Statistical significance is denoted as * $p < 0.05$ and ** $p < 0.001$.

RUT (μM) + NaBu (mM)	Mean Difference	95% CI of Difference	Summary	Adjusted *p* Value
PC-3				
Control vs. RUT 500 + NaBu 1	52.71	51.05 to 54.36	**	<0.0001
Control vs. RUT 500 + NaBu 2.5	41.57	39.92 to 43.22	**	<0.0001
Control vs. RUT 500 + NaBu 5	45.76	44.11 to 47.42	**	<0.0001
Control vs. RUT 500 + NaBu 10	48.41	46.76 to 50.06	**	<0.0001
Control vs. RUT 750 + NaBu 1	72.06	70.41 to 73.72	**	<0.0001
Control vs. RUT 750 + NaBu 2.5	61.67	60.01 to 63.32	**	<0.0001
Control vs. RUT 750 + NaBu 5	63.47	61.82 to 65.13	**	<0.0001
Control vs. RUT 750 + NaBu 10	66.97	65.32 to 68.62	**	<0.0001
HUVEC				
Control vs. RUT 500	2.102	−0.1289 to 4.333	ns	0.0699
Control vs. RUT 750	7.892	5.662 to 10.12	**	<0.0001
Control vs. NaBu 1	2.965	0.7339 to 5.196	*	0.0066
Control vs. NaBu 2.5	5.916	3.685 to 8.147	**	<0.0001
Control vs. RUT 500 + NaBu 1	7.809	5.578 to 10.04	**	<0.0001
Control vs. RUT 500 + NaBu 2.5	11.61	9.384 to 13.85	**	<0.0001
Control vs. RUT 750 + NaBu 1	8.273	6.042 to 10.50	**	<0.0001
Control vs. RUT 750 + NaBu 2.5	13.65	11.42 to 15.88	**	<0.0001

CI: confidence intervals, ns: no significance.

Table 3. The RUT and NaBu interaction in PC-3 cells was determined by CI values for 24 h.

RUT	500 μM	750 μM
CI at 1 mM Nabu	0.39	0.28
CI at 2.5 mM Nabu	0.74	0.46
CI at 5 mM Nabu	0.82	0.51
CI at 10 mM Nabu	1.13	0.59

CI: Combination index, CI < 1 Synergism; CI = 1 Additive Effect; CI > 1 Antagonism.

Table 4. The combined treatment of RUT and NaBu was analyzed by dose reduction index (DRI) values for 24 h in PC-3 cells.

RUT	500 μM		750 μM	
	NaBu	RUT	NaBu	RUT
DRI at 1 mM Nabu	16.35	3.01	50.12	3.70
DRI at 2.5 mM Nabu	3.55	2.15	10.83	2.64
DRI at 5 mM Nabu	2.35	2.51	6.08	2.82
DRI at 10 mM Nabu	1.31	2.67	3.64	3.11

DRI: Dose reduction index; DRI < 1: not favorable dose reduction; DRI = 1: no-dose reduction; DRI > 1: favorable dose reduction.

3.3. The Effect of Combined the Treatment of RUT with NaBu on Cell and Nucleus Morphology in PC-3 Cells

The combined effects of RUT and NaBu on cell and nuclear morphology in PC-3 cells were evaluated using AO and DAPI staining (Figure 3). Following treatment with RUT and NaBu combinations, apoptotic morphological changes, including a rounded cell shape, membrane blebbing, and cell shrinkage, were observed in PC-3 cells (Figure 3a). Among the treatments, the combination of 750 μM RUT + 1 mM NaBu was the most effective in inducing apoptotic cell morphology (Figure 3b, Table 6, $p < 0.001$). To further

assess apoptotic cell death, the nuclear morphology of PC-3 cells was examined using DAPI staining (Figure 3a). The results revealed irregular nuclear shapes and nuclear condensation in PC-3 cells treated with RUT and NaBu combinations, particularly with the 750 μM RUT + 1 mM NaBu treatment (Figure 3b, Table 6, $p < 0.001$). These findings align with the ELISA and ROS analysis results, supporting the role of RUT and NaBu combinations in inducing apoptosis in PC-3 cells.

Table 5. The statistical analysis results of ANXA5 V ELISA and ROS generation in PC-3 cells after the combination treatment of RUT with NaBu. A two-way ANOVA analysis with Tukey's multiple comparisons test was used for multiple comparisons. Statistical significance is denoted as * $p < 0.05$ and ** $p < 0.001$.

	Mean Difference	95% CI of Difference	Summary	Adjusted *p* Value
ANXA5 ELISA				
Control vs. 1 mM NaBu	0.8962	0.002110 to 1.790	*	0.0493
Control vs. 2.5 mM NaBu	2.914	2.020 to 3.808	**	<0.0001
Control vs. 500 mM RUT	1.628	0.7340 to 2.522	*	0.0003
Control vs. 750 mM RUT	2.619	1.725 to 3.513	**	<0.0001
Control vs. RUT 500 + NaBu 1	2.696	1.802 to 3.590	**	<0.0001
Control vs. RUT 500 + NaBu 2.5	3.914	3.020 to 4.808	**	<0.0001
Control vs. RUT 750 + NaBu 1	5.678	4.784 to 6.572	**	<0.0001
Control vs. RUT 750 + NaBu 2.5	4.619	3.725 to 5.513	**	<0.0001
ROS				
Control vs. 1 mM NaBu	86.00	82.13 to 89.87	**	<0.0001
Control vs. 2.5 mM NaBu	67.50	63.63 to 71.37	**	<0.0001
Control vs. 500 mM RUT	76.50	72.63 to 80.37	**	<0.0001
Control vs. 750 mM RUT	66.50	62.63 to 70.37	**	<0.0001
Control vs. RUT 500 + NaBu 1	58.00	54.13 to 61.87	**	<0.0001
Control vs. RUT 500 + NaBu 2.5	46.50	42.63 to 50.37	**	<0.0001
Control vs. RUT 750 + NaBu 1	29.50	25.63 to 33.37	**	<0.0001
Control vs. RUT 750 + NaBu 2.5	36.50	32.63 to 40.37	**	<0.0001

CI: confidence intervals, ns: no significance.

Table 6. The statistical analysis results of AO and DAPI staining in PC-3 cells after the combination treatment of RUT with NaBu. A two-way ANOVA analysis with Dunnett's multiple comparisons test was used for multiple comparisons. Statistical significance is denoted as ** $p < 0.001$.

RUT (μM) + NaBu (mM)	Mean Difference	95% CI of Difference	Summary	Adjusted *p* Value
AO staining cells				
Control vs. RUT 500 + NaBu 1	49.80	49.02 to 50.58	**	<0.0001
Control vs. RUT 500 + NaBu 2.5	35.80	35.02 to 36.58	**	<0.0001
Control vs. RUT 750 + NaBu 1	74.70	73.92 to 75.48	**	<0.0001
Control vs. RUT 750 + NaBu 2.5	15.90	15.12 to 16.68	**	<0.0001
DAPI staining cells				
Control vs. RUT 500 + NaBu 1	44.80	44.02 to 45.58	**	<0.0001
Control vs. RUT 500 + NaBu 2.5	38.80	38.02 to 39.58	**	<0.0001
Control vs. RUT 750 + NaBu 1	64.70	63.92 to 65.48	**	<0.0001
Control vs. RUT 750 + NaBu 2.5	25.90	25.12 to 26.68	**	<0.0001

CI: confidence intervals.

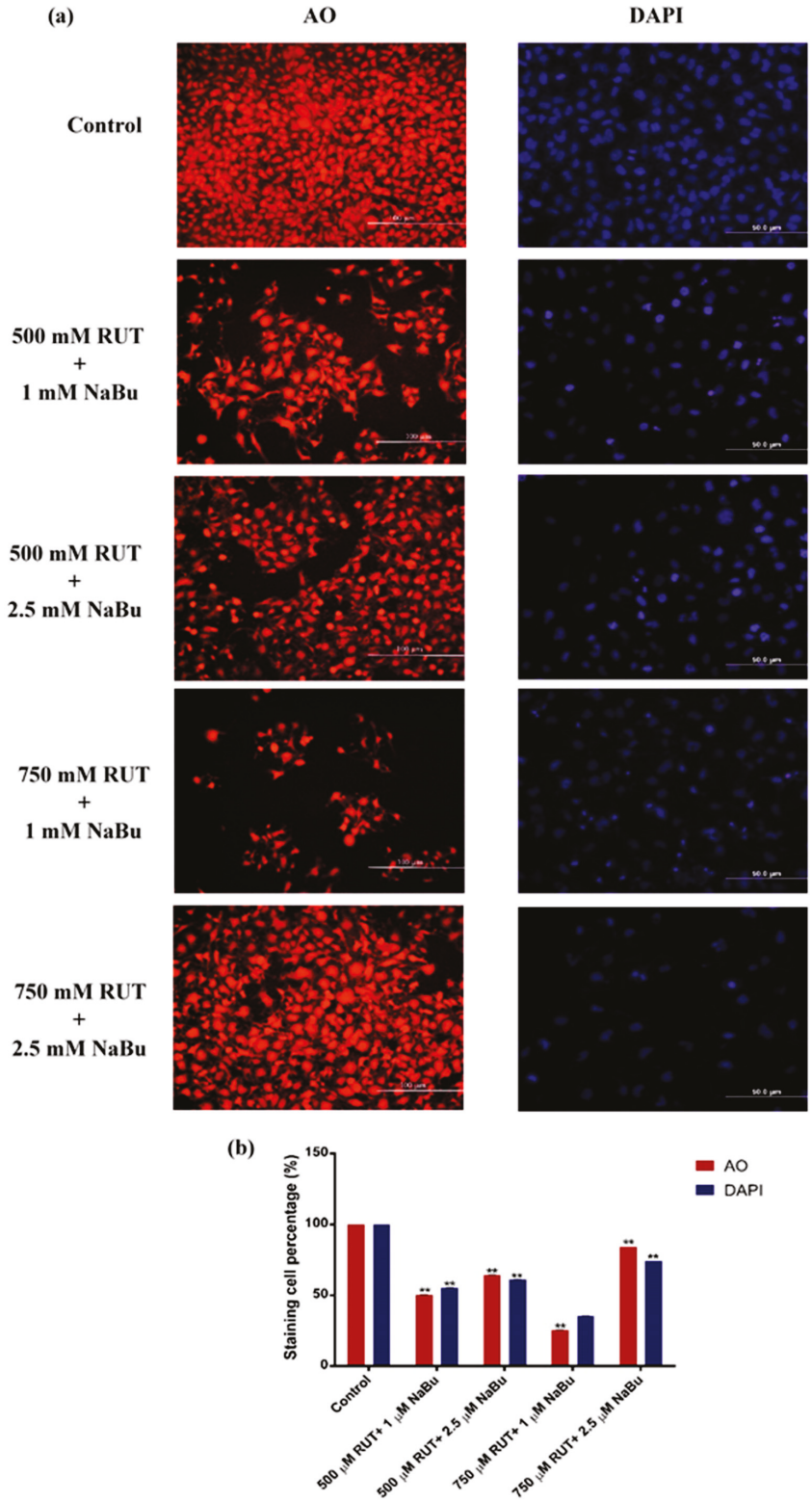

Figure 3. The effect of the combination treatment of RUT and NaBu on cell morphology and nuclear integrity. (**a**) PC-3 cells were treated with RUT (500 and 750 μM) in combination with NaBu (1 and 2.5 mM) for 48 h. Acridine orange (AO) staining was used to visualize cellular morphology, and 4′,6-diamidino-2-phenylindole (DAPI) staining was used to observe nuclear morphology. Fluorescence microscopy images were captured at 20× magnification for AO staining and 40× magnification for DAPI staining. Scale bar = 100 and 50 μm, respectively. (**b**) A quantitative analysis of AO and DAPI-positive cells is shown as a percentage. Data are presented as the mean ± SD (n = 3). ** $p < 0.001$ compared to control.

3.4. The Effect of the Combined Treatment of RUT with NaBu on mRNA Expression Levels

To evaluate the apoptotic potential of the RUT and NaBu combination treatment, the relative mRNA expression levels of *Bax* (pro-apoptotic), *Bcl-2* (anti-apoptotic), and *SOD* (antioxidant) were quantified using RT-PCR and normalized to the control group. (Figure 4). The combination treatment of 750 μM RUT + 1 mM NaBu for 48 h resulted in a significant increase in the relative expression levels of *Bax* and *SOD*, with 7.4- and 2.8-fold increases, respectively. Conversely, the mRNA expression level of *Bcl-2* was reduced by 0.7-fold (Figure 4, Table 7, $p < 0.01$). A significant upregulation of *Bax* mRNA expression was observed, particularly in the combination treatment of 750 μM RUT and 2.5 mM NaBu, suggesting a synergistic pro-apoptotic effect. No significant upregulation of *Bcl-2* was noted, while *SOD* showed moderate changes under some conditions. These findings indicate that the 750 μM RUT + 1 mM NaBu combination treatment exhibits a greater potency and synergistic cytotoxicity against metastatic prostate cancer cells.

Table 7. The statistical analysis results of a RT-PCR analysis in PC-3 cells after combination treatment of RUT with NaBu. A two-way ANOVA analysis with Tukey's multiple comparisons test was used for multiple comparisons. Statistical significance is denoted as * $p < 0.05$ and ** $p < 0.001$.

	Mean Difference	95% CI of Difference	Summary	Adjusted *p* Value
Bax				
Control vs. 1 mM NaBu	−0.2500	−0.7507 to 0.2507	ns	0.6124
Control vs. 2.5 mM NaBu	−0.7500	−1.251 to −0.2493	*	0.0016
Control vs. 500 mM RUT	−0.1500	−0.6507 to 0.3507	ns	0.9431
Control vs. 750 mM RUT	−0.4500	−0.9507 to 0.05066	ns	0.0925
Control vs. RUT 500 + NaBu 1	−1.870	−2.371 to −1.369	**	<0.0001
Control vs. RUT 500 + NaBu 2.5	−0.1650	−0.6657 to 0.3357	ns	0.9109
Control vs. RUT 750 + NaBu 1	−6.480	−6.981 to −5.979	**	<0.0001
Control vs. RUT 750 + NaBu 2.5	−0.5450	−1.046 to −0.04434	*	0.0283
Bcl-2				
Control vs. 1 mM NaBu	0.05000	−0.4507 to 0.5507	ns	0.9996
Control vs. 2.5 mM NaBu	0.3750	−0.1257 to 0.8757	ns	0.2108
Control vs. 500 mM RUT	0.1300	−0.3707 to 0.6307	ns	0.9730
Control vs. 750 mM RUT	0.2750	−0.2257 to 0.7757	ns	0.5142
Control vs. RUT 500 + NaBu 1	0.4950	−0.005658 to 0.9957	ns	0.0537
Control vs. RUT 500 + NaBu 2.5	0.3850	−0.1157 to 0.8857	ns	0.1901
Control vs. RUT 750 + NaBu 1	0.2600	−0.2407 to 0.7607	ns	0.5725
Control vs. RUT 750 + NaBu 2.5	0.2700	−0.2307 to 0.7707	ns	0.5334
SOD				
Control vs. 1 mM NaBu	−0.5500	−1.051 to −0.04934	*	0.0265
Control vs. 2.5 mM NaBu	−0.7500	−1.251 to −0.2493	*	0.0016
Control vs. 500 mM RUT	−0.4500	−0.9507 to 0.05066	ns	0.0925
Control vs. 750 mM RUT	−0.6500	−1.151 to −0.1493	*	0.0067
Control vs. RUT 500 + NaBu 1	−0.4450	−0.9457 to 0.05566	ns	0.0980
Control vs. RUT 500 + NaBu 2.5	−0.4700	−0.9707 to 0.03066	ns	0.0729
Control vs. RUT 750 + NaBu 1	−1.795	−2.296 to −1.294	**	<0.0001
Control vs. RUT 750 + NaBu 2.5	−1.460	−1.961 to −0.9593	**	<0.0001

CI: confidence intervals; ns: no significance.

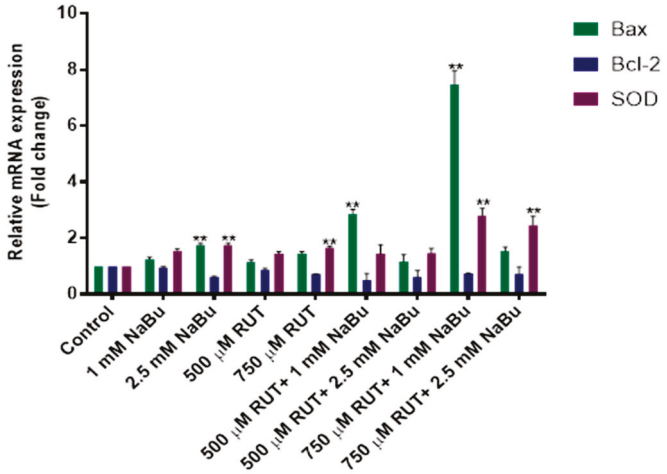

Figure 4. The effect of the combination treatment of RUT and NaBu on *Bax*, *Bcl-2*, and *SOD* mRNA expression in PC-3 cells. PC-3 cells were treated with RUT (500 μM and 750 μM) and NaBu (1 mM and 2.5 mM), either individually or in combination, for 48 h. The relative mRNA expression levels of *Bax*, *Bcl-2*, and *SOD* were quantified using RT-PCR and normalized to the control group. Data are presented as fold changes (mean ± SD). Statistical significance is denoted by ** $p \leq 0.05$.

4. Discussion

This study revealed that the combination therapy of RUT and NaBu had a significantly stronger inhibitory effect on PC-3 cells compared to their separate administrations, primarily by inducing apoptosis. Moreover, the combined treatment increased cellular ROS levels more effectively than either RUT or NaBu alone. The synergistic effect observed in this combination therapy not only enhanced its therapeutic efficacy but also reduced the systemic toxicity associated with NaBu. This highlights the potential of RUT and NaBu combination therapy as a potent and synergistic approach to cytotoxicity in mCRPC cells.

The use of natural plant extracts and flavonoids has demonstrated great potential in addressing various health challenges [10,11]. Among bioflavonoids, RUT is one of the most extensively studied, with significant contributions to inhibiting various types of cancers [12,16]. In this investigation, RUT was shown to dramatically reduce the viability of PC-3 cells, consistent with findings from Satari et al. [16], who reported the anti-proliferative effects of RUT on PC-3 cells. Although there is no prior research on the combined effects of RUT and NaBu, studies involving RUT in combination with other chemotherapeutic agents have shown highly effective results in various cancer cells [17,18]. In this study, the interaction of RUT and NaBu demonstrated a synergistic effect with a combination index (CI) as low as 0.28, which is even lower than the CI of 0.33 reported by Satari et al. [12] for the combination of RUT and 5-FU in PC-3 cells. In a recent study, we investigated the combined cytotoxic effects of sodium butyrate (NaBu) and the flavonoid quercetin on MCF-7 breast cancer cells and a synergistic interaction between NaBu and quercetin was observed, resulting in enhanced cytotoxicity compared to individual treatments [19]. These findings suggest that combining NaBu with quercetin could be a promising therapeutic strategy for targeting MCF-7 cells. Similar to our previous study, the results of this study also indicate that the combination of RUT and NaBu not only reduced NaBu's systemic toxicity but also retained its therapeutic efficacy.

The synergistic interactions between flavonoids and various drugs are mediated by multiple molecular mechanisms, such as enzyme inhibition, the modulation of drug efflux pumps, induction of apoptosis, and anti-inflammatory as well as antioxidant activities [20–23]. These mechanisms underscore the therapeutic potential of flavonoid–drug combinations. For instance, certain flavonoid mixtures demonstrate significant synergistic effects on α-glucosidase inhibition, a key enzyme in carbohydrate metabolism, through

the formation of hydrophobic interactions and hydrogen bonds with its active sites [20]. Additionally, taxifolin has been found to inhibit the overexpression of P-glycoprotein, a drug efflux protein, thereby preventing chemoresistance by blocking the action of rhodamine 123 and doxorubicin [21]. The co-administration of flavonoids with paclitaxel has also been shown to enhance the efficacy of chemotherapy by inducing apoptosis in cancer cells [22]. Furthermore, the combination of total saponins and flavonoids has displayed synergistic effects in reducing inflammation and myocardial cell apoptosis [23]. Although direct studies on the combined effects of NaBu and RUT are limited, research on similar compounds suggests potential synergistic mechanisms and the obtained data also suggested that NaBu and RUT synergistically increased apoptosis for the first time. However, further studies are required to clarify the specific interactions between NaBu and RUT, especially the downstream signaling cascades that control apoptosis.

Apoptosis is a crucial genetic process that ensures growth and cellular equilibrium. Cancer cells, however, evade apoptosis through mechanisms such as angiogenesis, uncontrolled proliferation, and the suppression of the intrinsic apoptotic pathway [24,25]. The primary function of apoptosis is to prevent cancer [26]. Cancer cells can inhibit apoptosis in various ways, such as blocking caspase activation or preventing the initiation of apoptosis. The overexpression of anti-apoptotic *Bcl-2* proteins and/or inactivation of pro-apoptotic proteins such as *Bax* or *Bak* are common mechanisms of evasion. While Bcl-2 is not classified as an oncogene, its altered expression contributes to malignancy development. An overexpression of Bcl-2 has been observed in more than 50% of cancer cases, regardless of subtype [27]. The findings of this study are consistent with those of Satari et al. [12], who reported that RUT, when combined with 5-FU, reduced Bcl-2 protein levels in prostate cancer cells. Similarly, Taylor et al. [27] found that NaBu, either alone or in combination with quercetin, significantly reduced cell growth or increased apoptosis by activating the pro-apoptotic *Bax* gene in human T986 glioblastoma cells. Additionally, a study investigating the effects of Curcuminoids and sodium butyrate, both individually and in combination, on three glioblastoma cell lines revealed that their combined treatment synergistically decreased glioblastoma cell viability [28]. This effect was achieved by inducing apoptosis, causing cell cycle arrest, and modulating ROS production and gene expression [28].

Antioxidant systems, comprising both enzymatic and non-enzymatic components, play a critical role in regulating ROS levels to mitigate oxidative stress. Cells adapt by activating antioxidant enzymes such as superoxide dismutase (SOD), which neutralizes ROS and minimizes damage [29,30]. During oxidative stress, these enzymes are often upregulated to counteract potential harm. RUT has been shown in several studies to reduce lipid peroxidation and alleviate oxidative stress [12,28]. Similarly, NaBu has been reported to exhibit genotoxic and anticancer effects, partly through its modulation of antioxidant enzymes [8]. In this study, the combination of RUT and NaBu significantly upregulated *SOD* expression compared to their separate administrations, suggesting that this combination effectively enhances the cellular capacity to combat oxidative damage by neutralizing free radicals.

5. Conclusions

NaBu is often administered as a combination therapy with other chemotherapeutic drugs to reduce the required therapeutic dose, thereby minimizing its toxic properties and clinical side effects. RUT, when administered alone, has demonstrated the ability to inhibit several aberrant signaling pathways associated with apoptosis, inflammation, autophagy, and angiogenesis, employing diverse mechanisms to impede cancer progression and metastasis. Our initial findings indicate that the combination therapy of RUT and NaBu

holds considerable promise as an anticancer therapeutic approach and warrants further molecular investigation, particularly focusing on its effects on pro- and anti-apoptotic pathways. However, further research, including studies in animal models or other cell lines, is necessary to fully evaluate and optimize its potential efficacy in cancer treatment.

Author Contributions: Conceptualization, J.A., Z.B. and A.D.O.; methodology, J.A., Z.B. and A.D.O.; software, J.A.; validation, Z.B.; formal analysis, A.D.O.; investigation, J.A. and A.D.O.; resources, J.A. and Z.B.; data curation, J.A.; writing—original draft preparation, J.A., Z.B. and A.D.O.; writing—review and editing, J.A., Z.B. and A.D.O.; visualization, A.D.O.; supervision, J.A. and Z.B. All authors have read and agreed to the published version of the manuscript.

Funding: This research was funded by Kocaeli University BAP grant number [FYL-2021-2774].

Institutional Review Board Statement: Not applicable.

Informed Consent Statement: Not applicable.

Data Availability Statement: Data are contained within the article.

Conflicts of Interest: The authors declare no conflicts of interest.

Abbreviations

The following abbreviations are used in this manuscript:

RUT	Rutin
NaBu	Sodium Butyrate
PCa	Prostate Cancer
ROS	Reactive oxygen species
mCRPC	Metastatic castration-resistant prostate cancer
AR	Androgen receptors

References

1. Siegel, R.L.; Miller, K.D.; Wagle, N.S.; Jemal, A. Cancer Statistics, 2023. *CA Cancer J. Clin.* **2023**, *73*, 17–48. [CrossRef] [PubMed]
2. Schultz, N.M.; Flanders, S.C.; Wilson, S.; Brown, B.A.; Song, Y.; Yang, H.; Lechpammer, S.; Kassabian, V. Treatment Duration, Healthcare Resource Utilization, and Costs Among Chemotherapy-Naïve Patients with Metastatic Castration-Resistant Prostate Cancer Treated with Enzalutamide or Abiraterone Acetate: A Retrospective Claims Analysis. *Adv. Ther.* **2018**, *35*, 1639–1655. [CrossRef]
3. Ferro, M.; Crocetto, F.; Lucarelli, G.; Lievore, E.; Barone, B. Radiotherapy to the Primary Tumor: The First Step of a Tailored Therapy in Metastatic Prostate Cancer. *Diagnostics* **2022**, *12*, 1981. [CrossRef]
4. Tiwari, R.; Manzar, N.; Ateeq, B. Dynamics of Cellular Plasticity in Prostate Cancer Progression. *Front. Mol. Biosci.* **2020**, *7*, 130. [CrossRef] [PubMed]
5. Guney Eskiler, G.; Deveci, A.O.; Bilir, C.; Kaleli, S. Synergistic Effects of Nobiletin and Sorafenib Combination on Metastatic Prostate Cancer Cells. *Nutr. Cancer* **2019**, *71*, 1299–1312. [CrossRef] [PubMed]
6. Deveci Ozkan, A.; Guney Eskiler, G.; Kaleli, S.; Sahin, E. Immunotherapeutic Role of Cabazitaxel Treatment in the Activation of TLR3 Signalling in Metastatic Castration-Resistant Prostate Cancer in Vitro. *Mol. Biol. Rep.* **2022**, *49*, 1261–1271. [CrossRef] [PubMed]
7. Kaushik, D.; Vashistha, V.; Isharwal, S.; Sediqe, S.A.; Lin, M.-F. Histone Deacetylase Inhibitors in Castration-Resistant Prostate Cancer: Molecular Mechanism of Action and Recent Clinical Trials. *Ther. Adv. Urol.* **2015**, *7*, 388–395. [CrossRef] [PubMed]
8. Yuksel, B.; Deveci Ozkan, A.; Aydın, D.; Betts, Z. Evaluation of the Antioxidative and Genotoxic Effects of Sodium Butyrate on Breast Cancer Cells. *Saudi J. Biol. Sci.* **2022**, *29*, 1394–1401. [CrossRef] [PubMed]
9. Ruzic, D.; Djoković, N.; Srdić-Rajić, T.; Echeverria, C.; Nikolic, K.; Santibanez, J.F. Targeting Histone Deacetylases: Opportunities for Cancer Treatment and Chemoprevention. *Pharmaceutics* **2022**, *14*, 209. [CrossRef] [PubMed]
10. Imani, A.; Maleki, N.; Bohlouli, S.; Kouhsoltani, M.; Sharifi, S.; Maleki Dizaj, S. Molecular Mechanisms of Anticancer Effect of Rutin. *Phytother. Res.* **2021**, *35*, 2500–2513. [CrossRef] [PubMed]
11. Hoai, T.T.; Yen, P.T.; Dao, T.T.B.; Long, L.H.; Anh, D.X.; Minh, L.H.; Anh, B.Q.; Thuong, N.T. Evaluation of the Cytotoxic Effect of Rutin Prenanoemulsion in Lung and Colon Cancer Cell Lines. *J. Nanomater.* **2020**, *2020*, 8867669. [CrossRef]

12. Satari, A.; Ghasemi, S.; Habtemariam, S.; Asgharian, S.; Lorigooini, Z. Rutin: A Flavonoid as an Effective Sensitizer for Anticancer Therapy; Insights into Multifaceted Mechanisms and Applicability for Combination Therapy. *Evid.-Based Complement. Altern. Med.* **2021**, *2021*, 9913179. [CrossRef] [PubMed]
13. Scherbakov, A.M.; Andreeva, O.E. Apigenin Inhibits Growth of Breast Cancer Cells: The Role of ERα and HER2/Neu. *Acta Naturae* **2015**, *7*, 133–139. [CrossRef]
14. Khurana, R.K.; Jain, A.; Jain, A.; Sharma, T.; Singh, B.; Kesharwani, P. Administration of Antioxidants in Cancer: Debate of the Decade. *Drug Discov. Today* **2018**, *23*, 763–770. [CrossRef] [PubMed]
15. Walker, J.H.; Boustead, C.M.; Koster, J.J.; Bewley, M.; Waller, D.A. Annexin V, a Calcium-Dependent Phospholipid-Binding Protein. *Biochem. Soc. Trans.* **1992**, *20*, 828–833. [CrossRef] [PubMed]
16. Pandey, P.; Khan, F.; Qari, H.A.; Oves, M. Rutin (Bioflavonoid) as Cell Signaling Pathway Modulator: Prospects in Treatment and Chemoprevention. *Pharmaceuticals* **2021**, *14*, 1069. [CrossRef]
17. Guruvayoor, C.; Girija Kuttan, G.K. Antiangiogenic Effect of Rutin and Its Regulatory Effect on the Production of VEGF, IL-1β and TNF-α in Tumor Associated Macrophages. *J. Biol. Sci.* **2007**, *7*, 1511–1519. [CrossRef]
18. Ghavami, G.; Muhammadnejad, S.; Amanpour, S.; Sardari, S. Bioactivity Screening of Mulberry Leaf Extracts and Two Related Flavonoids in Combination with Cisplatin on Human Gastric Adenocarcinoma Cells. *Iran. J. Pharm. Res.* **2020**, *19*, 371–382. [CrossRef] [PubMed]
19. Betts, Z.; Deveci Ozkan, A.; Yuksel, B.; Alimudin, J.; Aydin, D.; Aksoy, O.; Yanar, S. Investigation of the combined cytotoxicity induced by sodium butyrate and a flavonoid quercetin treatment on MCF-7 breast cancer cells. *J. Toxicol. Environ. Health A* **2023**, *86*, 833–845. [CrossRef] [PubMed]
20. Pan, J.; Nawaz, M.; Liu, J.; Liu, H.; Lv, Z.; Yang, W.; Jiao, Z.; Zhang, Q. Exploring synergistic inhibitory mechanisms of flavonoid mixtures on α-glucosidase by experimental analysis and molecular dynamics simulation. *Food Chem.* **2025**, *464*, 141560. [CrossRef] [PubMed]
21. Das, A.; Baidya, R.; Chakraborty, T.; Samanta, A.K.; Roy, S. Pharmacological basis and new insights of taxifolin: A comprehensive review. *Biomed. Pharmacother.* **2021**, *142*, 112004. [CrossRef]
22. Asnaashari, S.; Amjad, E.; Sokouti, B. Synergistic effects of flavonoids and paclitaxel in cancer treatment: A systematic review. *Cancer Cell Int.* **2023**, *23*, 211. [CrossRef]
23. Fang, M.; Meng, Y.; Du, Z.; Guo, M.; Jiang, Y.; Tu, P.; Hua, K.; Lu, Y.; Guo, X. The Synergistic Mechanism of Total Saponins and Flavonoids in Notoginseng–Safflower against Myocardial Infarction Using a Comprehensive Metabolomics Strategy. *Molecules* **2022**, *27*, 8860. [CrossRef] [PubMed]
24. Xu, W.; Jing, L.; Wang, Q.; Lin, C.-C.; Chen, X.; Diao, J.; Liu, Y.; Sun, X. Bax-PGAM5L-Drp1 Complex Is Required for Intrinsic Apoptosis Execution. *Oncotarget* **2015**, *6*, 30017–30034. [CrossRef]
25. Arbiser, J.L.; Bonner, M.Y.; Gilbert, L.C. Targeting the Duality of Cancer. *NPJ Precis. Oncol.* **2017**, *1*, 23. [CrossRef]
26. Pfeffer, C.; Singh, A. Apoptosis: A Target for Anticancer Therapy. *Int. J. Mol. Sci.* **2018**, *19*, 448. [CrossRef]
27. Taylor, M.A.; Khathayer, F.; Ray, S.K. Quercetin and Sodium Butyrate Synergistically Increase Apoptosis in Rat C6 and Human T98G Glioblastoma Cells Through Inhibition of Autophagy. *Neurochem. Res.* **2019**, *44*, 1715–1725. [CrossRef]
28. Majchrzak-Celińska, A.; Kleszcz, R.; Stasiłowicz-Krzemień, A.; Cielecka-Piontek, J. Sodium Butyrate Enhances Curcuminoids Permeability through the Blood-Brain Barrier, Restores Wnt/β-Catenin Pathway Antagonists Gene Expression and Reduces the Viability of Glioblastoma Cells. *Int. J. Mol. Sci.* **2021**, *22*, 11285. [CrossRef]
29. Lou, J.; Qualls, M.L.; Hudson, M.M.; McBee, D.P.; Baccile, J.A.; Best, M.D. Reactive Oxygen Species (ROS) Activated Liposomal Cell Delivery Using a Boronate-Caged Guanidine Lipid. *Chem. A Eur. J.* **2022**, *28*, e202201057. [CrossRef] [PubMed]
30. Wang, G.S.; Hoyte, C. Review of Biguanide (Metformin) Toxicity. *J. Intensive Care Med.* **2019**, *34*, 863–876. [CrossRef]

Disclaimer/Publisher's Note: The statements, opinions and data contained in all publications are solely those of the individual author(s) and contributor(s) and not of MDPI and/or the editor(s). MDPI and/or the editor(s) disclaim responsibility for any injury to people or property resulting from any ideas, methods, instructions or products referred to in the content.

biomedicines

MDPI

Article

Therapeutic Target Discovery for Multiple Myeloma: Identifying Druggable Genes via Mendelian Randomization

Shijun Jiang, Fengjuan Fan, Qun Li, Liping Zuo, Aoshuang Xu and Chunyan Sun *

Institute of Hematology, Union Hospital, Tongji Medical College, Huazhong University of Science and Technology, Wuhan 430022, China; guazhoudu123@sina.com (S.J.); kittyfan0120@163.com (F.F.); liqun97@126.com (Q.L.); zuo5258@126.com (L.Z.); xas_medicine@163.com (A.X.)
* Correspondence: suncy0618@163.com

Abstract: Background: Multiple myeloma (MM) is a hematological malignancy originating from the plasma cells present in the bone marrow. Despite significant therapeutic advancements, relapse and drug resistance remain major clinical challenges, highlighting the urgent need for novel therapeutic targets. **Methods**: To identify potential druggable genes associated with MM, we performed Mendelian randomization (MR) analysis. Causal candidates were further validated using a single-tissue transcriptome-wide association study (TWAS), and colocalization analysis was conducted to assess shared genetic signals between gene expression and disease risk. Potential off-target effects were assessed through an MR phenome-wide association study (MR-PheWAS). Additionally, molecular docking and functional assays were used to evaluate candidate drug efficacy. **Results**: The MR analysis identified nine druggable genes (FDR < 0.05), among which Orosomucoid 1 (*ORM1*) and Oviductal Glycoprotein 1 (*OVGP1*) were supported by both TWAS and colocalization evidence (PPH4 > 0.75). Experimental validation demonstrated the significant downregulation of ORM1 and OVGP1 in MM cells ($p < 0.05$). Pregnenolone and irinotecan, identified as agonists of ORM1 and OVGP1, respectively, significantly inhibited MM cell viability, while upregulating their expression ($p < 0.05$). **Conclusions**: Our study highlights ORM1 and OVGP1 as novel therapeutic targets for MM. The efficacy of pregnenolone and irinotecan in suppressing MM cell growth suggests their potential for clinical application. These findings provide insights into MM pathogenesis and offer a promising strategy for overcoming drug resistance.

Keywords: multiple myeloma; mendelian randomization; *ORM1*; *OVGP1*; pregnanolone; irinotecan

1. Introduction

Multiple myeloma (MM) is a blood cancer characterized by the unchecked expansion of plasma cells in the bone marrow. Plasma cells, a subset of B lymphocytes responsible for antibody production, undergo malignant transformation in MM, leading to uncontrolled proliferation and the secretion of abnormal monoclonal immunoglobulins (M-proteins). This aberrant cell growth disrupts normal hematopoiesis, causing clinical symptoms such as anemia, recurrent infections, bone fragility, fractures, and renal dysfunction. MM accounts for approximately 1% of all cancers and approximately 10% of blood cancers globally. Recent estimates indicate that the global incidence of MM is 2.1 per 100,000 individuals annually, with a mortality rate of 1.2 per 100,000 [1]. The condition predominantly impacts elderly individuals, with a median age of diagnosis of 69 years, and is slightly more common in males.

The etiology of MM remains incompletely understood, but accumulating evidence suggests that genetic predisposition, chronic inflammation, and environmental exposures are major contributing factors [2–4]. Genome-wide association studies (GWASs) have identified multiple susceptibility loci associated with MM risk, including variants of TULK4, ATG5, and WAC [5]. Notably, mutations in KRAS, NRAS, TP53, and MYC are frequently observed in MM, playing key roles in disease progression [6]. Additionally, chromosomal translocations involving the IGH loci—such as t(4;14), t(11;14), and t(14;16)—have been implicated in MM pathogenesis [7]. The bone marrow microenvironment is crucial in MM progression, providing survival signals through cytokines (e.g., IL-6, TNF-α, TGF-β, etc.), adhesion molecules, and extracellular matrix interactions [8–10]. MM cells frequently exploit these interactions to evade immune surveillance and resist apoptosis [11]. The dysregulation of several key signaling pathways, including RAS/MAPK, NF-κB, JAK/STAT, and PI3K/AKT/mTOR, further contributes to tumor growth and drug resistance [12].

Despite significant therapeutic advances, MM remains an incurable disease. The introduction of proteasome inhibitors (e.g., bortezomib, carfilzomib), immunomodulatory drugs (e.g., lenalidomide, pomalidomide), and monoclonal antibodies (e.g., daratumumab, elotuzumab) has substantially improved patient outcomes [13]. However, most patients eventually experience relapse or develop resistance to treatment, necessitating the development of novel therapeutic strategies [14]. Several mechanisms contribute to drug resistance in MM, including clonal evolution, epigenetic modifications, and alterations in drug metabolism pathways [15,16]. For instance, mutations in proteasome subunits (PSMB5) reduce bortezomib sensitivity, while the upregulation of anti-apoptotic proteins (BCL2, MCL1, etc.) enhances survival signaling [17,18]. The recent emergence of chimeric antigen receptor (CAR)-T cell therapy, bispecific T cell engagers (BiTEs), and antibody–drug conjugates (ADCs) has provided promising alternatives [19]. However, these therapies are expensive and are associated with significant immune-related toxicities, highlighting the need for novel, cost-effective druggable targets.

Targeting druggable genes is a promising strategy for overcoming drug resistance and improving treatment outcomes [20]. For example, B Cell Lymphoma 2 (BCL2) inhibitors such as venetoclax have shown efficacy in patients with t(11;14) translocations, providing a personalized treatment approach. Additionally, inhibitors targeting the MEK/ERK and JAK/STAT pathways have demonstrated potential in preclinical and early clinical studies, underscoring their relevance to the pathophysiology of MM.

Mendelian randomization (MR) has emerged as a powerful approach for investigating causal relationships between genetic variants and disease outcomes. This method utilizes genetic variants, such as instrumental variables (IVs), to infer causality, while minimizing the impact of confounding factors and reverse causation, thereby mimicking a randomized controlled trial (RCT) at the genetic level [21]. Since genetic variants are randomly assigned at conception according to Mendel's laws, their associations with disease risk factors are generally less influenced by environmental or behavioral factors. MR has been widely applied in epidemiological and genetic studies to uncover the causal links between risk factors and disease outcomes. For example, MR has provided evidence that high-density lipoprotein cholesterol (HDL-C) is not causally protective against coronary artery disease, challenging prior observational findings [22]. Furthermore, MR has been instrumental in evaluating the causal effects of lifestyle factors, such as smoking and alcohol consumption, on various health outcomes, thereby informing public health policies and intervention strategies [23].

A specialized application of MR, drug target Mendelian randomization (DTMR), integrates genome-wide association study (GWAS) data with genetic variants located in druggable genes to infer potential therapeutic targets. DTMR is particularly valuable in

oncology, where it enables the identification of genes that not only contribute to disease risk, but also represent viable intervention points for drug development [24,25]. For instance, Wang et al. employed a proteome-wide MR analysis to integrate plasma proteomic data with GWAS data, identifying 13 proteins causally associated with MM risk, including nicotinamide phosphoribosyl transferase (NAMPT) and suppressor of cytokine signaling 3 (SOCS3) [26]. This approach has been applied to study key regulatory pathways in diseases, including bone marrow microenvironment interactions, immune modulation, and cell signaling networks, thereby accelerating drug discovery and facilitating clinical translation [27,28]. Given the complex pathophysiology of MM, which involves dynamic interactions between malignant plasma cells and the bone marrow microenvironment, DTMR provides a robust strategy to prioritize genes for targeted therapy.

In this study, we employed MR-based approaches to identify and validate novel druggable targets for MM. By integrating GWAS data, colocalization analysis, and experimental validation, we aimed to identify new druggable genes causally associated with MM risk, validate these targets through colocalization analysis and in vitro experiments, assess potential off-target effects using an MR phenome-wide association study (MR-PheWAS), and evaluate the therapeutic potential of candidate drugs through molecular docking and functional assays. Our findings provide new insights into MM pathogenesis and may facilitate the development of targeted therapies aimed at overcoming drug resistance and improving patient outcomes.

2. Materials and Methods

2.1. Study Design

The STROBE-MR checklist was completed to ensure the integrity of this observational MR study (Supplementary Table S1) [29]. This study integrated both previously established methodologies and newly implemented approaches to investigate the causal relationship between druggable gene expression and MM susceptibility and progression. The workflow consisted of five key steps:

Two-sample Mendelian randomization (MR) was used to assess causality between cis-eQTL-associated druggable genes and MM susceptibility. This method has been widely used in genetic epidemiology, and follows established procedures [30].

To further assess whether these genes contribute to MM susceptibility via gene expression regulation, we performed a single-tissue transcriptome-wide association study (TWAS). A TWAS investigates the impact of gene expression on disease risk in a tissue-specific manner by utilizing expression prediction models generated from large-scale transcriptomic resources such as GTEx, eQTLGen, and DGN [31,32].

Bayesian colocalization analysis was conducted to confirm whether shared genetic variants influence both gene expression and MM risk. This study followed standard colocalization approaches, but the choice of PPH4 > 0.75 as a threshold was specifically optimized for MM [33].

A Mendelian randomization phenome-wide association study (MR-PheWAS) was employed to systematically explore the potential off-target effects of ORM1 and OVGP1 modulation (a novel addition to this research pipeline to evaluate safety risks across multiple traits).

In silico molecular docking analysis and in vitro validation:

Computational molecular docking was used to predict candidate small-molecule agonists for ORM1 and OVGP1, a method commonly used in drug discovery. However, the selection of compounds from DSigDB, rather than a general compound library, is a novel approach tailored to MM drug repurposing [34,35].

In vitro functional assays (qRT-PCR, Western blot, CCK-8, etc.) were performed to validate the efficacy of the identified small-molecule agonists, following standardized experimental procedures, but extending their application to ORM1 and OVGP1 in MM cells.

This integrative framework combines existing methodologies with novel analytical pipelines, particularly the combined use of MR-PheWAS and molecular docking in MM drug target discovery, thus advancing the field of genetics-driven target identification (Figure 1).

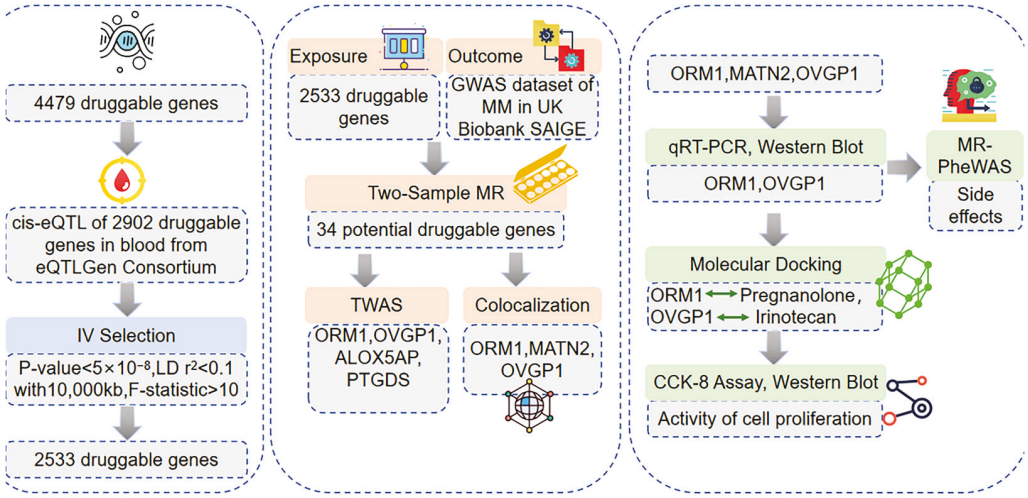

Figure 1. A diagram illustrating the design of our study.

2.2. Antibodies and Reagents

The marker used was the WJ103 model from Yamei, China. The antibodies used for Western blotting were ORM1 (16439-1-AP, Proteintech, Wuhan, China, 1:1000), MATN2 (24064-1-AP, Proteintech, Wuhan, China, 1:1000), OVGP1 (22324-1-AP, Proteintech, China, 1:1000), and GAPDH (10494-1-AP, Proteintech, Wuhan, China, 1:10,000). The secondary antibody used was horseradish peroxidase (HRP)-conjugated goat anti-rabbit antibody (ANT020; Antgen, Wuhan, China; 1:10,000). All the antibodies were diluted in Tris-buffered saline with Tween, supplemented with either 5% skim milk or bovine serum albumin, according to the manufacturer's instructions.

Pregnanolone (MedChemExpress, catalog: HY-B0151, Shanghai, China) and irinotecan (MedChemExpress, catalog: HY-16562, Shanghai, China) were used. All drugs were dissolved in dimethyl sulfoxide (DMSO) and stored at −20 °C in the dark.

The primers for the real-time qPCR targeting of ORM1, MATN2, OVGP1, and GAPDH were purchased from Beijing Qingke Biotechnology Co., Ltd., Beijing China. The primer sequences are provided in Table 1.

Table 1. Sequences of primers for ORM1, MATN2, OVGP1, and GAPDH.

Gene	Forward (5′–3′)	Reverse (5′–3′)
ORM1	ACCTACATGCTTGCTTTTGACG	CCCCCAAGTCTCTGTCCTGA
MATN2	GTGTCAACACCCATGACTATGC	CATCAGGACCAATGTCCAAG
OVGP1	AGCGAAGAAGCACTGGATTGA	ATTCACAGCAGATGACAGCCA
GAPDH	GAAGGTGAAGGTCGGAGTC	GAAGATGGTGATGGGATTTC

2.3. Exposure Data

Finan et al. identified 4479 druggable genes in total, which were categorized into three tiers according to their relevance in therapeutic development. Tier 1, which includes

1427 genes, consists of targets for licensed small molecules and biological therapies, as well as those currently in clinical development. Tier 2, consisting of 682 genes, represents those encoding proteins that bind to bioactive small molecules or share substantial sequence similarity with existing drug targets. Tier 3, with 2370 genes, encompasses genes responsible for extracellular or secreted proteins of major druggable families, such as G-protein-coupled receptors (GPCRs), ion channels, kinases, and nuclear hormone receptors, which are not part of the first two tiers [36]. Among these genes, 2902 are linked to the cis-eQTL data from the eQTLGen Consortium, which integrates genomic information from 37 datasets encompassing 31,684 individuals of European descent. These cis-eQTL data underscore the connection between gene expression levels and genetic variants within a 1 Mb region surrounding the gene, with a focus on variants having a minor allele frequency (MAF) greater than 0.01 [37]. These findings provide a comprehensive framework for understanding the therapeutic potential of druggable genes (Supplementary Table S2).

2.4. Instrumental Variable (IV) Selection

The cis-eQTLs associated with potential druggable genes from the eQTLGen database were selected as IVs for MR analysis [38,39]. To guarantee the reliability and robustness of these IVs, a set of rigorous criteria was applied:

2.4.1. Statistical Significance ($p < 5 \times 10^{-8}$)

A genome-wide significance threshold was set at $p < 5 \times 10^{-8}$, which is commonly used in GWAS and eQTL studies to minimize false-positive associations [40]. This threshold ensures that only high-confidence eQTLs are included, reducing the influence of weak genetic instruments.

2.4.2. Linkage Disequilibrium (LD) Clumping ($r^2 < 0.1$; Window Size = 10,000 kb)

To maintain independence among IVs, we applied LD clumping using a reference panel from the 1000 Genomes European population. An $r^2 < 0.1$ threshold ensured that the selected SNPs were not in high LD, minimizing collinearity and bias in MR estimates. The 10,000 kb window was chosen to prioritize variants with the strongest cis-regulatory effects on the target gene, while avoiding distant trans-eQTLs.

2.4.3. Instrument Strength (F-Statistic > 10)

The F-statistic was used to quantify instrument strength, ensuring that weak instruments did not bias MR estimates. According to Staiger and Stock's rule of thumb, an F-statistic > 10 is necessary to minimize weak instrument bias in MR studies [41]. The F-statistic is computed using the following formula:

$$F = \frac{R^2}{(1 - R^2)} \times \frac{(N - k - 1)}{k}.$$

where R^2 represents the proportion of variance explained by the IV, N is the sample size, and k is the number of instruments.

2.4.4. Software and Filtering Parameters

PLINK (version 1.9) was used for LD pruning and variant filtering.

By applying the aforementioned criteria, a high-quality set of IVs was selected for MR analysis to investigate the causal link between druggable gene expression and the risk of MM.

2.5. Outcome Data

The outcome data were derived from the GWAS dataset of MM in the UKB Scalable and Accurate Implementation of Generalized Mixed Model (SAIGE) database for association analysis. The UKB-SAIGE database, one of the largest health and genetic databases in the world, includes detailed health and genetic information of approximately 500,000 participants in the UK, facilitating extensive genetic research on complex diseases [42].

In this study, data from 552 patients with MM and 404,466 controls were utilized. The SAIGE model efficiently handles large-scale data, also accounting for genetic correlations, sex, birth year, and principal components for population stratification [43]. This model is particularly effective in the case of rare diseases, reducing false positives and improving the detection of rare variants.

2.6. Two-Sample Mendelian Randomization Analysis (Two-Sample MR)

MR analysis was conducted via the R package "TwoSampleMR" (version 0.5.6). For analyses involving a Single-Nucleotide Polymorphism (SNP) as the IV, the Wald ratio method was used to estimate the causal effects. For analyses involving multiple SNP IVs, five established techniques were utilized, i.e., inverse variance weighted (IVW), MR-Egger, weighted median, simple mode, and weighted mode [44]. Among these methods, the IVW approach was selected as the primary analytical tool because of its high efficiency and reliability, assuming that all SNPs function as valid IVs without horizontal pleiotropy. By integrating SNP-specific causal estimates through inverse variance weighting, the IVW method optimizes statistical power while minimizing standard errors, making it the most commonly employed technique in MR studies when the validity of instruments is ensured.

FDR corrections were performed to control for multiple testing, thereby enhancing the dependability of the significant findings. The final results were primarily based on the estimates derived from IVW, given its superior statistical robustness and precision, assuming valid instruments.

Sensitivity analyses:

Heterogeneity test (Cochran's Q-statistic): Cochran's Q test was used to assess heterogeneity among the IVs. A significant Q-statistic ($p < 0.05$) indicates potential heterogeneity in causal effects, necessitating additional tests, such as MR–Egger regression.

Directional pleiotropy test (MR–Egger intercept): MR–Egger regression was performed to evaluate the presence of directional pleiotropy, which occurs when IVs influence the outcome through pathways other than the exposure gene. A significant MR–Egger intercept ($p < 0.05$) suggests the presence of pleiotropy, in which case, weighted median MR is considered [45].

This comprehensive methodology enabled a robust causal inference for exposures and outcomes, while addressing biases and confounding factors.

2.7. Transcriptome-Wide Association Study (TWAS)

To further validate candidate causal genes for MM identified through two-sample Mendelian randomization (MR), we conducted a single-tissue TWAS using the FUSION pipeline [46]. This approach integrates GWAS summary statistics with gene expression prediction models derived from GTEx v8 whole blood data from individuals of European ancestry (GTExv8.EUR.Whole_Blood).

Cis-regulated expression was imputed within a $\pm$500 kb window around each gene using pre-trained expression weights. To accurately model linkage disequilibrium (LD) among SNPs in the cis region, we employed the 1000 Genomes Project Phase 3 European LD reference panel provided by FUSION in PLINK binary format, stratified by chromosome.

The TWAS analysis was limited to genes prioritized by two-sample MR, and statistical significance was evaluated using false discovery rate (FDR) correction. Genes with FDR-adjusted *p*-values < 0.05 were considered significantly associated with MM susceptibility.

2.8. Colocalization

The false positives resulting from LD were eliminated through the Bayesian colocalization analysis. This method evaluates whether exposure (e.g., gene expression) and outcomes (e.g., disease) are driven by the same genetic variant. This colocalization analysis led to five hypotheses:

H0. *Neither gene expression nor disease is associated with causal variants in the region*.

H1. *Only gene expression is associated with a causal variant*.

H2. *Only the disease is associated with a causal variant*.

H3. *Gene expression and disease are linked to separate causal variants*.

H4. *Gene expression and disease share a common causal variant*.

2.8.1. Single Causal Variant per Region

For this analysis, we used the "coloc" R package (version 4.0.6) [47]. The "coloc" model assumes that each genomic locus contains at most one causal variant affecting either the gene expression or disease risk. If multiple independent variants exist within the same region, this assumption may be violated, leading to misinterpretation of colocalization results.

2.8.2. Effect Sizes Are Derived from GWAS and eQTL Summary Statistics

The method assumes that effect sizes and standard errors are correctly estimated from large-scale GWAS and eQTL studies. Poorly estimated effect sizes can lead to incorrect posterior probabilities.

2.8.3. Rationale for $PPH_4 > 0.75$ Threshold

We adopted $PPH_4 > 0.75$ as the colocalization threshold based on the previous literature and statistical considerations: a threshold of 0.75–0.80 is widely used in genetic studies to define high-confidence colocalization [48,49]. PPH_4 values close to 1.0 indicate strong colocalization, while values below 0.50 suggest weak or no colocalization. This threshold balances specificity and sensitivity, ensuring that selected genes are likely causal, while minimizing false positives.

2.8.4. Visualization of Colocalization Results

Colocalization results were visualized using the "locuscomparer" R package (version 1.0.0), which generates regional association plots comparing GWAS and eQTL signals within the selected loci. These visualizations help to confirm whether the eQTL and GWAS peaks align, supporting shared genetic regulation.

2.9. Mendelian Randomization Phenome-Wide Association Study (MR-PheWAS)

An MR-PheWAS was utilized to investigate whether these genes might serve as potential therapeutic targets for various diseases. This study specifically employed cis-eQTLs of two core proteins, ORM1 and OVGP1, as exposure variables, while analyzing 1403 disease phenotypes from the UKB-SAIGE dataset as outcomes. By systematically conducting thousands of MR analyses, this approach examined the causal influence of

genetic variants across a broad spectrum of disease traits. The IVW method was employed to estimate causal relationships, with statistical significance defined as an FDR of <0.05. This robust analytical framework provides a comprehensive means to uncover novel associations between gene expression and disease phenotypes, offering critical insights into potential therapeutic targets [50,51].

This comprehensive approach allows for the identification of novel associations between gene expression and disease phenotypes, offering critical insights into potential therapeutic targets. For instance, a recent MR-PheWAS investigating the causal role of immune response to varicella zoster virus (VZV) in multiple traits identified associations with conditions such as Dupuytren disease, mononeuropathies of the upper limb, sarcoidosis, coeliac disease, and teeth problems. This study highlighted the potential of MR-PheWASs to uncover previously unrecognized links between immune response and various health conditions [52].

Furthermore, another MR-PheWAS focusing on insomnia symptoms revealed potential causal effects on a diverse range of outcomes, including anxiety, depression, pain, body composition, respiratory, musculoskeletal traits, and cardiovascular traits. This underscores the broad applicability of MR-PheWASs in elucidating the impact of specific exposures on multiple health outcomes [53].

By systematically conducting thousands of MR analyses, an MR-PheWAS serves as a powerful tool to uncover novel associations between gene expression and disease phenotypes, thereby offering critical insights into potential therapeutic targets.

2.10. Molecular Docking

To investigate the potential interactions between OVGP1 and ORM1 and their respective agonists, we performed molecular docking simulations using AutoDock Vina. This computational approach enabled us to predict the binding affinity and interaction modes of selected ligand molecules with their target proteins.

2.10.1. Retrieval and Preparation of Protein Structures

The three-dimensional structures of OVGP1 and ORM1 were obtained from the UniProt database: for ORM1, the crystal structure was obtained from 3KQ0 (PDB ID), and for OVGP1, the predicted structure was obtained from AF-Q12889-F1 (AlphaFold ID). Protein structures were preprocessed using AutoDockTools (version 1.5.7), including the removal of water molecules, the addition of polar hydrogens to account for hydrogen bonding interactions, and the assignment of Gasteiger charges to ensure accurate electrostatic calculations.

2.10.2. Selection and Preparation of Ligands

The potential agonists for OVGP1 and ORM1 were identified through the Drug Signatures Database (DSigDB), prioritizing compounds with reported gene expression modulation effects. Ligand structures were downloaded from PubChem, and optimized using Open Babel (version 3.1.1) to convert them into an AutoDock-compatible PDBQT format [54].

2.10.3. Docking Parameters and Scoring Functions

Molecular docking was conducted using AutoDock Vina (version 1.2.3) [55], employing the following grid box settings: ORM1: center at x = 32.1, y = 27.8, z = 40.7, with grid dimensions of 60 × 60 × 60 Å; OVGP1: center at x = 45.2, y = 38.6, z = 52.4, with grid dimensions of 60 × 60 × 60 Å. A grid spacing of 1.0 Å was used to ensure there was sufficient search space for flexible docking. The AutoDock Vina scoring function was used

to rank docking poses based on their binding energy (ΔG, kcal/mol), where lower ΔG values indicate a higher ligand–protein affinity [56].

2.10.4. Visualization and Interaction Analysis

The top-ranked docking complexes were visualized using PyMOL (version 2.5.5) to analyze binding site interactions.

The results provided intuitive insights and reliably supported the interaction between potential ligands and target proteins.

2.11. Cell Lines and Cell Culture

Human MM cell lines (RPMI-8226, NCI-H929, MM.1S, and OPM-2) were acquired from the Cell Bank of the Chinese Academy of Sciences, Beijing, China. GM12878 cells were purchased from Shanghai QuiCell Biotechnology Co., Ltd., Shanghai, China. The cells were cultured in RPMI-1640 medium enriched with 10% FBS and 1% penicillin-streptomycin, and incubated at 37 °C under a 5% CO_2 atmosphere with 95% humidity. They were passaged when their density reached 1×10^6–2×10^6 cells/mL at a 1:2 or 1:3 ratio, ensuring exponential growth.

2.12. RT-qPCR

To ensure the accurate quantification of gene expression, we performed reverse transcription quantitative PCR (RT-qPCR), following the Minimum Information for Publication of Quantitative Real-Time PCR Experiments (MIQE) guidelines [57].

2.12.1. RNA Extraction and Quality Control

Total RNA was extracted from cells using the TRIzol reagent (Invitrogen, Waltham, MA, USA) and by following the manufacturer's protocol. RNA purity and concentration were assessed using a NanoDrop 2000 spectrophotometer (Thermo Fisher Scientific, Waltham, MA, USA) by measuring the A260/A280 and A260/A230 ratios. Samples with an A260/A280 ratio between 1.8 and 2.0 were considered highly pure.

2.12.2. cDNA Synthesis

Reverse transcription (RT) was performed using the HiScript III RT SuperMix Kit (Vazyme, Nanjing, China). Genomic DNA contamination was eliminated by including a gDNA wiper step before cDNA synthesis. cDNA synthesis reactions were carried out in a total volume of 20 μL, with 500 ng of total RNA per reaction.

2.12.3. RT-qPCR Experimental Conditions

qPCR was conducted using the QuantStudio 5 Real-Time PCR System (Applied Biosystems, Waltham, MA, USA) in a 20 μL reaction volume containing 10 μL ChamQ SYBR qPCR Master Mix (Vazyme, Nanjing, China), 0.4 μL forward primer (10 μM), 0.4 μL reverse primer (10 μM), 1 μL cDNA template, and 8.2 μL RNase-free water. Melt curve analysis was performed from 65 °C to 95 °C to confirm reaction specificity.

2.12.4. Normalization and Quantification Method

The ΔΔCt method was used for relative gene expression analysis [58]. GAPDH was selected as the reference gene, after confirming its stable expression across experimental conditions.

2.13. Western Blotting

Western blotting was performed to evaluate the expression of target proteins [59].

2.13.1. Protein Extraction and Quantification

Cell lysates were prepared using RIPA lysis buffer (Beyotime, Shanghai, China) supplemented with protease and phosphatase inhibitors (Thermo Fisher, Waltham, MA, USA) to prevent protein degradation. Samples were incubated on ice for 30 min, with vortexing carried out every 5 min, followed by centrifugation at 12,000× *g* for 15 min at 4 °C, using an Eppendorf 5430 R centrifuge (Hamburg, Germany), to remove cell debris. Protein concentration was measured using the Bicinchoninic Acid (BCA) Assay with a NanoDrop 2000 spectrophotometer (Thermo Fisher, Waltham, MA, USA). Loading amounts were normalized to ensure equal protein input across all samples.

2.13.2. SDS-PAGE and Membrane Transfer

Equal protein quantities (20–30 μg per lane) were loaded and separated via sodium dodecyl sulfate–polyacrylamide gel electrophoresis (SDS-PAGE, 12% gels) using a Bio-Rad Mini-PROTEAN Tetra System (Hercules, CA, USA). Proteins were transferred to PVDF membranes (Millipore, Burlington, MA, USA) using a Bio-Rad Trans-Blot Cell wet transfer system at 100 V for 1.5 h at 4 °C.

2.13.3. Blocking and Antibody Incubation

Blocking step: membranes were incubated with 5% skim milk (Bio-Rad, Hercules, CA, USA) in Tris-buffered saline with 0.1% Tween-20 (TBST) for 1 h at room temperature, to reduce nonspecific binding. Primary antibody incubation: membranes were incubated with primary antibodies overnight at 4 °C, with gentle shaking. Secondary antibody incubation: after three washes (5 min each) with TBST, membranes were incubated with secondary antibodies for 1 h at room temperature. Protein detection: bands were visualized using an Enhanced Chemiluminescence (ECL) (Beyotime, Shanghai, China) substrate and detected using a GE Healthcare Amersham Imager 600 (Chicago, IL, USA).

2.13.4. Quantification of Band Intensity

Band intensity was quantified using the ImageJ software (version 1.54d) (Bethesda, MD, USA), and protein expression levels were normalized with the loading control (GAPDH).

2.14. Cell Counting Kit-8 (CCK-8) Assays

To evaluate the proliferation and viability of multiple myeloma (MM) cells in response to drug treatment, we performed CCK-8 assays, following standardized in vitro validation protocols.

2.14.1. Experimental Conditions

Used cell lines: RPMI-8226 and NCI-H929. Seeding density: 1×10^4 cells per well in 96-well plates (Corning, Corning, NY, USA).

2.14.2. Drug Treatment and Experimental Setup

Tested compounds: pregnenolone (ORM1 agonist) and irinotecan (OVGP1 agonist). Concentration gradient: cells were treated with 10, 20, 30, and 40 μM of each compound. Control conditions: DMSO (0.1%) was used as a negative control (vehicle control) to rule out solvent effects. Untreated cells served as an additional control to measure baseline proliferation.

2.14.3. CCK-8 Assay

Drug incubation: after plating, cells were treated with the compounds for 24 h at 37 °C in 5% CO_2. Addition of CCK-8 reagent: a 10 μL volume of CCK-8 solution (Beyotime, China) was added to each well. Incubation: cells were incubated for 1 h at 37 °C, allowing viable

cells to reduce the CCK-8 substrate into a formazan product. Absorbance measurement: the optical density (OD) at 450 nm was measured using a microplate reader (Thermo Fisher Scientific, Waltham, MA, USA).

2.14.4. Data Analysis and Statistical Methods

Normalization: The OD values were normalized with the negative control (DMSO-treated group) to calculate relative viability. Background absorbance (from only the medium) was subtracted from all readings.

Calculation of cell viability (%):

$$\text{Cell viability} = \left(\frac{\text{OD}_{\text{treated}} - \text{OD}_{\text{blank}}}{\text{OD}_{\text{control}} - \text{OD}_{\text{blank}}} \right) \times 100. \quad (1)$$

IC50 determination: the half-maximal inhibitory concentration (IC50) was calculated using nonlinear regression curve fitting (log [inhibitor] vs. response, variable slope model) in GraphPad Prism (version 9.0).

2.15. Statistical Analysis

All quantitative experiments were performed in triplicate or higher, unless otherwise specified, and values are reported as mean ± standard deviation (SD). Statistical analyses were carried out using GraphPad Prism 9 (GraphPad Software, La Jolla, CA, USA). For comparisons between two groups, an unpaired two-tailed Student's *t*-test was used. For multi-group comparisons (e.g., multiple cell lines or drug concentrations), MR and TWAS analyses were conducted as described, with multiple-testing corrections applied for high-dimensional analyses (the FDR method). Significance was defined as a p of <0.05 (or an FDR of <0.05 for adjusted results).

3. Results

3.1. Identification of Exposure Genes

On the basis of the selection criteria ($p < 5 \times 10^{-8}$, $r^2 < 0.1$, window size of 10,000 kb, and F statistic > 10), 2533 potential druggable genes were identified. These genes were selected to ensure their relevance to MM and statistical significance through rigorous bioinformatic and genetic screening processes.

A total of 40,447 SNPs were identified as IVs for these 2533 druggable genes, meeting the specified criteria. All IVs had an F-statistic of >10, suggesting the absence of any weak instrumental bias. The IVs are explained in detail in Supplementary Table S3.

3.2. Two-Sample MR Analysis Validated Druggable Genes

After identifying the 2533 potential druggable genes, two-sample MR analysis was used to evaluate the causal link between MM risk and the expression of these genes. To improve accuracy, all p-values were examined via FDR correction. After correction, 34 genes were significantly associated with MM risk (FDR < 0.05) (Figure 2).

Heterogeneity test: The reliability of the results was ensured by performing heterogeneity tests on the 34 significant genes. These tests examined the variability of effects across different IVs to confirm consistency in the causal link between gene expression and the risk for MM. The findings indicated consistent association effects across IVs, and no significant heterogeneity was observed (Supplementary Table S4).

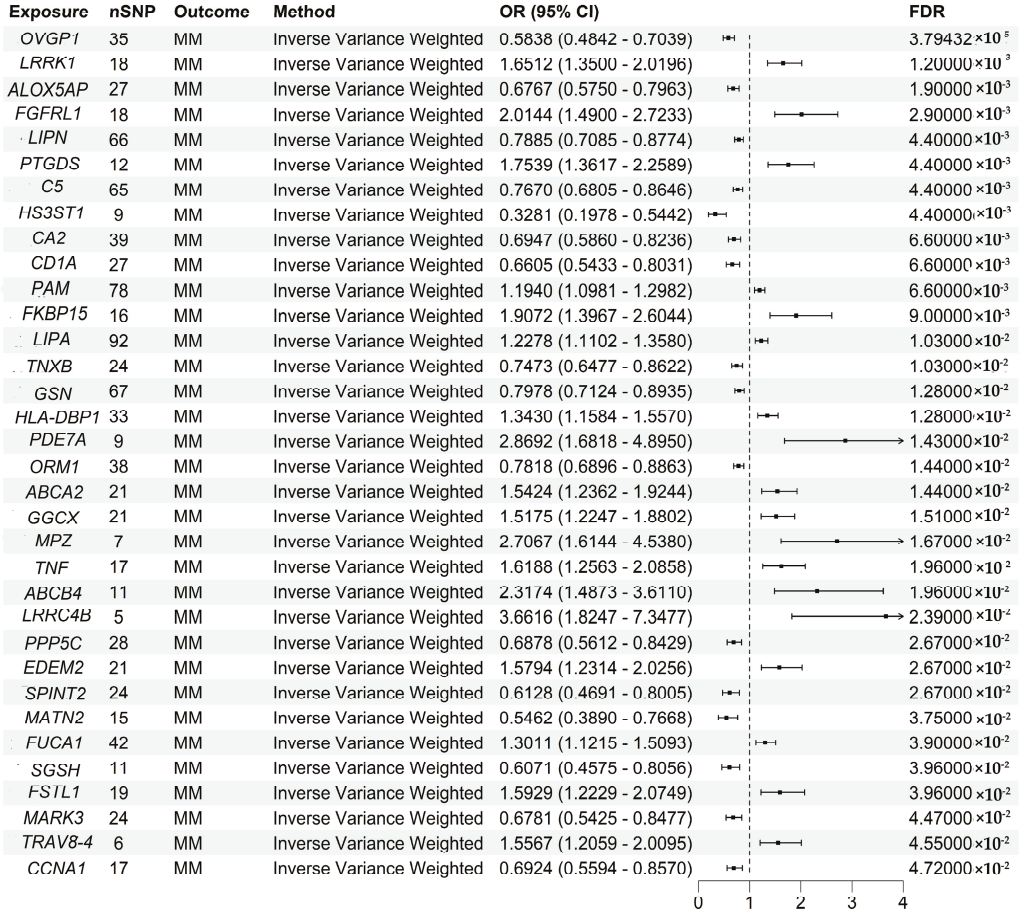

Figure 2. Key Mendelian randomization findings showing the association of druggable gene expression with susceptibility to multiple myeloma, adjusted for false discovery rate correction.

Horizontal Pleiotropy Test: Horizontal pleiotropy tests were performed to exclude the possibility that the IVs influence MM risk through pathways other than target gene expression. Using methods such as MR-Egger regression, the evidence of horizontal pleiotropy was noted only for Carbonic Anhydrase 2 *(CA2)* and Tumor Necrosis Factor *(TNF)* ($p < 0.05$), further supporting the causal role of these genes in MM (Supplementary Table S5).

3.3. Transcriptome-Wide Association Study (TWAS) Identified Susceptibility Genes for MM

We performed a single-tissue TWAS using gene expression prediction models from GTExv8.EUR.Whole_Blood to evaluate associations between genetically predicted expression and multiple myeloma (MM) risk for candidate genes identified by two-sample Mendelian randomization. The analysis identified four genes that remained statistically significant after false discovery rate (FDR) correction (FDR < 0.05): *OVGP1*, *ORM1*, *ALOX5AP*, and *PTGDS* (Table 2).

Table 2. TWAS analysis of MR-prioritized candidate genes.

ID	CHR	SNPID	pos	Z	FDR
OVGP1	1	rs1264878	111947430	−3.442623	0.013824
ORM1	9	rs7851482	117078286	−2.95	0.03416
ALOX5AP	13	rs6490461	30976845	−2.8571	0.03416
PTGDS	9	rs2811786	139683224	2.75	0.03594

Among them, *OVGP1* (rs1264878) exhibited the strongest negative association with MM risk (Z = −3.4), suggesting that increased genetically predicted expression of *OVGP1* in whole blood may be associated with a reduced risk of MM. Similarly, *ORM1* (rs7851482) and *ALOX5AP* (rs6490461) also showed negative TWAS Z-scores (Z = −2.95 and −2.8571), indicating potential protective roles. In contrast, *PTGDS* (rs2811786) demonstrated a positive association (Z = 2.75), implying that higher expression of *PTGDS* may contribute to increased MM susceptibility.

These findings provide transcriptome-level evidence supporting the involvement of these genes in MM pathogenesis, and warrant further investigation to elucidate their functional roles in disease development.

3.4. Colocalization Confirmed Shared Genetic Variants for Gene Expression and MM

Colocalization analysis was conducted to verify whether a single genetic variant contributes to both gene expression and disease phenotypes. This analysis calculated the posterior probability of shared causal variants (PPH4) to determine shared causality (Supplementary Table S6). Among the identified genes, only Orosomucoid 1 *(ORM1)*, Matrilin-2 *(MATN2)*, and Oviductal Glycoprotein 1 *(OVGP1)* had PPH4 values > 0.75, strongly indicating that these genes are causally linked to MM through the same genetic variants (Figure 3).

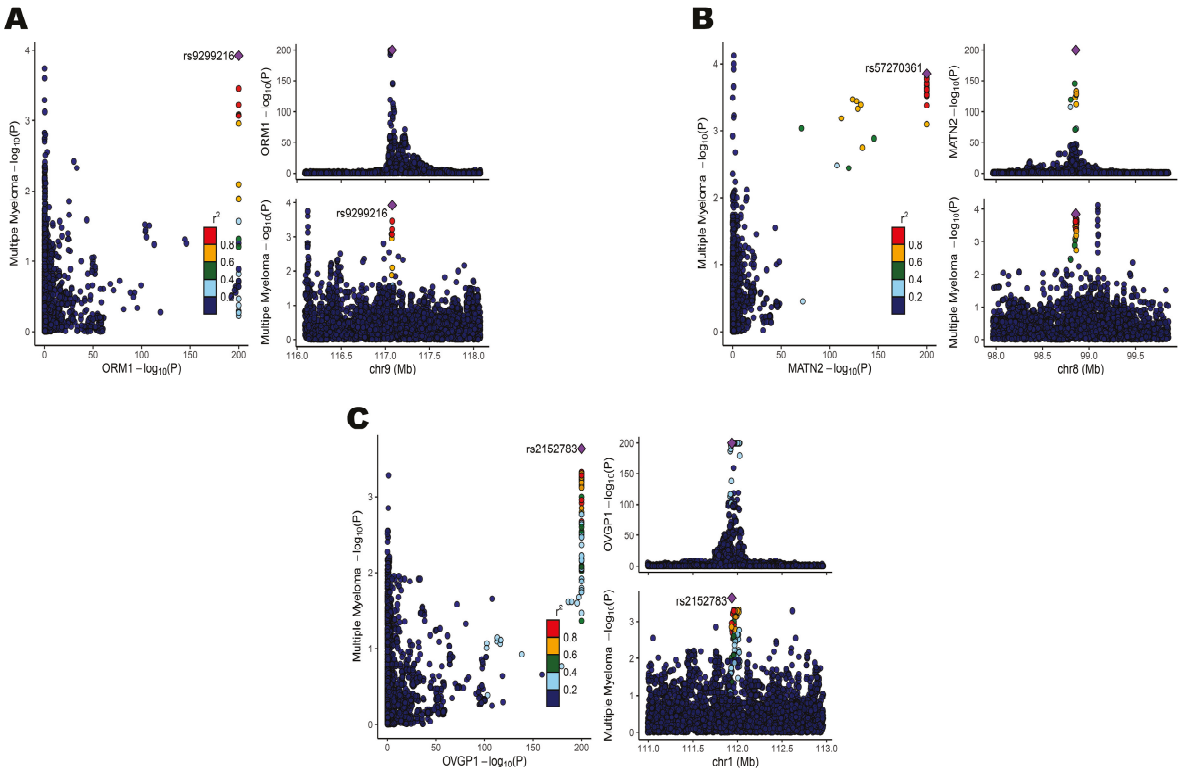

Figure 3. (**A**) Colocalization results of Orosomucoid 1 *(ORM1)* with MM; (**B**) colocalization results of Matrilin-2 *(MATN2)* with MM; and (**C**) colocalization results of Oviductal Glycoprotein 1 *(OVGP1)* with MM.

The multi-step pipeline applied in this study—including exposure gene identification, two-sample MR, TWAS, colocalization, and functional validation—represents a systematic framework for identifying and prioritizing therapeutic targets in MM. While each individual method has been previously used in complex disease genetics, the comprehensive integration of these approaches in MM research is a novel aspect of this study.

Similar strategies have been employed to identify causal genes in other diseases. For instance, a study by Gamazon et al. integrated MR and colocalization to identify druggable targets in complex diseases [60]. Huang et al. applied MR in inflammatory diseases, validating their findings via multi-omics data integration [61]. Additionally, research on osteoarthritis and Sjogren syndrome has successfully leveraged multi-omics MR and Bayesian colocalization to pinpoint therapeutic targets [62,63]. These examples validate the robustness of this approach, as it has been successfully replicated across different diseases.

3.5. Experimental Validation of Target Genes

The mRNA expression levels of *ORM1*, *MATN2*, and *OVGP1* were quantified in various cell lines via qPCR. The mRNA levels of these genes were significantly lower in RPMI-8226, NCI-H929, OPM-2, and MM.1S cells than in GM12878 cells ($p < 0.05$), suggesting their potential pathogenic roles in MM (Figure 4A–C).

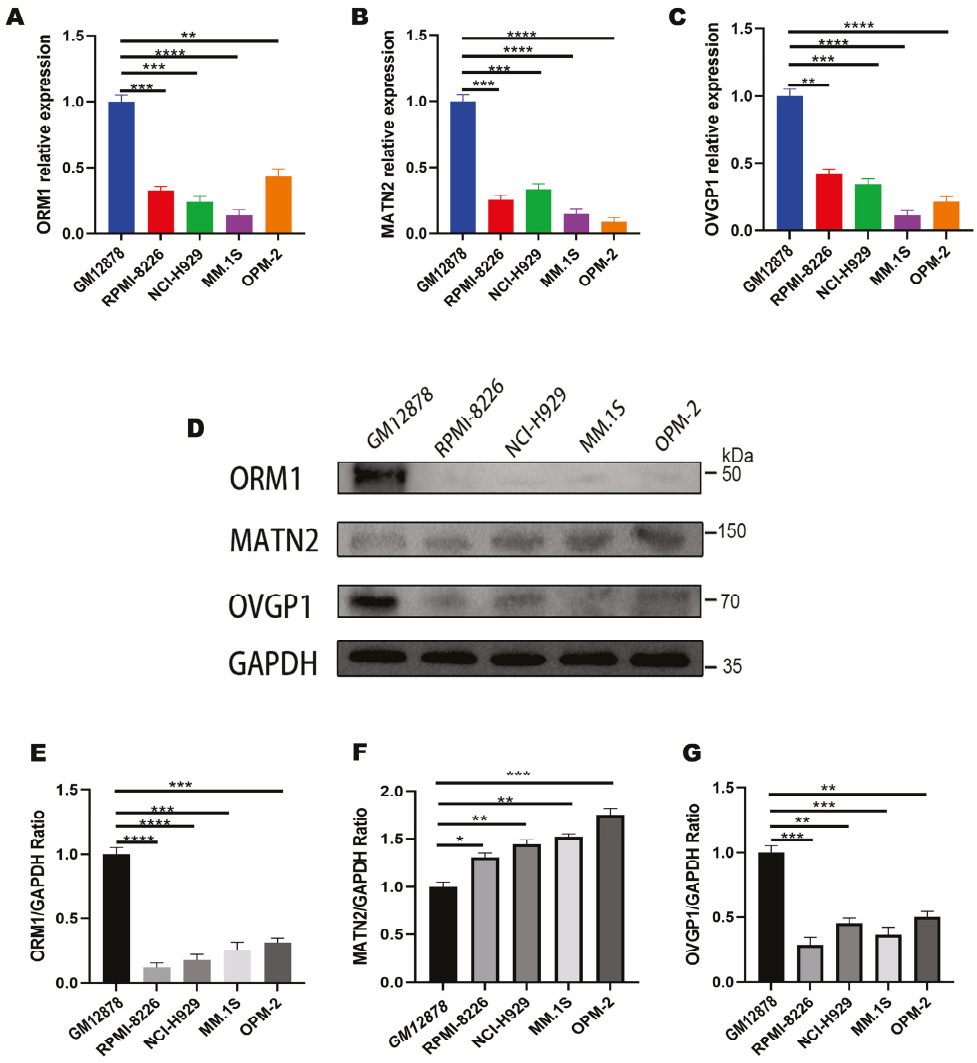

Figure 4. (**A**–**C**) qRT-PCR analysis of *ORM1*, *MATN2*, and *OVGP1* gene expression in GM12878, RPMI-8226, NCI-H929, MM.1S, and OPM-2 cells, with expression levels normalized with GAPDH; (**D**) Western blot analysis of ORM1, MATN2, and OVGP1 from various cells; (**E**–**G**) quantification of ORM1, MATN2, and OVGP1 levels after normalization with GAPDH levels.* indicates $p < 0.05$; ** indicates $p < 0.01$; *** indicates $p < 0.001$; **** indicates $p < 0.0001$.

Western blot analysis was performed to validate the mRNA expression trends reflected at the protein level (Figure 4D). The ORM1 and OVGP1 protein levels were significantly lower in MM cell lines than in GM12878 cell lines ($p < 0.05$), indicating the role of these genes in MM pathogenesis and progression (Figure 4E,G). In contrast, MATN2 exhibited an inverse trend; although its mRNA levels were lower in MM cell lines, the WB results revealed significantly higher protein expression in these lines than in GM12878 cells ($p < 0.05$) (Figure 4F). The full-length Western blot images of ORM1, MATN2, OVGP1, and GAPDH are provided in Supplementary Figure S1, including the molecular weight markers.

ORM1: this has been previously identified as an inflammatory biomarker of MM, but has never been linked to MM progression [64]. OVGP1: this has not been previously associated with MM, but is known as a tumor suppressor in ovarian cancer, where low OVGP1 expression correlates with poor prognosis [65,66].

3.6. MR-PheWAS Explored Off-Target Effects of Target Genes

The potential side effects of *ORM1* and *OVGP1* as drug targets were investigated through MR-PheWAS analysis for all 1403 phenotypes in the UKB-SAIGE database (Supplementary Tables S7 and S8). IVW methods with FDR correction revealed significant associations of *ORM1* with phenotypes of blindness, low vision, and acute posthemorrhagic anemia (FDR < 0.05) (Figure 5A). Thus, *OVGP1* was significantly associated with chronic pain and disorders of parathyroid glass (FDR < 0.05) (Figure 5B).

These findings suggest that ORM1 and OVGP1 modulation should be carefully evaluated for potential off-target effects in clinical applications. However, the identified associations do not suggest immediate life-threatening risks, indicating the feasibility of ORM1/OVGP1-based therapies with appropriate monitoring. These results align with previous MR-PheWAS analyses that have explored genetic targets for drug repurposing and adverse event prediction [67].

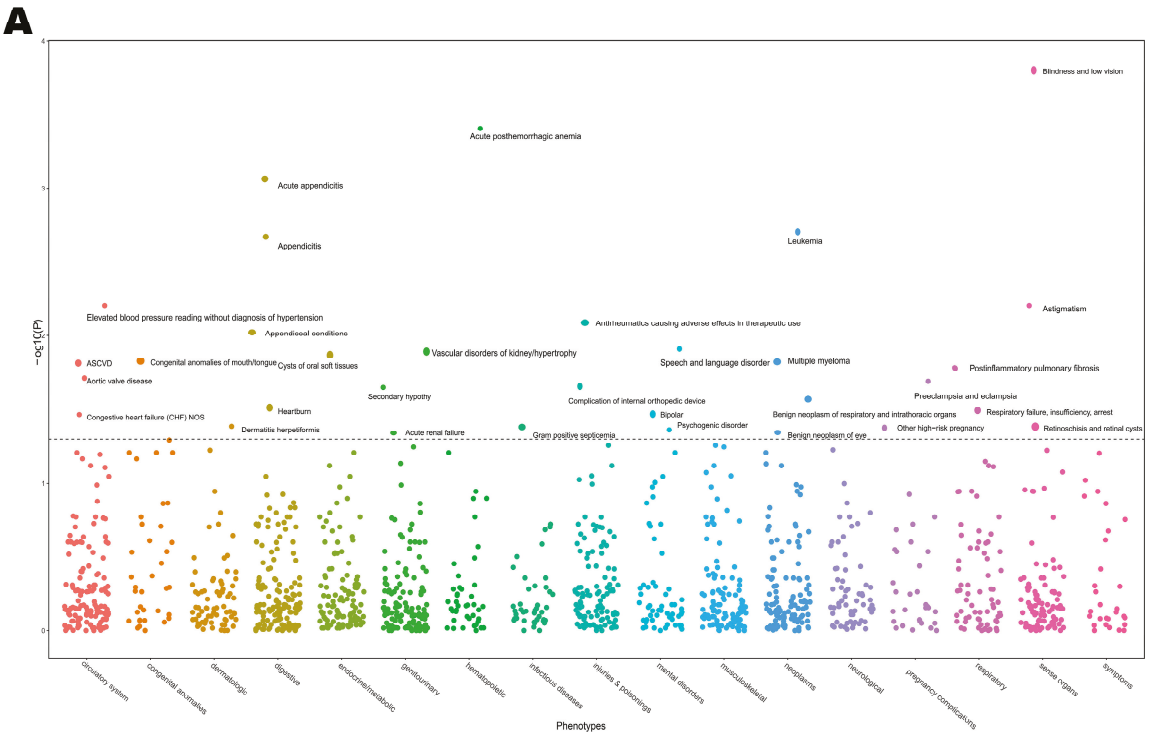

Figure 5. *Cont.*

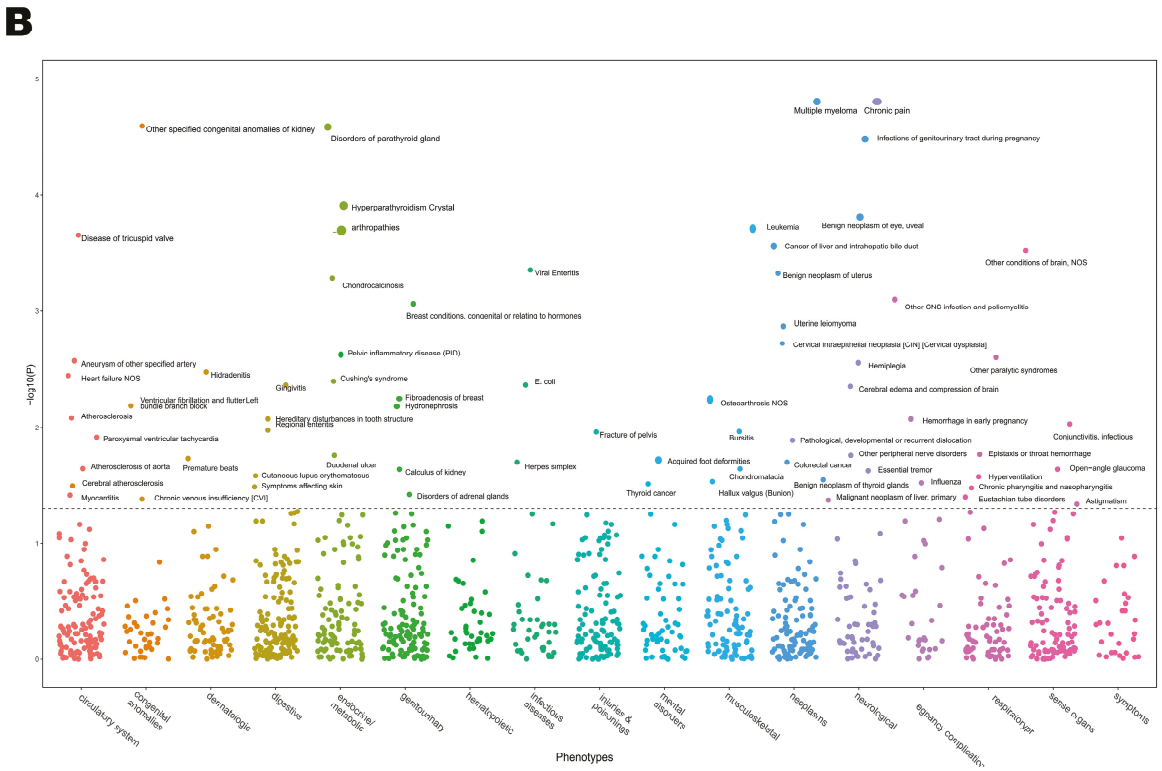

Figure 5. (**A**). MR-PheWAS results for *ORM1* and UKB-SAIGE-associated phenotypes; (**B**) MR-PheWAS results for OVGP1 and UKB-SAIGE-associated phenotypes.

3.7. Pregnanolone and Irinotecan as Effective Agonists of ORM1 and OVGP1

As ORM1 and OVGP1 are negatively correlated with MM progression, potential agonists of these targets were predicted via the DSigDB database. Molecular docking through AutoDock Vina identified pregnanolone and irinotecan as effective agonists for ORM1 and OVGP1, respectively (Supplementary Tables S9 and S10). The docking complexes with the lowest binding energies were visualized via PyMOL (Figure 6).

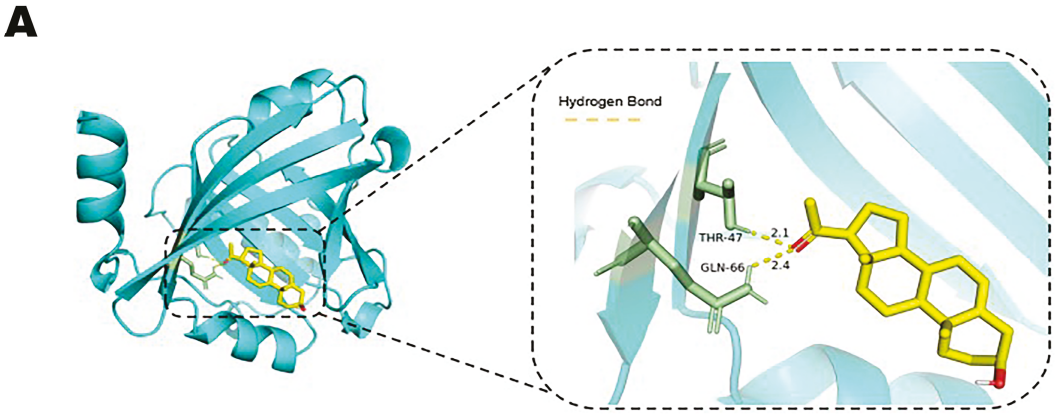

Figure 6. *Cont.*

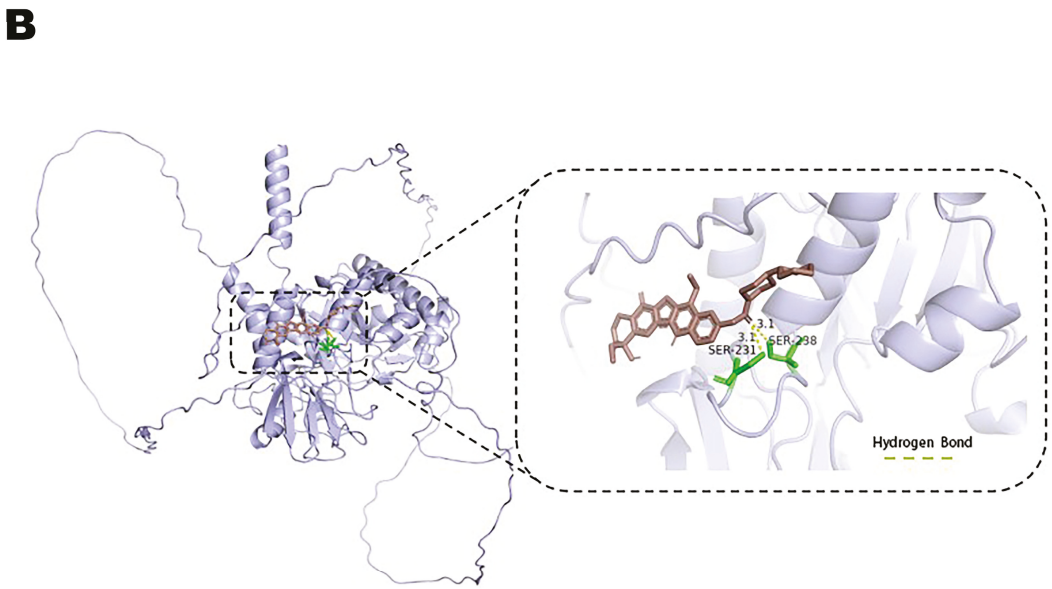

Figure 6. (**A**). Visualization of molecular docking between ORM1 and pregnanolone (hydrogen bonds are represented by yellow dashed lines); (**B**) visualization of molecular docking between OVGP1 and irinotecan (hydrogen bonds are represented by yellow dashed lines).

3.8. Effects of Pregnanolone and Irinotecan on Multiple Myeloma Cell Viability

CCK-8 assays demonstrated a significant decrease in the viability of RPMI-8226 and NCI-H929 cells after pregnanolone and irinotecan treatment. The IC50 values for pregnanolone and irinotecan were 32.97 μM and 30.34 μM, and 29.79 μM and 26.97 μM, in RPMI-8226 and NCI-H929 cells, respectively. Subsequently, 30 μM pregnanolone and 25 μM irinotecan were used to treat objective cells (Figure 7A–D). After 24 h, the ORM1 protein levels were significantly greater in the pregnanolone-treated cells than in the control cells ($p < 0.05$) (Figure 7E,F). Similarly, OVGP1 protein levels were significantly greater in the irinotecan-treated cells than in the control cells ($p < 0.05$), indicating that pregnanolone and irinotecan could increase ORM1 and OVGP1 expression, thereby suppressing MM growth (Figure 7G,H). The full-length Western blot images of ORM1 and GAPDH are provided in Supplementary Figure S2, and the full-length Western blot images of OVGP1 and GAPDH are provided in Supplementary Figure S3, including molecular weight markers.

Previous studies have explored the use of pregnenolone derivatives in neurological disorders and irinotecan as a topoisomerase inhibitor in cancer treatment [68,69]. However, our study presents the first evidence of these compounds' potential regulatory effects on ORM1 and OVGP1 in MM.

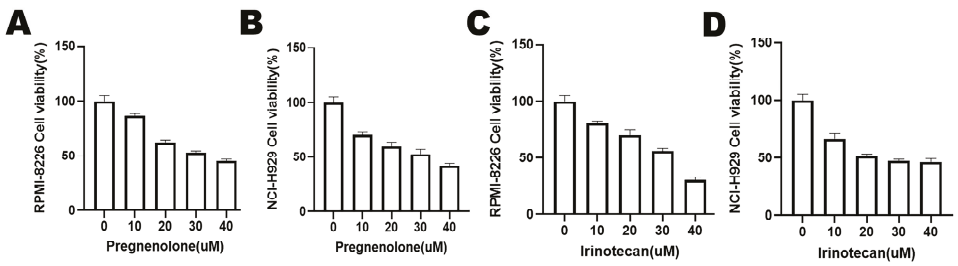

Figure 7. *Cont.*

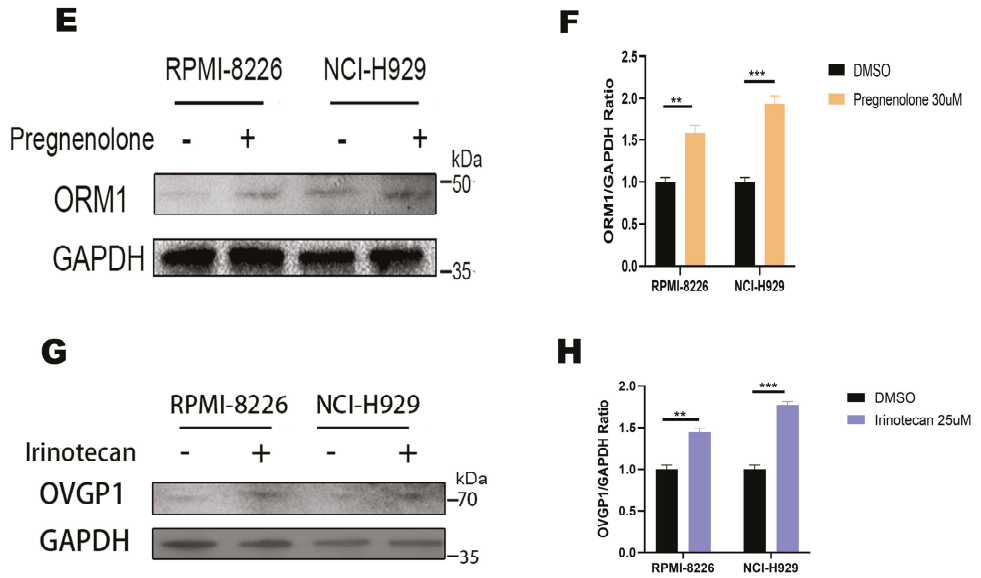

Figure 7. (**A**,**B**). Effects of pregnanolone on viability of RPMI-8226 and NCI-H929 cells; (**C**,**D**) effects of irinotecan on viability of RPMI-8226 and NCI-H929 cells; (**E**) effects of pregnanolone on ORM1 protein expression levels in RPMI-8226 and NCI-H929 cells; (**F**) quantification of ORM1 normalized with GAPDH; (**G**) effects of irinotecan on OVGP1 protein expression levels in RPMI-8226 and NCI-H929 cells; (**H**) quantification of OVGP1 normalized with GAPDH. ** indicates $p < 0.01$; *** indicates $p < 0.001$.

4. Discussion

In this study, we applied a two-sample MR framework to identify and prioritize druggable genes that have a causal impact on multiple myeloma. Starting from thousands of candidate genes, we selected 34 genes associated with MM risk through MR, and then further validated these genes using a TWAS by integrating GWAS summary statistics with gene expression prediction models from GTExv8.EUR whole blood data. The TWAS enhanced the interpretability of the GWAS findings by linking disease-associated variants to gene expression regulation, thereby helping to pinpoint functional target genes. Colocalization analysis (PPH4 > 0.75) highlighted three top gene candidates—*ORM1*, *MATN2*, and *OVGP1*—with strong evidence that genetic variation in these genes drives MM susceptibility. Functional assays confirmed that *ORM1* and *OVGP1* are expressed at significantly lower levels in MM cells than in non-malignant cells, consistent with the notion that their reduced activity may contribute to MM pathogenesis. This finding is in line with the results of the single-tissue TWAS, in which both *ORM1* and *OVGP1* showed significant associations with MM risk, and increased genetically predicted expression was associated with decreased disease risk. We identified pregnenolone and irinotecan as compounds that can upregulate *ORM1* and *OVGP1*, respectively, and showed that these agents inhibit MM cell viability in vitro, while restoring the expression of their target proteins. Together, these findings support ORM1 and OVGP1 as potential therapeutic targets in MM, and suggest a repurposing opportunity for pregnenolone and irinotecan as modulators of these targets. We also leveraged MR-PheWAS to examine the broader effects of *ORM1*/*OVGP1*, and the results did not reveal any prohibitive safety concerns, although some pleiotropic associations were noted, and should be investigated further.

ORM1, also known as α-1-acid glycoprotein, functions as a key protein in the acute-phase response, particularly in inflammation and immune system regulation [70]. ORM1 is produced mainly in the liver, and is released into the bloodstream in response to inflammation, where it serves as an important modulator of immune responses. Its involvement in the tumor microenvironment has been widely recognized, where it influences immune

responses through interactions with cytokines and various immune cells [71]. ORM1 has been implicated in both anti-apoptotic and proangiogenic processes across various cancers, suggesting its potential role in tumor progression. Additionally, its interaction with inflammatory cytokines, such as Interleukin 1 Beta (IL-1β) and Interleukin 6 (IL-6), could establish a complex immune network, where ORM1 might either promote or alleviate inflammation, depending on the specific context [72,73]. To the best of our knowledge, our study provides the first genetic evidence linking *ORM1* to MM. Uniquely, we observed the downregulation of *ORM1* in MM cell lines compared to a non-malignant baseline, implying that in MM, *ORM1* might function as a protective factor whose loss promotes disease. This contrasts with reports suggesting that elevated *ORM1* expression correlates with chemotherapy resistance and increased metastasis in certain solid tumors, such as breast cancer and hepatocellular carcinoma, highlighting how the role of a protein can vary across different malignancies [74,75]. The beneficial effect of increasing ORM1 in our MM models (via pregnenolone treatment, which raised ORM1 levels and slowed MM cell growth) highlights a potential therapeutic strategy: enhancing ORM1 activity might suppress MM progression. The exact mechanism by which *ORM1* downregulation favors MM remains to be elucidated. It may involve diminished immunoregulatory support, and since ORM1 can dampen excessive inflammation, its low levels in MM could contribute to a chronic inflammatory milieu that supports tumor growth. ORM1 has been implicated in the PI3K/AKT and ERK pathways [76], which regulate proliferation and apoptosis resistance. Decreased *ORM1* expression may impair negative feedback mechanisms, giving MM cells a survival advantage. Additionally, low levels of ORM1 might impair the negative feedback for angiogenesis or cell survival signals, giving MM cells a growth advantage. These hypotheses merit further investigation, possibly through *ORM1* overexpression or knockdown experiments in MM models.

OVGP1 is a secretory glycoprotein predominantly expressed in the reproductive system, especially in the fallopian tubes, where it is crucial in regulating oocyte fertilization and in the early stages of embryo development. Traditionally, OVGP1 was considered to have a reproduction-specific function, but recent studies have revealed its unexpected involvement in various malignancies, including breast, ovarian, and colorectal cancers [77,78]. Although the role of OVGP1 in the reproductive system is well established, its emerging importance in tumor biology highlights its broader function that extends beyond reproduction. While its role in the reproductive tract is well documented, emerging evidence points to its potential contribution to tumor progression. OVGP1 appears to modulate key processes, such as extracellular matrix (ECM) integrity and cell adhesion, both of which are essential for cancer cell migration and metastasis [79,80]. The glycoprotein may influence tumor cell movement by facilitating interactions between tumor cells and the ECM, thereby promoting invasion into adjacent tissues [81]. Indeed, our discussion of OVGP1's role in MM is somewhat speculative, given that MM is confined to the bone marrow; however, MM cells interact with the bone marrow ECM and stroma, and a protein like OVGP1 might influence these interactions if expressed or present in that niche. Our genetic data strongly suggest that higher *OVGP1* expression protects against MM (*OVGP1* expression is low in MM, and its low genetic expression increases MM risk). We validated that MM cell lines have markedly reduced OVGP1 levels, aligning with a potential tumor-suppressor role for OVGP1 in myeloma. The identification of irinotecan as an agent that increases *OVGP1* expression in cells is intriguing. It is well documented that irinotecan exerts cytotoxic effects by targeting topoisomerase I, leading to DNA damage and apoptosis [82,83]. However, in our study, irinotecan increased *OVGP1* expression, while simultaneously reducing MM cell viability. This suggests that *OVGP1* upregulation might contribute to the apoptotic response in MM cells, potentially by activating endoplasmic reticulum

(ER) stress or interfering with survival pathways. The tumor microenvironment in MM is highly immunosuppressive, allowing MM cells to evade immune detection [84,85]. Some glycoproteins, including mucins, are involved in immune modulation by interacting with immune checkpoint molecules [86,87]. If OVGP1 participates in immune recognition processes, its downregulation in MM could contribute to immune evasion. Future studies should explore whether OVGP1 interacts with immune cells in the bone marrow, such as T cells or macrophages, and whether its expression influences anti-tumor immunity.

Our MR-PheWAS analysis provided additional context for ORM1 and OVGP1 by highlighting phenotypes that might be affected by these proteins. The association of ORM1 with visual impairment and anemia could relate to ORM1's known function in modulating inflammation; chronic inflammation is an influencing factor in chronic disease conditions like macular degeneration or anemia, and thus, genetically higher levels of *ORM1* (anti-inflammatory) might be protective in these contexts. For OVGP1, the link to chronic pain could be coincidental or via an unknown pathway; the parathyroid association is also not straightforward, though one could speculate about calcium-binding properties of mucins or indirect endocrine effects. These findings are hypothesis-generating, and suggest that the systemic effects of modulating ORM1/OVGP1 should be carefully monitored. Nonetheless, none of the MR-PheWAS hits are acute life-threatening conditions; thus, targeting ORM1 or OVGP1 in MM appears feasible from a safety standpoint, provided that any chronic implications (vision-related, pain-related, metabolic) are managed.

Despite the promising results, our study has several limitations. First, the MR analysis was based on publicly available GWAS summary data, predominantly from individuals of European ancestry. This may limit the generalizability of our findings to other populations with different genetic architectures. Future replication in diverse cohorts or using ancestry-specific GWASs would bolster the evidence for these targets and ensure they are relevant globally. Additionally, while MR is powerful in inferring causality, it can be affected by biases such as residual confounding (if genetic instruments affect the outcome through other traits) and the winner's curse (the overestimation of effects in discovery datasets). We attempted to mitigate these issues through pleiotropy tests and validation steps, but unmeasured confounders could still have influenced the results. Second, although TWAS and colocalization analyses support the causal roles of *ORM1* and *OVGP1* in MM, these computational methods rely on certain assumptions and the quality of input data. Our experimental validation is still preliminary, although it confirms the differential expression of target genes. We made useful correlations (low *ORM1*/*OVGP1* expression is present in MM cells, and their upregulation reduces MM cell viability), but we have not yet deciphered the mechanism behind the effect of pregnenolone or irinotecan on cell viability that is mediated by *ORM1*/*OVGP1*. Further experiments such as rescue or knockdown studies would be valuable; for example, an assessment of whether silencing *ORM1* inhibits the effect of pregnenolone on MM cells. Such studies would solidify the causal chain from gene to phenotype in a biological sense. Third, the identified compounds (pregnenolone and irinotecan) are existing drugs with known profiles, which is advantageous for repurposing, but their use in MM is novel. Pregnenolone is a precursor steroid hormone, and has been explored mostly for neurological conditions; its effects on immune cells or cancer cells are not well characterized, and could involve off-target pathways. Irinotecan is a chemotherapy agent, and using it at lower doses to modulate *OVGP1* might or might not separate its *OVGP1*-related effects from its DNA-damaging cytotoxicity. Any clinical applications would require careful dosing strategies, and possibly the development of more specific analogues that preferentially enhance OVGP1 without severe toxicity. Fourth, a key consideration in our expression analysis is the choice of GM12878 lymphoblastoid cells as a control group. While GM12878 is widely used in hematologic malignancy studies, it

presents several limitations: GM12878 cells are Epstein–Barr virus (EBV)-transformed B lymphocytes, which may not fully reflect the gene expression profile of normal plasma cells. Plasma cells and lymphoblastoid cells have distinct transcriptional landscapes, which could lead to baseline expression differences unrelated to MM pathogenesis. Primary normal plasma cells are difficult to obtain, making GM12878 a practical alternative, albeit with certain caveats. To mitigate these concerns, we validated *ORM1* and *OVGP1* expression across multiple MM cell lines, ensuring the consistency of differential expression patterns. However, future studies should use primary bone marrow-derived plasma cells from healthy donors or integrate single-cell RNA sequencing datasets to establish a more accurate baseline [88,89]. Finally, MM is a complex and heterogeneous disease, and our study focused on single-gene targets in isolation. In reality, MM pathogenesis involves networks of interactions within the bone marrow microenvironment. Proteins like ORM1 and OVGP1 might influence MM progression through multiple mechanisms, for example, by modulating immune evasion, affecting cell adhesion in the marrow niche, or altering sensitivity to other drugs. Fully understanding their roles will require more comprehensive models, potentially co-culture systems with bone marrow stromal cells or in vivo models, to capture the context in which these genes operate. Additionally, future studies should investigate how these targets interact with known MM drivers, and whether combining an ORM1/OVGP1-targeted approach with existing therapies (like proteasome inhibitors or immunotherapies) yields synergistic benefits.

5. Conclusions

Multiple genetic analyses and experimental validation were integrated to elucidate the critical roles of ORM1 and OVGP1 in MM. This study also identified two effective agonists, irinotecan and pregnenolone, that target the aforementioned proteins, thereby broadening the scope of therapeutic targets for MM. These results increase our understanding of MM pathogenesis and provide a basis for future drug development. Future research should focus on the specific signaling pathways associated with ORM1 and OVGP1 and their potential in MM treatment, with the aim of developing more precise and effective strategies for the treatment of patients with MM.

Supplementary Materials: The following supporting information can be downloaded at: https://www.mdpi.com/article/10.3390/biomedicines13040885/s1, Figure S1: Uncropped Western blot images of ORM1 (A), MATN2 (B), OVGP1 (C), and GAPDH (D). Molecular weight markers are indicated on left; Figure S2: Uncropped Western blot images of ORM1 (A) and GAPDH (B). Molecular weight markers are indicated on left; Figure S3: Uncropped Western blot images of OVGP1 (A) and GAPDH (B). Molecular weight markers are indicated on left; Table S1: STROBE-MR checklist; Table S2: Summary of druggable genes with cis-eQTL data from eQTLGen Consortium; Table S3: Identification of potential druggable genes and SNPs as instrumental variables; Table S4: Heterogeneity test results for significant genes and instrumental variables; Table S5: Horizontal pleiotropy test results for instrumental variables and multiple myeloma risk; Table S6: Colocalization results of potentially druggable genes; Table S7: Potential side effects of ORM1 as drug target identified through MR-PheWAS analysis; Table S8: Potential side effects of OVGP1 as drug target identified through MR-PheWAS analysis; Table S9: Molecular docking results of ORM1 with potential agonists; Table S10: Molecular docking results of OVGP1 with potential agonists. References [90,91] are cited in the Supplementary Materials.

Author Contributions: Conceptualization, S.J.; methodology, S.J.; data analysis, F.F.; bioinformatics validation, Q.L.; in vitro experiments, L.Z. and A.X.; interpretation of results, L.Z. and A.X.; manuscript revision, C.S. All authors have read and agreed to the published version of the manuscript.

Funding: This research was funded by the National Natural Science Foundation of China (No. 82270214, 82470205, and 82270215).

Institutional Review Board Statement: Ethical review and approval were waived for this study, because all data were obtained from publicly available sources (UK Biobank, eQTLGen Consortium) that have been ethically approved for research use.

Informed Consent Statement: Not applicable. This study used only commercially available human cell lines.

Data Availability Statement: All datasets used and analyzed in this study are publicly available. The genetic association data for multiple myeloma (MM) were obtained from the UK Biobank (https://pheweb.org/UKB-SAIGE/, accessed on 28 August 2024), while the cis-eQTL data were retrieved from the eQTLGen Consortium (https://www.eqtlgen.org/, accessed on 7 September 2024). The transcriptomic prediction models for the single-tissue TWAS (GTExv8.EUR.Whole_Blood) were obtained from the FUSION website (http://gusevlab.org/projects/fusion/, accessed on 19 March 2025). The protein function and annotation data were obtained from the UniProt database (https://www.uniprot.org/, accessed on 19 September 2024), and the drug–gene interaction data were sourced from the DSigDB database (https://maayanlab.cloud/DSigDB/, accessed on 6 October 2024).

Acknowledgments: The authors would like to acknowledge the eQTLGen Consortium and UK Biobank for providing access to valuable datasets. We also thank the researchers who provided administrative, technical, and laboratory support, and those who contributed materials used in the experiments. Their contributions were invaluable to the completion of this study.

Conflicts of Interest: The authors declare no conflicts of interest. The funders had no role in the design of the study; in the collection, analyses, or interpretation of data; in the writing of the manuscript; or in the decision to publish the results.

Abbreviations

The following abbreviations are used in this manuscript:

ADCs	antibody–drug conjugates
BCL2	B-Cell Lymphoma 2
BiTEs	bispecific T cell engagers
CA2	carbonic anhydrase 2
CAR	chimeric antigen receptor
CCK-8	Cell Counting Kit-8
cis-eQTL	cis-acting Expression Quantitative Trait Loci
DMSO	dimethyl sulfoxide
DSigDB	Drug Signatures Database
DTMR	drug target Mendelian randomization
EBV	Epstein–Barr virus
ECL	Enhanced Chemiluminescence
ECM	extracellular matrix
ER	endoplasmic reticulum
FDR	false discovery rate
GPCRs	G-protein-coupled receptors
GWASs	genome-wide association studies
HDL-C	high-density lipoprotein cholesterol
HEIDI	Heterogeneity in Dependent Instruments
HRP	horseradish peroxidase
IL-1β	Interleukin 1 Beta
IL-6	Interleukin 6

IVs	instrumental variables
IVW	inverse variance weighted
LD	linkage disequilibrium
MAF	minor allele frequency
MATN2	Matrilin-2
MM	multiple myeloma
M-proteins	monoclonal immunoglobulins
MR	Mendelian randomization
MR-PheWAS	Mendelian randomization phenome-wide association
NAMPT	nicotinamide phosphoribosyl transferase
ORM1	Orosomucoid 1
OVGP1	Oviductal Glycoprotein 1
PBS	phosphate-buffered saline
RCT	randomized controlled trial
RT	Reverse transcription
SAIGE	Scalable and Accurate Implementation of Generalized Mixed Model
SDS-PAGE	sodium dodecyl sulfate–polyacrylamide gel electrophoresis
SNP	Single-Nucleotide Polymorphism
SOCS3	suppressor of cytokine signaling 3
TNF	Tumor Necrosis Factor
TWAS	transcriptome-wide association study
VZV	varicella zoster virus

References

1. Ludwig, H.; Novis Durie, S.; Meckl, A.; Hinke, A.; Durie, B. Multiple myeloma incidence and mortality around the globe; interrelations between health access and quality, economic resources, and patient empowerment. *Oncologist* **2020**, *25*, e1406–e1413. [CrossRef]
2. Pertesi, M.; Went, M.; Hansson, M.; Hemminki, K.; Houlston, R.S.; Nilsson, B. Genetic predisposition for multiple myeloma. *Leukemia* **2020**, *34*, 697–708. [CrossRef]
3. Ostendorf, L.; Burns, M.; Durek, P.; Heinz, G.A.; Heinrich, F.; Garantziotis, P.; Enghard, P.; Richter, U.; Biesen, R.; Schneider, U.; et al. Targeting CD38 with daratumumab in refractory systemic lupus erythematosus. *N. Engl. J. Med.* **2020**, *383*, 1149–1155. [CrossRef] [PubMed]
4. Hvidtfeldt, U.A.; Chen, J.; Rodopoulou, S.; Strak, M.; de Hoogh, K.; Andersen, Z.J.; Bellander, T.; Brandt, J.; Forastiere, F.; Brynedal, B.; et al. Multiple myeloma risk in relation to long-term air pollution exposure—A pooled analysis of four European cohorts. *Environ. Res.* **2023**, *239*, 117230. [CrossRef]
5. Went, M.; Sud, A.; Försti, A.; Halvarsson, B.-M.; Weinhold, N.; Kimber, S.; van Duin, M.; Thorleifsson, G.; Holroyd, A.; Johnson, D.C.; et al. Identification of multiple risk loci and regulatory mechanisms influencing susceptibility to multiple myeloma. *Nat. Commun.* **2018**, *9*, 3707. [CrossRef] [PubMed]
6. White, B.S.; Lanc, I.; O'Neal, J.; Gupta, H.; Fulton, R.S.; Schmidt, H.; Fronick, C.; Belter, E.A.; Fiala, M.; King, J.; et al. A multiple myeloma-specific capture sequencing platform discovers novel translocations and frequent, risk-associated point mutations in IGLL5. *Blood Cancer J.* **2018**, *8*, 35. [CrossRef] [PubMed]
7. Paner, A.; Patel, P.; Dhakal, B. The evolving role of translocation t(11;14) in the biology, prognosis, and management of multiple myeloma. *Blood Rev.* **2020**, *41*, 100643. [CrossRef]
8. Fotiou, D.; Katodritou, E. From biology to clinical practice: The bone marrow microenvironment in multiple myeloma. *J. Clin. Med.* **2025**, *14*, 327. [CrossRef]
9. García-Ortiz, A.; Rodríguez-García, Y.; Encinas, J.; Maroto-Martín, E.; Castellano, E.; Teixidó, J.; Martínez-López, J. The role of tumor microenvironment in multiple myeloma development and progression. *Cancers* **2021**, *13*, 217. [CrossRef]
10. Alabanza, L.M.; Xiong, Y.; Vu, B.; Webster, B.; Wu, D.; Hu, P.; Zhu, Z.; Dropulic, B.; Dash, P.; Schneider, D. Armored BCMA CAR T cells eliminate multiple myeloma and are resistant to the suppressive effects of TGF-β. *Front. Immunol.* **2022**, *13*, 832645. [CrossRef]
11. Swamydas, M.; Murphy, E.V.; Ignatz-Hoover, J.J.; Malek, E.; Driscoll, J.J. Deciphering mechanisms of immune escape to inform immunotherapeutic strategies in multiple myeloma. *J. Hematol. Oncol.* **2022**, *15*, 17. [CrossRef]
12. Lu, Q.; Yang, D.; Li, H.; Niu, T.; Tong, A. Multiple myeloma: Signaling pathways and targeted therapy. *Mol. Biomed.* **2024**, *5*, 25. [CrossRef]

13. Wallington-Beddoe, C.T.; Sobieraj-Teague, M.; Kuss, B.J.; Pitson, S.M. Resistance to proteasome inhibitors and other targeted therapies in myeloma. *Br. J. Haematol.* **2018**, *182*, 11–28. [CrossRef]
14. Moreau, P.; Attal, M.; Facon, T. Frontline therapy of multiple myeloma. *Blood* **2015**, *125*, 3076–3084. [CrossRef]
15. Pinto, V.; Bergantim, R.; Caires, H.R.; Seca, H.; Guimarães, J.E.; Vasconcelos, M.H. Multiple myeloma: Available therapies and causes of drug resistance. *Cancers* **2020**, *12*, 407. [CrossRef]
16. Alaterre, E.; Ovejero, S.; Herviou, L.; de Boussac, H.; Papadopoulos, G.; Kulis, M.; Boireau, S.; Robert, N.; Requirand, G.; Bruyer, A.; et al. Comprehensive characterization of the epigenetic landscape in multiple myeloma. *Theranostics* **2022**, *12*, 1715–1729. [CrossRef]
17. Wu, Y.-X.; Yang, J.-H.; Saitsu, H. Bortezomib-resistance is associated with increased levels of proteasome subunits and apoptosis-avoidance. *Oncotarget* **2016**, *7*, 77622–77634. [CrossRef]
18. Pan, Y.; Zhang, Y.; Liu, W.; Huang, Y.; Shen, X.; Jing, R.; Pu, J.; Wang, X.; Ju, S.; Cong, H.; et al. LncRNA H19 overexpression induces bortezomib resistance in multiple myeloma by targeting MCL-1 via miR-29b-3p. *Cell Death Dis.* **2019**, *10*, 106. [CrossRef]
19. Yue, T.; Sun, Y.; Dai, Y.; Jin, F. Mechanisms for resistance to BCMA-targeted immunotherapies in multiple myeloma. *Blood Rev.* **2025**, *70*, 101256. [CrossRef]
20. Vaghari-Tabari, M.; Hassanpour, P.; Sadeghsoltani, F.; Malakoti, F.; Alemi, F.; Qujeq, D.; Asemi, Z.; Yousefi, B. CRISPR/Cas9 gene editing: A new approach for overcoming drug resistance in cancer. *Cell. Mol. Biol. Lett.* **2022**, *27*, 49. [CrossRef]
21. Davies, N.M.; Holmes, M.V.; Smith, G.D. Reading Mendelian randomisation studies: A guide, glossary, and checklist for clinicians. *BMJ* **2018**, *362*, k601. [CrossRef] [PubMed]
22. Prats-Uribe, A.; Sayols-Baixeras, S.; Fernández-Sanlés, A.; Subirana, I.; Carreras-Torres, R.; Vilahur, G.; Civeira, F.; Marrugat, J.; Fitó, M.; Hernáez, Á.; et al. High-density lipoprotein characteristics and coronary artery disease: A Mendelian randomization study. *Metabolism* **2020**, *112*, 154351. [CrossRef]
23. Georgiou, A.N.; Ntritsos, G.; Papadimitriou, N.; Dimou, N.; Evangelou, E. Cigarette smoking, coffee consumption, alcohol intake, and risk of Crohn's disease and ulcerative colitis: A Mendelian randomization study. *Inflamm. Bowel Dis.* **2021**, *27*, 162–168. [CrossRef] [PubMed]
24. Yarmolinsky, J.; Bouras, E.; Constantinescu, A.; Burrows, K.; Bull, C.J.; Vincent, E.E.; Martin, R.M.; Dimopoulou, O.; Lewis, S.J.; Moreno, V.; et al. Genetically proxied glucose-lowering drug target perturbation and risk of cancer: A Mendelian randomisation analysis. *Diabetologia* **2023**, *66*, 1481–1500. [CrossRef] [PubMed]
25. Yarmolinsky, J.; Díez-Obrero, V.; Richardson, T.G.; Pigeyre, M.; Sjaarda, J.; Paré, G.; Walker, V.M.; Vincent, E.E.; Tan, V.Y.; Obón-Santacana, M.; et al. Genetically proxied therapeutic inhibition of antihypertensive drug targets and risk of common cancers: A mendelian randomization analysis. *PLoS Med.* **2022**, *19*, e1003897. [CrossRef]
26. Wang, Q.; Shi, Q.; Wang, Z.; Lu, J.; Hou, J. Integrating plasma proteomes with genome-wide association data for causal protein identification in multiple myeloma. *BMC Med.* **2023**, *21*, 377. [CrossRef]
27. Lin, Z.; Pan, W. A robust cis-Mendelian randomization method with application to drug target discovery. *Nat. Commun.* **2024**, *15*, 6072. [CrossRef]
28. Schmidt, A.F.; Finan, C.; Gordillo-Marañón, M.; Asselbergs, F.W.; Freitag, D.F.; Patel, R.S.; Tyl, B.; Chopade, S.; Faraway, R.; Zwierzyna, M.; et al. Genetic drug target validation using Mendelian randomisation. *Nat. Commun.* **2020**, *11*, 3255. [CrossRef] [PubMed]
29. Yeung, S.L.A.; Gill, D. Standardizing the reporting of Mendelian randomization studies. *BMC Med.* **2023**, *21*, 187. [CrossRef]
30. Sun, Z.; Yun, Z.; Lin, J.; Sun, X.; Wang, Q.; Duan, J.; Li, C.; Zhang, X.; Xu, S.; Wang, Z.; et al. Comprehensive Mendelian randomization analysis of plasma proteomics to identify new therapeutic targets for the treatment of coronary heart disease and myocardial infarction. *J. Transl. Med.* **2024**, *22*, 404. [CrossRef]
31. Liu, A.E.; Kang, H.M. Meta-imputation of transcriptome from genotypes across multiple datasets by leveraging publicly available summary-level data. *PLoS Genet.* **2022**, *18*, e1009571. [CrossRef]
32. Evans, P.; Nagai, T.; Konkashbaev, A.; Zhou, D.; Knapik, E.W.; Gamazon, E.R. Transcriptome-Wide Association Studies (TWAS): Methodologies, Applications, and Challenges. *Curr. Protoc.* **2024**, *4*, e981. [CrossRef]
33. Rasooly, D.; Peloso, G.M.; Giambartolomei, C. Bayesian genetic colocalization test of two traits using coloc. *Curr. Protoc.* **2022**, *2*, e627. [CrossRef]
34. Agu, P.C.; Afiukwa, C.A.; Orji, O.U.; Ezeh, E.M.; Ofoke, I.H.; Ogbu, C.O.; Ugwuja, E.I.; Aja, P.M. Molecular docking as a tool for the discovery of molecular targets of nutraceuticals in diseases management. *Sci. Rep.* **2023**, *13*, 13398. [CrossRef]
35. Gong, W.; Sun, P.; Li, X.; Wang, X.; Zhang, X.; Cui, H.; Yang, J. Investigating the molecular mechanisms of resveratrol in treating cardiometabolic multimorbidity: A network pharmacology and bioinformatics approach with molecular docking validation. *Nutrients* **2024**, *16*, 2488. [CrossRef]
36. Finan, C.; Gaulton, A.; Kruger, F.A.; Lumbers, R.T.; Shah, T.; Engmann, J.; Galver, L.; Kelley, R.; Karlsson, A.; Santos, R.; et al. The druggable genome and support for target identification and validation in drug development. *Sci. Transl. Med.* **2017**, *9*, eaag1166. [CrossRef] [PubMed]

37. Võsa, U.; Claringbould, A.; Westra, H.-J.; Bonder, M.J.; Deelen, P.; Zeng, B.; Kirsten, H.; Saha, A.; Kreuzhuber, R.; Yazar, S.; et al. Large-scale cis- and trans-eQTL analyses identify thousands of genetic loci and polygenic scores that regulate blood gene expression. *Nat. Genet.* **2021**, *53*, 1300–1310. [CrossRef] [PubMed]
38. Liu, Z.; Peng, Z.; Lin, H.; Zhou, K.; Liang, L.; Cao, J.; Huang, Z.; Mei, J. Identifying potential drug targets for idiopathic pulmonary fibrosis: A Mendelian randomization study based on the druggable genes. *Respir. Res.* **2024**, *25*, 217. [CrossRef]
39. Mathieu, S.; Briend, M.; Abner, E.; Couture, C.; Li, Z.; Bossé, Y.; Thériault, S.; Esko, T.; Arsenault, B.J.; Mathieu, P. Genetic association and Mendelian randomization for hypothyroidism highlight immune molecular mechanisms. *iScience* **2022**, *25*, 104992. [CrossRef]
40. Yuan, S.; Chen, J.; Geng, J.; Zhao, S.S.; Yarmolinsky, J.; Arkema, E.V.; Abramowitz, S.; Levin, M.G.; Tsilidis, K.K.; Burgess, S.; et al. GWAS identifies genetic loci, lifestyle factors and circulating biomarkers that are risk factors for sarcoidosis. *Nat. Commun.* **2025**, *16*, 2481. [CrossRef]
41. Garfield, V.; Salzmann, A.; Burgess, S.; Chaturvedi, N. A guide for selection of genetic instruments in Mendelian randomization studies of type 2 diabetes and HbA1c: Toward an integrated approach. *Diabetes* **2023**, *72*, 175–183. [CrossRef] [PubMed]
42. Bycroft, C.; Freeman, C.; Petkova, D.; Band, G.; Elliott, L.T.; Sharp, K.; Motyer, A.; Vukcevic, D.; Delaneau, O.; O'Connell, J.; et al. The UK Biobank resource with deep phenotyping and genomic data. *Nature* **2018**, *562*, 203–209. [CrossRef] [PubMed]
43. Zhou, W.; Nielsen, J.B.; Fritsche, L.G.; Dey, R.; Gabrielsen, M.E.; Wolford, B.N.; LeFaive, J.; VandeHaar, P.; Gagliano, S.A.; Gifford, A.; et al. Efficiently controlling for case–control imbalance and sample relatedness in large-scale genetic association studies. *Nat. Genet.* **2018**, *50*, 1335–1341. [CrossRef]
44. Burgess, S.; Foley, C.N.; Allara, E.; Staley, J.R.; Howson, J.M.M. A robust and efficient method for Mendelian randomization with hundreds of genetic variants. *Nat. Commun.* **2020**, *11*, 376. [CrossRef]
45. Chen, S.; Sun, S.; Cai, M.; Zhou, Z.; Ma, Y.; Zhou, Z.; Wang, F.; Liu, J.; Song, W.; Liu, Y.; et al. A metabolome-wide Mendelian randomization study prioritizes causal circulating metabolites for reproductive disorders including primary ovarian insufficiency, polycystic ovary syndrome, and abnormal spermatozoa. *J. Ovarian Res.* **2024**, *17*, 166. [CrossRef]
46. Mai, J.; Lu, M.; Gao, Q.; Zeng, J.; Xiao, J. Transcriptome-wide association studies: Recent advances in methods, applications and available databases. *Commun. Biol.* **2023**, *6*, 899. [CrossRef]
47. Zuber, V.; Grinberg, N.F.; Gill, D.; Manipur, I.; Slob, E.A.; Patel, A.; Wallace, C.; Burgess, S. Combining evidence from Mendelian randomization and colocalization: Review and comparison of approaches. *Am. J. Hum. Genet.* **2022**, *109*, 767–782. [CrossRef]
48. Li, Y.; Song, X.; Huang, Y.; Zhou, S.; Zhong, L. Genetic associations of plasma metabolites with immune cells in hyperthyroidism revealed by Mendelian randomization and GWAS-sc-eQTLs xQTLbiolinks analysis. *Sci. Rep.* **2025**, *15*, 1377. [CrossRef]
49. Wallace, C. Eliciting priors and relaxing the single causal variant assumption in colocalisation analyses. *PLoS Genet.* **2020**, *16*, e1008720. [CrossRef]
50. Wang, Z.; Li, S.; Cai, G.; Gao, Y.; Yang, H.; Li, Y.; Liang, J.; Zhang, S.; Hu, J.; Zheng, J. Mendelian randomization analysis identifies druggable genes and drugs repurposing for chronic obstructive pulmonary disease. *Front. Cell. Infect. Microbiol.* **2024**, *14*, 1386506. [CrossRef]
51. Yuan, S.; Sun, J.; Lu, Y.; Xu, F.; Li, D.; Jiang, F.; Wan, Z.; Li, X.; Qin, L.-Q.; Larsson, S.C. Health effects of milk consumption: Phenome-wide Mendelian randomization study. *BMC Med.* **2022**, *20*, 55. [CrossRef] [PubMed]
52. Yu, X.; Lophatananon, A.; Mekli, K.; Muir, K.R.; Guo, H. Exploring the causal role of the immune response to varicella-zoster virus on multiple traits: A phenome-wide Mendelian randomization study. *BMC Med.* **2023**, *21*, 143. [CrossRef]
53. Gibson, M.J.; Lawlor, D.A.; Millard, L.A.C. Identifying the potential causal role of insomnia symptoms on 11,409 health-related outcomes: A phenome-wide Mendelian randomization analysis in UK Biobank. *BMC Med.* **2023**, *21*, 128. [CrossRef] [PubMed]
54. Valdés-Tresanco, M.S.; Valdés-Tresanco, M.E.; Valiente, P.A.; Moreno, E. AMDock: A versatile graphical tool for assisting molecular docking with Autodock Vina and Autodock4. *Biol. Direct.* **2020**, *15*, 12. [CrossRef]
55. Eberhardt, J.; Santos-Martins, D.; Tillack, A.F.; Forli, S. AutoDock Vina 1.2.0: New docking methods, expanded force field, and Python bindings. *J. Chem. Inf. Model.* **2021**, *61*, 3891–3898. [CrossRef]
56. Nguyen, N.T.; Nguyen, T.H.; Pham, T.N.H.; Huy, N.T.; Bay, M.V.; Pham, M.Q.; Nam, P.C.; Vu, V.V.; Ngo, S.T. AutoDock Vina adopts more accurate binding poses but AutoDock4 forms better binding affinity. *J. Chem. Inf. Model.* **2020**, *60*, 204–211. [CrossRef] [PubMed]
57. Bustin, S.A.; Benes, V.; Garson, J.A.; Hellemans, J.; Huggett, J.; Kubista, M.; Mueller, R.; Nolan, T.; Pfaffl, M.W.; Shipley, G.L.; et al. The MIQE guidelines: Minimum information for publication of quantitative real-time PCR experiments. *Clin. Chem.* **2009**, *55*, 611–622. [CrossRef]
58. Schmittgen, T.D.; Livak, K.J. Analyzing real-time PCR data by the comparative C_T method. *Nat. Protoc.* **2008**, *3*, 1101–1108. [CrossRef]
59. Taylor, S.C.; Rosselli-Murai, L.K.; Crobeddu, B.; Plante, I. A critical path to producing high quality, reproducible data from quantitative western blot experiments. *Sci. Rep.* **2022**, *12*, 17599. [CrossRef]

60. Gamazon, E.R.; GTEx Consortium; Wheeler, H.E.; Shah, K.P.; Mozaffari, S.V.; Aquino-Michaels, K.; Carroll, R.J.; Eyler, A.E.; Denny, J.C.; Nicolae, D.L.; et al. A gene-based association method for mapping traits using reference transcriptome data. *Nat. Genet.* **2015**, *47*, 1091–1098. [CrossRef]
61. Huang, M.; Wu, Y.; Li, Y.; Chen, X.; Feng, J.; Li, Z.; Li, J.; Chen, J.; Lu, Y.; Feng, Y. Circadian clock-related genome-wide Mendelian randomization identifies putatively genes for ulcerative colitis and its comorbidity. *BMC Genom.* **2024**, *25*, 130. [CrossRef]
62. Lu, Y.; Lu, D.; Zhang, H.; Li, H.; Yu, B.; Zhang, Y.; Hu, H.; Sheng, H. Causality between ankylosing spondylitis and osteoarthritis in European ancestry: A bidirectional Mendelian randomization study. *Front. Immunol.* **2024**, *15*, 1297454. [CrossRef]
63. Xu, J.; Si, S.; Han, Y.; Zeng, L.; Zhao, J. Genetic insight into dissecting the immunophenotypes and inflammatory profiles in the pathogenesis of Sjogren syndrome. *J. Transl. Med.* **2025**, *23*, 56. [CrossRef]
64. Ocio, E.M.; Motlló, C.; Rodríguez-Otero, P.; Martínez-López, J.; Cejalvo, M.J.; Martín-Sánchez, J.; Bladé, J.; García-Malo, M.D.; Dourdil, M.V.; García-Mateo, A.; et al. Filanesib in combination with pomalidomide and dexamethasone in refractory MM patients: Safety and efficacy, and association with alpha 1-acid glycoprotein (AAG) levels. Phase Ib/II Pomdefil clinical trial conducted by the Spanish MM group. *Br. J. Haematol.* **2021**, *192*, 522–530. [CrossRef]
65. Gao, Y.; Liu, X.; Li, T.; Wei, L.; Yang, A.; Lu, Y.; Zhang, J.; Li, L.; Wang, S.; Yin, F. Cross-validation of genes potentially associated with overall survival and drug resistance in ovarian cancer. *Oncol. Rep.* **2017**, *37*, 3084–3092. [CrossRef]
66. Gabbasov, R.; Xiao, F.; Howe, C.G.; Bickel, L.E.; O'Brien, S.W.; Benrubi, D.; Do, T.-V.; Zhou, Y.; Nicolas, E.; Cai, K.Q.; et al. NEDD9 promotes oncogenic signaling, a stem/mesenchymal gene signature, and aggressive ovarian cancer growth in mice. *Oncogene* **2018**, *37*, 4854–4870. [CrossRef] [PubMed]
67. Han, Q.-J.; Zhu, Y.-P.; Sun, J.; Ding, X.-Y.; Wang, X.; Zhang, Q.-Z. PTGES2 and RNASET2 identified as novel potential biomarkers and therapeutic targets for basal cell carcinoma: Insights from proteome-wide Mendelian randomization, colocalization, and MR-PheWAS analyses. *Front. Pharmacol.* **2024**, *15*, 1418560. [CrossRef]
68. Schverer, M.; Lanfumey, L.; Baulieu, E.-E.; Froger, N.; Villey, I. Neurosteroids: Non-genomic pathways in neuroplasticity and involvement in neurological diseases. *Pharmacol. Ther.* **2018**, *191*, 190–206. [CrossRef]
69. Bailly, C. Irinotecan: 25 years of cancer treatment. *Pharmacol. Res.* **2019**, *148*, 104398. [CrossRef]
70. Cheng, X.; Liu, D.; Xing, R.; Song, H.; Tian, X.; Yan, C.; Han, Y. Orosomucoid 1 attenuates doxorubicin-induced oxidative stress and apoptosis in cardiomyocytes via Nrf2 signaling. *Biomed Res. Int.* **2020**, *2020*, 5923572. [CrossRef]
71. Yin, D.-M.; Yuan, D.; Sun, R.-J.; Xu, H.-Z.; Hun, S.-Y.; Sui, X.-H.; Shan, N.-N. Identification of ORM1, vWF, SPARC, and PPBP as immune-related proteins involved in immune thrombocytopenia by quantitative LC–MS/MS. *Clin. Proteom.* **2023**, *20*, 24. [CrossRef] [PubMed]
72. Sun, Y.; Wang, F.; Zhou, Z.; Teng, J.; Su, Y.; Chi, H.; Wang, Z.; Hu, Q.; Jia, J.; Liu, T.; et al. Urinary proteomics identifying novel biomarkers for the diagnosis of adult-onset Still's disease. *Front. Immunol.* **2020**, *11*, 2112. [CrossRef]
73. Ramsay, T.G.; Stoll, M.J.; Blomberg, L.A.; Caperna, T.J. Regulation of cytokine gene expression by orosomucoid in neonatal swine adipose tissue. *J. Anim. Sci. Biotechnol.* **2016**, *7*, 25. [CrossRef]
74. Qiong, L.; Yin, J. Orosomucoid 1 promotes epirubicin resistance in breast cancer by upregulating the expression of matrix metalloproteinases 2 and 9. *Bioengineered* **2021**, *12*, 8822–8832. [CrossRef]
75. He, J.; Zheng, Z.; Liu, T.; Ao, Y.; Yang, Y.; Hu, H. Salivary orosomucoid 1 as a biomarker of hepatitis B associated hepatocellular carcinoma. *Sci. Rep.* **2022**, *12*, 15347. [CrossRef]
76. Yue, L.; Xu, X.; Dai, S.; Xu, F.; Zhao, W.; Gu, J.; Dai, X.; Qian, X. Orosomucoid 1 promotes colorectal cancer progression and liver metastasis by affecting PI3K/AKT pathway and inducing macrophage M2 polarization. *Sci. Rep.* **2023**, *13*, 14092. [CrossRef]
77. Meng, H.; Jiang, X.; Huang, H.; Shen, N.; Guo, C.; Yu, C.; Yin, G.; Wang, Y. A MUCINs expression signature impacts overall survival in patients with clear cell renal cell carcinoma. *Cancer Med.* **2021**, *10*, 5823–5838. [CrossRef]
78. Flesken-Nikitin, A.; Ralston, C.Q.; Fu, D.-J.; De Micheli, A.J.; Phuong, D.J.; Harlan, B.A.; Ashe, C.S.; Armstrong, A.P.; McKellar, D.W.; Ghuwalewala, S.; et al. Preciliated tubal epithelial cells are prone to initiation of high-grade serous ovarian carcinoma. *Nat. Commun.* **2024**, *15*, 8641. [CrossRef]
79. García-Vázquez, F.A.; Garrappa, G.; Luongo, C.; Hamze, J.G.; Caballero, M.; Marco-Jiménez, F.; Antón, J.S.V.; Molina-Cuberos, G.J.; Jiménez-Movilla, M. Magnetic-assisted control of eggs and embryos via zona pellucida-linked nanoparticles. *Adv. Sci.* **2024**, *11*, e2306901. [CrossRef]
80. Laheri, S.; Ashary, N.; Bhatt, P.; Modi, D. Oviductal glycoprotein 1 (OVGP1) is expressed by endometrial epithelium that regulates receptivity and trophoblast adhesion. *J. Assist. Reprod. Genet.* **2018**, *35*, 1419–1429. [CrossRef]
81. Cosentino, G.; Romero-Cordoba, S.; Plantamura, I.; Cataldo, A.; Iorio, M.V. miR-9-mediated inhibition of EFEMP1 contributes to the acquisition of pro-tumoral properties in normal fibroblasts. *Cells* **2020**, *9*, 2143. [CrossRef] [PubMed]
82. Thomas, A.; Pommier, Y. Targeting Topoisomerase I in the era of precision medicine. *Clin. Cancer Res.* **2019**, *25*, 6581–6589. [CrossRef]

83. Chen, C.-I.; Chen, Y.-C.; Kao, Y.-K.; Chen, C.-H.; Yang, P.-W.; Chen, P.-C.; Song, L.-C.; Tsai, K.L. Taurine protects irinotecan-induced muscle dysfunction by modulating oxidative stress and endoplasmic reticulum stress in human skeletal muscle cells. *Anticancer Res.* **2024**, *44*, 5371–5378. [CrossRef]
84. Giannotta, C.; Autino, F.; Massaia, M. The immune suppressive tumor microenvironment in multiple myeloma: The contribution of myeloid-derived suppressor cells. *Front. Immunol.* **2023**, *13*, 1102471. [CrossRef] [PubMed]
85. Maiso, P.; Mogollón, P.; Ocio, E.M.; Garayoa, M. Bone marrow mesenchymal stromal cells in multiple myeloma: Their role as active contributors to myeloma progression. *Cancers* **2021**, *13*, 2542. [CrossRef]
86. Agrawal, B.; Gupta, N.; Konowalchuk, J.D. MUC1 mucin: A putative regulatory (checkpoint) molecule of T cells. *Front. Immunol.* **2018**, *9*, 2391. [CrossRef]
87. Zhao, L.; Cheng, S.; Fan, L.; Zhang, B.; Xu, S. TIM-3: An update on immunotherapy. *Int. Immunopharmacol.* **2021**, *99*, 107933. [CrossRef]
88. Osorio, D.; Yu, X.; Yu, P.; Serpedin, E.; Cai, J.J. Single-cell RNA sequencing of a European and an African lymphoblastoid cell line. *Sci. Data* **2019**, *6*, 112. [CrossRef] [PubMed]
89. Xia, J.; Zhang, J.; Wu, X.; Du, W.; Zhu, Y.; Liu, X.; Liu, Z.; Meng, B.; Guo, J.; Yang, Q.; et al. Blocking glycine utilization inhibits multiple myeloma progression by disrupting glutathione balance. *Nat. Commun.* **2022**, *13*, 4007. [CrossRef]
90. Skrivankova, V.W.; Richmond, R.C.; Woolf, B.A.R.; Yarmolinsky, J.; Davies, N.M.; Swanson, S.A.; VanderWeele, T.J.; Higgins, J.P.T.; Timpson, N.J.; Dimou, N.; et al. Strengthening the Reporting of Observational Studies in Epidemiology using Mendelian Randomization (STROBE-MR) Statement. *JAMA* **2021**, *326*, 1614–1621.
91. Skrivankova, V.W.; Richmond, R.C.; Woolf, B.A.R.; Davies, N.M.; Swanson, S.A.; VanderWeele, T.J.; Timpson, N.J.; Higgins, J.P.T.; Dimou, N.; Langenberg, C.; et al. Strengthening the Reporting of Observational Studies in Epidemiology using Mendelian Randomisation (STROBE-MR): Explanation and Elaboration. *BMJ* **2021**, *375*, n2233.

Disclaimer/Publisher's Note: The statements, opinions and data contained in all publications are solely those of the individual author(s) and contributor(s) and not of MDPI and/or the editor(s). MDPI and/or the editor(s) disclaim responsibility for any injury to people or property resulting from any ideas, methods, instructions or products referred to in the content.

biomedicines

MDPI

Article

Diminishing Hepcidin via Reducing *IL-6*/STAT3 Pathway by Utilizing Ferulic Acid: An In Vitro Study

Ola M. Al-Sanabra [1,*], Luay F. Abu-Qatouseh [2], Mohammad I. A. Ahmad [3,4], Mutaz Jamal Al-Khreisat [3] and Majd M. Alsaleh [5,6]

[1] Department of Medical Laboratory Sciences, Faculty of Allied Medical Sciences, Al-Balqa Applied University, Al-Salt 19117, Jordan
[2] Department of Medical Analyses, Faculty of Pharmacy and Medical Sciences, University of Petra, Amman 11196, Jordan; labuqatouseh@uop.edu.jo
[3] Department of Medical Laboratory Sciences, Faculty of Allied Medical Sciences, Al-Ahliyya Amman University, Amman 19328, Jordan; m.malkawy@ammanu.edu.jo (M.I.A.A.); m.alkhreisat@ammanu.edu.jo (M.J.A.-K.)
[4] Pharmacological and Diagnostic Research Center (PDRC), Faculty of Pharmacy, Al-Ahliyya Amman University, Amman, 19328, Jordan
[5] Department of Allied Medical Sciences, Al-Balqa Applied University, Al-Salt 19117, Jordan; majd.alsaleh@bau.edu.jo
[6] Department of Biology, Faculty of Science, University of Jordan, Amman 11942, Jordan
* Correspondence: ola.sanabra@bau.edu.jo

Abstract: Background/Objectives: Hepcidin is a negative regulator of iron absorption that is released by hepatocytes. It is one of the main contributors to hypoferremia and anemia in inflammatory and oncological disorders that are mediated by the proinflammatory cytokine *IL-6*/STAT3 pathway. Ferulic acid (FA) is a phenolic compound with pleiotropic biological activities, including anti-inflammatory activity. However, its effect on hepcidin secretion is still unknown. Thus, this study aimed to explore the impact of FA on hepcidin levels and the underlying mechanism. **Methods**: HepG2 cells were treated with different log percentages of FA, and their viability was determined via the MTT assay. The relative expression of *IL-6* and *HAMP* in treated and untreated cells was measured via qRT-PCR, and the protein levels of hepcidin, *IL-6* and STAT3 were measured using ELISA. **Results**: The MTT test showed an inverse relationship between FA concentrations and HepG2 cell proliferation; FA's IC_{50} value was 0.07669%. The expression levels of *IL-6* and *HAMP* were significantly increased in HepG2 cells following 24 h of culture with 4 μg/mL LPS. Meanwhile, the addition of FA significantly decreased the relative expression levels of these two genes and the secretion levels of *IL-6*, STAT3 and hepcidin compared to the cells treated with LPS alone. **Conclusions**: Overall, these findings show that FA modifies inflammatory pathways, affecting hepcidin levels via the *IL-6*/STAT3 pathway. Thus, this suggests FA as a potential therapeutic agent against the hypoferremia and anemia developed due to dysregulated hepcidin levels in diseases such as inflammatory and oncological disorders.

Keywords: hepcidin; *IL-6*/STAT3 pathway; ferulic acid; hypoferremia; anemia

1. Introduction

Iron homeostasis is a critical physiological process that ensures the balance of iron levels in the body and prevents both iron deficiency and overload. The typical serum iron concentration in adults ranges from 60 to 200 μg/100 mL, and variations beyond this range have been observed in healthy individuals, indicating a potential variability in iron regulation [1]. Central to this regulation is hepcidin, a liver-derived hormone that

responds to changes in iron levels and inflammatory signals. Elevated iron stores or reduced erythropoietic activity stimulates hepcidin production, while conditions such as anemia and hypoxia suppress it [2]. Hepcidin regulates iron levels by binding to ferroportin, the primary cellular iron exporter, which leads to its internalization and degradation. This process, which occurs in the spleen, duodenum and placenta, reduces dietary iron absorption and iron release from cells, increasing intracellular iron stores and decreasing levels of circulating iron [3]. Inflammation significantly influences hepcidin production, with proinflammatory cytokines such as interlukein-6 (*IL-6*) playing a key role [4]. *IL-6* stimulates hepcidin synthesis in hepatocytes via the JAK2-STAT3 signaling pathway, which regulates hepcidin expression from the *HAMP* gene located on chromosome 19 [5,6].

Cancer has increasingly begun to be recognized as a metabolic disorder with inflammation playing a pivotal role in its initiation and progression. Metabolic alterations in cancer cells, including changes in glucose, fatty acids, glutamine, and iron metabolism, are driven by oncogenes and tumor suppressor genes. These changes not only meet the heightened energy demands of cancer cells but also create an inflammatory tumor microenvironment that promotes tumor proliferation and metastasis [7]. Iron, which is essential for DNA synthesis and repair [8], is often deregulated in cancer, leading to iron overload and the disruption of homeostasis. Elevated hepcidin levels are associated with poor survival outcomes in cancer patients, particularly during hematopoietic stem cell transplantation [9], and have been observed in various cancers, including colorectal carcinoma [10], breast carcinoma [11], esophageal carcinoma [12], urothelial and renal neoplasms [13] and hepatic carcinoma [14]. This suggests that hepcidin may serve as a prognostic biomarker in cancer.

Ferulic acid (FA), a natural compound with well-documented antioxidant and anti-inflammatory properties, has shown promise in mitigating the inflammation associated with hepatocellular carcinoma (HCC), the most common liver cancer [15]. Chronic liver injury and inflammation are the primary drivers of HCC, with inflammatory signaling pathways facilitating the transition from liver damage to malignancy [16]. Cytokines, which are critical mediators of inflammation, are implicated in HCC development, highlighting the importance of targeting these pathways in therapeutic interventions [17]. FA has been shown to modulate cytokine production, potentially alleviating the inflammatory environment that promotes liver cancer progression [18]. Furthermore, iron homeostasis, which is governed by hepcidin, is frequently disrupted in chronic liver disease and inflammation, thereby complicating the pathophysiology of HCC [16]. Given the frequent disruption of iron homeostasis in these conditions, the interplay between FA's anti-inflammatory effects and hepcidin regulation offers a promising strategy for reducing liver cancer risk. Investigating the synergistic effects of the modulation of FA and hepcidin could provide novel insights into therapeutic approaches for liver cancer prevention and management [16].

Despite FA's potential in treating inflammatory and oncological disorders, the complexity of liver diseases and the multifactorial nature of cancer necessitate further research. A deeper understanding of FA's role in iron homeostasis and its interaction with hepcidin is essential to determine its efficacy and safety in clinical applications. This study aimed to explore the impact of FA on hepcidin levels in vitro, marking the first investigation of the connection between FA and hepcidin modulation. By investigating this relationship, we hope to contribute to the development of innovative therapeutic strategies for liver cancer and iron-associated disorders.

2. Materials and Methods

2.1. Chemical Reagents and Ferulic Acid (FA) Preparation

A stock of FA solution was prepared by dissolving (100 mg) FA with purity > 98% (Abcam, Cambridge, UK) in 1 mL of dimethyl sulfoxide (DMSO) with purity > 99%

(ThermoFisher, Waltham, MA, USA). Afterwards, different log percentages of FA were prepared by diluting the stock solution.

2.2. Cell Line and Culture Conditions

The hepatocellular carcinoma-derived cell line HepG2 (HB-8065) was purchased from ATCC, Washington, DC, USA, and was cultured in modified Eagle medium (PAN-Biotech, GmbH, Aidenbach, Germany) supplemented with 10% fetal bovine serum (FBS) (Cytiva, Amersham, UK), 1% L-Glutamine (PAN-Biotech, GmbH), 1% penicillin–streptomycin (Capricorn Scientific GmbH, Ebsdorfergrund, Germany), 1% Amphotericin-B (PAN-Biotech, GmbH), 1% nonessential amino acids (EuroClone, Pero, Italy) and 1% sodium pyruvate (EuroClone) in a humified atmosphere of 5% of CO_2 and 37 °C. To ensure that the cell line was established, the HepG2 cells were passaged three times before starting the experiments. The medium was changed on alternate days to maintain optimal cell growth conditions.

2.3. Cell Viability Assessment

When the cell confluency was 70–80% in the fourth passage, the cells were detached via addition of 0.05% trypsin/EDTA (PAN-Biotech, GmbH). A total of 7×10^3 HepG2 cells were cultured in each well of a 96-well culture plate (SPL Life Science Co., Ltd., Pocheon-si, Republic of Korea), and the plate was incubated under the same culturing conditions mentioned previously. The seeded cells were treated with different log percentages of FA (−0.02−−0.5%) or vehicle (0.2%) DMSO and incubated for 24 h. Viability was examined via the MTT assay (Sigma, St. Louis, MO, USA). Briefly, after incubation for 24 h, 5 mg/mL of MTT reagent assay was added to the treated cells, and the plate was incubated for 3 h under similar culturing conditions. Next, as an indicator of the cell viability, the intensity and change in the reagent color in the plate were measured using a Multiskan GO spectrophotometer (Thermo Scientific, Cambridge, UK) at a wavelength of 570 nm. The cell viability assessment was conducted in triplicate.

2.4. Cell Treatment

At a concentration of 1×10^6, HepG2 cells were incubated in six-well plates containing the MEM with 10% FBS were incubated under a humified 5% CO_2 atmosphere at 37 °C for 24–48 h. Next, the medium was aspirated from each well and the following treatments were applied: fresh media, 0.1% stock FA only, 0.01% DMSO, 4 μg lipopolysaccharide (LPS from *E. coli O55:B5*, ChemCruz, London, UK), 0.1% stock FA + 4 μg LPS. The plates were then incubated for an additional 24 h. Afterwards, the cells were trypsinized and harvested for either the extraction and isolation of RNA or for STAT3 levels' measurement. The HepG2 cell treatment was performed in triplicate.

2.5. RNA Extraction, cDNA Synthesis, and qRT-PCR

Total RNA was extracted and isolated from the harvested cells using the EasyPure RNA Kit (Transgen Biotech, Beijing, China) as per the manufacturer's instructions. Purity assessment and quantification of the isolated RNA were performed using a μDrop plate and Multiskan GO spectrophotometer (Thermo Scientific) at 260 and 280 nm. Then, 70 ng of total RNA was reverse transcribed to cDNA using the EasyScript First-Strand cDNA synthesis SuperMix kit (Transgen Biotech) following the manufacturer's protocol. Next, the qPCR reaction was carried out by using AriaDx Real-Time PCR (Diatech, Jesi, Italy) and the real-time SYBR Green method. Briefly, the 20 μL of amplification reaction consisted of 1 μL of cDNA, 10 μL of PerfectStart Green qPCR SuperMix (Transgen Biotech), 0.4 μL of 50× Universal Passive Reference Dye, 0.8 μL of 10 μM primers (IDT, Coralville, IA, USA) and 7.8 μL of water. The reaction was performed starting with initial inactivation at 94 °C for 30 s, followed by 40 cycles of denaturation at 94 °C for 5 s, annealing at 60 °C for

30 s and, finally, melting at 94 °C for 1 min. The relative mRNA expression level was determined using *GAPHD* as a housekeeping gene following the comparative $2^{-\Delta\Delta CT}$ calculation formula. The sequences of the primers used are shown in Table 1.

Table 1. Target gene primer sequences for quantitative real-time polymerase chain reaction.

Target Gene	Forward (3′ to 5′)	Reverse (3′ to 5′)
HAMP	TTCCTTCCTGGGCATGGA GT	GCAATGATCTTGATCTTCATT
IL-6	CACAACAGACGGGACAACTT	CGCAGCAGAAAATGCAGATG
GAPDH	GCCAAAAGGGTCATCATCTC	GGTGCTAAGCAGTTGGTGGT

2.6. Quantification of IL-6, STAT3 and Hepcidin Levels

The culture supernatants from the incubated untreated and treated (LPS only, FA only and LPS + FA) cells were collected after 24 h by centrifugation at 3000 rpm for 20 min. Subsequently, commercial ELISA kits were used to measure the levels of secreted *IL-6* (Invitrogen ThermoFisher Scientific) and hepcidin (Sunlong Biotech Co., Ltd., Hangzhou, China) following the manufacturer's instructions. For measuring phospho-STAT3, untreated and treated cell lysates were assessed using a commercial ELISA kit (R&D, Minneapolis, MN, USA) as per the manufacturer's instructions on the protocol.

2.7. Statistical Analysis

Data are presented as mean ± standard deviation (M ± SD). Outlier removal and checks for normality of residuals were performed before statistical comparisons. Statistical analysis was performed via one-way analysis of variance (ANOVA) or Student's paired *t*-test using GraphPad Prism Software 8 (GraphPad Software Inc., La Jolla, CA, USA).

3. Results

3.1. Determination of the IC_{50} and Viability of HepG2 Cells Treated with Ferulic Acid

The effect of FA on HepG2 cells' growth and proliferation was investigated using the MTT test. The results indicated an inverse relationship between viability and FA concentration; specifically, as the logarithmic concentration of FA increases, the cell viability decreases. Furthermore, the IC_{50} of FA was determined to be 0.07669% (Figure 1).

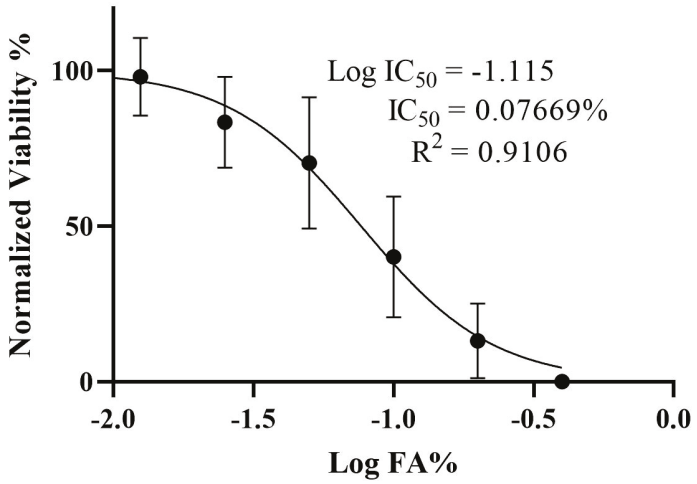

Figure 1. Determination of the IC_{50} and viability of HepG2 cells treated with ferulic acid. The viability percentage of viable HepG2 cells in response to treatment with different log percentages of ferulic acid was measured via MTT assay. Results represent M ± SD of independent triplicate experiments. IC_{50}: Half maximum inhibitory concentration.

3.2. Effect of Ferulic Acid on Hepcidin Secretion and Expression

In order to investigate the impact of FA on the secretion of hepcidin, we quantified the hepcidin levels induced by *IL-6* in HepG2 cells subjected to LPS treatment. This assessment was conducted following a 24 h exposure to 0.1% FA. A marked increase ($p \leq 0.01$) in the hepcidin secretion was observed in LPS-treated cells compared to the controls. Also, a significant reduction ($p \leq 0.05$) in the concentration of secreted hepcidin was observed in cells treated with 0.1% FA after they had been treated with LPS. Conversely, cells that received 4 μg/mL of LPS alone exhibited a marked elevation in hepcidin levels ($p \leq 0.05$). Furthermore, the hepcidin secretion from HepG2 cells treated with 0.1% FA after incubation with 4 μg/mL LPS demonstrated a marked decline (Figure 2A). Figure 2B shows the influence of LPS on the modulation of hepcidin following FA exposure in HepG2 cells; it specifically analyzes *HAMP* expression levels in the presence of FA or LPS. Treatment with FA alone led to a slight increase in *HAMP* expression compared to the controls. Meanwhile, cells treated with LPS alone had significantly ($p \leq 0.0001$) upregulated expression of the *HAMP* gene. However, the addition of 0.1% FA to the LPS-treated cells led to a significant ($p \leq 0.0001$) approximately four-fold decrease in *HAMP* expression levels.

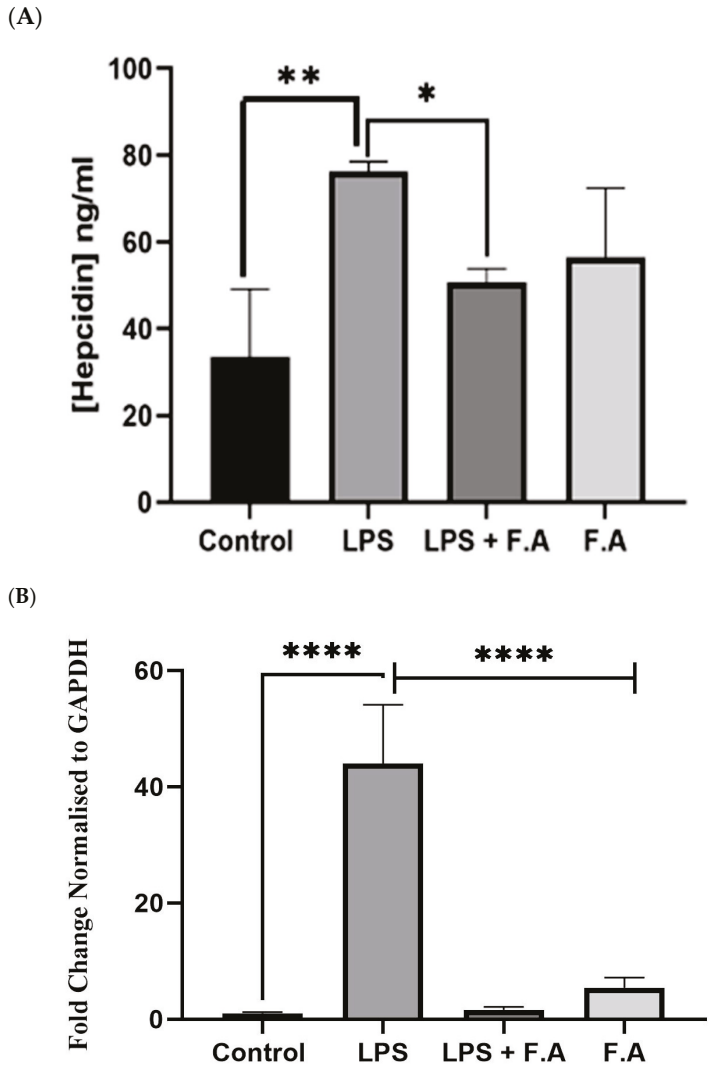

Figure 2. Reduction in hepcidin secretion and *HAMP* expression in response to ferulic acid. A 0.1% ferulic acid stock concentration diminishes (**A**) hepcidin secretion and (**B**) *HAMP* expression in HepG2 cells. Results represent the M ± SD of independent triplicate experiments. *p*-values indicate significance, as determined by Student's paired *t*-test or the one-way ANOVA test. Significance levels are represented as follows: * $p \leq 0.05$, ** $p \leq 0.01$, **** $p \leq 0.0001$.

3.3. Effect of Ferulic Acid on IL-6 Expression and Secretion

To measure the impact of LPS on *IL-6* levels after FA treatment in HepG2 cells, we looked at *IL-6* gene expression in response to treatment with either FA or LPS alone and their combination. The presence of 0.1% FA alone increased *IL-6* gene expression; however, this increase was significantly lower ($p \leq 0.01$) than that in cells treated with 4 µg/mL LPS alone. The combination of 0.1% FA and LPS caused a significant ($p \leq 0.001$) downregulation of *IL-6* gene expression compared to when cells were treated with LPS alone (Figure 3A). Additionally, to assess how FA affects inflammation in HepG2 cancer cells, we measured the increase in *IL-6* levels in cells treated with LPS for 24 h. Interestingly, *IL-6* levels showed a marked increase ($p \leq 0.0001$) in cells treated with LPS alone compared to controls. Meanwhile, cells treated with both FA and LPS exhibited a significant reduction in *IL-6* levels ($p \leq 0.01$). This reduction was about three times lower with FA than with LPS, as shown in Figure 3B.

(**A**)

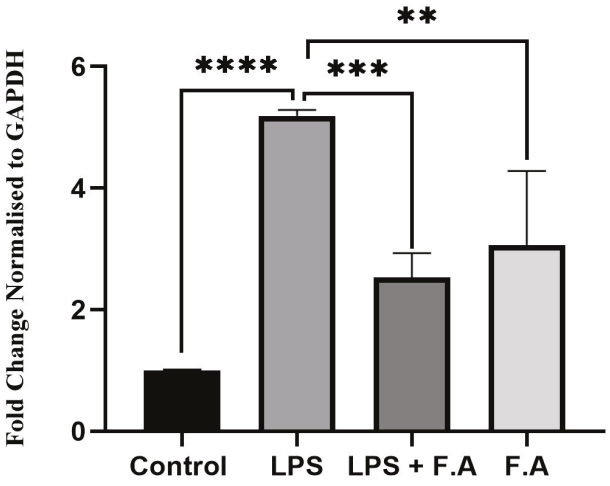

(**B**)

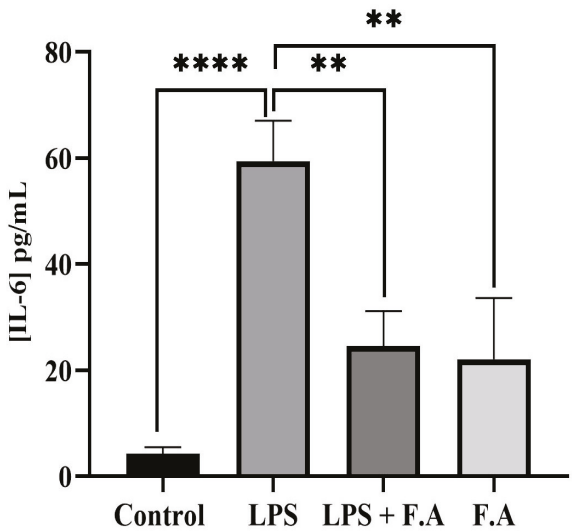

Figure 3. Reduction in proinflammatory *IL-6* expression and secretion via ferulic acid. A 0.1% of ferulic acid stock concentration decreased both the expression (**A**) and secretion of proinflammatory *IL-6* in HepG2 cells (**B**). Results represent the M ± SD of independent triplicate experiments. *p*-values indicate significance, as determined by the one-way ANOVA test. Significance levels are represented as follows: ** $p \leq 0.01$, *** $p \leq 0.001$, **** $p \leq 0.0001$.

3.4. Effect of Ferulic Acid on Phospho-STAT3 Secretion

To determine whether the modulation of hepcidin levels by ferulic acid occurred via the IL-STAT3 signaling cascade, we assessed phospho-STAT3 (Y-705) levels in HepG2 cells treated with FA alone, LPS alone or their combination. The results show that there was a significant ($p \leq 0.001$) increase in phospho-STAT3 (Y-705) levels in response to LPS alone compared to the controls. Meanwhile, the administration of 0.1% FA alone or 1% FA after LPS treatment resulted a significant reduction in phospho-STAT3 (Y-705) levels ($p \leq 0.0001$). However, the reduction in the phospho-STAT3 (Y-705) level in response to 1%FA after LPS induction was substantially larger than that when the cells were treated with FA alone, as illustrated in Figure 4.

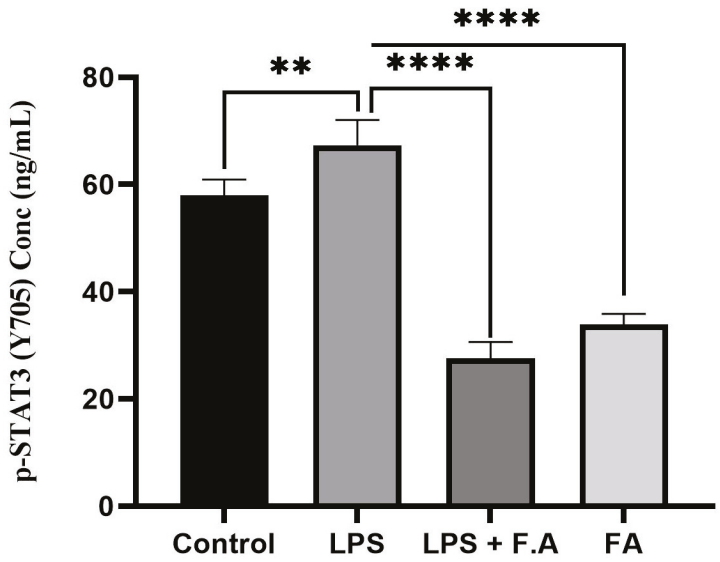

Figure 4. Reduction in phospho-STAT3 (Y-705) secretion in response to ferulic acid. A 0.1% ferulic acid stock concentration reduces secretion of phospho-STAT3 (Y-705) in HepG2 cells. Results represent the M ± SD of independent triplicate experiments. *p*-values indicate significance, as determined by one-way ANOVA test. Significance levels are represented as follows: ** $p \leq 0.01$, **** $p \leq 0.0001$.

4. Discussion

The importance of iron is not only simply restricted to its crucial role in hemoglobin synthesis and as an oxygen transporter throughout the body. It has fundamental importance extending to DNA synthesis and repair, cognitive development and immune system support [8,19]. Although iron deficiency is implicated in several health issues like anemia, excess iron levels can also lead to a serious health complications [20]. This highlights the importance of balanced consumption and meticulous oversight in medical environments.

Inflammatory environments can profoundly disrupt iron homeostasis, resulting in maladaptive iron metabolism that may aggravate disease mechanisms. Numerous studies have demonstrated the essential features of this interplay. For instance, Rosenblum, 2023 illustrated that the master regulator of iron metabolism, hepcidin, was induced by the proinflammatory cytokine *IL-6* and that this inducement leads to hypoferremia during the inflammation state [21]. This aligns with our study, which revealed that upon treating cells with LPS, there was an increase in *IL-6* gene expression and protein secretion, signifying a heightened state of inflammation (refer to Figure 3A,B). Furthermore, the expression of the hepcidin gene, along with its secretion, was notably upregulated and significantly elevated when the cell line was treated with LPS in this way. It was elucidated that this occurs via the STAT3 signaling pathway, emphasizing the pivotal role of *IL-6* and the interaction with its receptor, which results in the phosphorylation of STAT3 and the subsequent expression

of hepcidin [22]. The findings of that research correlate with our results, as illustrated in Figures 2–4.

The relationship between inflammatory responses and iron homeostasis is significant in numerous pathological states, such as cancer diseases and cardiovascular disorders [21]. Focusing on iron metabolism mechanisms offers prospective therapeutic avenues for the treatment of inflammatory disorders [23]. Thus, the aim of this study was to target iron metabolic pathways, particularly the STAT3 pathway, by using FA, which may present a potential alternate for therapeutic intervention in the treatment of these conditions.

FA is a multifaceted phenolic compound acknowledged for its broad spectrum of bioactive characteristics, rendering it advantageous across diverse domains [24]. Specifically, it demonstrates potential in the management of metabolic disorders through the mitigation of oxidative stress [25] and a protective role against the side effects of radiation therapy [26]. Cancer, as previously noted, is categorized as a metabolic disorder; consequently, FA was employed in this investigation as a prospective protective or therapeutic alternative for cancer treatment. Our study revealed that the *IL-6* concentration was approximately three-fold greater in cells treated with LPS compared to those receiving FA treatment after LPS stimulation. Nonetheless, the use of FA effectively mitigated the elevation of *IL-6* levels induced by LPS exposure. Specifically, the application of FA (0.1%) conferred protective effects against the inflammatory response elicited by LPS, resulting in a reduction in *IL-6* secretion to nearly one-third of the levels recorded in cells treated exclusively with LPS (Figure 3A). The investigation reported in [27] aligns with our research findings, i.e., using FA effectively reduces the LPS-mediated increase in *IL-6*. In particular, FA (0.1%) helped protect against the inflammatory reaction caused by LPS, lowering *IL-6* secretion to nearly one-third of what was seen in cells treated only with LPS (refer to Figure 3). In response to this reduction, the hepcidin level was also reduced, supporting the hypothesis that FA may confer a protective effect against the *IL-6*-mediated responses elicited by LPS, as shown in Figures 2 and 3. Curcumin, a natural compound, along with AG490 and a peptide that diminishes hepcidin expression in hepatocytes, together obstruct the *IL-6*-STAT3 signaling pathway and may present an innovative strategy for addressing iron dysregulation in the context of inflammatory diseases [27]. Another separate investigation undertaken by Li et al., 2022 corelates with our findings. In their study, it was demonstrated that caffeine attenuates hepcidin expression through the suppression of inflammation and the modulation of the *IL-6*/STAT3 signaling pathway [22], thereby presenting a compelling potential intervention for the management of anemia associated with inflammation. A study by Xin et al., 2016, showed that hydrogen sulfide reduces hepcidin production through the *IL-6*/STAT3 pathway; this also agrees with our findings [28]. Consequently, the correlation between the inflammatory milieu instigated by LPS stimulation, which leads to a reduction in hepcidin levels, has been empirically demonstrated to occur via the IL-STAT3 signaling cascade, as evidenced by our findings, which showed that FA treatment mitigated the rise in STAT3 levels subsequent to LPS stimulation in the HepG2 cell lines.

Conversely, FA not only confers a protective effect but also exhibits a cytotoxic effect against HepG2 cell lines, as demonstrated in Figure 1. This finding corelates with the observations made by the authors of [29], who indicated that FA enhances apoptosis in renal carcinoma (ACHN) and cervical carcinoma (HeLa and Caski) cell lines, with IC_{50} values recorded at 30 μM and 4–20 μM, respectively. Although the cytotoxic properties of FA appear promising, certain investigations suggest diminished efficacy at elevated concentrations in specific cancer cell lines, indicating that additional research is warranted to comprehensively elucidate its therapeutic potential.

FA has been demonstrated to be a potential therapeutic agent in vitro; however; its progress in this context may be impeded due to its inadequate solubility and bioavailability

and the complex nature of its metabolic pathways. These factors represent a considerable obstacle to its utilization as a therapeutic agent, as the absorption and distribution of FA within the in vivo system can be adversely affected [30]. Initiatives aimed at ameliorating these characteristics include the formulation of FA nanoemulsions and derivatives, which have led to improved solubility and bioavailability in vitro [31]. Additionally, synthesizing innovative derivatives of FA with enhanced physicochemical attributes has exhibited potential to bolster its therapeutic capacity [30]. Another limitation that remains unexplored in the current study is the intricate metabolic transformation of FA within the gut microbiome, where its metabolites exert diverse effects on microbial populations. This complexity has the potential to affect the therapeutic outcomes of using FA [32]. Although FA displays promise as a therapeutic agent, these limitations highlight the need for the development of additional future research targets' development to optimize its effectiveness in in vivo systems, i.e., via simulating an animal model of inflammation. Moreover, a co-culture of HepG2 and Caco-2 cell lines will allow a chance at the investigation of FA's effect on iron levels, other potential regulatory factors of *HAMP* expression like IL-1β and activin-B, ferroportin levels and molecular functional studies. Furthermore, future studies are needed to investigate the effect of FA on other cellular pathways such as activation of NF-κB and MAPK.

5. Conclusions

We have shown, for the first time, that FA significantly reduces hepcidin expression and secretion levels through attenuation of the *IL-6*-STAT3 pathway; hepcidin is one of the key regulators of iron metabolism. Thus, this collectively underscores the intricate interplay between FA and inflammatory mediators, thereby elucidating the potential therapeutic and protection implications of FA in the management of conditions characterized by dysregulated hepcidin levels such as cancer, anemia and chronic inflammation.

Author Contributions: O.M.A.-S. and L.F.A.-Q., Conceptualization, Supervision, Resources; M.I.A.A. and O.M.A.-S., Visualization, Methodology, Investigation, Validation, Project Administration, Formal Analysis; M.J.A.-K., Validation, Writing—Reviewing and Editing; O.M.A.-S. and M.M.A., Writing—Original Draft Preparation. All authors have read and agreed to the published version of the manuscript.

Funding: This research received no external funding.

Institutional Review Board Statement: Not applicable.

Informed Consent Statement: Not applicable.

Data Availability Statement: All the data are presented within the paper.

Acknowledgments: The authors would like to thank Aurum Biotech and Yazan Alkhawaldeh for their support during the conducting of this research.

Conflicts of Interest: The authors declare no conflict of interest.

Abbreviations

The following abbreviations are used in this manuscript:

FA	Ferulic acid
HCC	Hepatocellular carcinoma
DMSO	Dimethyl sulfoxide
ACHN	Apoptosis in renal carcinoma

References

1. Crosby, W.H.; Likhite, V.V.; O'Brien, J.E.; Forman, D. Serum iron levels in ostensibly normal people. *JAMA* **1974**, *227*, 310–312. [CrossRef] [PubMed]
2. Li, X.Y.; Li, J.H.; Jiang, Y.; Peng, B.S.; Li, J.; Zhu, S.L.; Su, Z.W.; Chang, J.P. Serum prohepcidin positively correlates with erythropoietin in normal adults. *Int. J. Lab. Hematol.* **2011**, *33*, 110–112. [CrossRef] [PubMed]
3. Camaschella, C.; Nai, A.; Silvestri, L. Iron metabolism and iron disorders revisited in the hepcidin era. *Haematologica* **2020**, *105*, 260–272. [CrossRef]
4. Soares, C.L.R.; Wilairatana, P.; Silva, L.R.; Moreira, P.S.; Vilar Barbosa, N.M.M.; da Silva, P.R.; Coutinho, H.D.M.; de Menezes, I.R.A.; Felipe, C.F.B. Biochemical aspects of the inflammatory process: A narrative review. *Biomed. Pharmacother.* **2023**, *168*, 115764. [CrossRef] [PubMed]
5. Wrighting, D.M.; Andrews, N.C. Interleukin-6 induces hepcidin expression through STAT3. *Blood* **2006**, *108*, 3204–3209. [CrossRef]
6. Kowdley, K.V.; Gochanour, E.M.; Sundaram, V.; Shah, R.A.; Handa, P. Hepcidin Signaling in Health and Disease: Ironing out the Details. *Hepatol. Commun.* **2021**, *5*, 723–735. [CrossRef]
7. Gyamfi, J.; Kim, J.; Choi, J. Cancer as a Metabolic Disorder. *Int. J. Mol. Sci.* **2022**, *23*, 1155. [CrossRef]
8. Zhang, Y.Y.; Han, Y.; Li, W.N.; Xu, R.H.; Ju, H.Q. Tumor iron homeostasis and immune regulation. *Trends Pharmacol. Sci.* **2024**, *45*, 145–156. [CrossRef]
9. Sakamoto, S.; Kawabata, H.; Kanda, J.; Uchiyama, T.; Mizumoto, C.; Kitano, T.; Kondo, T.; Hishizawa, M.; Tomosugi, N.; Takaori-Kondo, A. High pretransplant hepcidin levels are associated with poor overall survival and delayed platelet engraftment after allogeneic hematopoietic stem cell transplantation. *Cancer Med.* **2017**, *6*, 120–128. [CrossRef]
10. Schwartz, A.J.; Goyert, J.W.; Solanki, S.; Kerk, S.A.; Chen, B.; Castillo, C.; Hsu, P.P.; Do, B.T.; Singhal, R.; Dame, M.K.; et al. Hepcidin sequesters iron to sustain nucleotide metabolism and mitochondrial function in colorectal cancer epithelial cells. *Nat. Metab.* **2021**, *3*, 969–982. [CrossRef]
11. Mutlu, T.; Ozoran, E.; Trabulus, D.C.; Talu, C.K.; Erhan, D.; Mete, M.; Guven, M. Expression of genes related to iron homeostasis in breast cancer. *Mol. Biol. Rep.* **2023**, *50*, 5157–5163. [CrossRef] [PubMed]
12. Niu, R.; Zhao, F.; Dong, Z.; Li, Z.; Li, S. A stratification system of ferroptosis and iron-metabolism related LncRNAs guides the prediction of the survival of patients with esophageal squamous cell carcinoma. *Front. Oncol.* **2022**, *12*, 1010074. [CrossRef]
13. Traeger, L.; Ellermann, I.; Wiethoff, H.; Ihbe, J.; Gallitz, I.; Eveslage, M.; Moritz, R.; Herrmann, E.; Schrader, A.J.; Steinbicker, A.U. Serum Hepcidin and GDF-15 levels as prognostic markers in urothelial carcinoma of the upper urinary tract and renal cell carcinoma. *BMC Cancer* **2019**, *19*, 74. [CrossRef]
14. Joachim, J.H.; Mehta, K.J. Hepcidin in hepatocellular carcinoma. *Br. J. Cancer* **2022**, *127*, 185–192. [CrossRef] [PubMed]
15. Abdulal, Z.A.; Altahhan, M.Y.; Qindil, A.F.; Al-Juhani, A.M.; Alatawi, M.A.; Hassan, H.M.; Al-Gayyar, M.M. Ferulic acid inhibits tumor proliferation and attenuates inflammation of hepatic tissues in experimentally induced HCC in rats. *J. Investig. Med.* **2024**, *72*, 900–910. [CrossRef]
16. Bishayee, A. The role of inflammation and liver cancer. *Adv. Exp. Med. Biol.* **2014**, *816*, 401–435. [CrossRef] [PubMed]
17. Lee, C.C.; Wang, C.C.; Huang, H.M.; Lin, C.L.; Leu, S.J.; Lee, Y.L. Ferulic Acid Induces Th1 Responses by Modulating the Function of Dendritic Cells and Ameliorates Th2-Mediated Allergic Airway Inflammation in Mice. *Evid. Based Complement. Altern. Med.* **2015**, *2015*, 678487. [CrossRef]
18. Sakai, S.; Ochiai, H.; Nakajima, K.; Terasawa, K. Inhibitory effect of ferulic acid on macrophage inflammatory protein-2 production in a murine macrophage cell line, RAW264.7. *Cytokine* **1997**, *9*, 242–248. [CrossRef]
19. Iriarte-Gahete, M.; Tarancon-Diez, L.; Garrido-Rodriguez, V.; Leal, M.; Pacheco, Y.M. Absolute and functional iron deficiency: Biomarkers, impact on immune system, and therapy. *Blood Rev.* **2024**, *68*, 101227. [CrossRef]
20. Kotze, M.J.; van Velden, D.P.; van Rensburg, S.J.; Erasmus, R. Pathogenic Mechanisms Underlying Iron Deficiency and Iron Overload: New Insights for Clinical Application. *EJIFCC* **2009**, *20*, 108–123.
21. Rosenblum, S.L. Inflammation, dysregulated iron metabolism, and cardiovascular disease. *Front. Aging* **2023**, *4*, 1124178. [CrossRef] [PubMed]
22. Li, Z.D.; Geng, M.Y.; Dou, S.R.; Wang, X.; Zhang, Z.H.; Chang, Y.Z. Caffeine Decreases Hepcidin Expression to Alleviate Aberrant Iron Metabolism under Inflammation by Regulating the *IL-6*/STAT3 Pathway. *Life* **2022**, *12*, 1025. [CrossRef] [PubMed]
23. Kang, D.Y.; Sp, N.; Jo, E.S.; Lee, J.M.; Jang, K.J. New Insights into the Pivotal Role of Iron/Heme Metabolism in TLR4/NF-kappaB Signaling-Mediated Inflammatory Responses in Human Monocytes. *Cells* **2021**, *10*, 2549. [CrossRef]
24. Werneck Cerqueira, A.F.L.; de Mello Brandao, H.; Tavares, G.D.; Rodarte, M.P. Ferulic Acid: A Review of Mechanisms of Action, Absorption, Toxicology, Application on Wound Healing. *Antiinflamm. Antiallergy Agents Med. Chem.* **2024**, *23*, 205–214. [CrossRef]
25. Khatun, M.M.; Bhuia, M.S.; Chowdhury, R.; Sheikh, S.; Ajmee, A.; Mollah, F.; Al Hasan, M.S.; Coutinho, H.D.M.; Islam, M.T. Potential utilization of ferulic acid and its derivatives in the management of metabolic diseases and disorders: An insight into mechanisms. *Cell. Signal.* **2024**, *121*, 111291. [CrossRef] [PubMed]

26. Huang, M.; Ye, A.; Zhang, H.; Chen, J.; Yang, T.; Wei, X.; Gao, Y.; Ma, Z. Ferulic Acid Alleviates Radiation-Induced Immune Damage by Acting on JAK/STAT Signaling Pathway. *Pharmaceuticals* **2024**, *17*, 1175. [CrossRef]
27. Fatih, N.; Camberlein, E.; Island, M.L.; Corlu, A.; Abgueguen, E.; Detivaud, L.; Leroyer, P.; Brissot, P.; Loreal, O. Natural and synthetic STAT3 inhibitors reduce hepcidin expression in differentiated mouse hepatocytes expressing the active phosphorylated STAT3 form. *J. Mol. Med.* **2010**, *88*, 477–486. [CrossRef]
28. Xin, H.; Wang, M.; Tang, W.; Shen, Z.; Miao, L.; Wu, W.; Li, C.; Wang, X.; Xin, X.; Zhu, Y.Z. Hydrogen Sulfide Attenuates Inflammatory Hepcidin by Reducing *IL-6* Secretion and Promoting SIRT1-Mediated STAT3 Deacetylation. *Antioxid. Redox Signal.* **2016**, *24*, 70–83. [CrossRef]
29. Luo, L.; Zhu, S.; Tong, Y.; Peng, S. Ferulic Acid Induces Apoptosis of HeLa and Caski Cervical Carcinoma Cells by Down-Regulating the Phosphatidylinositol 3-Kinase (PI3K)/Akt Signaling Pathway. *Med. Sci. Monit.* **2020**, *26*, e920095. [CrossRef]
30. Janus, E.; Pinheiro, L.R.; Nowak, A.; Kucharska, E.; Swiatek, E.; Podolak, N.; Peruzynska, M.; Piotrowska, K.; Duchnik, W.; Kucharski, L.; et al. New Ferulic Acid and Amino Acid Derivatives with Increased Cosmeceutical and Pharmaceutical Potential. *Pharmaceutics* **2022**, *15*, 117. [CrossRef]
31. Abd-Allah, H.; Abdel Jaleel, G.A.; Hassan, A.; El Madani, M.; Nasr, M. Ferulic acid nanoemulsion as a promising anti-ulcer tool: In vitro and in vivo assessment. *Drug Dev. Ind. Pharm.* **2024**, *50*, 460–469. [CrossRef] [PubMed]
32. Lu, S.; Cheng, D.; Yao, H.; Wen, Y.; Yu, Y.; Li, H.; Wang, J.; Sun, B. Cascade Microbial Metabolism of Ferulic Acid In Vitro Fermented by the Human Fecal Inoculum. *J. Agric. Food Chem.* **2024**, *72*, 9807–9817. [CrossRef] [PubMed]

Disclaimer/Publisher's Note: The statements, opinions and data contained in all publications are solely those of the individual author(s) and contributor(s) and not of MDPI and/or the editor(s). MDPI and/or the editor(s) disclaim responsibility for any injury to people or property resulting from any ideas, methods, instructions or products referred to in the content.

biomedicines

MDPI

Article

Altered Expression of NK Receptors in Racially/Ethnically Diverse and Risk-of-Relapse Pediatric Acute Lymphoblastic Leukemia Patients

Stephen Mathew [1,*], Roslin Jose George [2], Alexsis Garcia [1], Sheila Powers [1], Subhash Aryal [3] and W. Paul Bowman [4]

[1] Department of Microbiology, Immunology and Genetics, University of North Texas Health Science Center, Fort Worth, TX 76107, USA; alexsisgarcia@my.unthsc.edu (A.G.); sheila_powers@yahoo.com (S.P.)
[2] Mayo Clinic Hospital, Rochester, MN 55902, USA; george.roslinjose@mayo.edu
[3] School of Nursing, Johns Hopkins University, Baltimore, MD 21205, USA; saryal5@jh.edu
[4] Cook Children's Medical Center, Fort Worth, TX 76104, USA; paul.bowman@cookchildrens.org
* Correspondence: stephen.mathew@unthsc.edu; Tel.: +1-817-735-5407

Abstract: Background/Objectives: Acute Lymphoblastic Leukemia (ALL) is a cancer that predominantly affects white blood cells within the blood and bone marrow of adults and children. Currently, ALL is one of the most prevalent malignancies in pediatric patients and is most seen among Caucasian and Hispanic descent, with lower incidence in African American children. The goal of the study was to investigate the expression of immune cell receptors in racial/ethnic populations and risk factors for relapse that could potentially influence the pediatric ALL outcomes. **Methods:** Twenty healthy subjects and forty-two pediatric ALL subjects were enrolled in the study and whole-blood was collected at diagnosis and post-chemotherapy, and the cell surface expression of various immune receptors, including 2B4, CS1, LLT1, Nkp30, and NKp46, was determined by flow cytometry. **Results:** Very high-risk and high-risk of relapse ALL subjects showed increased expression of LLT1 on NK cells, T cells, and monocytes at diagnosis compared to healthy subjects. CS1 was also significantly overexpressed on monocytes of very-high risk ALL subjects both at diagnosis and after the end of chemotherapy as compared to healthy subjects. Also, there was a significantly increased expression of NKp30 on T cells of Caucasians as compared to Hispanics and African Americans at diagnosis, and downregulation of CS1 and LLT1 on T cells of Caucasians post-induction chemotherapy. **Conclusions:** The altered expression of immune receptors in racial/ethnic and risk stratified groups may provide insights into the immune surveillance mediated by T cells and NK cells against pediatric ALL.

Keywords: acute lymphoblastic leukemia (ALL); health disparities; risk factors; natural killer (NK) cell; immune receptors

1. Introduction

Acute lymphoblastic leukemia (ALL) is marked by the formation of abnormal lymphoblasts, leading to a broad range of symptoms. While both children and adults can present with ALL, ALL remains the most prevalent childhood cancer in children under the age of 15, with incidence rates being higher in boys than in girls [1–5]. Predominantly, individuals of Caucasian and Hispanic descent present with ALL while African American children have relatively lower incidence [6–9]. Patients with ALL display symptoms related to bone marrow failure such as fatigue, pallor, and fever along with easy bruising and bleeding [10–13]. Currently, first-line treatments include vincristine, glucocorticoids,

and doxorubicin along with allogenic stem cell transplantation [2,3,9,14,15]. Despite the advances in various treatments, approximately 20% of pediatric patients experience a relapse [16] and of those treated with chemotherapeutic agents roughly 80–90% remained in remission [3,17–21].

Previously, age and white blood cell count were primarily used to risk stratify patients, with worse prognosis being associated with increased age [11]. Currently, various factors are used to assess risk stratification which include genetic information as well as age, white blood cell count, minimal residual disease (MRD) response, time of relapse from diagnosis, site of relapse, and immunophenotype (B-ALL or T-ALL) [4,11,22,23]. In addition to risk stratification, there have been various studies assessing the correlation between racial/ethnic health disparities and ALL [7,19,24–26]. Previous studies have noted that while African Americans have a lower incidence rate in comparison to their white and non-white counterparts, they often have worse treatment outcomes and lower rates of survival [6,27,28]. In addition, a link between genetic variations in African American and Hispanic pediatric patients and ALL risk/susceptibility have previously been investigated [24,28]. It has been noted that African Americans are more likely to have T-ALL, the more aggressive ALL lineage compared to B-ALL [29].

Some studies have investigated a link between ALL and natural killer (NK) cell dysfunction [20,30–32]. NK cells play a vital role in the innate immune system and are the body's first line of defense against foreign invaders and cancer cells [33,34]. Numerous recent studies have shed light on various membrane-bound receptors involved in the recognition, activation, and inhibition of NK cells through interactions with other immune cells [35,36]. Recent clinical studies have shown that chimeric antigen receptor (CAR)-T cells and CAR-NK cells are efficiently able to reduce relapses of ALL and more studies need to be conducted to fully realize the potential of this immunotherapy [37,38]. In this study, we have focused on five receptors/ligands, namely 2B4 (CD244, SLAMF4), CS1 (CD319, SLAMF7), LLT1 (CLEC2D), NKp30 (NCR3), and NKp46 (NCR1). Previously, our group had cloned 2B4, CS1, and LLT1 and evaluated their expression and function in various cancers including prostate cancer, triple-negative breast cancer, and acute lymphoblastic leukemia (ALL) [20,31,39,40]. These receptors have been linked to NK cell dysfunction via the disruption of optimal immune surveillance in ALL patients and various diseases [21,41–44]. Data collected from ALL subjects (ages 2–19, B-ALL and T-ALL) both at day 0 (diagnosis) and day 29 (post-chemotherapy treatment) were analyzed with a focus on the immune receptor expression in the following racial/ethnic populations: African Americans, Hispanics, and Caucasians. We also analyzed the expression of these receptors/ligands in risk-of-relapse stratified groups pre- and post-chemotherapeutic treatments. Overall, this study offers fresh insight into the dysregulation of immune receptor/ligand expression in ALL patients among various racial/ethnic and risk-stratified populations.

2. Materials and Methods

2.1. ALL and Healthy Subjects

Pediatric patients aged 2 to 21 years with newly diagnosed ALL were enrolled in the study at the Hematology and Oncology Clinic of Cook Children's Medical Center (CCMC) in Fort Worth, TX, USA. Informed consent/assent was obtained from each subject by Dr. W. Paul Bowman, MD or nursing staff per IRB approval from the University of North Texas Health Science Center (UNTHSC), Fort Worth, TX, USA and CCMC (UNTHSC IRB# 2008-094 & CCMC IRB#2008-57). Additionally, children under 21 years of age who visited the pediatric clinic at the UNTHSC Health Pavilion for routine medical check-ups were enrolled as healthy controls. Disease profile and demographic information were collected for every subject.

2.2. Blood Collection

One blood sample (8 mLs) indicated as the first blood draw (1BD) was collected by the staff from every ALL subject after obtaining written informed consent before any treatment was provided to them. A second blood sample indicated as the second blood draw (2BD) was collected on day 29 at the end of chemotherapy treatment, which typically lasts for 4 weeks. Healthy subjects only provided a single blood sample. A total of 42 ALL subjects and 20 healthy subjects were enrolled in the study.

2.3. Isolation of Peripheral Blood Mononuclear Cells (PBMC)

Peripheral blood mononuclear cells (PBMCs) were isolated from whole-blood collected in purple-top tubes containing ethylenediamine tetra acetic acid (EDTA) by Histopaque-1077 (Sigma Chemicals, St Louis, MO, USA) density gradient centrifugation using LeucoSep tubes (Greiner, Monroe, NC, USA). Red blood cells were lysed using ACK lysis buffer. The isolated PBMCs were subsequently utilized for flow cytometric analysis of immune receptor expression.

2.4. Antibodies and Immunostaining for Flow Cytometry

Prior to immunostaining, PBMCs were incubated with human IgG Fc fragments (Rockland Immunochemicals, Philadelphia, PA, USA) to block potential Fc receptor-mediated fluorescence. The antibodies used to distinguish immune cell populations included FITC-conjugated anti-human CD3 monoclonal antibody (mAb) for T cells, PE-Texas Red-conjugated anti-human CD19 mAb for B cells, APC-conjugated anti-human CD56 mAb for NK cells, and APC-Cy7-conjugated CD14 mAb for monocytes. To assess the percentage and quantitative cell surface expression of each immune receptor and its ligands, PE-conjugated monoclonal antibodies against human 2B4, CS1, LLT1, NKp30, and NKp46 were used for labeling. Immune cell populations were gated based on forward and side scatter to (Figure S1) distinguish lymphocytes and monocytes from other cells according to size and granularity, using a Beckman Coulter FC500 flow cytometer (Beckman Coulter Life Sciences, Indianapolis, IN, USA). All antibodies used in the study were obtained from BioLegend, San Diego, CA, USA. The median fluorescence intensity ratio (MFIR) was calculated by comparing the median fluorescence intensity (MFI) of test samples to that of isotype control samples. MFIR for each sample was determined by dividing the MFI of the test sample by the MFI of the corresponding isotype control.

2.5. Statistical Analysis

A multivariate analysis of variance (MANOVA) was conducted to evaluate differences in immune receptor expression among healthy individuals and ALL patient samples at diagnosis and after chemotherapy, across various racial/ethnic groups and risk stratification categories, using SAS version 9.4 (SAS, Cary, NC, USA). The statistical test adjusts for correlations among multiple measurements taken from the same subject. When a statistically significant overall difference was identified using MANOVA, each variable was individually assessed by race/ethnicity and risk-stratified groups using the ANOVA method. Significance was determined at alpha = 0.05. Graphs were created by using Graph Pad Prism version 10.2.3 software (GraphPad, San Diego, CA, USA).

3. Results

3.1. Altered Cell Surface Expression of CS1, LLT1 and NKp30 in CD3+ T Cells of Hispanic, Caucasian and African American ALL Subjects Pre- and Post-Chemotherapy Treatments

PBMCs were isolated from the whole blood of 42 ALL patients and 20 healthy individuals and the cell surface expressions of 2B4, CS1, LLT1, NKp30, and NKp46 were analyzed.

CS1 and LLT1 expression on CD3+ T cells of Caucasians was significantly downregulated as compared to Hispanics and African Americans post-chemotherapy (2BD), whereas at diagnosis (1BD) there was no significant difference in the expression of those receptors between the racial/ethnic populations (Figure 1C–F,K,L). As shown in Figure 1M, increased cell surface expression of NKp30 was observed on the CD3+ T cell population of Caucasians (36.2% positive cells) as compared to Hispanics (16.7% positive cells) and African Americans (8.4% positive cells) at diagnosis ($p < 0.01$; $p < 0.001$). However, following the completion of chemotherapy (2BD), NKp30 expression in Caucasians decreased to levels comparable to those observed in Hispanic and African American individuals (Figure 1N). There was no significant difference in the expression of 2B4, NKp30 (MFIR) and NKp46 among the different racial/ethnic populations (Figure 1A,B,G–J).

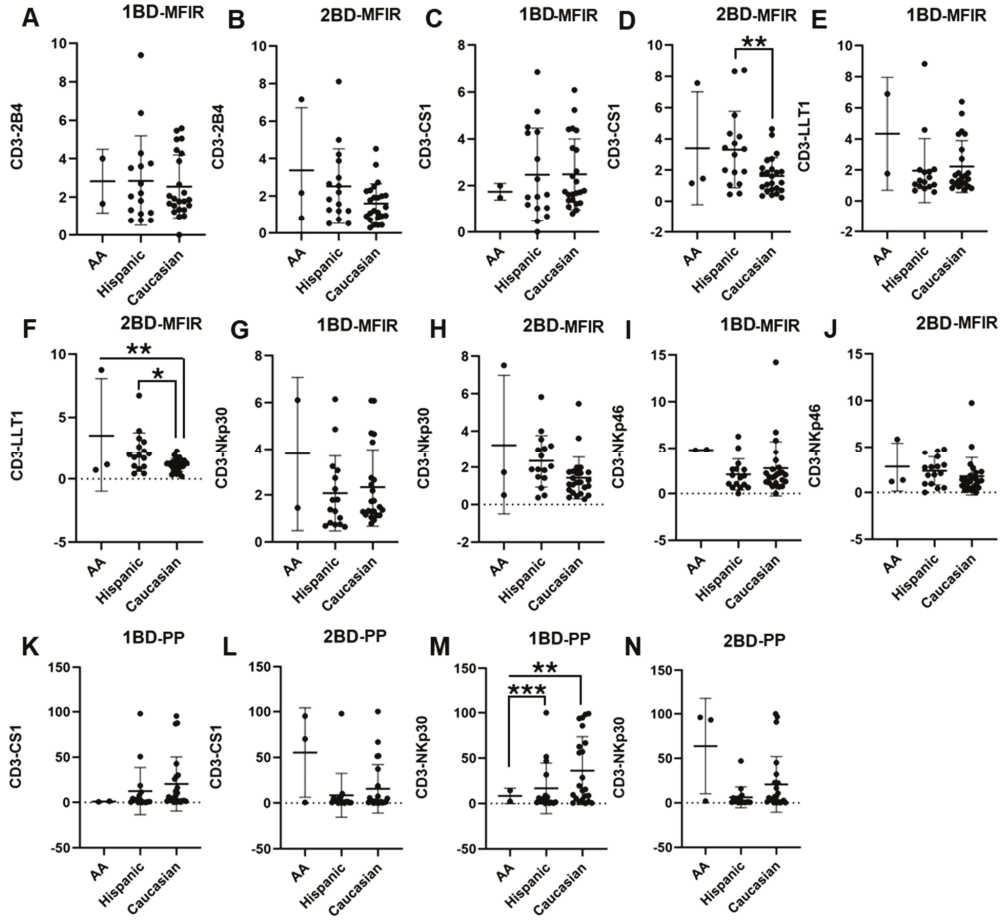

Figure 1. Differential expression of immune receptors on T cells of Hispanic, Caucasian, and African American ALL subjects before and after chemotherapy treatment. Flow cytometry analysis exhibits the cell surface expressions of 2B4 (**A**,**B**), CS1 (**C**,**D**), LLT1 (**E**,**F**), NKp30 (**G**,**H**), and NKp46 (**I**,**J**) on T cells of Hispanic, Caucasian, and African American ALL subjects pre- and post-chemotherapy treatments, as indicated by median fluorescence intensity ratio (MFIR). Flow cytometry analysis shows the percentage of positive (PP) cells expressing CS1 (**K**,**L**) and NKp30 (**M**,**N**) on T cells. The first blood draw is referred to as 1BD, which is collected at diagnosis or before the start of chemotherapy (day 0). The second blood draw is referred to as 2BD, which is collected at the end of induction chemotherapy or after treatment (day 29). * $p < 0.05$; ** $p < 0.01$; *** $p < 0.001$.

3.2. Increased Cell SurfaceEexpressions of LLT1 and NKp30 and Downregulation of CS1 in CD3+ T Cells of High-Risk ALL Subjects

ALL subjects were stratified into risk-of-relapse groups and were designated as very high-risk (VHR), high-risk (HR), or standard risk/low-risk (SR-LR) and the cell surface

immune receptor expression on CD3+ T cells was determined. The risk stratification was based on the subject's MRD status, age, white blood cell count, CNS status, DNA index, ALL subtype, hyperdiploidy, hypodiploidy, TEL/AML status, MLL translocations, Philadelphia (Ph) chromosome, t(1;19) translocation, and additional chromosomal abnormalities. The immune receptor expression was determined in both healthy (only one sample) and ALL subjects at diagnosis (day 0, 1BD) and post-induction chemotherapy (day 29, 2BD). As shown in Figure 2E, LLT1 was observed to be significantly overexpressed in CD3+ T cells of high-risk ALL (31.67%) subjects as compared to healthy (5.8%) subjects ($p < 0.01$) at diagnosis (day 0, 1BD), which dropped down post-induction chemotherapy (day 29, 2BD) treatment to comparable levels of expression (12.17%) with healthy subjects (Figure 2F). Similarly, cell surface expression of NKp30 was significantly upregulated on T cells of high-risk patients (40.55%) at diagnosis (1BD) as compared to standard risk/low-risk and healthy (13.4%) subjects (Figure 2G). NKp30 expression on T cells in high-risk subjects decreased to 27.3% following chemotherapy (2BD) treatment (Figure 2H). In contrast, CS1 expression on CD3+ T cells, measured by median fluorescence intensity ratio (MFIR), was significantly reduced at diagnosis (day 0, 1BD) in both very high-risk (1.76) and high-risk (2.47) ALL patients compared to healthy (3.89) individuals (Figure 2K). After induction chemotherapy (day 29, 2BD) there was no significant difference in CS1 expression on T cells in the different risk-stratified groups (very high-risk = 2.7, high-risk = 2.09, and standard risk/low-risk = 2.33) of ALL subjects as compared to healthy (3.89) subjects (Figure 2L). There was no significant difference in the percentage of positive cell expression of 2B4, CS1 and NKp46 on CD3+ T cells in the different risk-stratified groups of ALL subjects as compared to healthy subjects either at diagnosis (1BD) or post-induction chemotherapy (2BD) treatment (Figure 2A–D,I,J).

3.3. Increased Cell Surface Expression of LLT1 Was Observed in CD56+ NK Cells of Very High-Risk and Standard/Low-Risk ALL Patients

LLT1 cell surface expression was significantly elevated in CD56+ NK cells of very high-risk (49.91% and 49.77%) and standard risk/low-risk (34.64% and 31.38%) ALL subjects at diagnosis (1BD) and after chemotherapy (2BD), respectively, as compared to healthy (12.64%) subjects (Figure 3E,F). CD56+ NK cells from very high-risk ALL patients at diagnosis showed elevated expression of CS1 (61.34%), NKp30 (74.65%), and NKp46 (68.17%) as compared to healthy subjects (39.84%, 46.1%, and 49.9%, respectively), but it was not statistically significant (Figure 3C,G,I).

A similar trend of high expression of CS1 (67.88%), NKp30 (65.44%), and NKp46 (57.79%) was observed in the CD56+ NK cells of very high-risk ALL subjects post-induction (2BD) chemotherapy as compared to healthy subjects (39.84%, 46.1%, and 49.9%, respectively), but it was not statistically significant (Figure 3D,H,J). Contrastingly, a decrease in the expression of 2B4 on CD56+ NK cells was observed in the high-risk (72.16%) and standard risk/low-risk (60.2%) ALL subjects at diagnosis (1BD) as compared to healthy (77.04%) subjects (Figure 3A). After chemotherapy treatments (day 29, 2BD), there was a further decline in 2B4 expression on NK cells in the different risk-stratified groups (very high-risk = 71.6%, high-risk = 64.51%, and standard risk/low-risk = 55%) of ALL patients as compared to healthy (77.04%) individuals (Figure 3B).

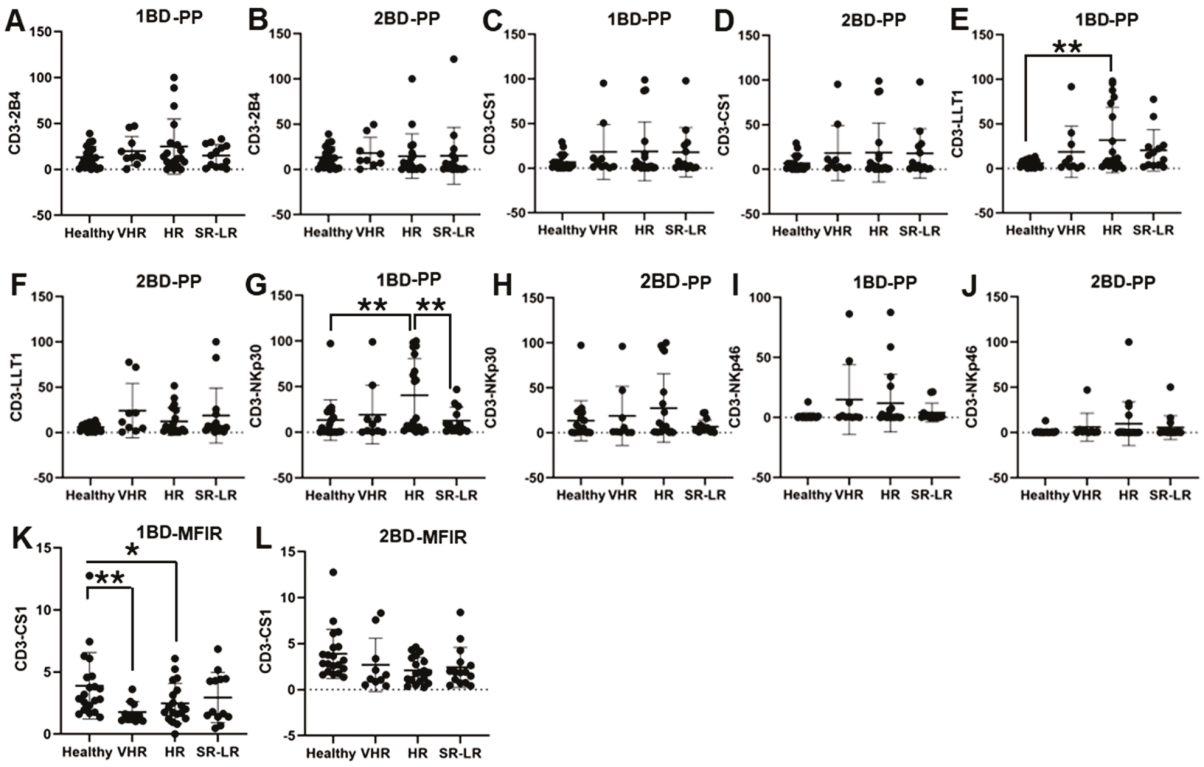

Figure 2. Cell surface expression of 2B4, CS1, LLT1, NKp30, and NKp46 on CD3+ T cells in high-risk ALL patients before and after chemotherapy treatment. Flow cytometry analysis of cell surface expression shows the percentage of positive (PP) cells expressing 2B4 (**A**,**B**), CS1 (**C**,**D**), LLT1 (**E**,**F**), NKp30 (**G**,**H**), NKp46 (**I**,**J**), and CS1 (**K**,**L**) indicated by median fluorescence intensity ratio (MFIR) on the CD3+ T cells of ALL subjects before and after chemotherapy treatments, stratified by risk-of-relapse. The first blood draw is referred to as 1BD, which is collected at diagnosis or before the start of chemotherapy (day 0). The second blood draw is referred to as 2BD, which is collected at the end of induction chemotherapy or after treatment (day 29). * $p < 0.05$, ** $p < 0.01$.

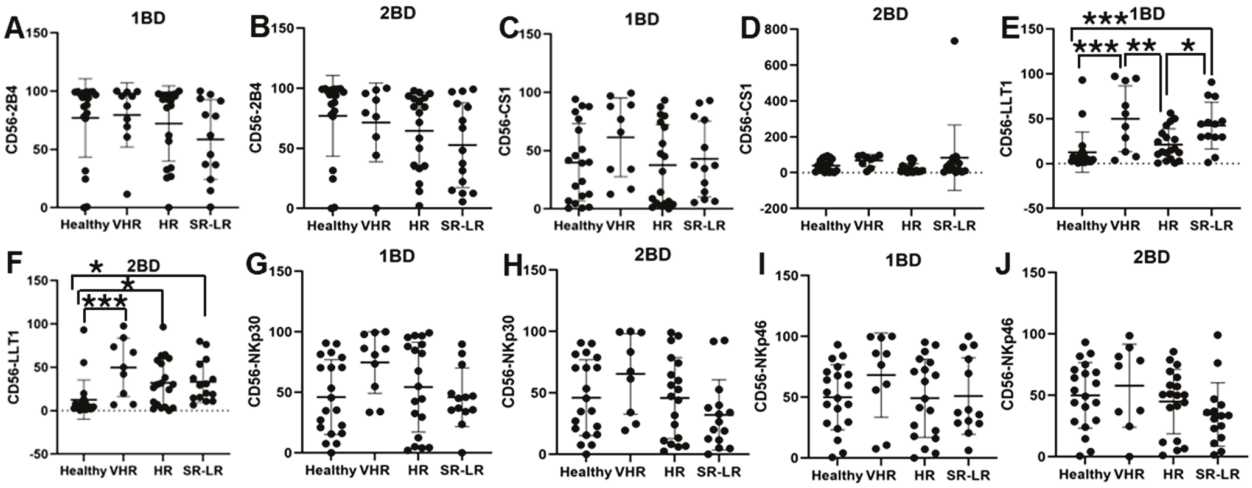

Figure 3. Cell surface expression of 2B4, CS1, LLT1, NKp30, and NKp46 on CD56+ NK cells of high-risk ALL subjects before and after chemotherapy treatments. Flow cytometry analysis of cell surface expression indicated by percentage of positive cells expressing 2B4 (**A**,**B**), CS1 (**C**,**D**), LLT1 (**E**,**F**), NKp30 (**G**,**H**), and NKp46 (**I**,**J**) on NK cells of ALL subjects before and after chemotherapy treatments stratified by risk-of-relapse. The first blood draw is referred to as 1BD, which is collected at diagnosis or before the start of chemotherapy (day 0). The second blood draw is referred to as 2BD, which is collected at the end of induction chemotherapy or after treatment (day 29). * $p < 0.05$, ** $p < 0.01$; *** $p < 0.001$.

3.4. Enhanced Cell Surface Expression of CS1 and LLT1 in CD14+ Monocytes of Very High-Risk and High-Risk ALL Subjects

CS1 cell surface expression was observed to be significantly higher in CD14+ monocytes of very high-risk (39.32%; $p < 0.05$) and high-risk (38.08%; $p < 0.01$) ALL subjects, respectively, at diagnosis (1BD) as compared to healthy (14.71%) subjects (Figure 4C). The standard risk/low-risk ALL subjects also showed high expression of CS1 (29.77%) in the monocyte population at diagnosis (1BD). The increased expression of CS1 on monocytes remained unchanged even after induction chemotherapy (2BD) in very high-risk (41.01%, $p < 0.05$) and standard risk/low-risk (36%, $p < 0.05$) and was significantly higher compared to healthy (14.71%) subjects (Figure 4D). High-risk and standard risk/low-risk ALL subjects showed significantly higher expression of 73.61% ($p < 0.05$) and 69.71% ($p < 0.05$) positive cells for LLT1 on CD14+ monocytes at diagnosis (1BD) as compared to healthy (44.9%) subjects (Figure 4E). The expression of LLT1 on monocytes decreased after induction chemotherapy (2BD) in very high-risk (45.23%), high-risk (60.8%), and standard risk/low-risk (47.29%) ALL subjects but was higher than the healthy (44.9%) subjects (Figure 4F). There was no significant difference in 2B4, NKp30, and NKp46 expression on CD14+ monocytes in the different risk-stratified groups of ALL patients as compared to healthy individuals either at diagnosis (1BD) or post-induction chemotherapy (2BD) treatment (Figure 4A,B,G–J).

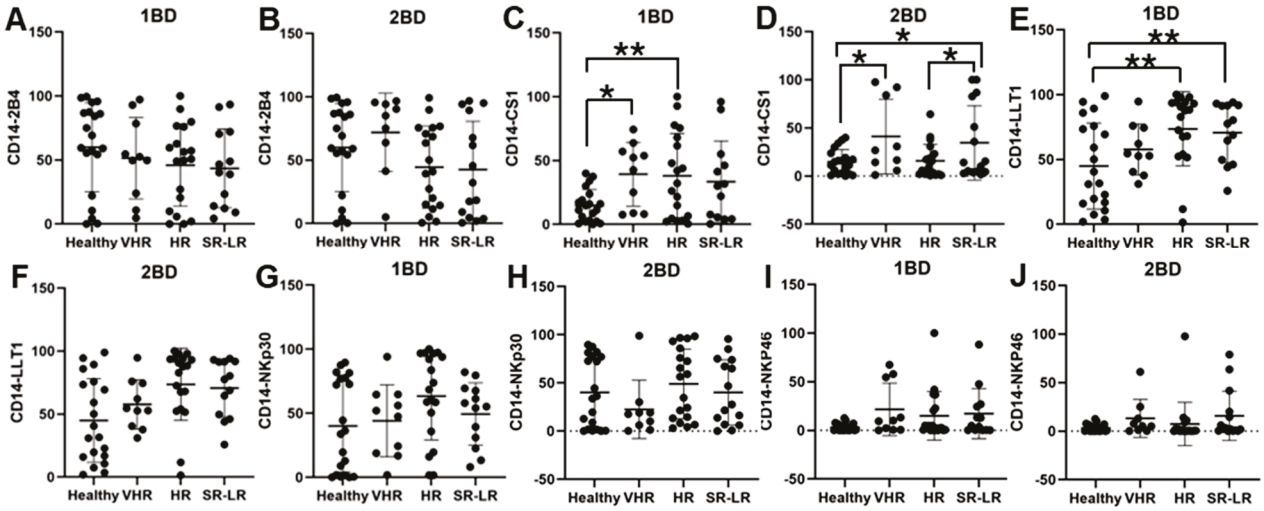

Figure 4. Cell surface expression of 2B4, CS1, LLT1, NKp30, and NKp46 on CD14+ monocytes of high-risk ALL subjects before and after chemotherapy treatments. Flow cytometry analysis of cell surface expression indicated by percentage of positive cells expressing 2B4 (**A**,**B**), CS1 (**C**,**D**), LLT1 (**E**,**F**), NKp30 (**G**,**H**), and NKp46 (**I**,**J**) on monocytes of ALL subjects before and after chemotherapy treatments, stratified by risk-of-relapse. The first blood draw is referred to as 1BD, which is collected at diagnosis or before the start of chemotherapy (day 0). The second blood draw is referred to as 2BD, which is collected at the end of induction chemotherapy or after treatment (day 29). * $p < 0.05$, ** $p < 0.01$.

3.5. Clinicopathological Features of ALL Subjects

Forty-six ALL patients and twenty healthy individuals were enrolled in this study. Four patients failed to satisfy the inclusion criteria or failed to complete the study and so were excluded from data analysis. There were equal number of male ($n = 21$) and female subjects ($n = 21$). A total of 93% of the subjects had B-ALL whereas 7% had T-ALL (Tables 1 and S1). We also enrolled twenty healthy subjects that we attempted to match with the patient groups regarding age, gender and race/ethnicity, but these were not perfectly matched due to the complexity of enrolling healthy pediatric subjects into the study.

Table 1. Demographic and clinicopathological features of ALL patients.

Clinical Features	No. of Patients
Sex	
Male	21
Female	21
ALL Subtype	
B-ALL	39
T-ALL	3
CNS status	
1 (no blasts in the CSF, regardless of WBC or RBC)	30
2a (<5 WBC/μL + blasts + <10 RBC/mL)	6
2b (<5 WBC/μL + blasts + ≥10 RBC/mL)	2
2c (≥5 WBC/μL + blasts + ≥10 RBC/mL)	2
3a (≥5 WBC/μL + blasts + <10 RBC/mL)	2
MRD	
Positive	6
Negative	34
Unknown	2
DNA index	
1.0	11
1.05–2.0	10
>2.0	9
Unknown	12
Hyperdiploidy	
Yes	12
No	19
Unknown	11
Hypodiploidy	
Yes	1
No	31
Unknown	10
TEL/AML	
Yes	2
No	40
Philadelphia chromosome	
Yes	6
No	36

The clinicopathological features revealed that 14.3% (n = 6) had a positive MRD status, whereas 81% (n = 34) had a negative MRD status and 5% (n = 2) were unknown. Analyzing the CNS status revealed that 76.2% (n = 32) of ALL subjects did not show any blasts in the cerebrospinal fluid (CSF) at diagnosis, with 12% (n = 5) showing CNS status 2a, 1 subject having CNS status 2b, and a couple of the subjects indicating CNS status 2c and 3a. A total of 24% (n = 10) of the ALL subjects showed a normal DNA index of 1.0, whereas 21.43% (n = 9) displayed an elevated DNA index (1.05–2.0) and another 21.43% (n = 9) reported a highly elevated DNA index (>2.0). For 33% (n = 14) of ALL subjects the DNA index was unknown. Among the ALL subjects, 28.5% (n = 12) displayed hyperdiploidy, characterized by trisomies of chromosomes 4, 10, or 17, occurring in one, two, or all three

chromosomes, whereas 2.38% (n = 1) showed hypodiploidy. A couple of the subjects were positive for TEL/AML, which is expressed from the t(12;21) chromosomal translocation in B-precursor ALL patients and six subjects were positive for Philadelphia chromosome [(Ph)/BCR/ABL-positive].

4. Discussion

Various risk factors can influence the chances of relapse in ALL patients, which includes immunophenotype specifically T cell ALL which is considered to be more aggressive in comparison to B-cell ALL. Survival rates among ALL patients vary based on gender, race/ethnicity, and socioeconomic status along with immunophenotype [20,26,45]. NK cells play a vital role in the immune surveillance of cancers and viral infections. NK cell activation is managed by a suite of activating, co-stimulatory, and inhibitory receptors and the regulation of these signals ultimately determines the cell function and activation [46–48]. The activating receptors are not able to activate NK cells on their own and so need the synergy of several receptors. The ITAMs (immunoreceptor tyrosine-based activation motifs) initiate activating signals when phosphorylated, leading to recruitment of kinases like Syk and activation of pathways such as PLCγ, PI3K, and calcium signaling. The inhibitory receptors' interaction with their corresponding ligands causes the phosphorylation of ITIMs (immunoreceptor tyrosine-based inhibitory motifs) sequences in the inhibitory receptor mediated by the Src-family kinase (SFK) [49,50]. The ITIMs activate protein tyrosine phosphatases (PT-Pases), mainly SHP-1 and SHP-2 after phosphorylation. SHP-1 further downregulates multiple activating signal molecules by dephosphorylation, inhibiting the NK cell activation signal and eventually inhibiting NK cell activity [50]. In this study we wanted to investigate the cell surface expression of immune receptors 2B4, CS1, LLT1, NKp30, and NKp46 in different racial/ethnic populations and risk-of-relapse stratified groups. These receptors are predominantly expressed on NK cells and other immune cells and play a role in cancers and other diseases. Our study has shown the differential expression of immune receptors in different immune cells in racial/ethnic populations and risk-of-relapse stratified groups.

The majority of the subjects recruited in our study were B-precursor ALL subtype, with only a few that were T cell ALL. Our results show that there is altered expression of CS1, LLT1, and NKp30 in different racial/ethnic populations at diagnosis and induction chemotherapy further caused a downregulation in the expression of these receptors in Caucasians as compared to Hispanics and African Americans that could impact the immune dysregulation (Figure 1). Prior studies have predominantly examined genetic polymorphisms and racial/ethnic influence on the risk to develop childhood ALL that may help explain varying susceptibilities across groups to environmental toxins [51]. de Smith et al. reported that Hispanic/Latino children with acute lymphoblastic leukemia (ALL) are more likely to carry high-risk germline SNPs, such as those in the *GATA3* and *IKZF1* genes. The *GATA3* SNP rs3824662, which is more prevalent in individuals with Indigenous American ancestry, has been strongly associated with Philadelphia chromosome-like (Ph-like) ALL—a subtype known for its poor response to standard chemotherapy and increased relapse risk. Similarly, *IKZF1* variants, also enriched in Latino populations, are associated with impaired lymphoid development and reduced survival [6]. Moreover, in pediatric acute myeloid leukemia (AML) a germline SNP in the epigenetic regulator gene *TET2* (rs2454206) has been identified as a prognostic marker influencing survival outcomes. This SNP shows variable prevalence across racial groups, with the $TET2^{AA}$ genotype being more common in Black patients showing higher non-relapse mortality, mainly due to infection-related complications during treatment, suggesting increased treatment toxicity rather than differences in relapse rates. Functional studies indicated

that rs2454206 affects the expression of *CXXC4*, a negative regulator of *TET2*, potentially altering epigenetic regulation and host susceptibility to chemotherapy toxicity [52]. These studies underscore the importance of racial/ethnic differences in SNP distribution that can influence not only chemoresistance but also treatment-related complications. A study on Axicabtagene ciloleucel (axi-cel), an autologous anti-CD19 chimeric antigen receptor (CAR) T cell therapy for relapsed/refractory (R/R) large B-cell lymphoma (LBCL), showed that non-Hispanic (NH) Black patients had a lower overall response rate and a lower complete response rate than NH White patients. NH Black patients also had a shorter progression-free survival vs. NH White and NH Asian patients. They did not find any difference in cytokine-release syndrome by race/ethnicity; however, higher rates of any-grade immune effector cell-associated neurotoxicity syndrome were observed in NH White patients than in other patients [53].

Increased expression of LLT1 was observed on T cells of high-risk ALL patients at diagnosis as compared to healthy individuals. But at the end of induction chemotherapy the expression of LLT1 on T cells of high-risk ALL patients were comparable to healthy individuals (Figure 2). It is well-documented that T cell exhaustion can result in failure of CAR-T cell therapy. B-cell recovery in pediatric B-ALL within 3 months of CD19 CAR-T cell therapy indicates a high-risk of relapse potentially due to T cell exhaustion [54]. Other studies have indicated that the spontaneous aggregation of antigen by CAR-T cells causes CAR-CD3ζ cells to accumulate and leads to CAR-T cell exhaustion [55]. Research has demonstrated that LLT1 on tumor cells interacts with the NK cell inhibitory receptor NKRP1A (CD161), leading to the suppression of NK cell-mediated tumor cytotoxicity [39,40,56–63]. Given that LLT1 is upregulated in various cancers and transmits inhibitory signals to T cells, it is plausible that increased LLT1 expression on ALL cells may potentially cause T cell exhaustion and increased risk-of-relapse. Elevated LLT1 expression on T cells in high-risk ALL patients may contribute to the inhibitory LLT1–NKRP1A interaction with NK cells, potentially enabling leukemic cells to evade NK cell-mediated cytotoxicity. Moreover, on NK cells we observed an increased expression of LLT1 in the very high-risk, high-risk, and standard risk/low-risk ALL patients both before and after chemotherapy treatment as compared to the healthy individuals (Figure 3E-F), which may potentially cause chronic activation of NK cells and be an indicator for NK cell exhaustion, which is where they are unable to recognize malignant cells and carry out the cytotoxic effects [33,64,65]. Similarly, LLT1 expression on CD14+ monocytes was significantly increased in very high-risk, high-risk, and standard risk/low-risk ALL subjects in comparison to their healthy counterparts (Figure 4E), suggesting that the high expression of LLT1 in different cell types could be a major contributor to cancer prognosis and risk in ALL.

At diagnosis, CD56+ NK cells from very high-risk ALL subjects exhibited high expression of CS1, NKp30, and NKp46 as compared to healthy subjects (Figure 3C,G,I) and even after chemotherapy the expression of these receptors did not change significantly but were higher than the expression in healthy subjects (Figure 3D,H,J). Studies have shown that there is increased expression of CS1 in plasma cells, multiple myeloma, and systemic lupus erythematosus [42,43,66–69]. Chretien et al. reported acute myeloid leukemia patients with higher expression of NKp46 had better progression free survival (PFS) and overall survival (OS) than their counterparts with lower expression [44]. Other studies found that NKp30 down-regulation plays a vital role in cervical cancer and HPV-16 immune evasion [70,71]. In contrast, our findings showed high expression of NKp30 on T cells, NK cells, and monocytes of high-risk ALL subjects, which could suggest that NKp30 may play a role in the relapse of ALL. These results align with previous studies which further indicate a connection between these receptors with cancer risk and severity.

In CD14+ monocytes, very high-risk and high-risk ALL subjects showed increased cell surface expression of CS1 that was statistically significant at diagnosis (1BD) as compared to healthy subjects (Figure 4C) and chemotherapy treatment (2BD) did not change the CS1 expression in very high-risk and standard risk/low-risk ALL subjects (Figure 4D). We previously demonstrated that CS1 is expressed in activated monocytes through PI3K- and NF-κB-dependent pathways and exerts an inhibitory effect by decreasing the production of proinflammatory cytokines in LPS-stimulated monocytes [43]. Li et al. reported that CS1 expressing monocytes may promote high-risk of relapse, progression of disease and immunosuppressive state to increase T cell exhaustion and suppression of NK cell function in multiple myeloma [54]. The inhibitory role of CS1 on monocytes could potentially contribute to poorer outcomes in very high-risk and high-risk ALL subjects.

5. Conclusions

Collectively, the results of our study demonstrate that there is differential expression of immune receptors in different racial/ethnic and risk-of-relapse stratified groups in pediatric ALL subjects. The results also suggest that variations in receptor and ligand expression among different racial/ethnic groups and risk stratifications may influence T cell- and NK cell-mediated immune surveillance in pediatric ALL. A major limitation to our study is the small sample size, and the altered expression of receptors observed in different racial/ethnic and risk-of-relapse groups needs to be validated in a larger cohort study. Although we have focused on immune receptor/ligand expression in racial/ethnic populations, other studies have shown genetic risk factors that contribute to the differences in incidences and overall survival in ALL, but the effect of environmental factors and tumor immune microenvironments cannot be ruled out. While our study brings greater understanding to the expression of various receptors/ligands, further studies are necessary to evaluate the function of these receptors and their effect on cancer prognosis and overall survival in risk stratified ALL patients from different racial/ethnic populations.

Supplementary Materials: The following supporting information can be downloaded at: https://www.mdpi.com/article/10.3390/biomedicines13061412/s1, Figure S1: Gating strategy for flow cytometry; Table S1: Clinical and demographic characteristics of pediatric patients with ALL.

Author Contributions: S.M. and W.P.B. designed the experiments. S.M., R.J.G. and S.A. analyzed the data. S.P., R.J.G. and S.M. performed the experiments. R.J.G. and S.M. prepared the figures. A.G. and S.M. wrote and edited the paper. Funding acquisition was performed by W.P.B. and S.M. All authors have read and agreed to the published version of the manuscript.

Funding: This work was supported by the Cancer Foundation of North Texas (CRFNT) (97313), Leukemia Texas Inc. (77313b), Institute for Cancer Research, UNTHSC (RI6062), and Team Connor Childhood Cancer Foundation (77313c).

Institutional Review Board Statement: The study was conducted according to the guidelines of the Declaration of Helsinki and approved by the Institutional Review Board (or Ethics Committee) of University of North Texas Health Science Center (UNTHSC IRB# 2008-094) and Cook Children's Medical Center (CCMC IRB# 2008-57).

Informed Consent Statement: Informed consent/assent was distributed and signed by all participants enrolled in the study.

Data Availability Statement: The data that support the findings of this study are available on request from the corresponding author, S.O.M. The data are not publicly available due to the information contained that could compromise the privacy of research participants.

Acknowledgments: Flow cytometry was performed in the Research Core lab facility at the University of North Texas Health Science Center, Fort Worth, TX, USA. We sincerely thank Steffi Daniel, Rashmi

Deshmukh, and Salwa Shoaib for helping with data analysis and Kim Aldy and Charise Tan for the collection of specimens. Special thanks to all the research subjects and the research staff at Cook Children's Medical Center, Fort Worth and UNT Health Science Center, Fort Worth for participating in the research study.

Conflicts of Interest: The authors declare no conflicts of interest.

Abbreviations

The following abbreviations are used in this manuscript:

ALL	Acute Lymphoblastic Leukemia
MRD	Minimal Residual Disease
B-ALL	B-cell Acute Lymphoblastic Leukemia
T-ALL	T-cell Acute Lymphoblastic Leukemia
NK cell	Natural Killer Cell
SLAMF	Signaling Lymphocyte Activation Molecule Family
NCR	Natural Cytotoxicity Receptor
LLT1	Lectin-Like Transcript 1
CCMC	Cook Children's Medical Center
IRB	Institutional Review Board
MFI	Median Fluorescence Intensity
MFIR	Median Fluorescence Intensity Ratio
PBMCs	Peripheral Blood Mononuclear Cells
VHR	Very High-Risk
HR	High-Risk
SR-LR	Standard-risk/Low-risk
MLL	Mixed Lineage Leukemia
CNS	Central Nervous System
1BD	1st Blood Draw
2BD	2nd Blood Draw
CSF	Cerebrospinal Fluid
CAR	Chimeric Antigen Receptor
LPS	Lipopolysaccharide
OS	Overall Survival

References

1. Aldoss, I.; Forman, S.J.; Pullarkat, V. Acute Lymphoblastic Leukemia in the Older Adult. *J. Oncol. Pract.* **2019**, *15*, 67–75. [CrossRef] [PubMed]
2. Einsiedel, H.G.; von Stackelberg, A.; Hartmann, R.; Fengler, R.; Schrappe, M.; Janka-Schaub, G.; Mann, G.; Hahlen, K.; Gobel, U.; Klingebiel, T.; et al. Long-term outcome in children with relapsed ALL by risk-stratified salvage therapy: Results of trial acute lymphoblastic leukemia-relapse study of the Berlin-Frankfurt-Munster Group 87. *J. Clin. Oncol.* **2005**, *23*, 7942–7950. [CrossRef] [PubMed]
3. Nguyen, K.; Devidas, M.; Cheng, S.C.; La, M.; Raetz, E.A.; Carroll, W.L.; Winick, N.J.; Hunger, S.P.; Gaynon, P.S.; Loh, M.L.; et al. Factors influencing survival after relapse from acute lymphoblastic leukemia: A Children's Oncology Group study. *Leukemia* **2008**, *22*, 2142–2150. [CrossRef] [PubMed]
4. O'Connor, D.; Enshaei, A.; Bartram, J.; Hancock, J.; Harrison, C.J.; Hough, R.; Samarasinghe, S.; Schwab, C.; Vora, A.; Wade, R.; et al. Genotype-Specific Minimal Residual Disease Interpretation Improves Stratification in Pediatric Acute Lymphoblastic Leukemia. *J. Clin. Oncol.* **2018**, *36*, 34–43. [CrossRef]
5. Tallen, G.; Ratei, R.; Mann, G.; Kaspers, G.; Niggli, F.; Karachunsky, A.; Ebell, W.; Escherich, G.; Schrappe, M.; Klingebiel, T.; et al. Long-term outcome in children with relapsed acute lymphoblastic leukemia after time-point and site-of-relapse stratification and intensified short-course multidrug chemotherapy: Results of trial ALL-REZ BFM 90. *J. Clin. Oncol.* **2010**, *28*, 2339–2347. [CrossRef]
6. de Smith, A.J.; Jimenez-Morales, S.; Mejia-Arangure, J.M. The genetic risk of acute lymphoblastic leukemia and its implications for children of Latin American origin. *Front. Oncol.* **2023**, *13*, 1299355. [CrossRef]

7. Liu, S.; Hu, B.; Zhang, J. Epidemiological characteristics and influencing factors of acute leukemia in children and adolescents and adults: A large population-based study. *Hematology* **2024**, *29*, 2327916. [CrossRef]
8. Puckett, Y.; Chan, O. *Acute Lymphocytic Leukemia*; StatPearls: Treasure Island, FL, USA, 2024.
9. Pui, C.H.; Relling, M.V.; Downing, J.R. Acute lymphoblastic leukemia. *N. Engl. J. Med.* **2004**, *350*, 1535–1548. [CrossRef]
10. Seth, R.; Singh, A. Leukemias in Children. *Indian J. Pediatr.* **2015**, *82*, 817–824. [CrossRef]
11. Terwilliger, T.; Abdul-Hay, M. Acute lymphoblastic leukemia: A comprehensive review and 2017 update. *Blood Cancer J.* **2017**, *7*, e577. [CrossRef]
12. Woo, J.S.; Alberti, M.O.; Tirado, C.A. Childhood B-acute lymphoblastic leukemia: A genetic update. *Exp. Hematol. Oncol.* **2014**, *3*, 16. [CrossRef] [PubMed]
13. Kato, M.; Manabe, A. Treatment and biology of pediatric acute lymphoblastic leukemia. *Pediatr. Int.* **2018**, *60*, 4–12. [CrossRef] [PubMed]
14. M Kamazani, F.; Bahoush-Mehdiabadi, G.; Aghaeipour, M.; Vaeli, S.; Amirghofran, Z. The Expression and Prognostic Impact of CD95 Death Receptor and CD20, CD34 and CD44 Differentiation Markers in Pediatric Acute Lymphoblastic Leukemia. *Iran J. Pediatr.* **2014**, *24*, 371–380.
15. Martin Stanulla, M.S. Acute Lymphoblastic Leukemia. *Semin. Hematol.* **2009**, *46*, 52–63. [CrossRef]
16. Rheingold, S.R.; Bhojwani, D.; Ji, L.; Xu, X.; Devidas, M.; Kairalla, J.A.; Shago, M.; Heerema, N.A.; Carroll, A.J.; Breidenbach, H.; et al. Determinants of survival after first relapse of acute lymphoblastic leukemia: A Children's Oncology Group study. *Leukemia* **2024**, *38*, 2382–2394. [CrossRef]
17. Hunger, S.P.; Mullighan, C.G. Redefining ALL classification: Toward detecting high-risk ALL and implementing precision medicine. *Blood* **2015**, *125*, 3977–3987. [CrossRef]
18. Marinescu, C.; Vladareanu, A.M.; Mihai, F. Acute Lymphocytic Leukemia in Adults. Pathologic Features and Prognosis. *Rom. J. Intern. Med.* **2015**, *53*, 31–36. [CrossRef]
19. Peng, L.; Dai, Q.; Wang, Y.; Yang, H.; Shi, R.; Zhang, G.; Jiang, Y.; Ye, L. Lymphocyte subsets in pediatric acute lymphoblastic leukemia and their prognostic value. *Medicine* **2024**, *103*, e40342. [CrossRef]
20. Powers, S.B.; Ahmed, N.G.; Jose, R.; Brezgiel, M.; Aryal, S.; Bowman, W.P.; Mathew, P.A.; Mathew, S.O. Differential Expression of LLT1, SLAM Receptors CS1 and 2B4 and NCR Receptors NKp46 and NKp30 in Pediatric Acute Lymphoblastic Leukemia (ALL). *Int. J. Mol. Sci.* **2023**, *24*, 3860. [CrossRef]
21. Allison, M.; Mathews, J.; Gilliland, T.; Mathew, S.O. Natural Killer Cell-Mediated Immunotherapy for Leukemia. *Cancers* **2022**, *14*, 843. [CrossRef]
22. Hunger, S.P.; Raetz, E.A. How I treat relapsed acute lymphoblastic leukemia in the pediatric population. *Blood* **2020**, *136*, 1803–1812. [CrossRef]
23. Witek, M.A.; Larkey, N.E.; Bartakova, A.; Hupert, M.L.; Mog, S.; Cronin, J.K.; Vun, J.; August, K.J.; Soper, S.A. Microfluidic Affinity Selection of B-Lineage Cells from Peripheral Blood for Minimal Residual Disease Monitoring in Pediatric B-Type Acute Lymphoblastic Leukemia Patients. *Int. J. Mol. Sci.* **2024**, *25*, 10619. [CrossRef] [PubMed]
24. Archer, N.P.; Perez-Andreu, V.; Scheurer, M.E.; Rabin, K.R.; Peckham-Gregory, E.C.; Plon, S.E.; Zabriskie, R.C.; De Alarcon, P.A.; Fernandez, K.S.; Najera, C.R.; et al. Family-based exome-wide assessment of maternal genetic effects on susceptibility to childhood B-cell acute lymphoblastic leukemia in hispanics. *Cancer* **2016**, *122*, 3697–3704. [CrossRef] [PubMed]
25. de Smith, A.J.; Wahlster, L.; Jeon, S.; Kachuri, L.; Black, S.; Langie, J.; Cato, L.D.; Nakatsuka, N.; Chan, T.F.; Xia, G.; et al. A noncoding regulatory variant in IKZF1 increases acute lymphoblastic leukemia risk in Hispanic/Latino children. *Cell Genom.* **2024**, *4*, 100526. [CrossRef] [PubMed]
26. Inaba, H.; Pui, C.H. Advances in the Diagnosis and Treatment of Pediatric Acute Lymphoblastic Leukemia. *J. Clin. Med.* **2021**, *10*, 1926. [CrossRef]
27. Pui, C.H.; Yang, J.J.; Hunger, S.P.; Pieters, R.; Schrappe, M.; Biondi, A.; Vora, A.; Baruchel, A.; Silverman, L.B.; Schmiegelow, K.; et al. Childhood Acute Lymphoblastic Leukemia: Progress Through Collaboration. *J. Clin. Oncol.* **2015**, *33*, 2938–2948. [CrossRef]
28. Kahn, J.M.; Keegan, T.H.; Tao, L.; Abrahao, R.; Bleyer, A.; Viny, A.D. Racial disparities in the survival of American children, adolescents, and young adults with acute lymphoblastic leukemia, acute myelogenous leukemia, and Hodgkin lymphoma. *Cancer* **2016**, *122*, 2723–2730. [CrossRef]
29. Lim, J.Y.; Bhatia, S.; Robison, L.L.; Yang, J.J. Genomics of racial and ethnic disparities in childhood acute lymphoblastic leukemia. *Cancer* **2014**, *120*, 955–962. [CrossRef]
30. Bi, J.; Tian, Z. NK Cell Dysfunction and Checkpoint Immunotherapy. *Front. Immunol.* **2019**, *10*, 1999. [CrossRef]
31. Buller, C.W.; Mathew, P.A.; Mathew, S.O. Roles of NK Cell Receptors 2B4 (CD244), CS1 (CD319), and LLT1 (CLEC2D) in Cancer. *Cancers* **2020**, *12*, 1755. [CrossRef]
32. Lee, L.J.; Hassan, N.; Idris, S.Z.; Subbiah, S.K.; Seow, H.F.; Mohtaruddin, N.; Chang, K.M.; Osman, R.; Ibrahim, H.M.; Nathan, S.; et al. Differential Regulation of NK Cell Receptors in Acute Lymphoblastic Leukemia. *J. Immunol. Res.* **2022**, *2022*, 7972039. [CrossRef] [PubMed]

33. Cózar, B.; Greppi, M.; Carpentier, S.; Narni-Mancinelli, E.; Chiossone, L.; Vivier, E. Tumor-Infiltrating Natural Killer Cells. *Cancer Discov.* **2021**, *11*, 34–44. [CrossRef] [PubMed]
34. Myers, J.A.; Miller, J.S. Exploring the NK cell platform for cancer immunotherapy. *Nat. Rev. Clin. Oncol.* **2021**, *18*, 85–100. [CrossRef] [PubMed]
35. Mizia-Malarz, A.; Sobol-Milejska, G. NK Cells as Possible Prognostic Factor in Childhood Acute Lymphoblastic Leukemia. *Dis. Markers* **2019**, *2019*, 3596983. [CrossRef]
36. Cheng, M.; Chen, Y.; Xiao, W.; Sun, R.; Tian, Z. NK cell-based immunotherapy for malignant diseases. *Cell Mol. Immunol.* **2013**, *10*, 230–252. [CrossRef]
37. Ibáñez-Navarro, M.; Fernández, A.; Escudero, A.; Esteso, G.; Campos-Silva, C.; Navarro-Aguadero, M.Á.; Leivas, A.; Caracuel, B.R.; Rodríguez-Antolín, C.; Ortiz, A.; et al. NKG2D-CAR memory T cells target pediatric T-cell acute lymphoblastic leukemia in vitro and in vivo but fail to eliminate leukemia initiating cells. *Front. Immunol.* **2023**, *14*, 1187665. [CrossRef]
38. Yang, N.; Zhang, C.; Zhang, Y.; Fan, Y.; Zhang, J.; Lin, X.; Guo, T.; Gu, Y.; Wu, J.; Gao, J.; et al. CD19/CD20 dual-targeted chimeric antigen receptor-engineered natural killer cells exhibit improved cytotoxicity against acute lymphoblastic leukemia. *J. Transl. Med.* **2024**, *22*, 274–288. [CrossRef]
39. Mathew, S.O.; Chaudhary, P.; Powers, S.B.; Vishwanatha, J.K.; Mathew, P.A. Overexpression of LLT1 (OCIL, CLEC2D) on prostate cancer cells inhibits NK cell-mediated killing through LLT1-NKRP1A (CD161) interaction. *Oncotarget* **2016**, *7*, 68650–68661. [CrossRef]
40. Marrufo, A.M.; Mathew, S.O.; Chaudhary, P.; Malaer, J.D.; Vishwanatha, J.K.; Mathew, P.A. Blocking LLT1 (CLEC2D, OCIL)-NKRP1A (CD161) interaction enhances natural killer cell-mediated lysis of triple-negative breast cancer cells. *Am. J. Cancer Res.* **2018**, *8*, 1050–1063.
41. Sung, P.S.; Jang, J.W. Natural Killer Cell Dysfunction in Hepatocellular Carcinoma: Pathogenesis and Clinical Implications. *Int. J. Mol. Sci.* **2018**, *19*, 3648. [CrossRef]
42. Kim, J.R.; Mathew, S.O.; Patel, R.K.; Pertusi, R.M.; Mathew, P.A. Altered expression of signalling lymphocyte activation molecule (SLAM) family receptors CS1 (CD319) and 2B4 (CD244) in patients with systemic lupus erythematosus. *Clin. Exp. Immunol.* **2010**, *160*, 348–358. [CrossRef] [PubMed]
43. Kim, J.R.; Horton, N.C.; Mathew, S.O.; Mathew, P.A. CS1 (SLAMF7) inhibits production of proinflammatory cytokines by activated monocytes. *Inflamm. Res.* **2013**, *62*, 765–772. [CrossRef] [PubMed]
44. Chretien, A.S.; Devillier, R.; Fauriat, C.; Orlanducci, F.; Harbi, S.; Le Roy, A.; Rey, J.; Bouvier Borg, G.; Gautherot, E.; Hamel, J.F.; et al. NKp46 expression on NK cells as a prognostic and predictive biomarker for response to allo-SCT in patients with AML. *Oncoimmunology* **2017**, *6*, e1307491. [CrossRef]
45. Berkman, A.M.; Andersen, C.R.; Cuglievan, B.; McCall, D.C.; Lupo, P.J.; Parsons, S.K.; DiNardo, C.D.; Short, N.J.; Jain, N.; Kadia, T.M.; et al. Long-Term Outcomes among Adolescent and Young Adult Survivors of Acute Leukemia: A Surveillance, Epidemiology, and End Results Analysis. *Cancer Epidemiol. Biomark. Prev.* **2022**, *31*, 1176–1184. [CrossRef]
46. Lanier, L.L. Up on the tightrope: Natural killer cell activation and inhibition. *Nat. Immunol.* **2008**, *9*, 495–502. [CrossRef]
47. Lee, R.K.; Spielman, J.; Zhao, D.Y.; Olsen, K.J.; Podack, E.R. Perforin, Fas ligand, and tumor necrosis factor are the major cytotoxic molecules used by lymphokine-activated killer cells. *J. Immunol.* **1996**, *157*, 1919–1925. [CrossRef]
48. Perussia, B. Lymphokine-activated killer cells, natural killer cells and cytokines. *Curr. Opin. Immunol.* **1991**, *3*, 49–55. [CrossRef]
49. Isakov, N. ITIMs and ITAMs: The Yin and Yang of antigen and Fc receptor-linked signaling machinery. *Immunol. Res.* **1997**, *16*, 85–100. [CrossRef]
50. Chen, Y.; Lu, D.; Churov, A.; Fu, R. Research Progress on NK Cell Receptors and Their Signaling Pathways. *Mediat. Inflamm.* **2020**, *2020*, 6437057. [CrossRef]
51. Swinney, R.M.; Beuten, J.; Collier, A.B., 3rd; Chen, T.T.; Winick, N.J.; Pollock, B.H.; Tomlinson, G.E. Polymorphisms in CYP1A1 and ethnic-specific susceptibility to acute lymphoblastic leukemia in children. *Cancer Epidemiol. Biomark. Prev.* **2011**, *20*, 1537–1542. [CrossRef]
52. Kutny, M.A.; Alonzo, T.A.; Gamazon, E.R.; Gerbing, R.B.; Geraghty, D.; Lange, B.; Heerema, N.A.; Sung, L.; Aplenc, R.; Franklin, J.; et al. Ethnic variation of TET2 SNP rs2454206 and association with clinical outcome in childhood AML: A report from the Children's Oncology Group. *Leukemia* **2015**, *29*, 2424–2426. [CrossRef] [PubMed]
53. Locke, F.L.; Siddiqi, T.; Jacobson, C.A.; Ghobadi, A.; Ahmed, S.; Miklos, D.B.; Perales, M.A.; Munoz, J.; Fingrut, W.B.; Pennisi, M.; et al. Real-world and clinical trial outcomes in large B-cell lymphoma with axicabtagene ciloleucel across race and ethnicity. *Blood* **2024**, *143*, 2722–2734. [CrossRef] [PubMed]
54. Li, W.; Zhang, B.; Cao, W.; Zhang, W.; Li, T.; Liu, L.; Xu, L.; Gao, F.; Wang, Y.; Wang, F.; et al. Identification of potential resistance mechanisms and therapeutic targets for the relapse of BCMA CAR-T therapy in relapsed/refractory multiple myeloma through single-cell sequencing. *Exp. Hematol. Oncol.* **2023**, *12*, 44. [CrossRef] [PubMed]

55. Long, A.; Haso, W.; Shern, J.; Wanhainen, K.M.; Murgai, M.; Ingaramo, M.; Smith, J.P.; Walker, A.J.; Kohler, M.E.; Venkateshwara, V.R.; et al. 4-1BB costimulation ameliorates T cell exhaustion induced by tonic signaling of chimeric antigen receptors. *Nat. Med.* **2015**, *21*, 581–590. [CrossRef]
56. Sanchez-Canteli, M.; Hermida-Prado, F.; Sordo-Bahamonde, C.; Montoro-Jimenez, I.; Pozo-Agundo, E.; Allonca, E.; Vallina-Alvarez, A.; Alvarez-Marcos, C.; Gonzalez, S.; Garcia-Pedrero, J.M.; et al. Lectin-Like Transcript 1 (LLT1) Checkpoint: A Novel Independent Prognostic Factor in HPV-Negative Oropharyngeal Squamous Cell Carcinoma. *Biomedicines* **2020**, *8*, 535. [CrossRef]
57. Roth, P.; Mittelbronn, M.; Wick, W.; Meyermann, R.; Tatagiba, M.; Weller, M. Malignant glioma cells counteract antitumor immune responses through expression of lectin-like transcript-1. *Cancer Res.* **2007**, *67*, 3540–3544. [CrossRef]
58. Germain, C.; Guillaudeux, T.; Galsgaard, E.D.; Hervouet, C.; Tekaya, N.; Gallouet, A.S.; Fassy, J.; Bihl, F.; Poupon, G.; Lazzari, A.; et al. Lectin-like transcript 1 is a marker of germinal center-derived B-cell non-Hodgkin's lymphomas dampening natural killer cell functions. *Oncoimmunology* **2015**, *4*, e1026503. [CrossRef]
59. Braud, V.M.; Biton, J.; Becht, E.; Knockaert, S.; Mansuet-Lupo, A.; Cosson, E.; Damotte, D.; Alifano, M.; Validire, P.; Anjuere, F.; et al. Expression of LLT1 and its receptor CD161 in lung cancer is associated with better clinical outcome. *Oncoimmunology* **2018**, *7*, e1423184. [CrossRef]
60. de Vicente, J.C.; Lequerica-Fernandez, P.; Rodrigo, J.P.; Rodriguez-Santamarta, T.; Blanco-Lorenzo, V.; Prieto-Fernandez, L.; Corte-Torres, D.; Vallina, A.; Dominguez-Iglesias, F.; Alvarez-Teijeiro, S.; et al. Lectin-like Transcript-1 (LLT1) Expression in Oral Squamous Cell Carcinomas: Prognostic Significance and Relationship with the Tumor Immune Microenvironment. *Int. J. Mol. Sci.* **2024**, *25*, 4314. [CrossRef]
61. Hu, X.; Dong, Y.; Xie, S.; Song, Y.; Yu, C.; He, Y.; Wang, Z.; Hu, Q.; Ni, Y.; Ding, L. Immune checkpoint CD161/LLT1-associated immunological landscape and diagnostic value in oral squamous cell carcinoma. *J. Pathol. Clin. Res.* **2024**, *10*, e353. [CrossRef]
62. Mandal, T.; Gnanasegaran, S.; Rodrigues, G.; Kashipathi, S.; Tiwari, A.; Dubey, A.K.; Bhattacharjee, S.; Manjunath, Y.; Krishna, S.; Madhusudhan, M.S.; et al. Targeting LLT1 as a potential immunotherapy option for cancer patients non-responsive to existing checkpoint therapies in multiple solid tumors. *BMC Cancer* **2024**, *24*, 1365. [CrossRef] [PubMed]
63. Sun, Y.; Malaer, J.D.; Mathew, P.A. Lectin-like transcript 1 as a natural killer cell-mediated immunotherapeutic target for triple negative breast cancer and prostate cancer. *J. Cancer Metastasis Treat.* **2019**, *2019*, 80. [CrossRef] [PubMed]
64. Bi, J.; Tian, Z. NK Cell Exhaustion. *Front. Immunol.* **2017**, *8*, 760. [CrossRef] [PubMed]
65. Judge, S.J.; Murphy, W.J.; Canter, R.J. Characterizing the Dysfunctional NK Cell: Assessing the Clinical Relevance of Exhaustion, Anergy, and Senescence. *Front. Cell Infect. Microbiol.* **2020**, *10*, 49. [CrossRef]
66. Schlaphoff, V.; Lunemann, S.; Suneetha, P.V.; Jaroszewicz, J.; Grabowski, J.; Dietz, J.; Helfritz, F.; Bektas, H.; Sarrazin, C.; Manns, M.P.; et al. Dual function of the NK cell receptor 2B4 (CD244) in the regulation of HCV-specific CD8+ T cells. *PLoS Pathog.* **2011**, *7*, e1002045. [CrossRef]
67. Malaer, J.D.; Mathew, P.A. CS1 (SLAMF7, CD319) is an effective immunotherapeutic target for multiple myeloma. *Am. J. Cancer Res.* **2017**, *7*, 1637–1641.
68. Hsi, E.D.; Steinle, R.; Balasa, B.; Szmania, S.; Draksharapu, A.; Shum, B.P.; Huseni, M.; Powers, D.; Nanisetti, A.; Zhang, Y.; et al. CS1, a potential new therapeutic antibody target for the treatment of multiple myeloma. *Clin. Cancer Res.* **2008**, *14*, 2775–2784. [CrossRef]
69. Chu, J.; He, S.; Deng, Y.; Zhang, J.; Peng, Y.; Hughes, T.; Yi, L.; Kwon, C.H.; Wang, Q.E.; Devine, S.M.; et al. Genetic modification of T cells redirected toward CS1 enhances eradication of myeloma cells. *Clin. Cancer Res.* **2014**, *20*, 3989–4000. [CrossRef]
70. Gutierrez-Silerio, G.Y.; Bueno-Topete, M.R.; Vega-Magana, A.N.; Bastidas-Ramirez, B.E.; Gutierrez-Franco, J.; Escarra-Senmarti, M.; Pedraza-Brindis, E.J.; Pena-Rodriguez, M.; Ramos-Marquez, M.E.; Delgado-Rizo, V.; et al. Non-fitness status of peripheral NK cells defined by decreased NKp30 and perforin, and increased soluble B7H6, in cervical cancer patients. *Immunology* **2023**, *168*, 538–553. [CrossRef]
71. Garcia-Iglesias, T.; Del Toro-Arreola, A.; Albarran-Somoza, B.; Del Toro-Arreola, S.; Sanchez-Hernandez, P.E.; Ramirez-Duenas, M.G.; Balderas-Pena, L.M.; Bravo-Cuellar, A.; Ortiz-Lazareno, P.C.; Daneri-Navarro, A. Low NKp30, NKp46 and NKG2D expression and reduced cytotoxic activity on NK cells in cervical cancer and precursor lesions. *BMC Cancer* **2009**, *9*, 186. [CrossRef]

Disclaimer/Publisher's Note: The statements, opinions and data contained in all publications are solely those of the individual author(s) and contributor(s) and not of MDPI and/or the editor(s). MDPI and/or the editor(s) disclaim responsibility for any injury to people or property resulting from any ideas, methods, instructions or products referred to in the content.

biomedicines

MDPI

Article

Single-Cell Transcriptomic Analysis Unveils Key Regulators and Signaling Pathways in Lung Adenocarcinoma Progression

Jialu Ma [1,2], Caleb McQuay [3], John Talburt [2], Amit K. Tiwari [4] and Mary Qu Yang [1,2,*]

[1] MidSouth Bioinformatics Center and Joint Bioinformatics Graduate Program, University of Arkansas at Little Rock, Little Rock, AR 72204, USA
[2] Information Science, University of Arkansas at Little Rock, Little Rock, AR 72204, USA
[3] Computer Science, University of Arkansas at Little Rock, Little Rock, AR 72204, USA
[4] Department of Pharmaceutical Sciences, College of Pharmacy, University of Arkansas for Medical Sciences, Little Rock, AR 72205, USA; atiwari@uams.edu
* Correspondence: mqyang@ualr.edu

Abstract

Background: Lung adenocarcinoma (LUAD) remains a leading cause of cancer-related mortality despite advances in treatments, necessitating more effective therapeutic strategies. Single-cell RNA sequencing (scRNA-seq) technology has revolutionized our ability to dissect the cellular complexity of cancers, which is often obscured in conventional bulk transcriptomic experiments. **Methods:** In this study, we performed an integrative analysis of scRNA-seq data from multiple LUAD patient cohorts to investigate cell-type-specific transcriptomic changes across disease stages. Clustering, lineage trajectory analysis, and transcriptional regulatory network reconstruction were employed to identify stage-specific gene markers and their upstream regulators. Additionally, we constructed intercellular communication networks to evaluate signaling changes within the tumor microenvironment (TME) during LUAD progression. **Results:** Our analysis revealed that epithelial cells from stage IV tumors exhibited a distinct transcriptional profile compared to earlier stages, a separation not observed in immune or stromal cell populations. We identified a panel of gene markers that differentiated epithelial cells across disease stages and effectively stratified patients into subgroups with distinct survival outcomes and TME compositions. Regulatory network analysis uncovered key transcription factors, including ATF3, ATF4, HSF1, KLF4, and NFIC, as potential upstream regulators of these stage-specific genes. Moreover, cell–cell communication analysis revealed a significant increase in signaling originating from epithelial cells and a concomitant decrease in immune-derived signals in late-stage LUAD. We identified several signaling pathways enriched in stage-specific crosstalk, including Wnt, PTN, and PDGF pathways, which may play critical roles in LUAD progression. **Conclusions:** This study provides a comprehensive single-cell resolution map of LUAD progression, highlighting epithelial-driven regulatory programs and dynamic intercellular communication within the TME. Our findings uncover novel molecular markers and regulatory mechanisms with potential prognostic and therapeutic value for more precise treatment.

Keywords: lung adenocarcinoma progression; single-cell RNA sequencing; transcription regulator; signaling pathways

1. Introduction

Lung carcinoma is a leading cause of cancer-related mortality worldwide, with an estimated 18.4% of all cancer deaths in 2018 [1]. Lung cancer is classified into small-cell lung (SCLC) and non-small-cell lung cancers (NSCLC), the latter representing about 80–85% of total cases [2]. NSCLC can be further classified into adenocarcinoma and squamous cell carcinoma. Only around 20% of lung cancer patients are eligible for curative surgery, yet up to 80% of those who undergo resection experience postoperative recurrence [3]. Moreover, roughly one-third of NSCLC cases are diagnosed at stage III, where 5-year survival falls from 36% in stage IIIA to 13% in stage IIIC [4]. Among the subtypes of NSCLC, lung adenocarcinoma (LUAD) is the most prevalent. Major risk factors for LUAD include smoking, environmental exposure, and genetic predispositions. As smoking rates decline in the population [5], there has been a marked increase in the proportion of patients with lung cancer who have never smoked, particularly among younger people and women [6]. Nonsmoking lung cancer patients are frequently diagnosed with LUAD [7,8]. Despite improvements in early diagnosis and treatment, patients often experience relapses and metastases. Consequently, the prognosis and overall survival rate of LUAD remain very poor [9,10].

Conventional treatment for LUAD includes surgery, chemotherapy, and radiotherapy. Owing to discoveries in molecular translation and clinical research, newer treatment approaches such as immunotherapy and targeted therapy have emerged as important options, which offer improved survival rates and quality of life for many patients with LUAD. For example, immune checkpoint blockade has become a significant treatment method for various cancers, including LUAD. In particular, inhibitors of the programmed cell death protein-1/programmed cell death ligand-1 (PD-1/PD-L1) enhance the antitumor activity of cytotoxic T cells and have been proven to be effective in the treatment of locally advanced LUAD [11,12]. Tyrosine kinase inhibitors targeted at known oncogenic driver mutations, such as EGFR and BRAF gene mutations [13,14] and ALK and ROS1 fusions [15–17], demonstrate efficacy in treating patients harboring these mutations [18]. However, patient responses to targeted therapy and immunotherapy vary widely. While some patients achieve a complete response, others may experience partial responses, and many may not respond at all. Furthermore, tumor progression can still occur in patients who initially respond to treatment, often due to the development of acquired resistance [19]. The inherent heterogeneity of LUAD further complicates the efficacy and durability of these treatments. To address these challenges, preclinical models such as patient-derived xenografts (PDX) have been used to evaluate therapeutic responses in a more physiologically relevant context [20,21]. However, they often lack resolution at the single-cell level.

Single-cell sequencing technology, which allows the assessment of individual cells in the tumor microenvironment (TME), provides opportunities to gain novel insights into disease progression and cellular heterogeneity, potentially leading to new treatment strategies. LUAD originates mainly from epithelial cells located in the distal part of the lung [22]. Oncogenic mutations in pulmonary epithelial cells can cause uncontrolled cellular proliferation, contributing to the development of lung cancer [23,24]. Lung epithelial cells have self-renewal capacity and can regenerate other types of lung cells in response to injury and disease [25]. Dysregulation of inflammation has been reported to facilitate the transition of epithelial cells to mesenchymal cells, a process critical to the development of chronic obstructive pulmonary disease and lung cancer [26,27]. However, the molecular mechanisms underlying the progression of LUAD at the cellular level remain largely uncharacterized.

In this study, we analyzed the transcriptomic alterations of various cell types and their intercellular communications within the TME during the progression of LUAD by

incorporating multiple single-cell RNA sequencing (scRNA-seq) datasets. We discovered a clear separation between stage IV LUAD epithelial cells and those from earlier stages, a distinction not seen in immune and stromal cell populations, as demonstrated through both cell clustering and lineage analysis. This unique separation pattern allowed us to extract a set of differentially expressed genes in epithelial cells that may serve as gene markers for LUAD progression at the cellular level. Given the inherent complexity and heterogeneity of LUAD, as observed in many other cancers, we expanded our analysis to multiple independent LUAD patient cohorts. We found that the expression of these gene markers robustly segregated LUAD patients into subgroups with distinct survival outcomes and TME compositions. To investigate the regulation of these gene signatures, we constructed transcriptional regulatory networks and identified their master regulators. Furthermore, we inferred cell-cell communication networks within the TME to assess changes in cellular interactions in response to LUAD progression. Our analysis revealed significantly increased communication signals originating from epithelial cells, particularly in the crosstalk between epithelial and fibroblast cells; in contrast, communication from immune cells notably decreased in late-stage LUAD. We also identified several key signaling pathways associated with the dynamics of the intercellular communication networks during LUAD progression. These findings present promising cellular-level biomarkers and drug targets, offering more precise opportunities for managing disease progression and developing improved treatment strategies for better clinical outcomes in patients.

2. Materials and Methods

2.1. LUAD Datasets

We obtained two scRNA-seq datasets, GSE131907 [28] and GSE127465 [29], from Gene Expression Omnibus (GEO) for this study. The GSE131907 dataset was generated using the 10× Genomics Single Cell 3′ platform, with libraries prepared by the Single Cell 3′ library and Gel Bead Kit V2, and sequenced on the Illumina HiSeq 2500 [28]. The sequencing reads were aligned to the GRCh38 human genome. For our study, we utilized cells derived from 26 lung tissue samples, including 11 normal and 15 tumor samples spanning stages I to IV. The GSE127465 dataset was generated using the inDrop platform. Libraries were prepared on the Illumina NextSeq platform and mapped to the GRCh38 human genome [29]. A total of 29,313 cells from tumor tissue samples collected from five LUAD patients across stages I, III, and IV were included in our study. The detailed metadata for GSE131907 and GSE127465 are provided in Supp. Table S1.

Additionally, we obtained four LUAD datasets containing survival information: TCGA-LUAD, OncoSG-LUAD, GSE68465, and GSE72094 from public data repositories. The TCGA-LUAD dataset was sourced from The Cancer Genome Atlas (TCGA) project and downloaded from the cBioPortal database (https://www.cbioportal.org/ (accessed on 19 March 2025.)). This dataset includes 515 LUAD samples, providing tissue RNA sequencing data, clinical information, and overall survival data. The OncoSG dataset was also obtained from the cBioPortal database [30] and consists of RNA sequencing profiles and clinical data for 169 LUAD patients. The GSE68465 [31] and GSE72094 [32] datasets were downloaded from the Gene Expression Omnibus (GEO). GSE68465 contains gene expression microarray data, clinical information, and pathological data from 443 LUAD patients [31]. GSE72094 includes gene expression data derived from Affymetrix microarrays and clinical information for 442 LUAD patients [32]. Detailed metadata for these four datasets is provided in Supp. Table S2.

2.2. scRNA-seq Data Preprocessing

The scRNA-seq data were processed with the Seurat package (version 5.1.0) in R. Initially, we excluded genes that were detected in less than 0.1% of total cells. We quantified the expression of mitochondrial genes and filtered out cells where mitochondrial gene expression exceeded 20%. The cells that had expressed fewer than 200 or more than 5000 genes were also removed. The dataset was normalized using log transformation with a scale factor of 10,000 (scale factor = 1×10^4). Then, we centered the expression values for each gene to have a mean of zero and limited the maximum value to 10 for scaled expression values using the ScaleData function in Seurat by setting the parameters: do.scale = FALSE, do.center = TRUE, scale.max = 10.

2.3. Cell Clustering and Cell Lineage Analysis

We selected the top 3000 genes that displayed the highest variability for cell clustering analysis. Dimensionality reduction was performed via principal component analysis (PCA), and the first 20 principal components were selected based on an Elbow plot analysis. The 20 principal components with a resolution of 0.2 were used to identify cell neighbors and generate broad cell clusters. Subsequently, when focusing on specific cell subsets (such as immune, stromal, and epithelial cells), the resolution was lowered to 0.01 to achieve finer-grained clustering. The clustering results were visualized using the uniform model approximation and projection (UMAP) [33].

Purity and entropy were calculated to assess the homogeneity of stage-specific clusters in malignant and non-malignant epithelial cells. Purity quantifies the dominance of a single cell type in a cluster and is computed as follows:

$$\text{Purity} = \frac{1}{N} \sum_{i} \max_{j} |c_i \cap t_j| \tag{1}$$

where N is the total number of cells, c_i is the number of cells in the ith cluster, and t_j is the count of cells in the jth cluster represents true stage information. Purity ranges from 0 (no homogeneity) to 1 (complete homogeneity). Entropy measures the uncertainty within a cluster and is calculated as:

$$S = -\sum_{j=1}^{C} p_j \log_2(p_j) \tag{2}$$

where C is the number of unique cell types and p_j is the proportion of cells of type j. Entropy values range from 0 (complete homogeneity) to 1 (maximum heterogeneity). Higher purity and lower entropy indicate more homogeneous clusters.

We applied the 'FindMarkers' function in the Seurat package to identify differentially expressed genes (DEGs) between various cell clusters using a Wilcoxon rank-sum test. A minimum percentage (min.pct) threshold of 0.25 was applied. Genes with adjusted p-value less than 0.01 and $\log_2(FC)$ greater than 1 were considered differentially expressed.

The trajectory of the cell lineage was constructed using Monocle2 [34]. The raw count matrix, phenotype data, and feature data were extracted from the corresponding Seurat object to generate the 'newCellDataSet' object. The data were normalized using 'estimateSizeFactors()', and gene expression dispersion was estimated with 'estimateDispersions()'. A set of highly variable genes, previously identified in Seurat via the 'VariableFeatures' function, was used to define the ordering filter with the 'setOrderingFilter' function. Dimensionality reduction and trajectory construction were performed using the DDRTree method, and cells were subsequently arranged along a pseudotime axis using 'orderCells'. The resulting cell trajectories were visualized with 'plot_cell_trajectory', highlighting distinct cell states and disease stages.

2.4. Copy Number Variation from Single Cell RNAseq Data

To distinguish malignant cells from non-malignant cells in tumor tissues, we utilized a method developed by Nayoung Kim et al. [28] to identify aberrant copy number variations based on perturbations in chromosomal gene expression. First, normal cells were added to tumor cells to ensure that putative malignant cells comprised less than 20% of the total cell population. Genes expressed in fewer than ten cells or with a mean expression of less than 0.1 across all cells on the log2 scale were then filtered out. Gene expression was standardized to Z-scores, scaled from -3 to 3. We sorted the genes by chromosomal location and calculated the CNV signals using a window size of 100 genes. The CNV signal was then adjusted using centered values across all genes. Finally, the CNV signal was summarized using the mean squares of estimates across all windows and the correlation of the CNV for each window with the mean of the top 5% of cells. Tumor cells with a mean square larger than 0.02 or a correlation larger than 0.2 were considered malignant.

InferCNV (version 1.18.1) [35] R package was employed to establish CNV profiles in tumor epithelial cells. Following cluster identification, the scRNA-seq data were prepared for inferCNV by sorting genes according to their genomic locations on chromosomes. As the dataset included only malignant cells, a reference group was not created. The parameters used for the InferCNV run() were cutoff = 1, denoise = FALSE, HMM = FALSE, and cluster_by_groups = TRUE.

2.5. LUAD Patient Subgroups

The bulk RNA sequencing and clinical data of LUAD patients in the TCGA (The Cancer Genome Atlas) [23] project were downloaded from cBioPortal [36]. The expression profile was normalized using the $\log_2(x+1)$ transformation. ComplexHeatmap package in R [37] was employed to perform hierarchical cluster analysis using the expression levels of stage-specific DEGs derived from epithelial cells. Euclidean distance with the Ward.D method was adopted for the clustering analysis. The column dendrogram of the hierarchical clusters represented LUAD tissue sample subgroups, while the row dendrogram organized the genes into three subsets. The enriched pathways and biological processes associated with the gene subsets were identified using the enrichKEGG() and enrichGO() functions from the clusterProfiler package in R. The *p*-values were calculated using the hypergeometric distribution and adjusted with the Benjamini-Hochberg (BH) method.

The Kaplan-Meier curves were plotted for each patient subgroup using the R survival package. Patients without stage information were excluded from the survival analysis. The logarithmic ranking test was used to evaluate the significance of the survival rate difference among the patient subgroups.

The composition of stromal and immune cells within LUAD tissue samples was assessed using the ESTIMATE method [38], while tumor purity was calculated using the PUREE method [39]. Both approaches relied on transcriptomic data obtained by RNA sequencing.

2.6. Gene Expression Regulatory Networks

We utilized the pySCENIC [40] pipeline to infer gene regulatory networks from processed scRNA-seq data. In the initial step, we employed the 'grnboost2' method to identify transcription factor (TF) and target co-expression modules. To reduce the stochasticity of 'grnboost2', we repeated this step 100 times, each with a different random seed, generating 100 adjacency files containing TF-target pairs with their importance values. We then retained those TF-target pairs that appeared in at least 80 out of the 100 runs and calculated their importance scores as the average importance across these retained occurrences. We then refined these pairs based on the enrichment of TF binding motifs to

infer potential regulons for TFs and their direct targets. The genomic region considered for binding motif searching included 500 base pairs upstream and 100 base pairs downstream of the transcription start site, which defined the promoter region. Subsequently, we quantified the activity of each regulon using the area under the recovery curve [40]. The stage-specific specificity of each regulon was calculated based on Jensen-Shannon divergence [40]. Finally, active and stage-specific regulons containing at least one DEG were assembled into regulatory networks and visualized using Cytoscape.

The interactions in the STRING database were selected based on evidence from experiments, databases, and literature text mining to investigate their connections with the key TFs.

2.7. Intercelluar Communication Networks

The cell-cell communication networks were constructed using the CellChat R package [41]. The gene expression data from the scRNA-seq dataset were mapped to a signaling molecular database that consists of interactions among ligands, receptors, and cofactors [41]. Communication networks between cell types were established using mass action models, differential expression analysis, and statistical tests. For a better comparison between early and late stages, we excluded endothelial cells and mast cells because of the absence of data for these two cell types in the late stage. Separate CellChat objects were created for the early and latestage datasets using the normalized data from the Seurat object. We then merged the two CellChat objects using the mergeCellChat() function, allowing for a direct comparison of their intercellular communication networks. To assess differences in the overall number and strength of interactions, we utilized compareInteractions() and netVisual_diffInteraction() to visualize changes in network edges. We also employed netVisual_heatmap() to examine these differences, highlighting variations in incoming and outgoing signaling for each cell type. Additionally, we used rankNet() to evaluate and rank the significance of different signaling pathways. The significance of these signaling pathways was evaluated through a permutation test by randomly permuting cell labels. The random permutation was repeated 100 times, after which the *p*-value was calculated, with $p < 0.05$ considered significant.

3. Results

3.1. The Cellular Landscape of LUAD

The single-cell RNA sequencing dataset (GSE131907) used in our study was generated from 11 LUAD adjacent normal tissue samples and 15 LUAD tumor tissue samples from eight Stage I, one Stage II, two Stage III, and four Stage IV patients [28]. After removing low-quality and non-expressed genes, a total of 98,504 cells consisting of 55,655 from tumor tissues and 42,849 from normal tissues, and 18,900 genes were retained for further analysis.

A total of eight major cell types were identified (Figure 1a), including 16,046 epithelial cells, 5468 stromal cells composed of endothelial cells and fibroblasts, and 76,990 immune cells. The immune cell population comprised 6407 B lymphocytes, 32,591 T lymphocytes, 2888 mast cells, 26,693 myeloid cells, and 8411 natural killer cells (NK). The different cell types were clearly separated, as illustrated in the UMAP (Figure 1a).

Next, we mapped tumor stage information to cell clusters and observed distinct patterns among epithelial, immune, and stromal cells. The epithelial cells demonstrated clear stage-specific clustering, showing significant separation between cells derived from various stages of LUAD tissue samples (Figure 1b) and those from normal tissue samples. In contrast, while stromal and immune cells exhibited distinct separation based on cell subtype (Figure 1c,e), they did not show significant distinctions among cells from different stages or normal tissues. Immune and stromal cells from various stages of LUAD and

normal tissues were intermixed within the clusters (Figure 1d,f), indicating a lack of clear stage-specific expression profiles for these cell types.

To determine whether the same phenomenon occurs in other LUAD datasets, we examined an independent patient cohort (GSE127465) [29]. The single-cell RNA sequencing data for this cohort were generated from tumor tissue samples of five LUAD patients and included 2199 epithelial cells, 26,024 immune cells, and 1090 stromal cells. Among these, 9953 cells were from stage I, 9681 from stage III, and 9679 from stage IV. Consistent with the previous dataset, immune and stromal cells showed no distinct separation across different stages, while only epithelial cells formed stage-specific clusters (Supp. Figure S1).

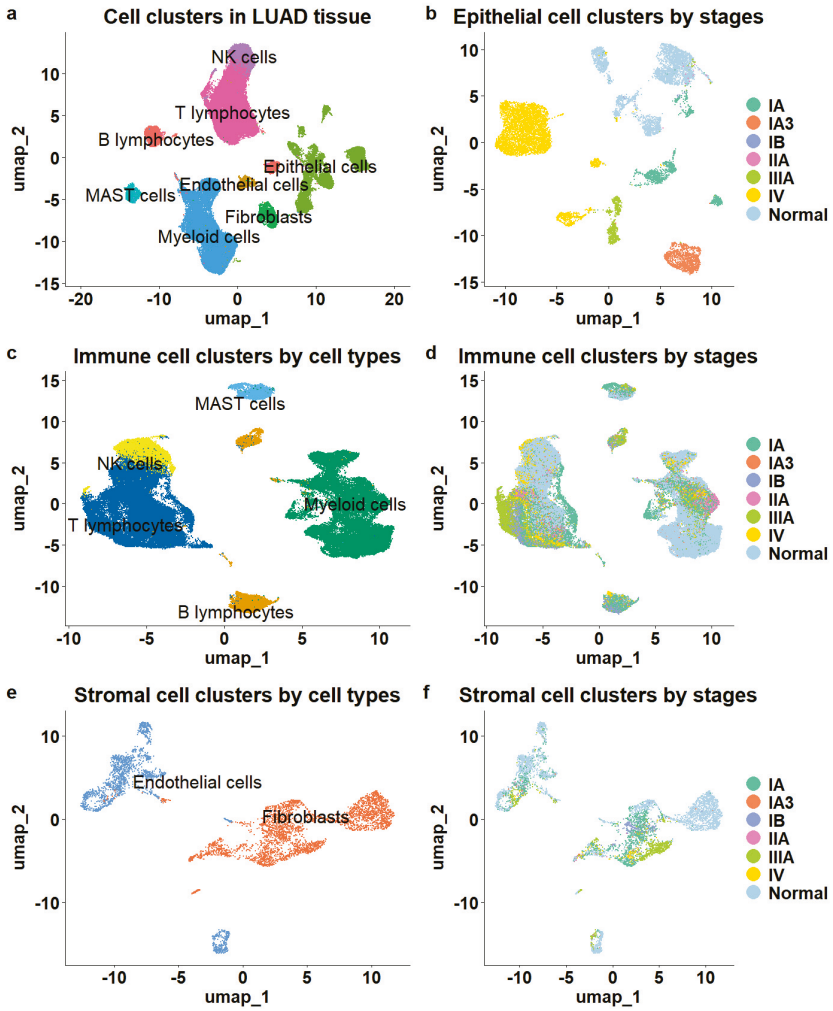

Figure 1. Overview of cell populations in the tumor microenvironment of LUAD. (**a**) The cellular composition of the TME. (**b**) Epithelial cells color-coded by stage demonstrated clear stage separation. (**c**) Immune cells color–coded by cell type showed clear separation. (**d**) Immune cells color–coded by stage lacked stage separation. (**e**) Stromal cells exhibited distinct cell type separation. (**f**) Stromal cells lacked stage–specific distinction.

Our findings align with the known roles of epithelial cells in cancer development [42]. In malignant neoplasms, epithelial cells undergo molecular alterations that lead to uncontrolled proliferation and loss of differentiation. Additionally, epithelial cells can acquire mesenchymal traits through processes like epithelial-mesenchymal transition (EMT), which are closely associated with tumor progression and metastasis. Therefore, genes that differentiate epithelial cells of different tumor stages could offer more precise cellular markers corresponding to LUAD progression.

3.2. Cellular Gene Markers Associated with LUAD Progression

As epithelial cells from tumor tissues may include residual non-malignant cells, we separated definitive malignant cells from non-malignant ones based on CNV estimation (Section 2). Out of the 12,410 epithelial cells extracted from tumor tissues, we identified 8460 (68.17%) as malignant, including 3572 cells in stages I, II and III and 4888 stage IV cells in the late stage.

The malignant epithelial cells formed four cell clusters with varied compositions (Figure 2a). The three clusters were homogeneous, consisting of epithelial cells from stages IV, IIIA, and IA3, respectively (Figure 2a). The heterogeneous cluster comprised a mix of different stages, including 1348 cells from stage IA (89.8%), 19 cells from stage IB (1.3%), 28 cells from stage IIA (1.9%), and 105 cells from stage IIIA (7%). Interestingly, we observed that non-malignant epithelial cells also displayed a stage-specific pattern; however, stage-specific clusters of non-malignant epithelial cells demonstrated lower levels of homogeneity, as indicated by purity and entropy measurements (see Section 2), compared to malignant epithelial cells (Supp. Figure S2). Only malignant cells were retained for further analysis.

Moreover, we reconstructed the cell lineage of epithelial cells. For comparison, we also established cell trajectories for stromal and various immune cells, including T cells, B cells, myeloid cells, and NK cells (Supp. Figure S3). Unlike the distinct separation observed in the trajectory of epithelial cells (Figure 2b), stromal and immune cells from different stages were distributed throughout all branches without clear delineation (Supp. Figure S3), consistent with the patterns observed in the cell clustering results.

We found that the epithelial cell trajectory was closely aligned with tumor progression. Stage IA3 cells were positioned in the bottom left branch of the trajectory, while Stage IA cells were predominantly found on the lower left and upper left branches (Figure 2b). Stage IIIA cells were located mainly on the upper left, some at the beginning of the right branch. The right branch started with a small number of stage III cells, transitioning to predominantly stage IV cells. This configuration illustrates a clear progression pattern through the branches (Figure 2c,d) and a distinct separation of stage IV epithelial cells from those in the earlier stages. Hence, we classified stages I, II, and III as early stages while considering stage IV as a late stage in this study.

We also investigated copy number variations in epithelial cells using InferCNV [43], a software tool that infers genomic amplifications and deletions from scRNA sequencing profiles. Our analysis revealed that epithelial cell transcriptomes in stage-specific clusters displayed unique amplification and deletion patterns on most chromosomes, chromosomes 14 and 8 exhibiting the most significant contrasts between the late and early stages (Figure 2e). In particular, chromosome 14 showed substantial deletions in cells from stage IV, while large amplifications were observed in cells from earlier stages. Conversely, chromosome 8 exhibited remarkable amplification in stage IV cells but showed deletions in the earlier stages.

Together, our results suggested that epithelial cells from stage IV LUAD exhibited significant transcriptional differences compared to those in earlier disease stages (I–III). To further investigate these stage-specific alterations, we conducted a differential expression analysis, comparing the epithelial cell populations isolated from earlier stage (I–III) tumors to those obtained from stage IV samples. This analysis identified the top 55 genes that were significantly upregulated (adjusted p-value < 0.01, log_2(fold change) > 1) in the stage IV epithelial cells. In contrast, these genes did not show significant expression changes in epithelial cells derived from normal tissues or non-malignant epithelium when comparing stage IV to earlier stages (Supp. Figure S4). Given the central role of epithelial cells in LUAD progression, we hypothesized that these stage-specific differentially expressed genes (DEGs) could serve as robust cellular markers characterizing disease progression.

To evaluate the validity and clinical relevance of these putative markers, we examined their expression patterns across multiple independent LUAD patient cohorts.

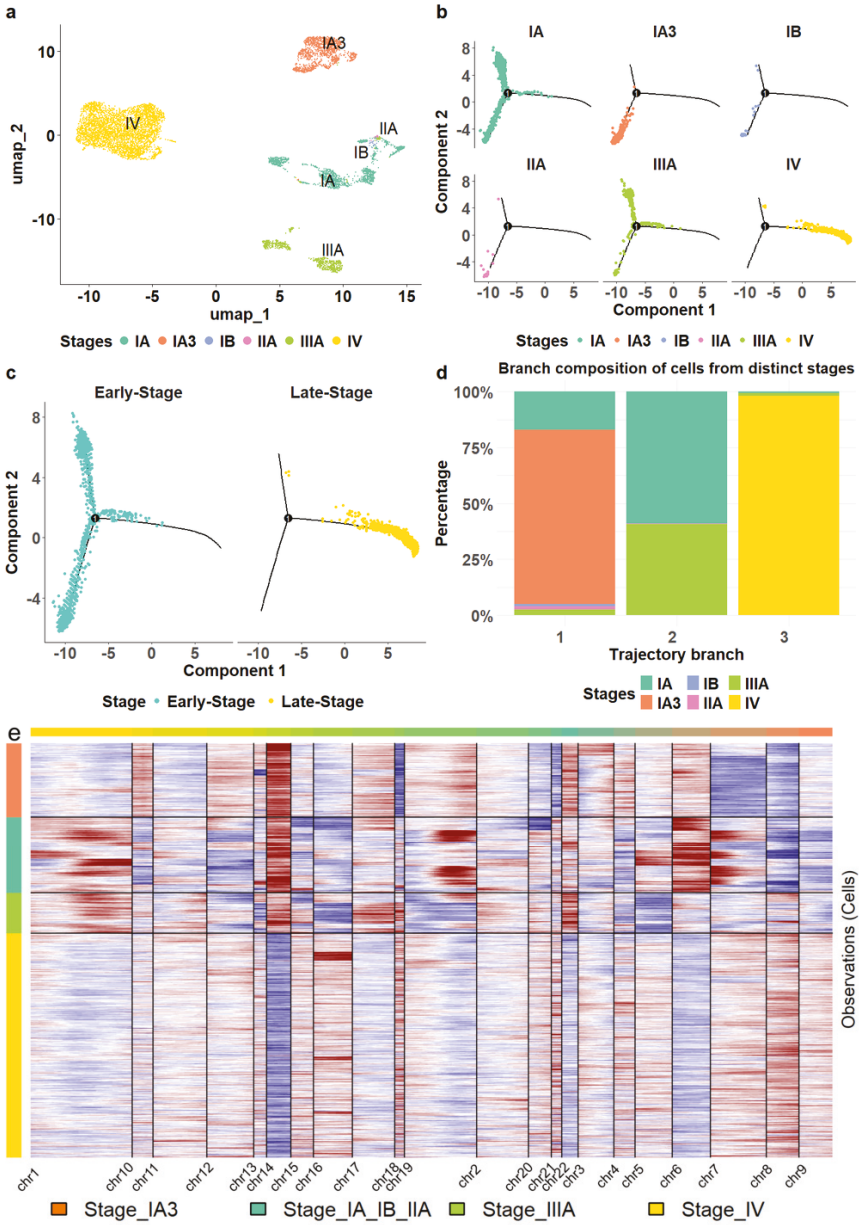

Figure 2. Transcriptomic alterations of epithelial cells during LUAD progression. (**a**) The malignant epithelial cells formed stage–specific clusters. (**b**) The location of epithelial cells from different stages in cell trajectory. (**c**) The comparison of the trajectory locations of epithelial cells from stage IV versus those from earlier stages. (**d**) The composition of epithelial cells in each trajectory branch. (**e**) The epithelial cells from stage IV exhibited distinct copy number variation patterns compared to those from earlier stages.

3.3. Clinical Implications of Cellular Marker Genes

We first analyzed a cohort of LUAD patients from the TCGA project. Hierarchical clustering of the expression levels of the identified stage-specific DEGs derived from epithelial cells classified the LUAD patients into three distinct subgroups: C1, C2, and C3, as illustrated in the column dendrogram of Figure 3a. Concurrently, the genes were organized into four groups according to the row dendrogram (Figure 3a), with each group exhibiting significant enrichment in biological processes and pathways relevant to tumor biology [44–49]. The statistical significance of these functional enrichments was

assessed using *p*-values calculated by the hypergeometric distribution and adjusted using the Benjamini-Hochberg (BH) method (Supp. Table S3).

Survival analysis revealed significantly distinct outcomes among the three patient subgroups. Patients classified into subgroup C1 demonstrated the best survival rates, while those in subgroup C3 experienced the poorest outcomes (Figure 3b). To further validate the clinical relevance of these stage-specific gene signatures, we evaluated their performance in three independent LUAD cohorts: OncoSG, GSE68465, and GSE72094. The results showed the consistency of these gene markers in segregating patients into subgroups with varying survival outcomes (Supp. Figure S5).

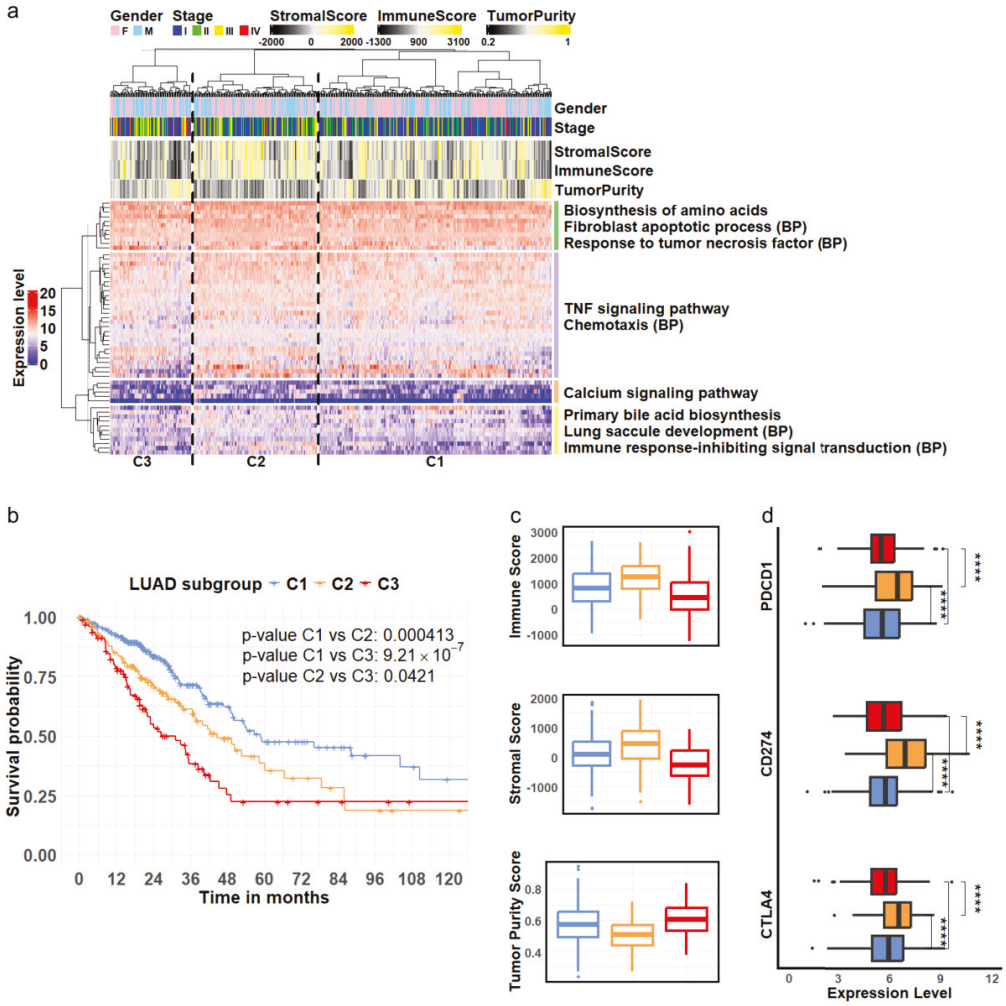

Figure 3. LUAD subgroups defined by cellular markers associated with disease progression. (**a**) Hierarchical clustering analysis of RNA−seq expression of 55 genes derived from epithelial cells revealed three LUAD subgroups, C1, C2, and C3. These genes were separated into four clusters enriched in distinct pathways and biological processes (BPs) related to tumor development. (**b**) Among the three identified subgroups, C1 (blue), C2 (orange) and C3 (red), Kaplan−Meier survival curves indicate that patients in subgroup C3 (red) had the poorest survival outcomes, while those in subgroup C1 (blue) exhibited the best survival. (**c**) The C3 (red) subgroup showed the highest tumor purity, accompanied by the lowest levels of stromal and immune cell content. (**d**) The three genes encoding immune inhibitors were expressed at significantly higher levels in subgroup C2 (orange) compared to subgroups C1 (blue) and C3 (red). (**** $p < 0.0001$).

Furthermore, we investigated the TME composition across the three patient subgroups identified through our clustering analysis. We assessed the immune and stromal cell content using the ESTIMATE algorithm [38] and evaluated tumor purity using the PUREE

method [39]. The results indicated that tumor samples in subgroup C3 had the lowest stromal cell composition, the lowest level of immune infiltration, and the highest tumor purity compared to subgroups C1 and C2 (Figure 3c, ANOVA test, $p < 0.05$). Interestingly, while subgroup C2 exhibited the highest immune infiltration, its patients had lower survival rates than those in subgroup C1. To further explore the potential mechanisms underlying these survival differences, we examined the expression levels of known immune checkpoint genes. We observed significantly higher expression of *PDCD1* (encoding PD-1), *CD274* (encoding PD-L1), and *CTLA4* in subgroup C2 (Figure 3d). PD-1 is an inhibitor of T-cell activation [50], while PD-L1 can downregulate immune responses by interacting with PD-1 [51]. Similarly, CTLA-4 acts as a negative regulator of T-cell activation [52]. The elevated expression of these immune checkpoint molecules in subgroup C2 suggested potential tumor evasion of immune surveillance and T-cell exhaustion, which may result in a negative impact on patient survival in this subgroup.

Collectively, our results indicated that the DEGs derived from epithelial cells captured critical molecular characteristics of LUAD progression and suggested that epithelial cells may significantly influence the biological behavior of other cell types within the TME.

3.4. Key Transcription Regulators of Progression-Related Gene Markers

To identify the upstream regulators of the 55 progression-related DEGs, we inferred transcriptional regulatory networks in epithelial cells using SCENIC [40]. This method integrates scRNA-seq data with transcription factor (TF) binding information to construct regulatory networks (see Section 2). Among the 1892 human TFs examined, 218 TFs and their downstream targets formed co-expression modules, with target gene promoters enriched for binding motifs corresponding to their respective TFs within each regulon. We assessed regulon activity using the area under the recovery curve and calculated stage specificity based on Jensen-Shannon divergence [40]. This analysis identified 36 regulons active in one or more cell types (Figure 4a), with nine regulons specific to stage IV (Figure 4b). We then assembled networks from active and stage-specific regulons containing at least one DEG.

In the identified regulatory networks, 32 of the 55 DEGs were classified as target genes, while *PITX1*, one of the DEGs, served as a transcription factor within the network. *PITX1* can activate the tumor suppressor gene *TP53* by binding to its promoter region [53]. Among the 32 target DEGs, 26 were regulated by five transcription factors (TFs): *ATF3*, *ATF4*, *HSF1*, *KLF4*, and *NFIC* (Figure 4c). Notably, these five TFs functioned as regulators within the regulons that were highly active and stage-specific in epithelial cells at stage IV (Figure 4a,b).

ATF3 and *ATF4*, belonging to the activating transcription factor (ATF) family, are involved in critical cancer biology pathways [54] and mediate cellular responses to stress [55,56]. *HSF1*, a vital regulator of the heat shock response, has been implicated in tumor malignancy and poor prognosis [57]. *KLF4* plays a crucial role in regulating cell growth and differentiation [58], and its low expression has been associated with poor survival outcomes in LUAD [59]. Finally, *NFIC*, a member of the nuclear factor I family, has been implicated in various types of cancer [60–63].

The five transcription factors (TFs) regulated the expression of 26 out of 55 differentially expressed genes (DEGs) (Figure 4c). Notably, *ATF4* and *NFIC* regulated 13 and 14 of these genes, respectively. To further investigate the functional relevance of the five key transcription factors (TFs), we performed Gene Ontology (GO) and KEGG pathway enrichment analyses on their predicted target genes. The results revealed that these TFs regulate diverse and biologically meaningful processes related to LUAD progression. ATF3 targets were significantly enriched in the fibroblast apoptotic process (p.adjust < 0.013) and

EGFR tyrosine kinase inhibitor resistance (*p*.adjust < 0.024). ATF4 targets were associated with TNF signaling (*p*.adjust < 0.00011), cytokine–receptor interactions (*p*.adjust < 0.034), and platinum drug resistance (*p*.adjust < 0.034). NFIC targets were enriched in tumor necrosis factor-mediated pathways (*p*.adjust < 0.038) and lung epithelium development (*p*.adjust < 0.040). KLF4 targets were involved in pathways related to epithelial proliferation and lung morphogenesis (*p*.adjust < 0.060). HSF1 targets showed significant enrichment in processes such as programmed necrotic cell death (*p*.adjust < 0.050) and nucleotide salvage (*p*.adjust < 0.041). Furthermore, incorporating interactions from the STRING database, we found that four genes, *TP53*, *KRAS*, *ROS1* and *BRAF*, the known targets of NSCLC drug therapy, were directly or indirectly interconnected with these TFs (Figure 4d). Collectively, our results, corroborated by multi-layered evidence from literature and databases, suggest that these TFs may function as critical molecular drivers in LUAD progression.

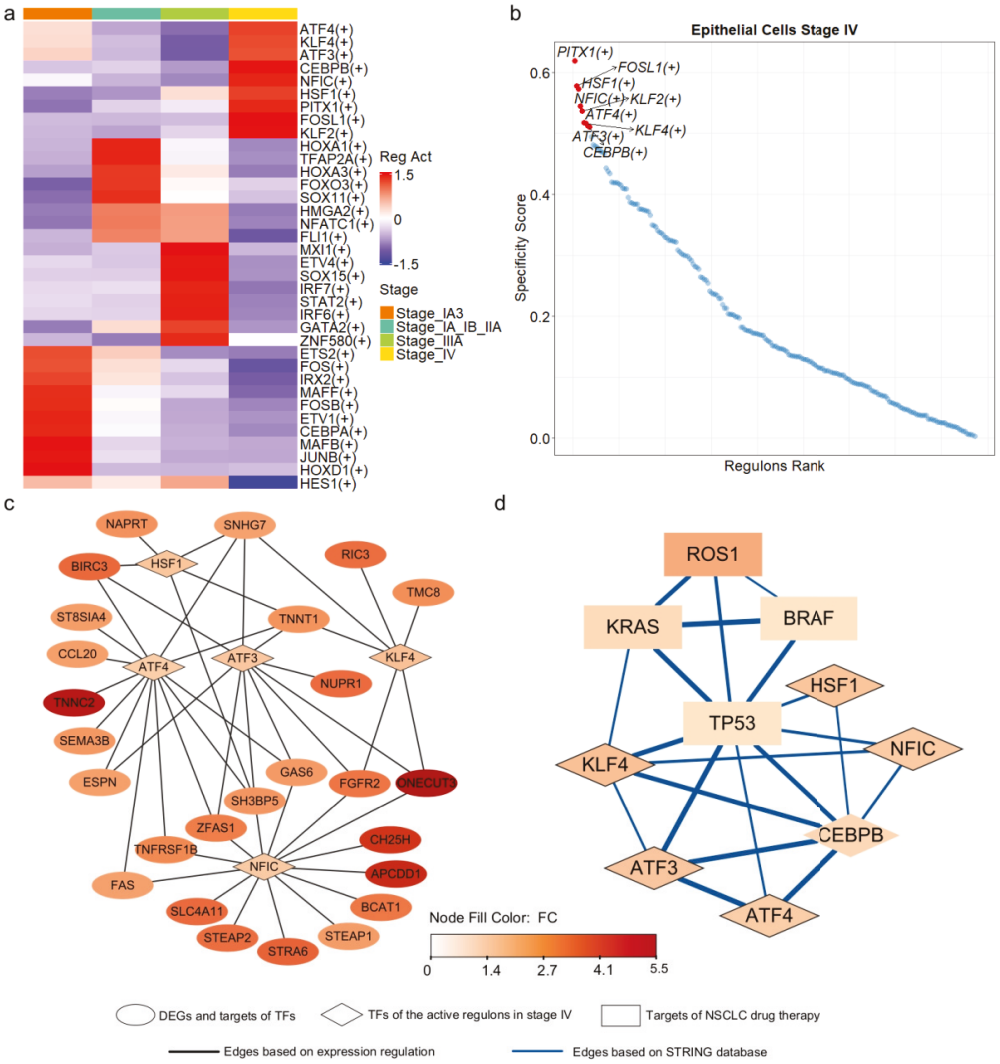

Figure 4. Transcriptional regulatory networks of stage–specific DEGs derived from epithelial cells. (**a**) Active regulons identified in epithelial cells across the four stages of LUAD, with each regulon being active in at least one stage. (**b**) Regulons ranked based on their specificity to stage IV epithelial cells. (**c**) Transcriptional regulatory networks of the DEGs, with TF represented by diamonds and target DEGs represented by ovals. Node color corresponded to fold change, indicating the level of expression variation between late–stage and early–stage epithelial cells. (**d**) Interaction network derived from the STRING database, with known targets of NSCLC drug therapy represented by rectangles and TF represented by diamonds.

3.5. Cellular Communication Alterations in Response to Tumor Progression

To understand how cellular interactions evolve during disease progression, we established cell-cell communication networks among various cell types in the TME. When comparing stage IV LUAD with earlier stages, we found a decrease in both the total number and strength of cellular signaling originating from T cells to other cell types (Figure 5a,b). A similar decline was observed for B cells (Figure 5a,b), indicating an overall reduction in immune response during the late stage of LUAD.

In contrast, there was a substantial increase in cellular communication originating from epithelial cells in stage IV, characterized by a greater number of interactions and enhanced interaction strength (Figure 5a,b).In particular, a significant rise in communications between epithelial cells and fibroblasts was observed (Figure 5a,b). Cancer-associated fibroblasts are known to promote angiogenesis, metastasis, immune evasion, and drug resistance [64–66]. Additionally, we detected heightened intercellular crosstalk between myeloid cells and epithelial cells, and the communication originating from myeloid cells to T cells also increased in stage IV. Research indicates that myeloid-related innate immunity can facilitate tumor progression by affecting T-cell activity [67]. Together, these results suggest that the complex cellular interplay centered around epithelial cells may significantly impact how the TME mediates LUAD development.

Next, we investigate the activity of signaling pathways that coordinate cell communications during LUAD progression, focusing on secreted signaling. Of 158 secreted signaling pathways, 22 exhibited significant changes ($p < 0.05$) between stage IV and earlier stages. Among the significant pathways, eight were exclusively active in late-stage LUAD, which included ncWNT (noncanonical Wnt pathway), CSF (colony-stimulating factors), BAG (BCL-2-associated athanogene), PDGF (platelet-derived growth factor), SEMA3 (semaphorin 3), IFN-γ (interferon gamma), TNF (tumor necrosis factor) and PTN (pleiotrophin) (Figure 5c).

The activation of the ncWNT pathway enhances cell migration and contributes to metastatic behavior. Dysregulation of this pathway promotes the EMT, allowing tumor cells to invade surrounding tissues and spread through the bloodstream [68]. The EMT mechanism can also cause drug resistance [69]. In the ncWNT pathway, the WNT5A $\rightarrow$ FZD1 interaction represented the dominant ligand-receptor pairing (Figure 5d(top left panel)).

PDGF signaling pathway involves angiogenesis and EMT, promoting tumor metastasis [70,71]. The significant ligand-receptor pairs involved in the PDGF signaling pathway were PDGFA $\rightarrow$ PDGFRB and PDGFA $\rightarrow$ PDGFRA, which facilitate signaling from epithelial cells to fibroblasts, whereas the PDGFC $\rightarrow$ PDGFRA interaction was involved in intracellular signaling in fibroblasts (Figure 5d(top right panel),e).

PTN is a multifunctional growth factor known for its angiogenic properties and role in tumor growth and metastasis [72]. Four key ligand $\rightarrow$ receptor pairs, including PTN $\rightarrow$ NCL, PTN $\rightarrow$ SDC4, PTN $\rightarrow$ SDC1, and PTN $\rightarrow$ SDC2, contributed to the activity of the PTN pathway (Figure 5d(bottom panel)), three contributed to the signal of fibroblasts to epithelial cells (Figure 5e) while PTN $\rightarrow$ SDC2 was involved in intracellular communication in fibroblasts. The PTN $\rightarrow$ NCL interaction is a primary driver of PTN pathway activity in late-stage LUAD. Nucleolin (NCL) is a protein that is often overexpressed in various cancers [73–77], and inhibiting nucleolin can reduce cancer cell viability [78].

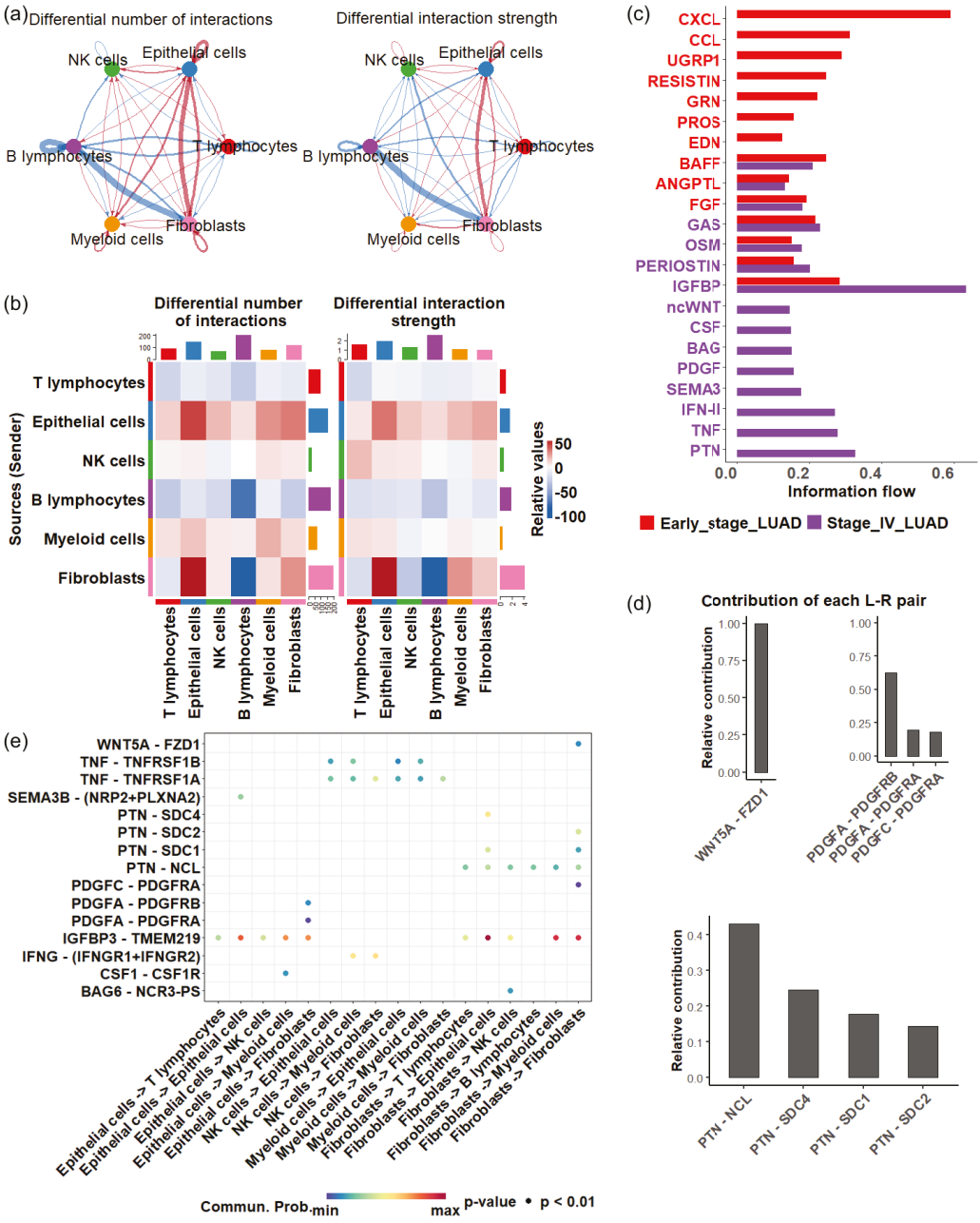

Figure 5. Cell–cell communications in early and late stage of LUAD. (**a**) Differential cell–cell communication number (left) and strength (right). Blue arrows represent a decrease in the number or strength of interactions in the late stage of LUAD compared with the early stage of LUAD, while red arrows represent an increase in interactions in the late stage of LUAD. (**b**) Differential cell–cell communication number (left) and strength (right). (**c**) Significant signaling pathways in the early and late stages of LUAD ($p < 0.05$). The active pathways in the early stage are represented by red bars, while those in the late stages are shown in purple bars. (**d**) Contribution of ligand–receptor pairs in the ncWNT pathway (upper) and PTN pathway (bottom). (**e**) Significant ligand–receptor interactions ($p < 0.01$), represented by dots, contribute to cellular communication in late–stage LUAD.

Most ligand-receptor interactions contributing to the unique pathways in late-stage LUAD were observed in the signaling between epithelial cells and fibroblasts (Figure 5e). The enhanced crosstalk between these two populations may play a vital role in shaping the TME, highlighting the central roles of epithelial cells in LUAD progression.

4. Discussion

In this study, we developed an integrated computational framework to investigate the cellular mechanisms underlying the development of LUAD. We began by analyzing scRNA-seq transcriptomes of various cell types, including stromal, immune, and epithelial cells, in the TME of early- and late-stage LUAD. Our analysis revealed distinct patterns in cell clustering and trajectory, particularly among epithelial cells, in contrast to stromal and immune cell populations. Late-stage LUAD epithelial cells formed a well-defined cell cluster and lineage branch, clearly distinguishing them from their early-stage counterparts. This separation was not observed in the stromal and immune cells. The results were further validated by the scRNA-seq dataset of an independent cohort of LUAD patients. Thus, we hypothesize that gene signatures differentiating early-stage from late-stage epithelial cells provide precise cellular markers related to LUAD progression and metastatic processes. Our analysis of the TCGA LUAD patient cohort revealed that the expression profiles of these marker genes delineated three distinct LUAD subgroups. Each subgroup showed significantly different survival outcomes and TME compositions.

Among LUAD subgroups, tumor tissue from patients with the poorest survival outcomes exhibited the highest tumor purity, the lowest levels of immune infiltration, and low stromal scores. Previous studies suggested that lower stromal scores are associated with better survival in gastric cancer [79] and colon cancer [80]. A low stromal component may limit blood vessel formation, hindering tumor growth; however, it might simultaneously reduce immune cell infiltration, possibly due to the complex crosstalk between stromal and immune cells within the TME. Moreover, the *TP53* mutation rate was significantly high in subgroup C3. Mutated *TP53* are often linked to aggressive tumor characteristics and poor clinical outcomes [81,82]. Additionally, p53 mutations can lead to chronic inflammation in cancer cells and foster an immunosuppressive environment [83,84]. Interestingly, while subgroup C2 was characterized by the highest levels of immune infiltration, this did not correlate with optimal survival outcomes. We observed elevated expression of genes encoding the immune checkpoint proteins in this subgroup. This suggested the phenomenon of T-cell exhaustion, where persistent exposure to tumor antigens diminishes T-cell functionality, ultimately compromising the immune response [85]. This result aligned with existing literature indicating that despite heightened immune infiltration in some cancer subtypes, the presence of immunosuppressive signals can hinder effective immune responses [86].

We observed that female patients were more prominently represented in the subgroups with favorable survival outcomes and less represented in the subgroup associated with poor survival outcomes (Chi-square test, $p < 0.052$, Supp. Table S4). This finding aligns with the existing literature indicating that female patients with LUAD tend to experience better survival outcomes than their male counterparts [87,88]. In addition, we noted variability in tumor stage distribution among the subgroups; each subgroup contained a mix of samples at various stages. However, in comparisons of stage composition across subgroups, stage I had the highest proportion in subgroup (C1) with the best survival rate, while stage IV had the highest proportion in subgroup (C3) with the poorest survival rate (Supp. Table S5). Thus, these progress-related genes derived from epithelial cells can effectively stratify patients into subgroups with distinct clinical characteristics. Although TCGA RNA-seq data reflected average gene expression across heterogeneous cell populations, our results implied that these epithelial cell-derived genes captured critical aspects of LUAD progression. Furthermore, they demonstrated that epithelial cells could significantly influence the biological behavior of other cell types within the TME.

Our investigation into the cell-cell communication networks within the TME revealed significant changes between early and late-stage lung adenocarcinoma (LUAD). Notably,

communications originating from T cells and B cells significantly decreased in late-stage LUAD, suggesting a compromised immune response. This decline in immune cell communication aligns with findings that late-stage tumors often exhibit characteristics associated with immune evasion [89]. Conversely, communication signals from epithelial cells to other cell types in the TME increased in the late stage, including interactions with T cells and B cells. This enhanced signaling includes interactions with T cells and B cells, indicating that epithelial cells may actively modulate the immune landscape within the TME. For instance, secreted factors from epithelial cells can influence T cell differentiation and activation, shaping the immune environment in ways that may either aid or hinder anti-tumor responses [90].

Specifically, we observed significant increases in intercellular communication between epithelial cells and fibroblasts in late-stage LUAD. Fibroblasts are key components of the TME, contributing to its architecture and influencing tumor biology through the secretion of growth factors and cytokines [91,92]. The interplay between epithelial cells and fibroblasts often results in the secretion of pro-inflammatory and pro-angiogenic factors, which can stimulate angiogenesis and further tumor growth [93,94]. The enhanced collaboration between these cell types in late-stage disease may suggest a shift toward a more aggressive tumor phenotype, enabling efficient nutrient supply and persistent tumor cell survival.

Moreover, our study identified multiple signaling pathways activated in late-stage LUAD, such as the ncWNT, PDGF and PTN pathways. The WNT signaling pathway, particularly through its non-canonical (ncWNT) branch, plays a crucial role in epithelial-mesenchymal transition (EMT) [69,95], a dynamic process wherein epithelial cells lose their cell polarity and adhesion properties, gaining invasive and migratory capabilities [96]. The ligand-receptor interactions that significantly contribute to the activity of these pathways represent promising therapeutic targets. For instance, antagonists targeting these late-stage specific pathways may help disrupt the communication that enables tumor survival and immune evasion [97,98]. PTN has been shown to promote tumorigenesis by enhancing cell proliferation and contributing to the tumor microenvironment [99,100], while PDGF plays a critical role in angiogenesis and fibrosis associated with tumor progression [101]. Preclinical models have demonstrated that inhibition of these pathways can reduce tumor growth and improve treatment responsiveness [99,102–104]. Additionally, research suggests that combining PTN and PDGF inhibitors with existing therapies, such as chemotherapy and immunotherapy, may produce synergistic effects, enhancing therapeutic efficacy and overcoming resistance mechanisms [105–107]. For example, studies have shown that concurrent targeting of PDGF signaling can enhance the effectiveness of anti-PD-1 therapies by modulating the tumor immune microenvironment [108,109].

The 55 stage-specific genes identified in our study demonstrate considerable potential as biomarkers for patient stratification and prognostic assessment in LUAD. Their consistent performance across multiple independent patient cohorts suggests their clinical utility. In addition, five key transcription factors (ATF3, ATF4, HSF1, KLF4, and NFIC) and critical signaling pathways (ncWNT, PDGF, and PTN) represent potential therapeutic targets, paving the way for the development of novel treatment strategies in advanced LUAD. Integrating these molecular insights into clinical workflows could enhance diagnostic precision and guide therapeutic decision making in LUAD treatment. Collectively, our findings, supported by existing literature, underscore the translational potential of targeting these genes and pathways to not only inhibit tumor progression but also to improve clinical outcomes when combined with current treatment regimens.

Recent literature has proposed a broader conceptual framework that characterizes cancer not solely as a genetic disease, but as an ecological pathology [110]. In this perspective, cancer cells are conceptualized as invasive species that interact dynamically with their

microenvironment through ecological principles such as mutualism, parasitism, and competition. Our findings of enhanced epithelial-fibroblast crosstalk and altered ligand-receptor signaling in late-stage LUAD align with this ecological model, suggesting that tumor progression results not only from cell-intrinsic genetic alterations but also from evolving ecological interactions within the tumor microenvironment. These interactions may play crucial roles in fostering immune suppression, therapeutic resistance, and metastasis through non-genetic mechanisms.

While our study provides valuable insights into the roles of epithelial cell subpopulations and cell–cell communication dynamics in LUAD progression, future research, including in vitro and in vivo experiments, is essential to validate the functional roles of the identified key transcription factors and signaling pathways.

In conclusion, our work underscores the pivotal role of epithelial cells in driving LUAD progression. The key transcription regulators and signaling pathways identified in this study offer valuable therapeutic targets for developing more effective and precise treatment strategies for LUAD patients.

Supplementary Materials: The following supporting information can be downloaded at: https://www.mdpi.com/article/10.3390/biomedicines13071606/s1, Figure S1: Cell clustering analysis of LUAD scRNA-seq dataset GSE127465.; Figure S2: Stage-specific cell clustering in malignant and nonmalignant epithelial cells.; Figure S3: Cell trajectories of stromal cells and various immune cell types at different LUAD stages.; Figure S4: Expression of 55-gene signatures across LUAD stages in normal, non-malignant, and malignant epithelial cells; Figure S5: LUAD patient stratification based on the DEGs derived from epithelial cells and survival analysis in independent cohorts.; Table S1: Single-cell RNA sequencing datasets; Table S2: LUAD datasets with survival information; Table S3: Significantly enriched pathways and biological processes; Table S4: Sex information in patient subgroups; Table S5: Stage information in patient subgroups.

Author Contributions: Conceptualization, M.Q.Y.; methodology, M.Q.Y. and J.M.; formal analysis, J.M. and M.Q.Y.; resources, J.M., C.M. and A.K.T.; data curation, J.M. and C.M.; writing—original draft preparation, M.Q.Y. and J.M.; writing—review and editing, A.K.T. and J.T. All authors have read and agreed to the published version of the manuscript.

Funding: This work was supported by grants R15GM137288 and P20GM103429 from the National Institutes of Health, grant OIA-1946391 from the National Science Foundation, and an award from the Arkansas Research Alliance.

Institutional Review Board Statement: Not applicable.

Informed Consent Statement: Not applicable.

Data Availability Statement: GSE131907, GSE127465 and GSE68465 are available in the Gene Expression Omnibus (GEO) database. TCGA breast cancer data are available at the Genomic Data Commons (GDC) Data Porter (https://portal.gdc.cancer.gov/ (accessed on 19 March 2025)). The OncoSG dataset was also obtained from the cBioPortal database.

Conflicts of Interest: The authors declare no conflicts of interest.

References

1. Bray, F.; Ferlay, J.; Soerjomataram, I.; Siegel, R.L.; Torre, L.A.; Jemal, A. Global cancer statistics 2018: GLOBOCAN estimates of incidence and mortality worldwide for 36 cancers in 185 countries. *CA Cancer J. Clin.* **2018**, *68*, 394–424. [CrossRef] [PubMed]
2. Thandra, K.C.; Barsouk, A.; Saginala, K.; Aluru, J.S.; Barsouk, A. Epidemiology of lung cancer. *Contemp. Oncol. Współczesna Onkol.* **2021**, *25*, 45–52. [CrossRef] [PubMed]
3. Lu, Y.; Zeng, T.; Zhang, H.; Li, Y.; Zhu, X.; Liu, H.; Sun, B.; Ji, C.; Li, T.; Huang, L.; et al. Nano-immunotherapy for lung cancer. *Nano TransMed* **2023**, *2*, e9130018. [CrossRef]

4. Wu, Y.L.; Lu, S.; Zhou, Q.; Zhang, L.; Cheng, Y.; Wang, J.; Wang, B.; Hu, C.; Lin, L.; Zhong, W.; et al. Expert consensus on treatment for stage III non-small cell lung cancer. *Med. Adv.* **2023**, *1*, 3–13. [CrossRef]
5. Cornelius, M.E.; Loretan, C.G.; Jamal, A.; Davis Lynn, B.C.; Mayer, M.; Alcantara, I.C.; Neff, L. Tobacco product use among adults–United States, 2021. *MMWR. Morb. Mortal. Wkly. Rep.* **2023**, *72*, 475–483. [CrossRef]
6. Pelosof, L.; Ahn, C.; Gao, A.; Horn, L.; Madrigales, A.; Cox, J.; McGavic, D.; Minna, J.D.; Gazdar, A.F.; Schiller, J. Proportion of never-smoker non–small cell lung cancer patients at three diverse institutions. *JNCI J. Natl. Cancer Inst.* **2017**, *109*, djw295. [CrossRef]
7. Gitlitz, B.J.; Novello, S.; Vavalà, T.; Bittoni, M.; Sable-Hunt, A.; Pavlick, D.; Hsu, R.; Park, S.L.; Chen, R.; Cooke, M.; et al. The genomics of young lung cancer: Comprehensive tissue genomic analysis in patients under 40 with lung cancer. *JTO Clin. Res. Rep.* **2021**, *2*, 100194. [CrossRef]
8. Dubin, S.; Griffin, D. Lung cancer in non-smokers. *Mo. Med.* **2020**, *117*, 375–379.
9. Ucvet, A.; Yazgan, S.; Gursoy, S.; Samancilar, O. Prognosis of resected non-small cell lung cancer with ipsilateral pulmonary metastasis. *Thorac. Cardiovasc. Surg.* **2020**, *68*, 176–182. [CrossRef]
10. Siegel, R.L.; Giaquinto, A.N.; Jemal, A. Cancer statistics, 2024. *CA Cancer J. Clin.* **2024**, *74*, 12–49. [CrossRef]
11. Calles, A.; Riess, J.W.; Brahmer, J.R. Checkpoint blockade in lung cancer with driver mutation: Choose the road wisely. In *Proceedings of the American Society of Clinical Oncology Educational Book*; American Society of Clinical Oncology, Annual Meeting: Chicago, IL, USA, 2020; Volume 40, pp. 372–384.
12. Mamdani, H.; Matosevic, S.; Khalid, A.B.; Durm, G.; Jalal, S.I. Immunotherapy in lung cancer: Current landscape and future directions. *Front. Immunol.* **2022**, *13*, 823618. [CrossRef] [PubMed]
13. Kamata, T.; Sunami, K.; Yoshida, A.; Shiraishi, K.; Furuta, K.; Shimada, Y.; Katai, H.; Watanabe, S.i.; Asamura, H.; Kohno, T.; et al. Frequent BRAF or EGFR mutations in ciliated muconodular papillary tumors of the lung. *J. Thorac. Oncol.* **2016**, *11*, 261–265. [CrossRef]
14. Cardarella, S.; Ogino, A.; Nishino, M.; Butaney, M.; Shen, J.; Lydon, C.; Yeap, B.Y.; Sholl, L.M.; Johnson, B.E.; Jänne, P.A. Clinical, pathologic, and biologic features associated with BRAF mutations in non–small cell lung cancer. *Clin. Cancer Res.* **2013**, *19*, 4532–4540. [CrossRef]
15. Takeuchi, K.; Soda, M.; Togashi, Y.; Suzuki, R.; Sakata, S.; Hatano, S.; Asaka, R.; Hamanaka, W.; Ninomiya, H.; Uehara, H.; et al. RET, ROS1 and ALK fusions in lung cancer. *Nat. Med.* **2012**, *18*, 378–381. [CrossRef] [PubMed]
16. Kohno, T.; Nakaoku, T.; Tsuta, K.; Tsuchihara, K.; Matsumoto, S.; Yoh, K.; Goto, K. Beyond ALK-RET, ROS1 and other oncogene fusions in lung cancer. *Transl. Lung Cancer Res.* **2015**, *4*, 156–164. [PubMed]
17. Conde, E.; Rojo, F.; Gómez, J.; Enguita, A.B.; Abdulkader, I.; González, A.; Lozano, D.; Mancheño, N.; Salas, C.; Salido, M.; et al. Molecular diagnosis in non-small-cell lung cancer: Expert opinion on ALK and ROS1 testing. *J. Clin. Pathol.* **2022**, *75*, 145–153. [CrossRef]
18. Takuma, S.; Inoue, Y.; Karayama, M.; Tsuchiya, K.; Tsukui, H.; Hozumi, H.; Suzuki, Y.; Furuhashi, K.; Enomoto, N.; Fujisawa, T.; et al. EGFR-Mutated lung adenocarcinoma successfully treated with Osimertinib after spontaneous Transformation to SCLC and Adenocarcinoma with neuroendocrine differentiation: Case Report. *JTO Clin. Res. Rep.* **2022**, *3*, 100264. [CrossRef]
19. Rivera-Concepcion, J.; Uprety, D.; Adjei, A.A. Challenges in the use of targeted therapies in non-small cell lung cancer. *Cancer Res. Treat.* **2022**, *54*, 315–329. [CrossRef]
20. Gu, A.; Li, J.; Li, M.Y.; Liu, Y. Patient-derived xenograft model in cancer: Establishment and applications. *MedComm* **2025**, *6*, e70059. [CrossRef]
21. Liu, W.; Cui, Y.; Zheng, X.; Yu, K.; Sun, G. Application status and future prospects of the PDX model in lung cancer. *Front. Oncol.* **2023**, *13*, 1098581. [CrossRef]
22. Yang, M.; Shen, H.; Flodby, P.; Koss, M.D.; Bassiouni, R.; Liu, Y.; Jashashvili, T.; Neely, A.; Ogbolu, E.; Castillo, J.; et al. Alveolar type I cells can give rise to KRAS-induced lung adenocarcinoma. *Cell Rep.* **2023**, *42*, 113286. [CrossRef] [PubMed]
23. Cancer Genome Atlas Research Network. Comprehensive molecular profiling of lung adenocarcinoma. *Nature* **2014**, *511*, 543–550. [CrossRef]
24. Westcott, P.M.; Halliwill, K.D.; To, M.D.; Rashid, M.; Rust, A.G.; Keane, T.M.; Delrosario, R.; Jen, K.Y.; Gurley, K.E.; Kemp, C.J.; et al. The mutational landscapes of genetic and chemical models of Kras-driven lung cancer. *Nature* **2015**, *517*, 489–492. [CrossRef] [PubMed]
25. Kotton, D.N.; Morrisey, E.E. Lung regeneration: Mechanisms, applications and emerging stem cell populations. *Nat. Med.* **2014**, *20*, 822–832. [CrossRef] [PubMed]
26. Kalluri, R.; Neilson, E.G. Epithelial-mesenchymal transition and its implications for fibrosis. *J. Clin. Investig.* **2003**, *112*, 1776–1784. [CrossRef]
27. Dohadwala, M.; Yang, S.C.; Luo, J.; Sharma, S.; Batra, R.K.; Huang, M.; Lin, Y.; Goodglick, L.; Krysan, K.; Fishbein, M.C.; et al. Cyclooxygenase-2–dependent regulation of E-cadherin: Prostaglandin E2 induces transcriptional repressors ZEB1 and Snail in non–small cell lung cancer. *Cancer Res.* **2006**, *66*, 5338–5345. [CrossRef]

28. Kim, N.; Kim, H.K.; Lee, K.; Hong, Y.; Cho, J.H.; Choi, J.W.; Lee, J.I.; Suh, Y.L.; Ku, B.M.; Eum, H.H.; et al. Single-cell RNA sequencing demonstrates the molecular and cellular reprogramming of metastatic lung adenocarcinoma. *Nat. Commun.* **2020**, *11*, 2285. [CrossRef]
29. Zilionis, R.; Engblom, C.; Pfirschke, C.; Savova, V.; Zemmour, D.; Saatcioglu, H.D.; Krishnan, I.; Maroni, G.; Meyerovitz, C.V.; Kerwin, C.M.; et al. Single-cell transcriptomics of human and mouse lung cancers reveals conserved myeloid populations across individuals and species. *Immunity* **2019**, *50*, 1317–1334. [CrossRef]
30. Chen, J.; Yang, H.; Teo, A.S.M.; Amer, L.B.; Sherbaf, F.G.; Tan, C.Q.; Alvarez, J.J.S.; Lu, B.; Lim, J.Q.; Takano, A.; et al. Genomic landscape of lung adenocarcinoma in East Asians. *Nat. Genet.* **2020**, *52*, 177–186. [CrossRef]
31. Gene expression–based survival prediction in lung adenocarcinoma: A multi-site, blinded validation study. *Nat. Med.* **2008**, *14*, 822–827. [CrossRef]
32. Schabath, M.B.; Welsh, E.A.; Fulp, W.J.; Chen, L.; Teer, J.K.; Thompson, Z.J.; Engel, B.E.; Xie, M.; Berglund, A.E.; Creelan, B.C.; et al. Differential association of STK11 and TP53 with KRAS mutation-associated gene expression, proliferation and immune surveillance in lung adenocarcinoma. *Oncogene* **2016**, *35*, 3209–3216. [CrossRef] [PubMed]
33. McInnes, L.; Healy, J.; Melville, J. Umap: Uniform manifold approximation and projection for dimension reduction. *arXiv* **2018**, arXiv:1802.03426.
34. Qiu, X.; Mao, Q.; Tang, Y.; Wang, L.; Chawla, R.; Pliner, H.A.; Trapnell, C. Reversed graph embedding resolves complex single-cell trajectories. *Nat. Methods* **2017**, *14*, 979–982. [CrossRef] [PubMed]
35. Tirosh, I.; Izar, B.; Prakadan, S.M.; Wadsworth, M.H.; Treacy, D.; Trombetta, J.J.; Rotem, A.; Rodman, C.; Lian, C.; Murphy, G.; et al. Dissecting the multicellular ecosystem of metastatic melanoma by single-cell RNA-seq. *Science* **2016**, *352*, 189–196. [CrossRef]
36. de Bruijn, I.; Kundra, R.; Mastrogiacomo, B.; Tran, T.N.; Sikina, L.; Mazor, T.; Li, X.; Ochoa, A.; Zhao, G.; Lai, B.; et al. Analysis and visualization of longitudinal genomic and clinical data from the AACR project GENIE biopharma collaborative in cBioPortal. *Cancer Res.* **2023**, *83*, 3861–3867. [CrossRef] [PubMed]
37. Gu, Z.; Eils, R.; Schlesner, M. Complex heatmaps reveal patterns and correlations in multidimensional genomic data. *Bioinformatics* **2016**, *32*, 2847–2849. [CrossRef]
38. Yoshihara, K.; Shahmoradgoli, M.; Martínez, E.; Vegesna, R.; Kim, H.; Torres-Garcia, W.; Treviño, V.; Shen, H.; Laird, P.W.; Levine, D.A.; et al. Inferring tumour purity and stromal and immune cell admixture from expression data. *Nat. Commun.* **2013**, *4*, 2612. [CrossRef]
39. Revkov, E.; Kulshrestha, T.; Sung, K.W.K.; Skanderup, A.J. PUREE: Accurate pan-cancer tumor purity estimation from gene expression data. *Commun. Biol.* **2023**, *6*, 394. [CrossRef]
40. Van de Sande, B.; Flerin, C.; Davie, K.; De Waegeneer, M.; Hulselmans, G.; Aibar, S.; Seurinck, R.; Saelens, W.; Cannoodt, R.; Rouchon, Q.; et al. A scalable SCENIC workflow for single-cell gene regulatory network analysis. *Nat. Protoc.* **2020**, *15*, 2247–2276. [CrossRef]
41. Jin, S.; Guerrero-Juarez, C.F.; Zhang, L.; Chang, I.; Ramos, R.; Kuan, C.H.; Myung, P.; Plikus, M.V.; Nie, Q. Inference and analysis of cell-cell communication using CellChat. *Nat. Commun.* **2021**, *12*, 1088. [CrossRef]
42. Ribatti, D.; Tamma, R.; Annese, T. Epithelial-mesenchymal transition in cancer: A historical overview. *Transl. Oncol.* **2020**, *13*, 100773. [CrossRef] [PubMed]
43. Tickle, T.; Tirosh, I.; Georgescu, C.; Brown, M.; Haas, B. inferCNV of the Trinity CTAT Project. 2019. Available online: https://github.com/broadinstitute/inferCNV (accessed on 21 October 2024).
44. Wang, X.; Lin, Y. Tumor necrosis factor and cancer, buddies or foes? *Acta Pharmacol. Sin.* **2008**, *29*, 1275–1288. [CrossRef]
45. Roussos, E.T.; Condeelis, J.S.; Patsialou, A. Chemotaxis in cancer. *Nat. Rev. Cancer* **2011**, *11*, 573–587. [CrossRef]
46. Sadras, F.; Monteith, G.R.; Roberts-Thomson, S.J. An emerging role for calcium signaling in cancer-associated fibroblasts. *Int. J. Mol. Sci.* **2021**, *22*, 11366. [CrossRef] [PubMed]
47. Monteith, G.R.; Prevarskaya, N.; Roberts-Thomson, S.J. The calcium–cancer signalling nexus. *Nat. Rev. Cancer* **2017**, *17*, 373–380. [CrossRef]
48. Fu, J.; Yu, M.; Xu, W.; Yu, S. Research progress of bile acids in cancer. *Front. Oncol.* **2022**, *11*, 778258. [CrossRef] [PubMed]
49. Vettore, L.; Westbrook, R.L.; Tennant, D.A. New aspects of amino acid metabolism in cancer. *Br. J. Cancer* **2020**, *122*, 150–156. [CrossRef]
50. Boussiotis, V.A.; Chatterjee, P.; Li, L. Biochemical signaling of PD-1 on T cells and its functional implications. *Cancer J.* **2014**, *20*, 265–271. [CrossRef]
51. Parvez, A.; Choudhary, F.; Mudgal, P.; Khan, R.; Qureshi, K.A.; Farooqi, H.; Aspatwar, A. PD-1 and PD-L1: Architects of immune symphony and immunotherapy breakthroughs in cancer treatment. *Front. Immunol.* **2023**, *14*, 1296341. [CrossRef]
52. Walunas, T.L.; Lenschow, D.J.; Bakker, C.Y.; Linsley, P.S.; Freeman, G.J.; Green, J.M.; Thompson, C.B.; Bluestone, J.A. CTLA-4 can function as a negative regulator of T cell activation. *Immunity* **1994**, *1*, 405–413. [CrossRef]
53. Liu, D.; Lobie, P. Transcriptional activation of p53 by Pitx1. *Cell Death Differ.* **2007**, *14*, 1893–1907. [CrossRef] [PubMed]

54. Chen, M.; Liu, Y.; Yang, Y.; Qiu, Y.; Wang, Z.; Li, X.; Zhang, W. Emerging roles of activating transcription factor (ATF) family members in tumourigenesis and immunity: Implications in cancer immunotherapy. *Genes Dis.* **2022**, *9*, 981–999. [CrossRef] [PubMed]
55. Wortel, I.M.; van der Meer, L.T.; Kilberg, M.S.; van Leeuwen, F.N. Surviving stress: Modulation of ATF4-mediated stress responses in normal and malignant cells. *Trends Endocrinol. Metab.* **2017**, *28*, 794–806. [CrossRef]
56. Pakos-Zebrucka, K.; Koryga, I.; Mnich, K.; Ljujic, M.; Samali, A.; Gorman, A.M. The integrated stress response. *EMBO Rep.* **2016**, *17*, 1374–1395. [CrossRef]
57. Gumilar, K.E.; Chin, Y.; Ibrahim, I.H.; Tjokroprawiro, B.A.; Yang, J.Y.; Zhou, M.; Gassman, N.R.; Tan, M. Heat Shock Factor 1 Inhibition: A Novel Anti-Cancer Strategy with Promise for Precision Oncology. *Cancers* **2023**, *15*, 5167. [CrossRef] [PubMed]
58. Ghaleb, A.M.; Yang, V.W. Krüppel-like factor 4 (KLF4): What we currently know. *Gene* **2017**, *611*, 27–37. [CrossRef]
59. Li, S.; Huang, L.; Gu, J.; Wu, J.; Ou, W.; Feng, J.; Liu, B.; Cui, X.; Zhou, Y. Restoration of KLF4 inhibits invasion and metastases of lung adenocarcinoma through suppressing MMP2. *J. Cancer* **2017**, *8*, 3480–3489. [CrossRef]
60. Chen, K.S.; Lim, J.W.; Richards, L.J.; Bunt, J. The convergent roles of the nuclear factor I transcription factors in development and cancer. *Cancer Lett.* **2017**, *410*, 124–138. [CrossRef]
61. Nilsson, J.; Helou, K.; Kovács, A.; Bendahl, P.O.; Bjursell, G.; Fernö, M.; Carlsson, P.; Kannius-Janson, M. Nuclear Janus-activated kinase 2/nuclear factor 1-C2 suppresses tumorigenesis and epithelial-to-mesenchymal transition by repressing Forkhead box F1. *Cancer Res.* **2010**, *70*, 2020–2029. [CrossRef]
62. Brun, M.; Jain, S.; Monckton, E.A.; Godbout, R. Nuclear factor I represses the notch effector HEY1 in glioblastoma. *Neoplasia* **2018**, *20*, 1023–1037. [CrossRef]
63. Zhang, H.; Luo, Z.; Tang, J.; Tian, J.; Xiao, Y.; Sun, C.; Wang, T. Transcription factor NFIC functions as a tumor suppressor in lung squamous cell carcinoma progression by modulating lncRNA CASC2. *Cell Cycle* **2022**, *21*, 63–73. [CrossRef] [PubMed]
64. Affo, S.; Nair, A.; Brundu, F.; Ravichandra, A.; Bhattacharjee, S.; Matsuda, M.; Chin, L.; Filliol, A.; Wen, W.; Song, X.; et al. Promotion of cholangiocarcinoma growth by diverse cancer-associated fibroblast subpopulations. *Cancer Cell* **2021**, *39*, 866–882. [CrossRef] [PubMed]
65. Unterleuthner, D.; Neuhold, P.; Schwarz, K.; Janker, L.; Neuditschko, B.; Nivarthi, H.; Crncec, I.; Kramer, N.; Unger, C.; Hengstschläger, M.; et al. Cancer-associated fibroblast-derived WNT2 increases tumor angiogenesis in colon cancer. *Angiogenesis* **2020**, *23*, 159–177. [CrossRef]
66. Su, S.; Chen, J.; Yao, H.; Liu, J.; Yu, S.; Lao, L.; Wang, M.; Luo, M.; Xing, Y.; Chen, F.; et al. CD10+ GPR77+ cancer-associated fibroblasts promote cancer formation and chemoresistance by sustaining cancer stemness. *Cell* **2018**, *172*, 841–856. [CrossRef]
67. Deng, J.; Fleming, J.B. Inflammation and myeloid cells in cancer progression and metastasis. *Front. Cell Dev. Biol.* **2022**, *9*, 759691. [CrossRef] [PubMed]
68. Lamouille, S.; Xu, J.; Derynck, R. Molecular mechanisms of epithelial–mesenchymal transition. *Nat. Rev. Mol. Cell Biol.* **2014**, *15*, 178–196. [CrossRef]
69. Xue, W.; Yang, L.; Chen, C.; Ashrafizadeh, M.; Tian, Y.; Sun, R. Wnt/β-catenin-driven EMT regulation in human cancers. *Cell. Mol. Life Sci.* **2024**, *81*, 79. [CrossRef]
70. Jechlinger, M.; Grunert, S.; Tamir, I.H.; Janda, E.; Lüdemann, S.; Waerner, T.; Seither, P.; Weith, A.; Beug, H.; Kraut, N. Expression profiling of epithelial plasticity in tumor progression. *Oncogene* **2003**, *22*, 7155–7169. [CrossRef]
71. Jechlinger, M.; Sommer, A.; Moriggl, R.; Seither, P.; Kraut, N.; Capodiecci, P.; Donovan, M.; Cordon-Cardo, C.; Beug, H.; Grünert, S.; et al. Autocrine PDGFR signaling promotes mammary cancer metastasis. *J. Clin. Investig.* **2006**, *116*, 1561–1570. [CrossRef]
72. Elahouel, R.; Blanc, C.; Carpentier, G.; Frechault, S.; Cascone, I.; Destouches, D.; Delbé, J.; Courty, J.; Hamma-Kourbali, Y. Pleiotrophin exerts its migration and invasion effect through the neuropilin-1 pathway. *Neoplasia* **2015**, *17*, 613–624. [CrossRef]
73. Masiuk, M.; Urasinska, E.; Domagala, W. Intranuclear nucleolin distribution during cell cycle progression in human invasive ductal breast carcinomas in relation to estrogen receptor status. *Anticancer Res.* **2007**, *27*, 3957–3962. [PubMed]
74. Cicchillitti, L.; Di Michele, M.; Urbani, A.; Ferlini, C.; Donati, M.B.; Scambia, G.; Rotilio, D. Comparative proteomic analysis of paclitaxel sensitive A2780 epithelial ovarian cancer cell line and its resistant counterpart A2780TC1 by 2D-DIGE: The role of ERp57. *J. Proteome Res.* **2009**, *8*, 1902–1912. [CrossRef] [PubMed]
75. Qiu, W.; Zhou, F.; Zhang, Q.; Sun, X.; Shi, X.; Liang, Y.; Wang, X.; Yue, L. Overexpression of nucleolin and different expression sites both related to the prognosis of gastric cancer. *Apmis* **2013**, *121*, 919–925. [CrossRef] [PubMed]
76. Rosenberg, J.E.; Bambury, R.M.; Van Allen, E.M.; Drabkin, H.A.; Lara, P.N.; Harzstark, A.L.; Wagle, N.; Figlin, R.A.; Smith, G.W.; Garraway, L.A.; et al. A phase II trial of AS1411 (a novel nucleolin-targeted DNA aptamer) in metastatic renal cell carcinoma. *Investig. New Drugs* **2014**, *32*, 178–187. [CrossRef]
77. Xu, J.y.; Lu, S.; Xu, X.y.; Hu, S.l.; Li, B.; Li, W.x.; Chang, J.Y. Prognostic significance of nuclear or cytoplasmic nucleolin expression in human non-small cell lung cancer and its relationship with DNA-PKcs. *Tumor Biol.* **2016**, *37*, 10349–10356. [CrossRef]
78. Chen, Z.; Xu, X. Roles of nucleolin: Focus on cancer and anti-cancer therapy. *Saudi Med. J.* **2016**, *37*, 1312–1318. [CrossRef]

79. Ren, Q.; Zhu, P.; Zhang, H.; Ye, T.; Liu, D.; Gong, Z.; Xia, X. Identification and validation of stromal-tumor microenvironment-based subtypes tightly associated with PD-1/PD-L1 immunotherapy and outcomes in patients with gastric cancer. *Cancer Cell Int.* **2020**, *20*, 92. [CrossRef] [PubMed]
80. Jia, J.; Dai, Y.; Zhang, Q.; Tang, P.; Fu, Q.; Xiong, G. Stromal score-based gene signature: A prognostic prediction model for colon cancer. *Front. Genet.* **2021**, *12*, 655855. [CrossRef]
81. Ahrendt, S.A.; Hu, Y.; Buta, M.; McDermott, M.P.; Benoit, N.; Yang, S.C.; Wu, L.; Sidransky, D. p53 mutations and survival in stage I non-small-cell lung cancer: Results of a prospective study. *J. Natl. Cancer Inst.* **2003**, *95*, 961–970. [CrossRef]
82. Robles, A.I.; Jen, J.; Harris, C.C. Clinical outcomes of TP53 mutations in cancers. *Cold Spring Harb. Perspect. Med.* **2016**, *6*, a026294. [CrossRef]
83. Cui, Y.; Guo, G. Immunomodulatory function of the tumor suppressor p53 in host immune response and the tumor microenvironment. *Int. J. Mol. Sci.* **2016**, *17*, 1942. [CrossRef] [PubMed]
84. Agupitan, A.D.; Neeson, P.; Williams, S.; Howitt, J.; Haupt, S.; Haupt, Y. P53: A guardian of immunity becomes its saboteur through mutation. *Int. J. Mol. Sci.* **2020**, *21*, 3452. [CrossRef] [PubMed]
85. Wherry, E.J. T cell exhaustion. *Nat. Immunol.* **2011**, *12*, 492–499. [CrossRef]
86. Binnewies, M.; Roberts, E.W.; Kersten, K.; Chan, V.; Fearon, D.F.; Merad, M.; Coussens, L.M.; Gabrilovich, D.I.; Ostrand-Rosenberg, S.; Hedrick, C.C.; et al. Understanding the tumor immune microenvironment (TIME) for effective therapy. *Nat. Med.* **2018**, *24*, 541–550. [CrossRef] [PubMed]
87. Pinto, J.A.; Vallejos, C.S.; Raez, L.E.; Mas, L.A.; Ruiz, R.; Torres-Roman, J.S.; Morante, Z.; Araujo, J.M.; Gómez, H.L.; Aguilar, A.; et al. Gender and outcomes in non-small cell lung cancer: An old prognostic variable comes back for targeted therapy and immunotherapy? *ESMO Open* **2018**, *3*, e000344. [CrossRef]
88. Sakurai, H.; Asamura, H.; Goya, T.; Eguchi, K.; Nakanishi, Y.; Sawabata, N.; Okumura, M.; Miyaoka, E.; Fujii, Y.; Japanese Joint Committee for Lung Cancer Registration. Survival differences by gender for resected non-small cell lung cancer: A retrospective analysis of 12,509 cases in a Japanese Lung Cancer Registry study. *J. Thorac. Oncol.* **2010**, *5*, 1594–1601. [CrossRef]
89. Kim, S.K.; Cho, S.W. The evasion mechanisms of cancer immunity and drug intervention in the tumor microenvironment. *Front. Pharmacol.* **2022**, *13*, 868695. [CrossRef]
90. Schleimer, R.P.; Kato, A.; Kern, R.; Kuperman, D.; Avila, P.C. Epithelium: At the interface of innate and adaptive immune responses. *J. Allergy Clin. Immunol.* **2007**, *120*, 1279–1284. [CrossRef]
91. Sahai, E.; Astsaturov, I.; Cukierman, E.; DeNardo, D.G.; Egeblad, M.; Evans, R.M.; Fearon, D.; Greten, F.R.; Hingorani, S.R.; Hunter, T.; et al. A framework for advancing our understanding of cancer-associated fibroblasts. *Nat. Rev. Cancer* **2020**, *20*, 174–186. [CrossRef]
92. Sarkar, M.; Nguyen, T.; Gundre, E.; Ogunlusi, O.; El-Sobky, M.; Giri, B.; Sarkar, T.R. Cancer-associated fibroblasts: The chief architect in the tumor microenvironment. *Front. Cell Dev. Biol.* **2023**, *11*, 1089068. [CrossRef]
93. De Visser, K.E.; Joyce, J.A. The evolving tumor microenvironment: From cancer initiation to metastatic outgrowth. *Cancer Cell* **2023**, *41*, 374–403. [CrossRef] [PubMed]
94. Jiang, X.; Wang, J.; Deng, X.; Xiong, F.; Zhang, S.; Gong, Z.; Li, X.; Cao, K.; Deng, H.; He, Y.; et al. The role of microenvironment in tumor angiogenesis. *J. Exp. Clin. Cancer Res.* **2020**, *39*, 204. [CrossRef] [PubMed]
95. Chen, H.C.; Zhu, Y.T.; Chen, S.Y.; Tseng, S.C. Wnt signaling induces epithelial–mesenchymal transition with proliferation in ARPE-19 cells upon loss of contact inhibition. *Lab. Investig.* **2012**, *92*, 676–687. [CrossRef]
96. Kalluri, R.; Weinberg, R.A. The basics of epithelial-mesenchymal transition. *J. Clin. Investig.* **2009**, *119*, 1420–1428. [CrossRef]
97. Martin-Orozco, E.; Sanchez-Fernandez, A.; Ortiz-Parra, I.; Ayala-San Nicolas, M. WNT signaling in tumors: The way to evade drugs and immunity. *Front. Immunol.* **2019**, *10*, 2854. [CrossRef]
98. Dostert, C.; Grusdat, M.; Letellier, E.; Brenner, D. The TNF family of ligands and receptors: Communication modules in the immune system and beyond. *Physiol. Rev.* **2018**, *99* , 115–160. [CrossRef] [PubMed]
99. Shi, Y.; Ping, Y.F.; Zhou, W.; He, Z.C.; Chen, C.; Bian, B.S.J.; Zhang, L.; Chen, L.; Lan, X.; Zhang, X.C.; et al. Tumour-associated macrophages secrete pleiotrophin to promote PTPRZ1 signalling in glioblastoma stem cells for tumour growth. *Nat. Commun.* **2017**, *8*, 15080. [CrossRef] [PubMed]
100. Mikelis, C.; Koutsioumpa, M.; Papadimitriou, E. Pleiotrophin as a possible new target for angiogenesis-related diseases and cancer. *Recent Patents Anti-Cancer Drug Discov.* **2007**, *2*, 175–186. [CrossRef]
101. Pandey, P.; Khan, F.; Upadhyay, T.K.; Seungjoon, M.; Park, M.N.; Kim, B. New insights about the PDGF/PDGFR signaling pathway as a promising target to develop cancer therapeutic strategies. *Biomed. Pharmacother.* **2023**, *161*, 114491. [CrossRef]
102. Zou, X.; Tang, X.Y.; Qu, Z.Y.; Sun, Z.W.; Ji, C.F.; Li, Y.J.; Guo, S.D. Targeting the PDGF/PDGFR signaling pathway for cancer therapy: A review. *Int. J. Biol. Macromol.* **2022**, *202*, 539–557. [CrossRef]
103. Sorrelle, N.; Dominguez, A.T.; Brekken, R.A. From top to bottom: Midkine and pleiotrophin as emerging players in immune regulation. *J. Leukoc. Biol.* **2017**, *102*, 277–286. [CrossRef]
104. Heldin, C.H. Targeting the PDGF signaling pathway in tumor treatment. *Cell Commun. Signal.* **2013**, *11*, 97. [CrossRef] [PubMed]

105. Pietras, K.; Rubin, K.; Sjoblom, T.; Buchdunger, E.; Sjoquist, M.; Heldin, C.H.; Ostman, A. Inhibition of PDGF receptor signaling in tumor stroma enhances antitumor effect of chemotherapy. *Cancer Res.* **2002**, *62*, 5476–5484.
106. Liu, J.; Liao, S.; Huang, Y.; Samuel, R.; Shi, T.; Naxerova, K.; Huang, P.; Kamoun, W.; Jain, R.K.; Fukumura, D.; et al. PDGF-D improves drug delivery and efficacy via vascular normalization, but promotes lymphatic metastasis by activating CXCR4 in breast cancer. *Clin. Cancer Res.* **2011**, *17*, 3638–3648. [CrossRef] [PubMed]
107. Wang, J.C.; Li, G.Y.; Wang, B.; Han, S.X.; Sun, X.; Jiang, Y.N.; Shen, Y.W.; Zhou, C.; Feng, J.; Lu, S.Y.; et al. Metformin inhibits metastatic breast cancer progression and improves chemosensitivity by inducing vessel normalization via PDGF-B downregulation. *J. Exp. Clin. Cancer Res.* **2019**, *38*, 235. [CrossRef]
108. Akiyama, T.; Yasuda, T.; Uchihara, T.; Yasuda-Yoshihara, N.; Tan, B.J.; Yonemura, A.; Semba, T.; Yamasaki, J.; Komohara, Y.; Ohnishi, K.; et al. Stromal reprogramming through dual PDGFRα/β blockade boosts the efficacy of anti–PD-1 immunotherapy in fibrotic tumors. *Cancer Res.* **2023**, *83*, 753–770. [CrossRef] [PubMed]
109. Yang, J.; Guo, Z.; Song, M.; Pan, Q.; Zhao, J.; Huang, Y.; Han, Y.; Ouyang, D.; Yang, C.; Chen, H.; et al. Lenvatinib improves anti-PD-1 therapeutic efficacy by promoting vascular normalization via the NRP-1-PDGFRβ complex in hepatocellular carcinoma. *Front. Immunol.* **2023**, *14*, 1212577. [CrossRef]
110. Luo, W. Nasopharyngeal carcinoma ecology theory: Cancer as multidimensional spatiotemporal "unity of ecology and evolution" pathological ecosystem. *Theranostics* **2023**, *13*, 1607–1631. [CrossRef]

Disclaimer/Publisher's Note: The statements, opinions and data contained in all publications are solely those of the individual author(s) and contributor(s) and not of MDPI and/or the editor(s). MDPI and/or the editor(s) disclaim responsibility for any injury to people or property resulting from any ideas, methods, instructions or products referred to in the content.

biomedicines

MDPI

Review

Pharmacological Modulation of Mutant *TP53* with Oncotargets Against Esophageal Cancer and Therapy Resistance

Pei-I Lin [1], Yu-Cheng Lee [2], I-Hung Chen [3] and Hsien-Hui Chung [4,5,6,7,*]

[1] Department of Nursing, Kaohsiung Chang Gung Memorial Hospital, Kaohsiung City 833401, Taiwan; t3810@cgmh.org.tw
[2] Graduate Institute of Medical Sciences, College of Medicine, Taipei Medical University, Taipei City 110301, Taiwan; yclee0212@tmu.edu.tw
[3] Division of Urology, Department of Surgery, National Cheng Kung University Hospital Douliu Branch, Yunlin County 640003, Taiwan; josephcmed@gmail.com
[4] Department of Pharmacy & Clinical Trial Pharmacy, Kaohsiung Veterans General Hospital, Kaohsiung City 813414, Taiwan
[5] St. Edmund Hall, University of Oxford, Oxford OX1 4AR, UK
[6] Preventive Medicine Program, Center for General Education, Chung Yuan Christian University, Taoyuan City 320314, Taiwan
[7] Department of Pharmacy and Master Program, College of Pharmacy and Health Care, Tajen University, Pingtung County 907101, Taiwan
* Correspondence: clinicaltrialchung@gmail.com

Abstract: The prevalence and deaths from esophageal cancer (EC) have recently increased. Although therapeutic strategies depend on the EC stage and recurrence, such as surgical intervention, chemotherapy, radiation therapy, chemoradiation therapy, targeted therapy, and immunotherapy, a more effective and novel treatment for EC is still required. This review briefly describes and summarizes some insightful oncotargets involved in the metabolic modulation of EC, including (1) cancer stem cells (CSCs) for EC progression, poor prognosis, tumor recurrence, and therapy resistance; (2) retinoic acid receptors (RARs) for esophageal carcinogenesis and regeneration; (3) phosphofructokinase (PFK) for EC-reprogrammed glycolysis; (4) lactate dehydrogenase (LDH) as an EC peripheral blood biomarker; and (5) hypoxia-inducible factor-1 alpha (HIF-1α) for the tumor microenvironment under hypoxic conditions. Moreover, the aforementioned oncotargets can be modulated by mutant *TP53* and have their own features in the carcinogenesis, differentiation, proliferation, and metastasis of EC. Thus, the clarification of pharmacological mechanisms regarding the interaction between mutant *TP53* and the abovementioned oncotargets could provide precise and perspective opinions for minimizing prediction errors, reducing therapy resistance, and developing novel drugs against EC.

Keywords: esophageal cancer; metabolic modulation; mutant *TP53*; oncotargets; therapy resistance

1. Introduction

Esophageal cancer (EC) is a highly prevalent and well-known digestive disease. Recently, EC has become the sixth most common cause of cancer-related deaths worldwide. According to the EC trends from the World Health Organization statistical database, the male age-standardized mortality rate (ASMR)/100,000 in Europe, the United States, and Japan was 4.01, 4.28, and 5.10 in 2015-19, respectively. Additionally, the global range of female ASMRs was from 0.82 to 0.85/100,000 [1].

Patients with EC have difficulty swallowing, accompanied by body weight loss, and risk factors, such as smoking, heavy alcohol use, acid reflux, and Barrett's esophagus (BE). Esophageal adenocarcinoma (EAC) and esophageal squamous cell carcinoma (ESCC) are the two main types of EC based on histological evaluation and the location of malignancies in the lower and upper esophagus, which are related to transitional and squamous basal cells, respectively. Moreover, the risk factors involved in EAC include obesity, gastroesophageal reflux disease (GERD), single-nucleotide polymorphisms (SNPs), BE, decreased estrogen exposure, and Helicobacter pylori infection. Meanwhile, risk factors involved in ESCC are family history, genetic changes (mutation and SNPs), habits (smoking and drinking), chemical factors, infection, and signal transduction [2]. Clinically, the combination of chemotherapy and radiotherapy can be applied to attenuate EC based on the stages of EC progression. Unfortunately, there is no proper therapeutic strategy once the acquired chemo- or radio-resistance occurs because the failure to treat EC results from chemotherapy resistance linked to complicated mechanisms. Although some promising immunotherapies have attracted much attention, including cancer vaccines for specific targets (preventive type and therapeutic type), immune checkpoint inhibitors (ICIs) for cancer cells and T cells, and chimeric antigen receptor (CAR) T-cell therapy for recognizing specific target antigens, patients with EC receiving immunotherapy have an overall response rate lower than 30% and most patients initially receiving immunotherapy have acquired resistance. Moreover, the immunotherapy resistance in EC still results in clinical challenges owing to drug resistance and immunosuppression associated with oncological characteristics and the heterogeneity of immune microenvironments [3]. Recently, targeting epithelial-mesenchymal conversion by miR-200 has provided a therapeutic direction for ESCC patients with acquired concurrent chemoradiotherapy resistance [4]. Thus, developing therapeutic strategies for improving EC therapy resistance by exploring novel oncotargets and biomarkers is crucial.

2. Metabolic Modulation of Oncotargets in Esophageal Cancer

2.1. Effects of Cancer Stem Cells on Esophageal Cancer

Generally, normal stem cells represent physiological development, whereas cancer stem cells (CSCs) have distinct morphological features associated with pathological carcinogenesis and tumor-initiating cells. CSCs play crucial roles in the molecular mechanisms of metabolic reprogramming, quiescence, epigenetic modification, progression, poor prognosis, tumor recurrence, and therapeutic resistance in EC. Additionally, impaired mitochondrial function of CSCs, such as imbalanced mitochondrial dynamics, subcellular localization, metabolic plasticity, mitophagy, excessive mitochondria biogenesis, and defective mtDNA, is associated with drug resistance. Moreover, the factors involved in the therapy resistance of esophageal CSCs include DNA repair, the cycle distribution, free radical and reactive oxygen species (ROS) scavenging, the tumor microenvironment, epithelial-mesenchymal transition (EMT), hypoxia, oxidative ROS modulation, autophagy, inflammation, metabolic mechanisms, CSC plasticity, drug transporters, miRNAs, and long noncoding RNAs (lncRNAs) [5]. Some CSC markers—including CD44, CD133, CD271, CD90, leucine-rich repeat-containing G-protein coupled receptor 5 (LgR5), aldehyde dehydrogenase 1 (ALDH1), intercellular cell adhesion molecule-1 (ICAM-1), ATP-binding cassette superfamily G member 2 (ABCG2), integrin subunit alpha 7 (ITGA7), $CD44^+/CD24^-$, $CD44^+/CD133^+$, $CD133^+/CXCR4^+$, B-lymphoma Mo-MLV insertion region 1 (BMI1), NANOG, glioma-associated oncogene homolog 1 (GLI-1), octamer-binding transcription factor 4 (OCT-4), spalt-like transcription factor 4 (SALL4), sex-determining region Y-box2 (SOX2), epithelial cell adhesion molecule (Ep-CAM), and podoplanin—were involved in the diagnosis and prognosis of EC. Moreover, the regulation of CSC prolif-

eration, invasiveness, metastasis, differentiation capacity, and self-renewal in EC may be associated with Notch, Hedgehog, Hippo, Wnt/β-catenin, JAK/STAT3, transforming growth factor-β (TGF-β)/Smad, and phosphatidylinositol 3-kinase (PI3K)/AKT/c-MYC signal transduction pathways [6]. Thus, clarifying metabolic modulation and pathological mechanisms in esophageal CSCs would be helpful for us in finding effective strategies to eradicate EC and control its progression [7]. Most importantly, the clinical targeting CSCs combined with surgical intervention, chemotherapy, radiotherapy, chemoradiation therapy, targeted therapy, and immunotherapy for patients with EC effectively reduce therapy resistance and should be considered.

2.2. Effects of Retinoic Acid Receptors (RARs) on Esophageal Carcinogenesis and Regeneration

Retinoic acid, mainly derived from vitamin A, is involved in physiological cell growth, differentiation, and metabolic homeostasis, which has anti-oxidant, pro-apoptotic, and anti-proliferative effects. Meanwhile, RARs belong to nuclear receptors involved in the modulation of cell functions, including the maintenance of cellular differentiation, proliferation, and survival. Thus, disruption of the retinoic acid pathway by targeting RARs in EC should be elucidated and is worth investigating. Interestingly, in addition to the canonically intracellular role of RARs, a previous study has revealed that the application of exosomes associated with RARs in regenerative medicine, including tissue repair and regeneration, has attracted much attention [8]. Noticeably, activation of RARγ enhances the formation of esophageal epithelial cells (EECs) differentiated from the human-induced pluripotent stem cell (hiPSCs)-derived foregut, providing a novel strategy for regenerative therapy [9]. Nevertheless, the difference in RAR subtypes (RARα, RARβ, and RARγ) involved in esophageal carcinogenesis and regeneration should be further addressed. Thus, I have shared some viewpoints regarding the comparison of RAR subtype-mediated mechanisms in esophageal carcinogenesis and regeneration.

2.2.1. Differential Expressions of RAR Subtypes in Esophageal Carcinogenesis

All-trans retinoic acid (ATRA) has anti-tumor and anti-angiogenesis effects on human ESCC by inhibiting vascular endothelial growth factor (VEGF)-mediated signal transduction [10]. Additionally, CSCs in ESCC that express higher levels of CD44 surface markers are positively correlated with tumorigenicity and chemotherapy resistance. The combination of chemotherapy reagents (cisplatin and 5-fluorouracil) with low concentrations of ATRA enhances tumor cell cycle arrest and apoptosis, exhibiting a synergistic cytotoxic effect against human EC stem cells by suppressing CD44 [11]. As ATRA can non-selectively activate RAR subtypes, the association between distinct RAR subtypes in esophageal carcinogenesis and chemotherapy sensitivity should be investigated. First, it has been demonstrated that RARα was overexpressed in human esophageal carcinoma, whereas silencing RARα expression can attenuate ESCC tumor cell proliferation and metastatic ability through suppressing the Wnt/β-catenin mechanism to resensitize ESCC to chemotherapy treatment [12]. Second, compared to the gain-of-function role of RARα in ESCC tumors, the formation of esophageal carcinogenesis is attributed to the loss of RARβ expressions, but the induction of RARβ expressions in EC cells enhances cell apoptosis via reducing cyclooxygenase-2 expression [13]. Moreover, RARβ silencing in human ESCC associated with hypermethylation of the RARβ promoter region led to the progression and severity of esophageal carcinogenesis, but esophageal carcinogenesis could be ameliorated by DNA methyltransferase inhibitors to partially restore RARβ expressions [14].

Furthermore, the other subtype of RARs and RARγ demonstrates no significantly differential expressions in ESCC compared to those in the same matched distant normal tissues [15]. Conversely, patients with smoking and alcohol drinking habits exhibited

relatively lower RARγ expressions in ESCC than those in surrounding normal tissues [16], suggesting the possibility of the RARγ response to chronic chemical stimulation and the variation based on different normal tissues. In the above evaluation of the differential expressions of RAR subtype in esophageal carcinogenesis, RARα, RARβ, and RARγ expressions may have similar and distinct characteristics. Moreover, lifestyles, environmental factors, and genetic differences would directly or indirectly alter RAR subtype expressions, which contribute to esophageal carcinogenesis. Using RAR, subtype expressions between patients with EC and healthy humans identified through a genetic analysis of the biobank can be considered as the reference clinical therapy and the identification of compounds applied in pharmacotherapy. The above differential expressions of RAR subtypes in esophageal carcinogenesis are summarized in Table 1.

Table 1. The comparison of the differential expressions of retinoic acid receptor (RAR) subtype in esophageal regeneration and carcinogenesis.

RAR Subtype	Esophageal Regeneration	Esophageal Carcinogenesis
RARα	Unknown	RARα Overexpression (RARα ↑) [12]
RARβ	Unknown	The loss of RARβ expressions with hypermethylation (RARβ ↓) [14]
RARγ	The differentiation of esophageal epithelial cells from hiPSC-derived foregut through the specific activation of RARγ [9]	Lower RARγ expression (RARγ ↓) [16]

hiPSCs: human-induced pluripotent stem cells.

2.2.2. Differential Expressions of RAR Subtypes During Esophageal Regeneration

Esophageal carcinogenesis is driven by epigenetic mutations, environmental risk factors, GERD, and BE. Although chemotherapy, radiotherapy, and immunotherapy currently serve as the therapeutic options for ESCC treatment, identifying the most effective therapy is essential. Regarding the physiological role of RARs, it is remarkable to mention the beneficial role of ATRA in a single progenitor cell population in the maintenance and repair of the esophageal epithelium, which provides a switching behavior for esophageal regeneration related to wound healing [17].

Surprisingly, the analysis of marker genes during the EEC differentiated process relies on RARγ signaling, not RARα and RARβ, and suitable differentiation protocols. Thus, RARγ activation has a critical and specific impact on esophageal regeneration linked to tissue repair [9]. Furthermore, the application of genetically modified animal models to observe the detailed mechanisms and influence of RARγ linked to the regenerative potential of exosomes on esophageal regeneration is essential because of the complicated interaction of in vivo mimicking that, in humans, has clinical value. Given the above evaluation for the differential expressions of RAR subtype in esophageal regeneration, the stimulation of retinoic acid and RARγ-mediated signaling may induce tissue repair and esophageal regeneration. Thus, retinoic acid synthesis and RARγ expressions involved in esophageal regeneration could provide an alternative therapy against EC and replace abnormal tissues. The differential expressions of RAR subtypes in esophageal regeneration are summarized in Table 1.

2.2.3. Clinical Application of RAR Subtypes in EC

Collectively, the diverse functions and underlying mechanisms of the differential expressions of RAR subtypes in esophageal carcinogenesis or regeneration should be further clarified. The well-understanding in the regulation and mechanisms of distinct RAR subtypes is clinically significant for providing new insights into the combination of anti-carcinogenic action and regenerative therapy through the use of specific RAR subtype agonists or antagonists in patients with ESCC. Thus, the development of RAR subtype compounds in attenuating EC through cellular models, animal models, and clinical trials can be practicably performed. Most importantly, the clinical application of RAR subtype compounds combined with surgical intervention, chemotherapy, radiotherapy, chemoradiation therapy, targeted therapy, and immunotherapy in patients with EC could effectively reduce therapy resistance and is worthwhile to expect.

2.3. Metabolic Role of Phosphofructokinase (PFK) in EC

Regarding the utilization of adenosine triphosphate (ATP) for cellular metabolism, compared to normal cells, cancer cells have the preference of glycolysis in the cytosol rather than mitochondrial oxidative phosphorylation based on the requirement of more ATP, which is known as the Warburg effect. When EC exhibits a greater Warburg effect, it is more aggressive and malignant. Thus, focusing on the metabolic reprogramming of EC during glycolysis may help identify potential targets or biomarkers. During the glycolysis process, PFK catalyzes the phosphorylation of fructose-6-phosphate to fructose-1,6-bisphosphate, which is allosterically activated by adenosine monophosphate (AMP) and inhibited by ATP. The aberrant regulation of PFK on glucose metabolism is closely associated with insulin resistance in animal models fed high amounts of fructose [18–20]. Currently, two types of PFK have been identified in humans: PFK1 and PFK2. Based on tissue-specific functions and expressions, PFK1 isoforms can be classified as liver-specific PFK (PFKL), skeletal muscle-specific PFK (PFKM), and platelet-specific PFK (PFKP). Although PFK is thought to be associated with cancer progression [21], the metabolic modulation of PFK in EC has not been fully investigated. Patients with ESCC with poor survival and advanced stages had higher PFKL expression levels, but the antipsychotic drug, penfluridol, significantly attenuated ESCC by suppressing PFKL to activate AMP-activated protein kinase (AMPK), forkhead box-containing protein 3a (FOXO3a), and Bcl-2-interacting mediator of cell death (BIM) signaling for glycolysis inhibition and apoptosis induction [22]. In addition, the 6-phosphofructo-2-kinase/fructose-2,6-bisphosphatase isoform 3 (PFKFB3) has biofunctional roles as an effective modulator of glycolytic flux and a critical regulator of angiogenesis, cell death, and cell stemness [23]. An observational study has reported that ESCC tissues exhibited higher protein and gene expression levels of 6-phosphofructo-2-kinase/fructose-2,6-bisphosphatase isoform 3 (PFKFB3) than adjacent non-tumor tissues, indicating the carcinogenic effect of PFKFB3 on the development, occurrence, and prognosis of ESCC. Moreover, the 3-year survival by PFKFB3 mRNA changes could also be predicted in patients with ESCC [24]. However, the genetic absence of PFK or impaired insulin signaling enhanced the extracellular matrix hyaluronan synthesis involved in tumor development and progression by using the nude mouse xenograft model with ESCC induced by streptozotocin, indicating the divergent metabolic regulation of PFK in diabetic EC [25]. Thus, the development of targeting PFK compounds in attenuating EC through cellular models, animal models, and clinical trials can be practicably performed. Certainly, the compounds, by targeting PFK or other related enzymes combined with surgical intervention, chemotherapy, radiotherapy, chemoradiation therapy, targeted therapy, and immunotherapy for patients with EC, could effectively reduce therapy resistance, and this is worthwhile to verify.

2.4. Metabolic Role of Lactate Dehydrogenase (LDH) in EC

The metabolic enzyme LDH is primarily responsible for converting pyruvate to lactate. The enhancement of tumor glycolysis contributes to increased lactate production, which is linked to an acidified tumor microenvironment, metastasis, invasion, angiogenesis, immunosuppression, and therapy resistance. LDH was involved in the tumorigenesis of EC because LDHA was overexpressed in ESCC, which was modulated by decreased cleavage of PARP and caspase 8 and increased AKT activation and cyclin D1 expressions. Relatively, the silencing of LDHA expressions significantly attenuates ESCC migration and growth both in vitro and in vivo [26]. Moreover, some small molecules, such as LDHA antagonists, have been designed for tumor regression and cancer therapeutics, including notinamide adenine dinucleotide and hydrogen (NADH) competitive inhibitors through competition with cofactor NADH; pyruvate competitive inhibitors through competition with substrate pyruvate; and substrate and cofactor competitive inhibitors through competition with substrate pyruvate, as well as NADH, peptides, and galloflavin, which can be potentially considered as EC treatments [27]. Regarding the effects of LDH on therapy resistance, the correlation between LDH levels and EC progression should be investigated. In a single-center retrospective study, patients with ESCC receiving chemoradiotherapy showed that the high-LDH group had shorter overall survival (OS) and progression-free survival (PFS) than the low-LDH group [28]. In a phase 1 clinical trial, compared to patients with normal serum LDH levels at baseline, the increased serum LDH levels at baseline in patients with ESCC exhibited a poorer tumor response, such as complete remission and partial remission, as well as shorter PFS and OS. Moreover, the reduced serum LDH levels are associated with better disease control than the elevated serum LDH levels in patients with ESCC treated with a novel anti-PD-1 antibody, camrelizumab, indicating that the changes of serum LDH levels can be used for evaluating EC prognosis in immunotherapy [29]. Moreover, the metabolic modulation of EC by targeting LDH can be clarified, and the identification of targeting LDH compounds in attenuating EC through cellular models, animal models, and clinical trials can be practicably performed. Furthermore, the compounds, by targeting LDH combined with surgical intervention, chemotherapy, radiation therapy, chemoradiation therapy, targeted therapy, and immunotherapy in patients with EC, can effectively reduce therapy resistance and are worthwhile to evaluate.

2.5. Effects of Hypoxia-Inducible Factor-1 (HIF-1) Alpha on EC

HIF-1 is mainly assembled by oxygen-sensitive subunit HIF-1α and constitutively expressed subunit HIF-1β as a heterodimer, and HIF-1α subunit in hypoxia or normoxia can be modulated through post-translation, including phosphorylation, acetylation, hydroxylation, and ubiquitination [30]. The induction of HIF-1 via tumor hypoxia regulates cell survival, angiogenesis, proliferation, invasion, and cancer metabolism. The anaerobic glycolysis is responsible for the metabolic modulation of cancer cells in hypoxic environments. Regarding the effects of HIF-1α expressions on EC, the shorter OS of patients with EC is associated with glycolysis-related proteins and higher HIF-1α expressions [31]. Moreover, the ESCC pathological tumor–node–metastasis stage, T classification, lymph node metastasis, and differentiation can be evaluated via HIF-1α expressions [32]. Compared with local control of low HIF-1α expression (72.5%), poor local control of high HIF-1α expression levels (42.7%) was observed in patients with EC receiving concurrent chemoradiotherapy. The low HIF-1α expression group had a significantly higher 5-year recurrence-free survival (39.8%) than the high HIF-1α expression group (18.2%) [33]. Additionally, the glycolysis of EC in hypoxic conditions may be related to PI3K/AKT and HIF-1α, whereas wortmannin decreased lactic acid and glycolytic enzyme levels (LDHA, hexokinase II, and glucose transporter-1) by inhibiting the PI3K/AKT pathway [34]. The upregulation of G077640, an

uncharacterized hypoxia-responsive lncRNA, promotes ESCC proliferation and migration involved in tumorigenesis by interacting with histone H2AX and HIF-1α, which altered hypoxia-related glycolysis, including PDK1, HK2, and GLUT4, but G077640 knockdown attenuates ESCC progression [35]. The C–X–C motif chemokine receptor 4 (CXCR4) antagonist (MSX-122) or CXCR4 knockdown reverses the induction of ESCC migration and invasion by HIF-1α [36]. Furthermore, compared with the absent treatment of berberine, the treatment with berberine significantly increases radiosensitivity in ESCC by blocking VEGF and HIF-1α, which can be clinically applied to radiotherapy resistance [37]. Meanwhile, to observe the tumor microenvironment of EC, non-invasive molecular imaging techniques via ^{18}F-HX4 or positron-emission tomography with 2-nitroimidazole derivatives have been used, and some factors for EC, named local control, complete response, disease-free survival, and OS, were evaluated using a hypoxia-associated marker called carbonic anhydrase IX [38]. Thus, the metabolic modulation of EC by targeting HIF-1α can be elucidated, and the identification of targeting HIF-1α compounds in attenuating EC through cellular models, animal models, and clinical trials can be practicably performed. Furthermore, the compounds, by targeting HIF-1α combined with surgical intervention, chemotherapy, radiation therapy, chemoradiation therapy, targeted therapy, and immunotherapy in patients with EC, can effectively reduce therapy resistance and are worth exploring.

3. Metabolic Interaction Between Mutant *TP53* and Oncotargets as a Driver of EC Progression

The mutant *TP53* gene initiates the dysfunction of the tumor suppressor protein p53 in carcinogenesis, metastasis, progression, and therapy resistance in patients with EC [39]. Under the glycolytic metabolism of EAC, missense mutations are the most common type, and the *TP53* mutation frequency is 87% based on the cBioPortal database, greatly affecting the tumor microenvironment and immune response through metabolic reprogramming [40]. p53 modulates cancer metabolism via the liver kinase B1 (LKB1) and AMPK pathways [41], and reduced expression of LKB1 in EAC enhances tumor metastasis and the tumor stage and decreases OS in patients with EAC [42]. However, cross-linking between mutant *TP53* and the aforementioned oncotargets in EC progression has rarely been investigated. Interactions between mutant *TP53* and the aforementioned oncotargets are summarized in Table 2 as follows. First, the *TP53* mutation (R175H mutant p53) enhances proliferation, migration, and invasion in ESCC linked to overexpressed WNT10A and increases the self-renewal capability of CSCs by higher $CD44^+/CD24^-$ population induction [43]. Second, the *TP53* mutation in the patients with EAC downregulates the retinoic acid metabolic process, and adapalene inhibits EAC cell lines through activating RARβ and RARγ [44], indicating the beneficial roles of RARβ and RARγ against esophageal carcinogenesis (Table 1). Third, metabolic reprogramming involved in glycolysis related to ESCC proliferation, invasion, and migration is associated with esophageal *TP53* mutation, accompanied by posttranslational modifications of PFKFB3. Moreover, the enhancement of ESCC proliferation is mediated by the interaction between lncRNA Actin Gamma 1 Pseudogene (*AGPG*) and PFKFB3 against proteasomal degradation [45]. These molecular mechanisms can be applied to develop specific drugs for ESCC patients by targeting the p53-*AGPG*-PFKFB3 axis. Fourth, the overexpression of *TP53*-induced glycolysis and apoptosis regulator (TIGAR) is associated with the progression and therapy resistance of ESCC owing to reduced intracellular lactate levels and metabolic reprogramming from glycolysis to glutamine metabolism [46]. Moreover, the expression of TIGAR and MUC1 transmembrane C-terminal subunit (MUC1-C) in ESCC cells is positively correlated with tumor growth, which is attenuated by targeting MUC1-C and inhibiting the AKT-mTOR-S6K1 pathway [47]. Lastly, the higher HIF-1α expressions under hypoxic regions are positively

correlated with higher p53 expressions both in the patients with ESCC and EAC compared to those under normoxic regions [48], which are associated with upregulated TIGAR by HIF-1α in metabolic changes of the tumor microenvironment and therapy sensitivity [49]. Based on the above illustration, pharmacological intervention of mutant *TP53* and its oncotargets may be practical and effective in attenuating EC progression and improving therapy resistance.

Table 2. The interaction of mutant *TP53* with oncotargets in esophageal cancer.

EC Type	Oncotargets	Main Outcomes	References
ESCC	CSCs	WNT10A was overexpressed in invasive mutant *TP53* cells, and CD44 induction increased self-renewal capability of CSCs	Long et al., 2015 [43]
EAC	RARs	The retinoic acid metabolic process was downregulated in patients with esophageal *TP53* mutation, and the RARβ and RARγ agonist had beneficial effect against EAC cell lines	Zhang et al., 2022 [44]
ESCC	PFK	Esophageal *TP53* mutation induced the activation of glycolysis and the enhancement of cell cycle progression through the upregulation of AGPG and PFKFB3 accumulation	Liu et al., 2020 [45]
ESCC	LDH	The overexpressed TIGAR decreased intracellular lactate levels through the reprogramming of glycolysis to glutamine metabolism for esophageal cancer progression and therapy resistance	Chu et al., 2020 [46]
ESCC and EAC	HIF-1α	HIF-1α upregulated p53 expressions in hypoxic regions compared to normoxic regions	Igbo et al., 2022 [48]

AGPG: Actin Gamma 1 Pseudogene; PFKFB3: 6-phosphofructo-2-kinase/fructose-2,6-bisphosphatase isoform 3; TIGAR: TP53-induced glycolysis and apoptosis regulator.

4. Metabolic Attenuation of Therapy Resistance in EC via Oncotarget Compounds and the Mutant *TP53* Modulator

Mutant *TP53* can be restored by targeting Cys124 and Cys277 with methylene quinuclidinone converted from APR-246 [50], and eprenetapopt (APR-246) inhibits esophageal cellular proliferation and xenograft tumor growth by inducing ferroptosis, inhibiting NFS1 cysteine desulfurase, and synergizing with dietary serine and glycine restriction [51]. APR-246 has significant antitumor activity and effectively improves chemosensitivity to cisplatin and 5-fluorouracil (5-FU) in preclinical EAC cell lines, cell line xenograft (CLX), and patient-derived xenograft (PDX) models via p53 modification [52]. Moreover, APR-246 induces apoptosis in ESCC cell lines, CLX, and PDX models with a p53 missense mutation through ROS induction and upregulated p73-Noxa signaling, which is enhanced by the combination of 5-FU [53]. In clinical trials, the pharmacotherapeutic sensitivity of APR-246 in patients with EC with the *TP53* mutation was determined by modulating the expressions of solute carrier family 7 member 11 [54]. Thus, the beneficial effects of APR-246 by targeting mutant *TP53* on both preclinical models and clinical trials exhibit therapeutic potential in combating EC and therapy resistance (Table 3). The direct or indirect metabolic regulation

and clinical pharmacotherapy in EC by targeting mutant *TP53* and oncotargets should be further verified (Figure 1).

Table 3. The amelioration of esophageal cancer by restoring *TP53* mutation with APR-246.

EC Type Models	Main Findings	References
EAC cell lines and Xenograft mice models	APR-246 inhibited esophageal cancer by inducing ferroptosis, inhibiting NFS1 cysteine desulfurase, and synergizing with dietary serine and glycine restriction	Fujihara et al., 2022 [51]
EAC cell lines, CLX and PDX models	APR-246 inhibited EAC cell survival, induced apoptosis and enhanced chemosensitivity to a cisplatin/5-FU-resistant xenograft model	Liu et al., 2015 [52]
ESCC cell lines, CLX and PDX models	APR-246 induced apoptosis in ESCC with p53 mutation through ROS induction and p73-Noxa signaling, which was enhanced by the combination of 5-FU	Kobayashi et al., 2021 [53]
EC patients	The sensitivity of APR-246 to EC with *TP53* mutation can be determined by the modulation of SLC7A11 expressions	Fujihara et al., 2021 [54]

5-FU: 5-fluorouracil; CLX: cell line xenograft; PDX: patient-derived xenograft; ROS: reactive oxygen species; SLC7A11: solute carrier family 7 member 11.

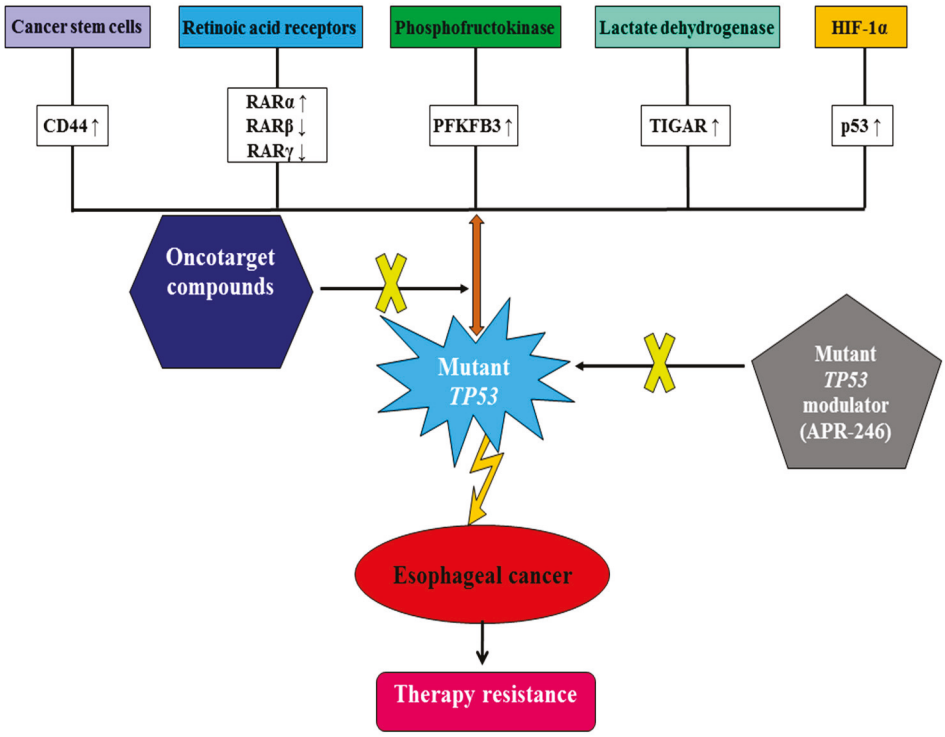

Figure 1. The metabolic attenuation of therapy resistance in esophageal cancer via oncotarget compounds and the mutant *TP53* modulator (APR-246).

5. Conclusions

Collectively, the multiple integration of CSCs, RARs, PFK, LDH, and HIF-1α with mutant *TP53* provides a promising direction for the precise application of pharmacotherapy, including chemotherapy, gene therapy, chemoradiation therapy, targeted therapy,

and immune therapy in the metabolic modulation of therapy resistance due to EC. Most importantly, the algorithmic integration of EC clinical features, biomedical data, genomics, transcriptomics, proteomics, biobank, and clinical trials to develop artificial intelligence models can accelerate the identification of oncotarget compounds and mutant *TP53* modulators as therapeutic drugs to treat EC and improve therapy resistance in the future.

Author Contributions: Conceptualization, H.-H.C.; investigation, P.-I.L.; supervision, I.-H.C.; writing-original draft preparation, H.-H.C.; writing—review & editing, Y.-C.L. and H.-H.C. All authors have read and agreed to the published version of the manuscript.

Funding: Article processing charges were provided in part by Kaohsiung Veterans General Hospital (KSVGH-114-126).

Institutional Review Board Statement: Not applicable.

Informed Consent Statement: Not applicable.

Data Availability Statement: No new data were analyzed or created in this study, and data sharing was not applicable to this article.

Acknowledgments: Many thanks for Benjamin Fairfax's professional and sincere suggestions in the present manuscript.

Conflicts of Interest: The authors declare no conflicts of interest.

References

1. Santucci, C.; Mignozzi, S.; Malvezzi, M.; Collatuzzo, G.; Levi, F.; La Vecchia, C.; Negri, E. Global trends in esophageal cancer mortality with predictions to 2025, and in incidence by histotype. *Cancer Epidemiol.* **2023**, *87*, 102486. [CrossRef] [PubMed]
2. Liu, K.; Zhao, T.; Wang, J.; Chen, Y.; Zhang, R.; Lan, X.; Que, J. Etiology, cancer stem cells and potential diagnostic biomarkers for esophageal cancer. *Cancer Lett.* **2019**, *458*, 21–28. [CrossRef] [PubMed]
3. Fang, P.; Zhou, J.; Liang, Z.; Yang, Y.; Luan, S.; Xiao, X.; Li, X.; Zhang, H.; Shang, Q.; Zeng, X.; et al. Immunotherapy resistance in esophageal cancer: Possible mechanisms and clinical implications. *Front. Immunol.* **2022**, *13*, 975986. [CrossRef] [PubMed]
4. Lee, Y.-C.; Lin, C.-H.; Chang, W.-L.; Lin, W.-D.; Pan, J.-K.; Wang, W.-J.; Su, B.-C.; Chung, H.-H.; Tsai, C.-H.; Lin, F.-C.; et al. Concurrent Chemoradiotherapy-Driven Cell Plasticity by miR-200 Family Implicates the Therapeutic Response of Esophageal Squamous Cell Carcinoma. *Int. J. Mol. Sci.* **2022**, *23*, 4367. [CrossRef]
5. Sun, G.; Yang, Y.; Liu, J.; Gao, Z.; Xu, T.; Chai, J.; Xu, J.; Fan, Z.; Xiao, T.; Jia, Q.; et al. Cancer stem cells in esophageal squamous cell carcinoma. *Pathol. Res. Pract.* **2022**, *237*, 154043. [CrossRef]
6. Zhou, C.; Fan, N.; Liu, F.; Fang, N.; Plum, P.S.; Thieme, R.; Gockel, I.; Gromnitza, S.; Hillmer, A.M.; Chon, S.-H.; et al. Linking Cancer Stem Cell Plasticity to Therapeutic Resistance-Mechanism and Novel Therapeutic Strategies in Esophageal Cancer. *Cells* **2020**, *9*, 1481. [CrossRef]
7. Das, P.K.; Islam, F.; Smith, R.A.; Lam, A.K. Therapeutic Strategies Against Cancer Stem Cells in Esophageal Carcinomas. *Front. Oncol.* **2021**, *10*, 598957. [CrossRef]
8. Jing, H.; He, X.; Zheng, J. Exosomes and regenerative medicine: State of the art and perspectives. *Transl. Res.* **2018**, *196*, 1–16. [CrossRef]
9. Koterazawa, Y.; Koyanagi-Aoi, M.; Uehara, K.; Kakeji, Y.; Aoi, T. Retinoic acid receptor γ activation promotes differentiation of human induced pluripotent stem cells into esophageal epithelium. *J. Gastroenterol.* **2020**, *55*, 763–774. [CrossRef]
10. Lu, T.-Y.; Li, W.-C.; Chen, R.-Y.; Fan, Q.-X.; Wang, L.-X.; Wang, R.-L.; Lu, S.-X.; Meng, H. Inhibition effects of all trans-retinoic acid on the growth and angiogenesis of esophageal squamous cell carcinoma in nude mice. *Chin. Med. J.* **2011**, *124*, 2708–2714.
11. Najafzadeh, N.; Mazani, M.; Abbasi, A.; Farassati, F.; Amani, M. Low-dose all-trans retinoic acid enhances cytotoxicity of cisplatin and 5-fluorouracil on CD44(+) cancer stem cells. *Biomed. Pharmacother.* **2015**, *74*, 243–251. [CrossRef] [PubMed]
12. Mao, X.-M.; Li, H.; Zhang, X.-Y.; Zhou, P.; Fu, Q.-R.; Chen, Q.-E.; Shen, J.-X.; Liu, Y.; Chen, Q.-X.; Shen, D.-Y. Retinoic Acid Receptor α Knockdown Suppresses the Tumorigenicity of Esophageal Carcinoma via Wnt/β-catenin Pathway. *Dig. Dis. Sci.* **2018**, *63*, 3348–3358. [CrossRef] [PubMed]
13. Li, M.; Song, S.; Lippman, S.M.; Zhang, X.-K.; Liu, X.; Lotan, R.; Xu, X.-C. Induction of retinoic acid receptor-beta suppresses cyclooxygenase-2 expression in esophageal cancer cells. *Oncogene* **2002**, *21*, 411–418. [CrossRef]
14. Wang, Y.; Fang, M.Z.; Liao, J.; Yang, G.-Y.; Nie, Y.; Song, Y.; So, C.; Xu, X.; Wang, L.-D.; Yang, C.S. Hypermethylation-associated inactivation of retinoic acid receptor beta in human esophageal squamous cell carcinoma. *Clin. Cancer Res.* **2003**, *9*, 5257–5263.

15. Kumar, A.; Kaur, J.; Chattopadhyay, T.K.; Mathur, M.; Ralhan, R. Differential expression of retinoic acid receptors in normal and malignant esophageal tissues. *J. Exp. Ther. Oncol.* **2004**, *4*, 1–8.
16. Bergheim, I.; Wolfgarten, E.; Bollschweiler, E.; Hölscher, A.H.; Bode, C.H.; Parlesak, A. Role of retinoic acid receptors in squamous-cell carcinoma in human esophagus. *J. Carcinog.* **2005**, *4*, 20. [CrossRef]
17. Doupé, D.P.; Alcolea, M.P.; Roshan, A.; Zhang, G.; Klein, A.M.; Simons, B.D.; Jones, P.H. A single progenitor population switches behavior to maintain and repair esophageal epithelium. *Science* **2012**, *337*, 1091–1093. [CrossRef]
18. Chiu, Y.-J.; Chung, H.-H.; Yeh, C.-H.; Cheng, J.-T.; Lo, S.-H. Improvement of insulin resistance by Chlorella in fructose-rich chow-fed rats. *Phytother. Res.* **2011**, *25*, 1306–1312. [CrossRef]
19. Ko, W.-C.; Liu, I.-M.; Chung, H.-H.; Cheng, J.-T. Activation of I(2)-imidazoline receptors may ameliorate insulin resistance in fructose-rich chow-fed rats. *Neurosci. Lett.* **2008**, *448*, 90–93. [CrossRef]
20. Huang, D.-W.; Chang, W.-C.; Wu, J.S.; Shih, R.-W.; Shen, S.-C. Gallic acid ameliorates hyperglycemia and improves hepatic carbohydrate metabolism in rats fed a high-fructose diet. *Nutr. Res.* **2016**, *36*, 150–160. [CrossRef]
21. Al Hasawi, N.; Alkandari, M.F.; Luqmani, Y.A. Phosphofructokinase: A mediator of glycolytic flux in cancer progression. *Crit. Rev. Oncol. Hematol.* **2014**, *92*, 312–321. [CrossRef] [PubMed]
22. Zheng, C.; Yu, X.; Liang, Y.; Zhu, Y.; He, Y.; Liao, L.; Wang, D.; Yang, Y.; Yin, X.; Li, A.; et al. Targeting PFKL with penfluridol inhibits glycolysis and suppresses esophageal cancer tumorigenesis in an AMPK/FOXO3a/BIM-dependent manner. *Acta Pharm. Sin. B* **2022**, *12*, 1271–1287. [CrossRef] [PubMed]
23. Yan, S.; Li, Q.; Li, S.; Ai, Z.; Yuan, D. The role of PFKFB3 in maintaining colorectal cancer cell proliferation and stemness. *Mol. Biol. Rep.* **2022**, *49*, 9877–9891. [CrossRef] [PubMed]
24. Bao, J.; Wu, Y.; Wang, L.; Zhu, Y. The role of 6-phosphofructo-2-kinase/fructose-2,6-bisphosphatase-3 in esophageal squamous cell carcinoma. *Medicine* **2020**, *99*, e19626. [CrossRef] [PubMed]
25. Twarock, S.; Reichert, C.; Peters, U.; Gorski, D.J.; Röck, K.; Fischer, J.W. Hyperglycaemia and aberrated insulin signalling stimulate tumour progression via induction of the extracellular matrix component hyaluronan. *Int. J. Cancer* **2017**, *141*, 791–804. [CrossRef]
26. Yao, F.; Zhao, T.; Zhong, C.; Zhu, J.; Zhao, H. LDHA is necessary for the tumorigenicity of esophageal squamous cell carcinoma. *Tumour Biol.* **2013**, *34*, 25–31. [CrossRef]
27. Sharma, D.; Singh, M.; Rani, R. Role of LDH in tumor glycolysis: Regulation of LDHA by small molecules for cancer therapeutics. *Semin. Cancer Biol.* **2022**, *87*, 184–195. [CrossRef]
28. Liu, C.; Han, J.; Han, D.; Huang, W.; Li, B. A new risk score model based on lactate dehydrogenase for predicting prognosis in esophageal squamous cell carcinoma treated with chemoradiotherapy. *J. Thorac. Dis.* **2023**, *15*, 2116–2128. [CrossRef]
29. Wang, X.; Zhang, B.; Chen, X.; Mo, H.; Wu, D.; Lan, B.; Li, Q.; Xu, B.; Huang, J. Lactate dehydrogenase and baseline markers associated with clinical outcomes of advanced esophageal squamous cell carcinoma patients treated with camrelizumab (SHR-1210), a novel anti-PD-1 antibody. *Thorac. Cancer* **2019**, *10*, 1395–1401. [CrossRef]
30. Ke, Q.; Costa, M. Hypoxia-inducible factor-1 (HIF-1). *Mol. Pharmacol.* **2006**, *70*, 1469–1480. [CrossRef]
31. Yu, M.; Chen, S.; Hong, W.; Gu, Y.; Huang, B.; Lin, Y.; Zhou, Y.; Jin, H.; Deng, Y.; Tu, L.; et al. Prognostic role of glycolysis for cancer outcome: Evidence from 86 studies. *J. Cancer Res. Clin. Oncol.* **2019**, *145*, 967–999. [CrossRef] [PubMed]
32. Jing, S.W.; Wang, J.; Xu, Q. Expression of hypoxia inducible factor 1 alpha and its clinical significance in esophageal carcinoma: A meta-analysis. *Tumour Biol.* **2017**, *39*, 1010428317717983. [CrossRef] [PubMed]
33. Ogawa, K.; Chiba, I.; Morioka, T.; Shimoji, H.; Tamaki, W.; Takamatsu, R.; Nishimaki, T.; Yoshimi, N.; Murayama, S. Clinical significance of HIF-1alpha expression in patients with esophageal cancer treated with concurrent chemoradiotherapy. *Anticancer Res.* **2011**, *31*, 2351–2359. [PubMed]
34. Zeng, L.; Zhou, H.-Y.; Tang, N.-N.; Zhang, W.-F.; He, G.-J.; Hao, B.; Feng, Y.-D.; Zhu, H. Wortmannin influences hypoxia-inducible factor-1 alpha expression and glycolysis in esophageal carcinoma cells. *World J. Gastroenterol.* **2016**, *22*, 4868–4880. [CrossRef]
35. Huang, X.; Liu, C.; Li, H.; Dai, T.; Luo, G.; Zhang, C.; Li, T.; Lü, M. Hypoxia-responsive lncRNA G077640 promotes ESCC tumorigenesis via the H2AX-HIF1α-glycolysis axis. *Carcinogenesis* **2023**, *44*, 383–393. [CrossRef]
36. Wu, X.; Zhang, H.; Sui, Z.; Gao, Y.; Gong, L.; Chen, C.; Ma, Z.; Tang, P.; Yu, Z. CXCR4 promotes the growth and metastasis of esophageal squamous cell carcinoma as a critical downstream mediator of HIF-1α. *Cancer Sci.* **2022**, *113*, 926–939. [CrossRef]
37. Yang, X.; Yang, B.; Cai, J.; Zhang, C.; Zhang, Q.; Xu, L.; Qin, Q.; Zhu, H.; Ma, J.; Tao, G.; et al. Berberine enhances radiosensitivity of esophageal squamous cancer by targeting HIF-1α in vitro and in vivo. *Cancer Biol. Ther.* **2013**, *14*, 1068–1073. [CrossRef]
38. Peerlings, J.; Van De Voorde, L.; Mitea, C.; Larue, R.; Yaromina, A.; Sandeleanu, S.; Spiegelberg, L.; Dubois, L.; Lambin, P.; Mottaghy, F.M. Hypoxia and hypoxia response-associated molecular markers in esophageal cancer: A systematic review. *Methods* **2017**, *130*, 51–62. [CrossRef]
39. Zhong, L.; Li, H.; Chang, W.; Ao, Y.; Wen, Z.; Chen, Y. TP53 Mutations in Esophageal Squamous Cell Carcinoma. *Front. Biosci. Landmark Ed.* **2023**, *28*, 219. [CrossRef]
40. Zhu, L.; Yang, F.; Li, X.; Li, Q.; Zhong, C. Glycolysis Changes the Microenvironment and Therapeutic Response Under the Driver of Gene Mutation in Esophageal Adenocarcinoma. *Front. Genet.* **2021**, *12*, 743133. [CrossRef]

41. Gomes, A.S.; Ramos, H.; Soares, J.; Saraiva, L. p53 and glucose metabolism: An orchestra to be directed in cancer therapy. *Pharmacol. Res.* **2018**, *131*, 75–86. [CrossRef] [PubMed]
42. Whitsett, T.G.; Mittal, S.K.; Eschbacher, J.M.; Carson, V.M.; Smith, M.A.; Bremner, R.M.; Inge, L.J. LKB1 inactivation occurs in a subset of esophageal adenocarcinomas and is sufficient to drive tumor cell proliferation. *J. Thorac. Cardiovasc. Surg.* **2018**, *155*, 1891–1899. [CrossRef] [PubMed]
43. Long, A.; Giroux, V.; Whelan, K.A.; Hamilton, K.E.; Tétreault, M.-P.; Tanaka, K.; Lee, J.-S.; Klein-Szanto, A.J.; Nakagawa, H.; Rustgi, A.K. WNT10A promotes an invasive and self-renewing phenotype in esophageal squamous cell carcinoma. *Carcinogenesis* **2015**, *36*, 598–606. [CrossRef]
44. Zhang, Y.; Weh, K.M.; Howard, C.L.; Riethoven, J.-J.; Clarke, J.L.; Lagisetty, K.H.; Lin, J.; Reddy, R.M.; Chang, A.C.; Beer, D.G.; et al. Characterizing isoform switching events in esophageal adenocarcinoma. *Mol. Ther. Nucleic Acids* **2022**, *29*, 749–768. [CrossRef] [PubMed]
45. Liu, J.; Liu, Z.-X.; Wu, Q.-N.; Lu, Y.-X.; Wong, C.-W.; Miao, L.; Wang, Y.; Wang, Z.; Jin, Y.; He, M.-M.; et al. Long noncoding RNA AGPG regulates PFKFB3-mediated tumor glycolytic reprogramming. *Nat. Commun.* **2020**, *11*, 1507. [CrossRef]
46. Chu, J.; Niu, X.; Chang, J.; Shao, M.; Peng, L.; Xi, Y.; Lin, A.; Wang, C.; Cui, Q.; Luo, Y.; et al. Metabolic remodeling by TIGAR overexpression is a therapeutic target in esophageal squamous-cell carcinoma. *Theranostics* **2020**, *10*, 3488–3502. [CrossRef]
47. GongSun, X.; Zhao, Y.; Jiang, B.; Xin, Z.; Shi, M.; Song, L.; Qin, Q.; Wang, Q.; Liu, X. Inhibition of MUC1-C regulates metabolism by AKT pathway in esophageal squamous cell carcinoma. *J. Cell. Physiol.* **2019**, *234*, 12019–12028. [CrossRef]
48. Igbo, B.T.; Linge, A.; Frosch, S.; Suckert, T.; Stolz-Kieslich, L.; Löck, S.; Kumaravadivel, M.S.; Welsch, T.; Weitz, J.; Sommer, U.; et al. Immunohistochemical analyses of paraffin-embedded sections after primary surgery or trimodality treatment in esophageal carcinoma. *Clin. Transl. Radiat. Oncol.* **2022**, *36*, 106–112. [CrossRef]
49. Maurer, G.D.; Heller, S.; Wanka, C.; Rieger, J.; Steinbach, J.P. Knockdown of the TP53-Induced Glycolysis and Apoptosis Regulator (TIGAR) Sensitizes Glioma Cells to Hypoxia, Irradiation and Temozolomide. *Int. J. Mol. Sci.* **2019**, *20*, 1061. [CrossRef]
50. Zhang, Q.; Bykov, V.J.N.; Wiman, K.G.; Zawacka-Pankau, J. APR-246 reactivates mutant p53 by targeting cysteines 124 and 277. *Cell Death Dis.* **2018**, *9*, 439. [CrossRef]
51. Fujihara, K.M.; Zhang, B.Z.; Jackson, T.D.; Ogunkola, M.O.; Nijagal, B.; Milne, J.V.; Sallman, D.A.; Ang, C.-S.; Nikolic, I.; Kearney, C.J.; et al. Eprenetapopt triggers ferroptosis, inhibits NFS1 cysteine desulfurase, and synergizes with serine and glycine dietary restriction. *Sci. Adv.* **2022**, *8*, eabm9427. [CrossRef] [PubMed]
52. Liu, D.S.; Read, M.; Cullinane, C.; Azar, W.J.; Fennell, C.M.; Montgomery, K.G.; Haupt, S.; Haupt, Y.; Wiman, K.G.; Duong, C.P.; et al. APR-246 potently inhibits tumour growth and overcomes chemoresistance in preclinical models of oesophageal adenocarcinoma. *Gut* **2015**, *64*, 1506–1516. [CrossRef] [PubMed]
53. Kobayashi, T.; Makino, T.; Yamashita, K.; Saito, T.; Tanaka, K.; Takahashi, T.; Kurokawa, Y.; Yamasaki, M.; Nakajima, K.; Morii, E.; et al. APR-246 induces apoptosis and enhances chemo-sensitivity via activation of ROS and TAp73-Noxa signal in oesophageal squamous cell cancer with TP53 missense mutation. *Br. J. Cancer* **2021**, *125*, 1523–1532. [CrossRef] [PubMed]
54. Fujihara, K.M.; Corrales Benitez, M.; Cabalag, C.S.; Zhang, B.Z.; Ko, H.S.; Liu, D.S.; Simpson, K.J.; Haupt, Y.; Lipton, L.; Haupt, S.; et al. SLC7A11 Is a Superior Determinant of APR-246 (Eprenetapopt) Response than TP53 Mutation Status. *Mol. Cancer Ther.* **2021**, *20*, 1858–1867. [CrossRef]

Disclaimer/Publisher's Note: The statements, opinions and data contained in all publications are solely those of the individual author(s) and contributor(s) and not of MDPI and/or the editor(s). MDPI and/or the editor(s) disclaim responsibility for any injury to people or property resulting from any ideas, methods, instructions or products referred to in the content.

biomedicines

MDPI

Systematic Review

Chemoimmunotherapy in Advanced Biliary Tract Cancers: A Meta-Analysis of Clinical Outcomes

Alireza Tojjari [1], Sepideh Razi [2], Osama M. Younis [3], Ramez M. Odat [4], Ibrahim Halil Sahin [1,5] and Anwaar Saeed [1,5,*]

[1] Department of Medicine, Division of Hematology & Oncology, University of Pittsburgh Medical Center (UPMC), Pittsburgh, PA 15213, USA; alirezatojjari@gmail.com (A.T.)
[2] Research Center for Immunodeficiencies, Children's Medical Center, Tehran University of Medical Sciences, Tehran 1416753955, Iran
[3] School of Medicine, The University of Jordan, Amman 11942, Jordan
[4] Faculty of Medicine, Jordan University of Science and Technology, Irbid 22110, Jordan
[5] UPMC Hillman Cancer Center, 5150 Centre Avenue, Pittsburgh, PA 15213, USA
* Correspondence: saeeda3@upmc.edu

Abstract

Background/Objectives: Biliary tract cancers (BTCs), encompassing tumors of the bile ducts, gallbladder, or ampulla of Vater, are notoriously hard to manage, especially when surgery is off the table and standard chemotherapy provides only modest benefits. While emerging treatments such as immune checkpoint inhibitors have shown promise, mixed clinical trial results and varied study endpoints have left their true impact unclear. This concise review consolidates current evidence on combining chemotherapy with immunotherapy to clarify whether these regimens can significantly improve outcomes and steer more effective treatment strategies for BTCs. **Methods:** A comprehensive literature search was conducted across PubMed, Embase, Web of Science, and ClinicalTrials.gov for randomized controlled trials (RCTs) and prospective comparative studies published from January 2010 to December 2024. Fixed-effect meta-analyses (inverse-variance method) were used as the primary approach, with random-effects models (REML) performed as sensitivity analyses to confirm robustness were performed to calculate pooled hazard ratios (HRs) for overall survival (OS) and progression-free survival (PFS). Leave-one-out sensitivity analyses and Egger's tests assessed result stability and publication bias. The review was conducted in accordance with PRISMA 2020 guidelines and registered in OSF. **Results:** Two RCTs (n = 1754; chemoimmunotherapy n = 874, chemotherapy n = 880) were included in the quantitative meta-analysis. Compared to chemotherapy alone, chemoimmunotherapy significantly reduced the risk of death by 20% (OS, HR = 0.80; 95% CI 0.72–0.89; I^2 = 0%) and the risk of disease progression or death by 19% (PFS, HR = 0.81; 95% CI 0.73–0.90; I^2 = 33.5%). Leave-one-out sensitivity analyses confirmed result stability. Egger's tests showed no significant publication bias (OS p = 0.30; PFS p = 0.40). Two additional studies (IMbrave 151 and Monge 2022) lacking comparative survival data were qualitatively assessed. **Conclusions**: Chemoimmunotherapy significantly improves OS and PFS compared with chemotherapy alone in advanced BTC, with consistent findings across included trials. These results support the incorporation of chemoimmunotherapy as a first-line therapeutic strategy. Future research should prioritize biomarker-driven patient selection, evaluation of long-term clinical outcomes, and integration of targeted therapies with chemoimmunotherapy.

Keywords: biliary tract cancer; chemoimmunotherapy; immune checkpoint inhibitors; meta-analysis; chemotherapy; immunotherapy

1. Introduction

Biliary tract cancers (BTCs) include malignancies that arise from the intrahepatic and extrahepatic bile ducts, the gallbladder, and the ampulla of Vater. They are usually diagnosed at advanced stages when curative interventions are no longer possible [1]. Due to their aggressive biology and late presentation, BTCs are rarely eligible for surgical resection and have traditionally been managed with systemic chemotherapy. However, gemcitabine–cisplatin regimens, the longstanding standard, offer only modest survival benefits, underscoring the urgent need for more effective approaches [2–4]. Key late-phase trials include KEYNOTE-966 [5], TOPAZ-1 [6], and the phase II durvalumab ± tremelimumab study [7] evaluating gemcitabine–cisplatin plus checkpoint inhibitors.

In recent years, immune checkpoint inhibitors have spurred a paradigm shift in oncology, prompting their investigation in BTCs. Preclinical data support synergy between chemotherapy and programmed cell death protein 1 (PD-1)/programmed death-ligand 1 (PD-L1) blockade through enhanced antigen presentation and immune cell infiltration, laying the groundwork for clinical exploration [8,9].

This rapid evolution in treatment modalities marks a significant shift toward personalized medicine in managing BTCs, enabling clinicians to tailor regimens based on tumor biology and patient characteristics. Despite promising mechanistic insights, heterogeneous outcomes across early-phase and pivotal trials underscore the need for a comprehensive evaluation of chemoimmunotherapy strategies. This meta-analysis systematically synthesizes data from randomized controlled trials (RCTs) and prospective comparative studies published between 2010 and 2024 to assess the effect of adding immunotherapy to chemotherapy versus chemotherapy alone on survival outcomes in patients with advanced BTCs. Such insights are critical for informing clinical practice and shaping future research in this challenging disease.

2. Materials and Methods

2.1. Literature Search

A comprehensive literature search was conducted in PubMed, Web of Science, ClinicalTrials.gov, and the Cochrane Library for studies published between 1 January 2010, and 31 December 2024. Search strategies combined terms for "biliary tract cancer" and "chemotherapy" and "immunotherapy" (see Supplementary File S1 for detailed strings). We applied the following filters: English-language articles only, human studies, and clinical trials. No other date, age, or gender restrictions were imposed. This systematic review and meta-analysis were conducted in accordance with the Preferred Reporting Items for Systematic Reviews and Meta-Analyses (PRISMA) 2020 guidelines (Figure 1). The review protocol was registered in the Open Science Framework (OSF) under the registration DOI: https://doi.org/10.17605/OSF.IO/5KYJ7.

2.2. Inclusion and Exclusion Criteria

The inclusion criteria for this meta-analysis required RCTs or prospective comparative studies enrolling adult patients with unresectable or metastatic BTCs, including intrahepatic and extrahepatic cholangiocarcinoma, gallbladder cancer, and ampullary carcinoma. Eligible studies had to compare chemotherapy combined with immunotherapy versus chemotherapy alone. To be included, studies were required to report at least one time-to-event survival outcome, overall survival (OS) as the primary outcome, and/or progression-free survival (PFS) as a secondary endpoint.

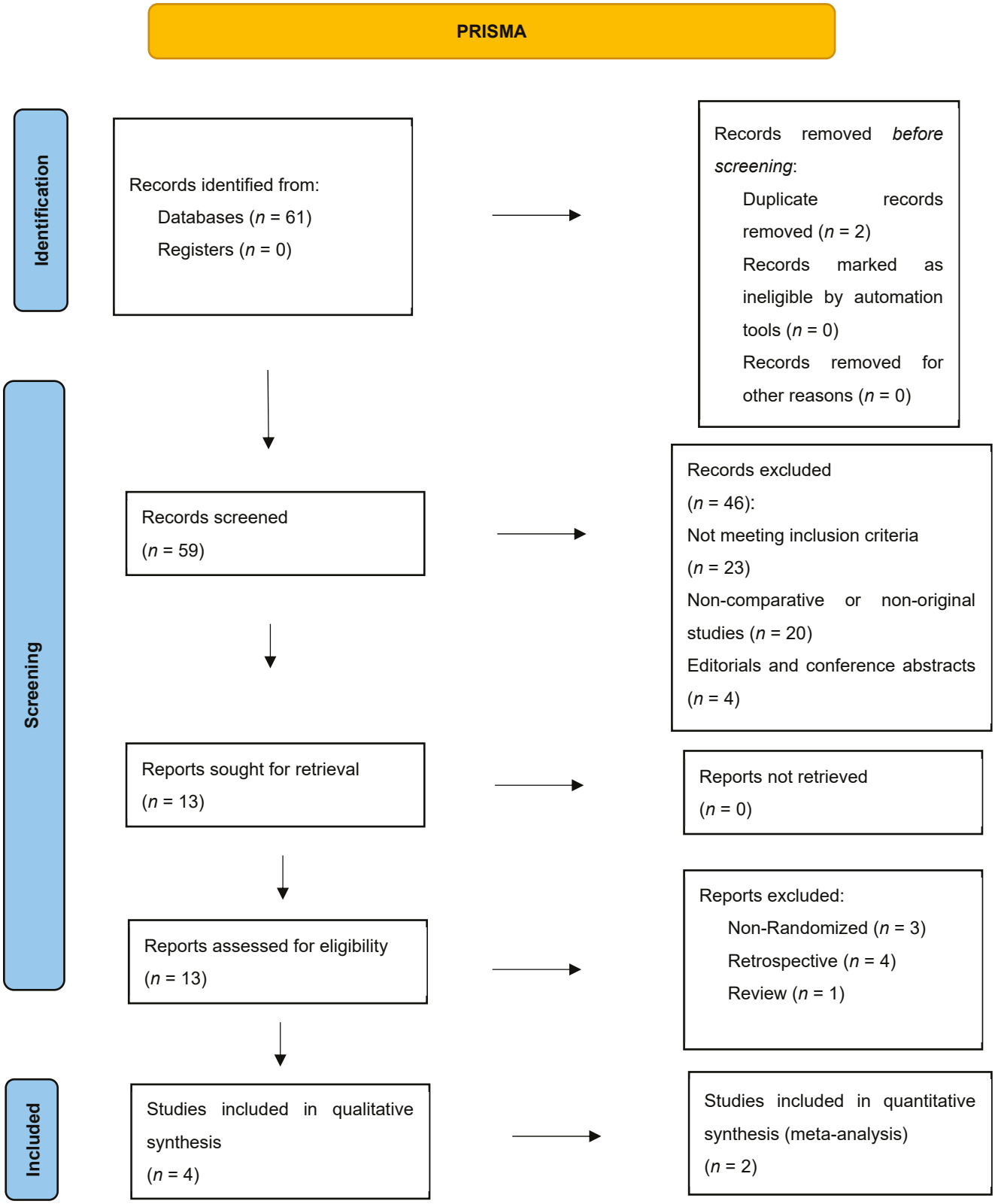

Figure 1. PRISMA flow diagram illustrating the systematic literature search and study selection process. A total of 61 records were identified through database searching; after removing 2 duplicates, 59 records were screened by title and abstract. Of these, 46 were excluded (non-original articles, abstracts, or not meeting PICO criteria), and 13 full-text articles were assessed for eligibility. Eight were excluded (non-randomized or retrospective), leaving four studies: two RCTs included in the quantitative meta-analysis and two studies (single-arm/protocol) included in the qualitative synthesis. The final qualitative and quantitative study selection is shown.

The exclusion criteria excluded papers from the meta-analysis that studied resectable BTCs, lacked a direct comparison between chemoimmunotherapy and chemotherapy alone, or did not report the primary outcome. Lastly, non-randomized trials, retrospective studies, case reports, editorials, and review articles were all excluded. For qualitative synthesis, studies not meeting the meta-analysis criteria, such as those lacking a chemotherapy-alone control arm or quantitative survival data, but providing relevant qualitative data on chemoimmunotherapy, were included.

2.3. Data Extraction and Quality Assessment

Title and abstract screening were independently conducted by two reviewers, with discrepancies resolved by a third reviewer. Full-text screening was also conducted independently by the same two reviewers. Study quality was assessed using the Cochrane Risk of Bias 2.0 (ROB-2) [10] tool and was conducted independently by two separate reviewers. The following data were extracted from each included study: study identifiers (author, year, country), patient and disease characteristics (tumor type, prior treatment, age, sex distribution, sample size), treatment arms (experimental and control regimens), response outcomes (objective response rate [ORR], complete response [CR], partial response [PR], stable disease [SD], progressive disease [PD], disease control rate [DCR]), and time-to-event outcomes (OS and PFS). For the three-arm Phase II trial by Oh et al. [7], hazard ratios (HRs) from the two experimental arms were combined using a fixed-effects variance-based method to avoid double-counting the shared control group. Certainty of evidence (e.g., using the GRADE approach) was not formally assessed due to the limited number of included randomized controlled trials.

2.4. Statistical Analysis

All analyses were performed in R (version 4.3.3) using the meta and metafor packages. For OS and PFS, pooled HRs with 95% confidence intervals (CIs) were estimated using a fixed-effect model (inverse-variance method), given the limited number of trials. Between-study heterogeneity was assessed via I^2 and Cochran's Q test (with corresponding *p*-values reported for heterogeneity only). The pooled analysis was repeated under a random-effects model using the restricted maximum-likelihood (REML) estimator to confirm the robustness of the fixed-effect results. Leave-one-out influence diagnostics and contour-enhanced funnel plots (with Egger's regression test) were conducted to assess the impact of individual studies and potential publication bias. Objective response rates, CR, PR, SD, and PD were pooled under a fixed-effect model after Freeman–Tukey double-arcsine transformation, then subjected to leave-one-out sensitivity checks and a random-effects REML model as a robustness check. Statistical significance was defined as $p < 0.05$ (two-sided). Heterogeneity was assessed separately using Cochran's Q test.

3. Results

We identified 61 records through database searches. After removing 2 duplicates, 59 titles and abstracts were screened; 46 were excluded (20 non-original studies, 4 conference abstracts, 23 not meeting PICO criteria). Thirteen full-text articles were assessed for eligibility: eight were excluded (3 non-randomized designs, 4 retrospective cohorts, and one review), leaving four studies for qualitative synthesis. Of these, two RCTs [5,6] provided complete time-to-event data and were included in the quantitative meta-analysis (Table 1).

Table 1. Baseline Demographic and Clinical Characteristics of Patients.

Study	Arm	*n*	% Male	Median Age (IQR), yrs	Disease Status (LA/M)	Site	ECOG	Virology (HBV/HCV %)	PD-L1 ≥1 (%)
KEYNOTE-966 [1] [5]	GemCis + Pembrolizumab	533	53%	64 (57–71)	60/473	Extrahepatic: 18% Gallbladder: 22% Intrahepatic: 60%	0: 48% 1: 51% ≥2: <1%	HBV: 31% HCV: 4%	68%
	GemCis	536	51%	63 (55–70)	66/470	Extrahepatic: 20% Gallbladder: 22% Intrahepatic: 58%	0: 43% 1: 57% ≥2: 0%	HBV: 31% HCV: 3%	68%
TOPAZ-1 [2] [6]	GemCis + Durvalumab	341	50%	64 (20–84)	11/89	Intrahepatic cholangiocarcinoma: 56% Extrahepatic cholangiocarcinoma: 19% Gallbladder cancer: 25%	0: 51% 1: 49%	HBV or HCV: 21%	58%
	GemCis	344	51%	64 (31–85)	17/83	Intrahepatic cholangiocarcinoma: 56% Extrahepatic cholangiocarcinoma: 19% Gallbladder cancer: 25%	0: 47% 1: 53%	HBV or HCV: 25%	60%
Oh et al. (2022) [3] [7]	GemCis followed by GemCis + Durvalumab + Tremelimumab	30	57%	64 (57–68)	-	Intrahepatic cholangiocarcinoma: 57% Gallbladder: 23% Extrahepatic cholangiocarcinoma: 7% Ampullary cancer: 13%	0: 100% 1: 0%	HBV: 10% HCV: 0%	NR
	GemCis + Durvalumab	47	40%	61 (57–71)	-	Intrahepatic cholangiocarcinoma: 67% Gallbladder: 15% Extrahepatic cholangiocarcinoma: 19% Ampullary cancer: 4%	0: 40% 1: 60%	HBV: 4% HCV: 0%	NR
	GemCis + Durvalumab + Tremelimumab	47	53%	66 (60–71)	-	Intrahepatic cholangiocarcinoma: 43% Gallbladder: 34% Extrahepatic cholangiocarcinoma: 6% Ampullary cancer: 17%	0: 49% 1: 51%	HBV: 4% HCV: 0%	NR
Monge 2022 [4] [11]	GemCis + Durvalumab (single arm)	11	64%	65 (57–72)	100/0	50/50	82	NR	NR

Abbreviations: LA, locally advanced; M, metastatic; IHC, intrahepatic. cholangiocarcinoma; EHC, extrahepatic cholangiocarcinoma; NR, not reported. [1] (KEYNOTE-966) [5]: randomized III trial, double-blind. [2] (TOPAZ-1) [6]: randomized III trial, open-label. [3] Oh et al. [7]: Phase II three-arm study; experimental arms pooled separately. IMbrave 151 [12]: Phase II study protocol only. [4] Monge [11]: Phase II single-arm study.

3.1. Baseline Demographic and Clinical Characteristics

Table 1 summarizes the baseline characteristics of 1889 patients enrolled across four clinical cohorts. In the two phase III trials, KEYNOTE-966 [5] randomized 1069 patients roughly equally between gemcitabine–cisplatin plus pembrolizumab (*n* = 533) and gemcitabine–cisplatin alone (*n* = 536); both arms were majority male (53% vs. 51%) with a median age of 64 years (IQR 57–71 vs. 55–70). Most patients (58–60%) had intrahepatic cholangiocarcinoma, with gallbladder (22%) and extrahepatic (18–20%) disease comprising the remainder. Performance status was good (ECOG 0–1 in >95%), chronic hepatitis B was present in about 31% (hepatitis C in 3–4%), and 68% had PD-L1 expression ≥ 1%. TOPAZ-1 [6] enrolled 685 patients into durvalumab plus gemcitabine–cisplatin (*n* = 341) or placebo plus gemcitabine–cisplatin (*n* = 344) arms; both arms were 50–51% male, median age 64 years, and had similar disease sites (56% intrahepatic, 19% extrahepatic, 25% gallbladder). ECOG 0–1 rates exceeded 98%, 21–25% had viral hepatitis, and PD-L1 ≥1% in 58–60%. In Oh et al.'s phase II study [7] (*n* = 124 across three experimental regimens), patients were slightly younger (median 61–66 years), 40–57% were male, predominantly

had intrahepatic disease (43–67%), they uniformly had an ECOG of 0, and there were low hepatitis rates (4–10%). Finally, Monge 2022's single-arm cohort [11] (n = 11) mirrored these demographics (64% male, median age 65, intrahepatic site in 100%, ECOG 0 in 82%). Across all studies, patients were well balanced with respect to age, sex, disease distribution, and functional status, ensuring the comparability of efficacy and safety outcomes. Notably, elderly patients aged ≥80 years were rare across all trials, limiting the available evidence for this subgroup.

3.2. Characteristics of Studies Included in the Quantitative Meta-Analysis

Table 2 outlines the two pivotal phase III, double-blind randomized trials that form the quantitative backbone of our meta-analysis. In 2023, the global KEYNOTE-966 study (5) enrolled 1069 patients with unresectable or metastatic biliary tract cancer across 175 sites, randomizing 533 patients to pembrolizumab plus gemcitabine–cisplatin and 536 patients to gemcitabine–cisplatin alone; the primary endpoint was overall survival, with a median follow-up of 25.6 months (IQR 21.7–30.4). The following year, the TOPAZ-1 trial (6) spanned 17 countries and similarly compared durvalumab plus gemcitabine–cisplatin (n = 341) against gemcitabine–cisplatin alone (n = 344) in a comparable patient population; overall survival again served as the primary endpoint, with a median follow-up of 23.4 months (IQR 20.6–25.2). Both studies offer high-quality, randomized data on first-line chemoimmunotherapy versus chemotherapy alone in advanced biliary tract carcinoma.

Table 2. Characteristics of Studies Included in the Quantitative Meta-analysis.

Author (Trial)	Year	Phase/Design	Region	Population	*n* (Exp)	*n* (Ctrl)	Regimen (Experimental vs. Control)	Primary Endpoint	Median Follow-Up (mo)
Kelley et al. (KEYNOTE-966) [5]	2023	III/RCT, double-blind	Global (175 sites)	Unresectable/metastatic BTC	533	536	Gem-Cis + Pembrolizumab vs. Gem-Cis	OS	25.6 (21.7–30.4) *
Oh et al. (TOPAZ-1) [6]	2024	III/RCT, double-blind	17 countries	Unresectable/metastatic BTC	341	344	Gem-Cis + Durvalumab vs. Gem-Cis	OS	23.4 (20.6–25.2)

Data are presented as *n* or median (interquartile range) unless otherwise specified. * Median follow-up is reported as the median (IQR). Abbreviations: RCT, randomized controlled trial; BTC, biliary tract cancer; OS, overall survival; Gem, gemcitabine; Cis, cisplatin.

3.3. Qualitative Summary of Two Single-Arm/Protocol Studies

Table 3 provides a concise overview of two non-comparative studies that were excluded from the quantitative synthesis due to their single-arm designs. Monge et al. (2022) [11] enrolled 11 patients in a phase II trial of durvalumab plus tremelimumab, reporting an objective response rate (ORR) of 18% and a six-month overall survival of approximately 54%, but, lacking a control arm, it could not inform direct comparisons. Oh et al.'s 2022 open-label phase II study [7] evaluated three experimental sequences—gemcitabine–cisplatin followed by gemcitabine–cisplatin with durvalumab and tremelimumab, gemcitabine–cisplatin plus durvalumab, and a triplet of gemcitabine–cisplatin, durvalumab, and tremelimumab in 124 patients, yielding ORRs between 50% and 73% and a median overall survival of roughly 18 months. Although these results underscore encouraging activity signals for chemo-immunotherapy combinations, their lack of a randomized control arm precluded their inclusion in the pooled meta-analysis.

Table 3. Qualitative Summary of Two Single-Arm/Protocol Studies.

Author (Trial)	Year	Phase/Design	Sample Size	Intervention Regimen	Comparator	Outcome Summary	Reason for Exclusion
Monge et al. [11]	2022	II/Single-arm	11	Durvalumab + Tremelimumab	None (no control group)	Reported ORR 18%, 6-mo OS ~54%; no comparative outcomes	No control arm; single-arm trial
Oh et al. (Phase II) [7]	2022	II/Single-arm, open-label	124	GemCis followed by GemCis + Durvalumab + Tremelimumab, GemCis + Durvalumab, GemCis + Durvalumab + Tremelimumab	-	ORR 50–73%, median OS ~18 months	Single-arm trial

This table provides a qualitative overview of studies that were excluded from the quantitative meta-analysis due to lack of comparative survival or response data. Oh et al. (2022) are single-arm studies evaluated against historical controls. Abbreviations: RCT, randomized controlled trial; ORR, objective response rate; OS, overall survival; Gem-Cis, gemcitabine plus cisplatin; NR, not reported.

3.4. Qualitative Synthesis

Two studies lacked a standalone chemotherapy-only comparator and were summarized qualitatively (Table 2):

Oh et al. [7]: Phase II single-arm (n = 45); ORR 67%, median OS ~18 mo; PFS not directly reported.

Monge [11]: single-arm (n = 11); ORR 18%, 6-mo OS 54%.

3.5. Risk of Bias Assessment

The Cochrane ROB-2 tool was applied to the two RCTs included. TOPAZ-1 trial [6] showed a low overall risk of bias; however, the KEYNOTE-966 [5] trial demonstrated some concerns specifically in the outcome measurement domain (Figure 2).

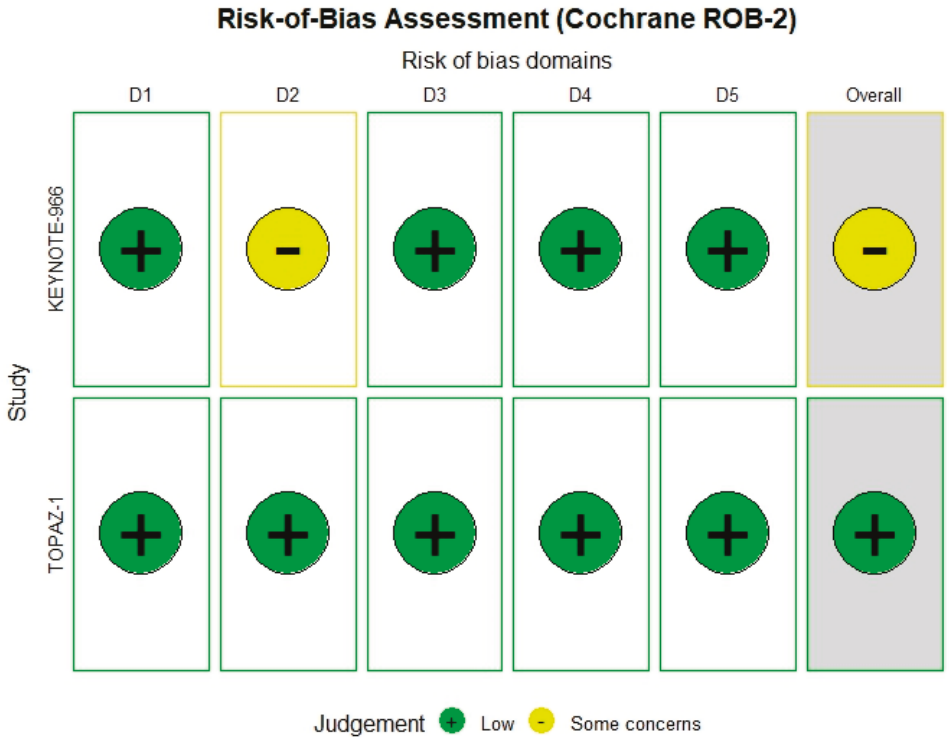

Figure 2. Risk of bias summary according to the Cochrane ROB-2 tool, indicating domain-level assessments for included randomized controlled trials (RCTs).

3.6. Overall Survival

A fixed-effects meta-analysis demonstrated a significant benefit for chemo-immunotherapy versus gemcitabine–cisplatin alone, with a pooled HR of 0.80 (95% CI 0.72–0.89; z = –4.20, $p < 0.001$) (Figure 3). Under a random-effects model using the REML estimator, the pooled HR remained 0.80 (95% CI 0.72–0.90; z = –3.81, $p < 0.001$) (Figure 3), with $\tau^2 = 0$ and $I^2 = 0\%$, confirming the robustness of the fixed-effect estimate. Between-study heterogeneity was negligible ($I^2 = 0.0\%$, $\tau^2 = 0$, $p = 0.44$). Egger's test for publication bias was non-significant ($p = 0.30$) (Figure 3).

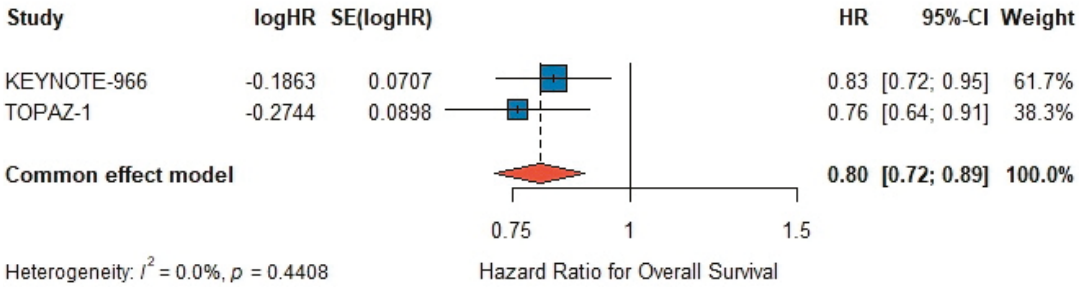

Figure 3. Forest plot for overall survival (OS). Individual hazard ratios (HR) with 95% confidence intervals (CI) for each included study (KEYNOTE-966 and TOPAZ-1) are shown as blue squares. The orange diamond represents the pooled HR calculated using a fixed-effect (common-effect) model (HR = 0.80; 95% CI 0.72–0.89). No significant heterogeneity was detected ($I^2 = 0\%$, $p = 0.44$). HR < 1 favors chemoimmunotherapy.

3.7. Subgroup Analysis (OS)

In trial using pembrolizumab, the pooled HR was 0.81 (95% CI 0.70–0.94; $I^2 = 0\%$; $p = 0.78$), while in this using durvalumab, it was 0.83 (95% CI 0.72–0.96; $I^2 = 0\%$; $p = 0.82$), indicating consistent benefit across agents.

3.8. Leave-One-Out Analysis (OS)

The leave-one-out sensitivity analysis for OS further validated the robustness of the pooled estimate. Sequential omission of each trial yielded HRs ranging from 0.76 (95% CI 0.64–0.91) to 0.83 (95% CI 0.72–0.95), consistently excluding unity, thus confirming the reliability and stability of the OS benefit.

3.9. Progression-Free Survival

The pooled fixed-effect HR for PFS was 0.81 (95% CI 0.73–0.90) (Figure 4), indicating a 19% reduction in the risk of progression or death. Under the random-effects model, heterogeneity remained moderate ($I^2 = 33.5\%$, $\tau^2 = 0.0031$, $p = 0.22$) as noted below (Figure 4).

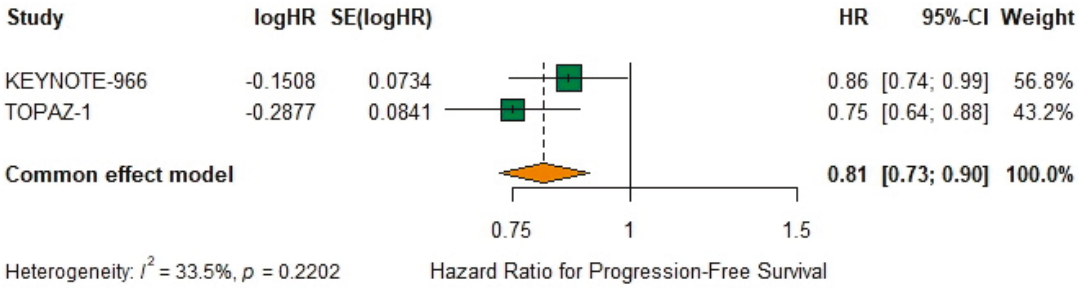

Figure 4. Forest plot for progression-free survival (PFS). Hazard ratios (HR) with 95% confidence intervals (CI) from each study (KEYNOTE-966 and TOPAZ-1) are shown as green squares. The orange diamond represents the pooled HR using a fixed-effect (common-effect) model (HR = 0.81; 95% CI 0.73–0.90). Low-to-moderate heterogeneity was observed ($I^2 = 33.5\%$, $p = 0.22$), which was not statistically significant. HR < 1 favors chemoimmunotherapy.

3.10. Sensitivity Analysis (PFS)

A random-effects meta-analysis using the REML estimator yielded a pooled log-HR of –0.2131 (SE 0.0682), corresponding to an HR of 0.81 (95% CI 0.71–0.92; z = –3.13, $p = 0.0018$). Between-study heterogeneity was moderate ($\tau^2 = 0.0031$; $I^2 = 33.5\%$; Q (1) = 1.50, $p = 0.22$), confirming the robustness of the fixed-effect estimate.

3.11. Subgroup Analysis (PFS)

Subgroup evaluation of PFS demonstrated that pembrolizumab (KEYNOTE-966) reduced the hazard of progression or death by 18% (HR 0.82, 95% CI 0.68–1.00; $I^2 = 0\%$), while durvalumab (TOPAZ-1) achieved a 21% reduction (HR 0.79, 95% CI 0.67–0.93; $I^2 = 0\%$). These concordant results attest to the efficacy of both agents in prolonging PFS.

3.12. Leave-One-Out Analysis (PFS)

The leave-one-out sensitivity analysis for PFS confirmed the robustness of the treatment effect. Omitting individual trials sequentially resulted in HR ranging from 0.75 (95% CI 0.64–0.88) to 0.86 (95% CI 0.74–0.99), with all confidence intervals remaining below 1.0. This consistency supports the stability and reliability of the observed benefit for PFS.

3.13. Objective Response Rates

The pooled analysis of objective response rates (ORR), comprising complete response (CR) and partial response (PR), demonstrated that chemoimmunotherapy significantly improved the response rate compared to chemotherapy alone. Based on the fixed-effect meta-analysis, the pooled ORR was calculated as follows:

Overall ORR: 34.8% (95% CI, 31.8–37.9%)
Pembrolizumab arm (KEYNOTE-966): ORR = 28.7% (95% CI, 25.0–32.4%)
Durvalumab arm (TOPAZ-1): ORR = 27.1% (95% CI, 22.4–31.8%)

These results indicate that chemoimmunotherapy enhances tumor shrinkage and improves clinical responses, supporting its incorporation into first-line therapy regimens.

Table 4 highlights the distribution of tumor responses across treatment arms in the two pivotal trials. In KEYNOTE-966 [5], the addition of pembrolizumab to gemcitabine–cisplatin yielded a slightly higher complete response rate (2.1% vs. 1.3%) and virtually identical partial response rates (26.6% vs. 27.2%) compared to chemotherapy alone, translating into overall response rates of 28.7% and 28.5%, respectively. Stable disease rates and progressive disease rates were also comparable between arms (46.2% vs. 47.4% for SD; 19.1% vs. 17.9% for PD), suggesting that pembrolizumab primarily shifts the balance toward deeper responses without markedly altering disease stabilization. In TOPAZ-1, the durvalumab combination demonstrated a more pronounced benefit: the overall response rate improved from 19% (CR + PR: 1% + 18%) with gemcitabine–cisplatin alone to 27.1% (2.1% + 25%) with the addition of durvalumab. This was accompanied by a reduction in progressive disease (14% vs. 15%) and a higher proportion of patients achieving stable disease (59% vs. 64%). Taken together, these findings indicate that while both immune-checkpoint inhibitors enhance response depth when added to standard chemotherapy, the magnitude of benefit appears greater with durvalumab in TOPAZ-1, particularly in boosting partial responses and maintaining disease control.

Pooled (fixed-effect) rates were:

- CR: 1.54% (95% CI 1.00–2.10)
- PR: 33.3% (95% CI 30.9–35.7)
- SD: 41.8% (95% CI 39.5–44.1)
- PD: 20.8% (95% CI 18.9–22.7)

Table 4. Individual Response Rates (CR, PR, SD, PD) by Study and Treatment Arm.

Study	Arm	*n*	CR *n* (%)	PR *n* (%)	SD *n* (%)	PD *n* (%)
KEYNOTE-966	GemCis + Pembrolizumab	533	11 (2.1)	142 (26.6)	246 (46.2)	102 (19.1)
KEYNOTE-966	GemCis	536	7 (1.3)	146 (27.2)	254 (47.4)	96 (17.9)
TOPAZ-1	GemCis + Durvalumab	341	7 (2.1)	84 (25)	200 (59)	47 (14)
TOPAZ-1	GemCis	343	2 (1)	62 (18)	220 (64)	51 (15)

Abbreviations: CR, complete response; PR, partial response; SD, stable disease; PD, progressive disease; GemCis, gemcitabine plus cisplatin.

To evaluate the robustness of our pooled response estimates, we performed a leave-one-out sensitivity analysis in which each trial arm was sequentially omitted and the overall complete response (CR), partial response (PR), stable disease (SD), and progressive disease (PD) rates were recalculated. As summarized in Table 5, excluding any single arm—whether pembrolizumab plus gemcitabine–cisplatin (KEYNOTE-966_E), its control (KEYNOTE-966_C), durvalumab plus gemcitabine–cisplatin (TOPAZ-1_E), or its control (TOPAZ-1_C)—resulted in minimal fluctuations in the pooled estimates (CR 1.49–1.60%; PR 33.0–33.6%; SD 41.5–42.0%; PD 20.4–21.2%). These narrow ranges underscore the stability of our meta-analytic findings and suggest that no individual study disproportionately drives the overall response profile.

Table 5. Leave-One-Out Sensitivity for Response Rates (CR, PR, SD, PD).

Omitted Study	CR (%) [95% CI]	PR (%) [95% CI]	SD (%) [95% CI]	PD (%) [95% CI]
None (all arms)	1.54 (1.00–2.10)	33.3 (30.9–35.7)	41.8 (39.5–44.1)	20.8 (18.9–22.7)
KEYNOTE-966 _E	1.58 (1.03–2.14)	33.0 (30.6–35.4)	41.9 (39.6–44.2)	20.5 (18.6–22.4)
KEYNOTE-966 _C	1.51 (0.97–2.05)	33.6 (31.1–36.0)	41.7 (39.4–44.0)	21.1 (19.2–23.0)
TOPAZ-1 _E	1.60 (1.05–2.15)	33.2 (30.8–35.6)	41.5 (39.2–43.8)	21.2 (19.3–23.1)
TOPAZ-1 _C	1.49 (0.95–2.03)	33.4 (31.0–35.8)	42.0 (39.7–44.3)	20.4 (18.5–22.3)

Leave-One-Out Sensitivity Analysis for Pooled Response Rates. Each row shows the pooled estimate and 95% confidence interval (CI) for complete response (CR), partial response (PR), stable disease (SD), and progressive disease (PD) after omitting the specified study. Abbreviations: KEYNOTE-966_E, pembrolizumab plus gemcitabine–cisplatin arm of KEYNOTE-966; KEYNOTE-966_C, gemcitabine–cisplatin control arm; TOPAZ-1_E, durvalumab plus gemcitabine–cisplatin arm of TOPAZ-1; TOPAZ-1_C, gemcitabine–cisplatin control arm.

3.14. Publication Bias and Sensitivity Analyses

Funnel plots were symmetric for both OS and PFS, and Egger's tests were non-significant (OS $p = 0.30$; PFS $p = 0.40$) (Figure 5). Leave-one-out sensitivity analyses confirmed that excluding any single study did not materially alter the pooled estimates. All supplementary materials used for statistical analyses are provided in the Supplementary File S1 for transparency and reproducibility.

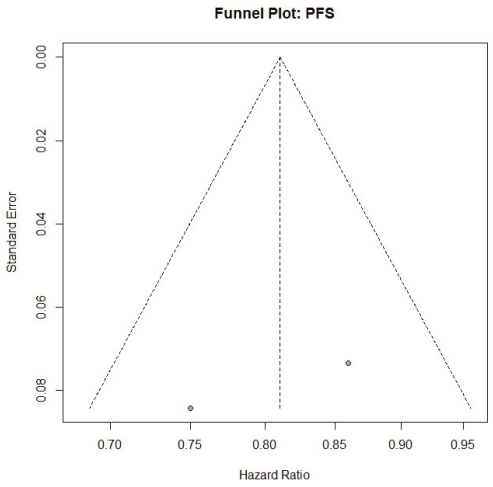

Figure 5. *Cont.*

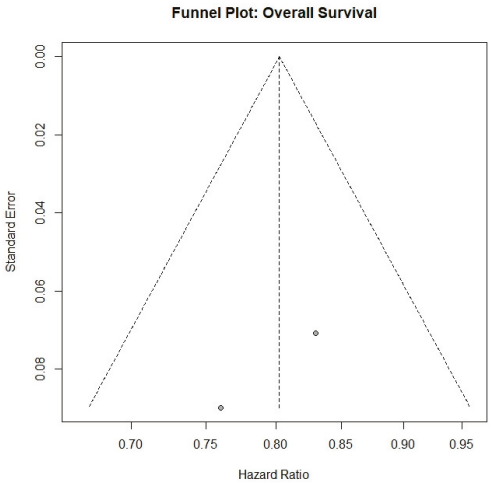

Figure 5. Funnel plots illustrating publication bias assessments for progression-free survival (PFS; upper panel) and overall survival (OS; lower panel). Each circle represents an individual study's hazard ratio (HR), plotted against its standard error. Visual inspection demonstrates symmetry around the pooled estimates, suggesting minimal publication bias. Egger's test confirmed no significant publication bias for both PFS ($p = 0.40$) and OS ($p = 0.30$).

4. Discussion

In total, two RCTs enrolling 1754 patients were included in this meta-analysis. Chemoimmunotherapy significantly improved OS (HR = 0.83, 95% CI: 0.72–0.96; $I^2 = 0.0\%$, $p = 0.44$) and PFS (HR = 0.80, 95% CI: 0.67–0.96; $I^2 = 33.5\%$, $p = 0.22$) compared with chemotherapy alone, indicating a 17% reduction in the risk of death and a 20% reduction in disease progression risk with combination therapy. Egger's test for publication bias was non-significant for both OS ($p = 0.30$) and PFS ($p = 0.40$).

4.1. Clinical Implications

Our meta-analysis demonstrates that adding immunotherapy to first-line chemotherapy yields a clear survival benefit for advanced BTCs over chemotherapy alone. Pooled results from randomized trials show a prolongation of median OS to roughly 12–13 months with chemoimmunotherapy, compared to ~10–11 months with chemotherapy alone [5,6]. This translates to a 17% reduction in the risk of death with combination therapy–a clinically meaningful improvement in a historically hard-to-treat disease. Notably, the addition of an immune checkpoint inhibitor doubled the 2-year survival rate in one study (≈24% vs. 11–12% with chemo alone), indicating a subset of patients achieving durable long-term remission. These gains were achieved without a trade-off in safety: immunotherapy did not markedly increase high-grade toxicities, and no new safety signals emerged in the combination arm. In practical terms, this means oncologists can improve survival outcomes by incorporating immunotherapy into first-line regimens without significantly worsening the expected chemotherapy-related side effects. Taken together, our findings confirm the paradigm shift in BTC management, establishing chemoimmunotherapy as a new standard of care for untreated advanced disease [6,13]. Therefore, while this meta-analysis supports the role of chemoimmunotherapy as the new first-line standard, it mainly corroborates the findings of the pivotal RCTs rather than providing novel evidence. More granular analyses with IPD would be required to evaluate the magnitude of benefit in each clinically relevant subgroup.

Beyond the statistical significance, these results carry important implications for daily practice. Until recently, gemcitabine–cisplatin was the only standard, yielding a median OS of under 1 year. The introduction of immunotherapy has broken this plateau, offering new hope in a cancer with an urgent need for better therapies. Physicians should now

consider a platinum/gemcitabine plus PD-1/L1 inhibitor combination as first-line therapy for eligible patients. Current evidence indicates that this benefit extends across broad patient subgroups. For example, improved survival was seen regardless of PD-L1 expression level or patient ethnicity, suggesting we should offer chemoimmunotherapy to all patients without restricting it to PD-L1–positive tumors. The combination appears effective in intrahepatic cholangiocarcinoma, extrahepatic cholangiocarcinoma, and gallbladder cancers alike, although one trial noted a somewhat less pronounced benefit in extrahepatic disease. This observation might relate to clinical factors (extrahepatic BTC patients often have more comorbidities and biliary complications), but it underscores that anatomical subtypes may respond differently, a nuance clinicians should be aware of. Overall, the broad efficacy of chemoimmunotherapy means that, for the first time in over a decade, patients with advanced BTC have a new frontline option that significantly improves survival and the chance of long-term tumor control [14].

Mechanistically, the success of chemotherapy–immunotherapy combinations in BTC is biologically plausible and likely synergistic. Biliary tract tumors are typically immunologically "cold," failing to elicit strong native immune responses [14]. Chemotherapy can favorably alter this tumor microenvironment: Gemcitabine and cisplatin induce immunogenic cell death, release tumor antigens, and deplete immunosuppressive cell populations. For instance, gemcitabine has been shown to enhance dendritic cell function and cross-prime $CD8^+$ T-cells against tumor antigens [15]. Such effects can convert a cold tumor into a more immune-reactive one, essentially priming the patient's immune system. Adding a PD-1/L1 blocker then amplifies this anti-tumor immunity by unleashing T-cell responses that chemotherapy alone could not sustain. Clinically, this synergy is reflected in our findings: while objective response rates with chemoimmunotherapy were similar to chemotherapy alone in trials, responses lasted longer with the addition of immunotherapy (e.g., median response duration ~9.7 vs. 6.9 months) [15]. This prolonged disease control in responders likely underpins the observed OS benefit despite only modest improvements in median PFS. In summary, the chemoimmunotherapy approach not only attacks the tumor with cytotoxins but also engages the patient's immune system for a more durable defense–a dual mechanism of action that is now clinically validated in BTC.

4.2. Clinical Considerations

Although the included trials were broadly representative of advanced BTC populations, patients aged $\geq$80 years were rarely enrolled. As a result, the applicability of chemoimmunotherapy in very elderly or frail patients remains uncertain. While gemcitabine–cisplatin has been used with dose adjustments in older adults, the tolerability of adding immune checkpoint inhibitors to chemotherapy in this subgroup requires prospective evaluation. Future studies should incorporate geriatric oncology frameworks and real-world cohorts to clarify efficacy and safety in this underrepresented population.

Another important limitation is the lack of data beyond two years of follow-up. Both KEYNOTE-966 and TOPAZ-1 demonstrated durable survival benefits at interim analyses, but mature data regarding long-term survival, progression-free survival plateaus, and late immune-related toxicities are not yet available. Understanding outcomes beyond 24 months is essential to determine whether chemoimmunotherapy can achieve sustained disease control or functional cure in a subset of patients. Extended follow-up of existing trials and pooled analyses from real-world registries will be crucial to address this gap.

4.3. Study Limitations

Despite the encouraging results, we must acknowledge several limitations of this meta-analysis and the underlying studies. First, the evidence is driven largely by two pivotal

trials, TOPAZ-1 and KEYNOTE-966, which had similar designs (gemcitabine/cisplatin with either durvalumab or pembrolizumab vs. chemo alone). The limited number of trials (and total sample size of 1754 patients) restricts our ability to perform extensive subgroup analyses and may overemphasize trial-specific biases. For instance, both trials were sponsored studies with rigorous patient selection, enrolling mostly patients with good performance status (ECOG 0–1) and without severe comorbidities. This selection criterion means the trial populations might not fully represent real-world BTC patients, who often are older or have liver dysfunction, etc. As a result, the generalizability of the findings could be somewhat constrained. Moreover, mature quality-of-life (QoL) data remain unavailable, limiting assessment of whether survival gains translate into meaningful patient benefit. Outcomes in routine practice might be different if patients are less fit than those in trials. Early real-world reports suggest the regimen is feasible outside of trials, but efficacy data in broader populations are still maturing. We also note that publication bias is a potential concern, albeit a minor one here–positive trials are available and were included, whereas any negative or small studies (if they exist) might be unpublished and thus not captured in our analysis. With only two randomized studies, formal tests such as Egger's test were non-significant, though underpowered due to the limited number of studies. While the qualitative studies [7,11] provided valuable preliminary efficacy data, their lack of comparative controls limited their inclusion in the quantitative meta-analysis. Nonetheless, their encouraging ORR highlights potential activity warranting further randomized comparisons.

Another limitation is the clinical heterogeneity inherent to BTC itself and across trials. BTCs comprise a diverse family of tumors (intrahepatic vs. extrahepatic cholangiocarcinoma vs. gallbladder cancer) with distinct biology and epidemiology. Our meta-analysis combined data across these subtypes; although this boosts statistical power, it introduces heterogeneity. Differences in regional patient demographics (about half of the patients in the trials were from Asia, half from Western countries) could also influence outcomes [13]. For example, etiologies like hepatitis, liver fluke infection, or gallstone disease vary by region and might affect tumor behavior and immune interactions. The trials stratified by primary tumor site and geography, and subgroup analyses so far, show consistently positive effects of immunotherapy across most groups. However, the trend toward a smaller benefit in extrahepatic cholangiocarcinoma hints at unrecognized heterogeneity–perhaps those tumors have a different tumor microenvironment or competing risks. Our analysis could not deeply explore such subgroup differences given the data available. Similarly, variations in trial protocol–e.g., KEYNOTE-966 allowed continuation of gemcitabine beyond 6 months in some cases, whereas TOPAZ-1 followed a more fixed chemotherapy course–might lead to minor outcome differences [14]. We did not detect significant statistical heterogeneity between studies for the primary endpoints, which is reassuring, but the clinical diversity of BTC warrants caution in over-generalizing findings to every patient scenario.

From a methodological standpoint, the lack of individual patient data (IPD) in our meta-analysis is a constraint. We relied on published aggregate outcomes (HRs, survival rates, etc.), which prevents nuanced analyses such as determining how specific patient factors (e.g., age, comorbidities, baseline immune markers) correlate with benefit. Only two randomized controlled trials (RCTs) with similar design and comparable study populations were included, limiting the depth of subgroup analyses. Without access to individual patient data (IPD), it is impossible to assess treatment benefit in clinically relevant subgroups, such as those defined by tumor site, ethnicity, or biomarker status. An IPD meta-analysis in the future could better identify which patients benefit the most or least. Additionally, some important outcomes remain insufficiently reported. Quality-of-life (QoL) data and patient-reported outcomes were not yet fully available from these trials at the time of

our analysis. Since adding immunotherapy can be costly and is intended to prolong life, it is crucial to know whether it maintains or improves QoL compared to chemo alone. The absence of mature QoL data is a current gap, though preliminary reports suggest patients tolerate the regimen well; formal QoL analyses will bolster the value proposition of chemoimmunotherapy. Finally, the follow-up duration in published studies, while the longest to date in BTC, is still relatively short for capturing tail-end survival [6]. The OS curves suggest some patients achieve long-term survival beyond 2 years; longer follow-up (3–5 years) is needed to determine if a plateau or cure fraction emerges. Ongoing updates (e.g., a 3-year OS showing continued separation of curves) are awaited to confirm the durability of the benefit.

Another important limitation relates to the lack of data in very elderly patients, particularly those aged 80 years or older. Both pivotal trials predominantly enrolled younger, fitter individuals (ECOG 0–1), limiting generalizability to frailer populations more commonly seen in real-world practice. Consequently, the applicability and tolerability of chemoimmunotherapy in the very elderly remain uncertain and warrant dedicated prospective evaluation. In addition, long-term outcomes beyond two years are not yet well established. Although one included trial demonstrated a doubling of the 2-year survival rate with chemoimmunotherapy versus chemotherapy alone, the durability of this benefit remains unclear given the relatively short follow-up. Longer observation ($\geq$3–5 years) will be critical to determine whether early gains translate into sustained survival benefit or even a plateau suggestive of cure.

Another limitation of this review is that the certainty of evidence across outcomes was not formally graded, which restricts the strength of recommendations derived from these findings.

In summary, while the findings are robust at a population level, uncertainties remain regarding applicability in very elderly or frail patients, durability of long-term benefit, and real-world generalizability.

5. Future Directions

Our findings highlight several avenues for future research to optimize patient selection and refine treatment strategies in advanced BTC. A top priority is the identification of predictive biomarkers that can distinguish which patients are most likely to benefit from immunotherapy. Currently, no reliable clinical or molecular markers exist to guide this decision [16]. PD-L1 expression did not predict differential benefit: patients experienced similar OS and PFS improvements with chemoimmunotherapy regardless of PD-L1 status. We therefore need to look beyond PD-L1. Comprehensive tumor profiling (genomic, transcriptomic, and immune microenvironment analysis) could uncover features associated with response or resistance. For instance, exploratory studies suggest certain molecular subtypes (e.g., tumors with TP53/KRAS co-mutations) have higher immune infiltration and might respond better to immunotherapy [15]. Similarly, microsatellite instability-high (MSI-H) or mismatch-repair-deficient BTCs, though rare (~1–2% of BTCs), have shown notable sensitivity to immunotherapy alone, with response rates around 40% in that subgroup [17]. Identifying such subsets prospectively and tailoring therapy accordingly will be a crucial step. In the future, we may refine treatment by intensifying or adding immunotherapy for those predicted to respond, while sparing expense and potential immune toxicities in patients unlikely to benefit (who might be better served by alternative strategies). Translational studies embedded in ongoing trials should collect tumor tissue and blood to search for predictive biomarkers (e.g., T-cell infiltrates, tumor mutational burden, specific cytokine or gene expression signatures). As our meta-analysis shows a

benefit in an unselected population, biomarker-driven enrichment could further improve the risk–benefit ratio of chemoimmunotherapy.

Mature quality-of-life (QoL) data from these trials remain essential to ensure that survival benefits translate into meaningful improvements in patient well-being, underscoring the importance of comprehensive patient-centered outcomes in future BTC studies.

Future trials should evaluate chemoimmunotherapy combinations with targeted agents (e.g., FGFR2 or IDH1 inhibitors) and integration with loco-regional treatments (e.g., radioembolization, hepatic arterial infusion) to assess potential synergistic effects.

We also see opportunities to enhance therapeutic strategies, building on the success of chemoimmunotherapy. One approach is to test additional or alternative immunomodulatory agents in combination. Ongoing trials are evaluating whether adding a second checkpoint inhibitor (such as an anti-CTLA-4 antibody) to PD-1 blockade plus chemotherapy can deepen responses, or if novel checkpoints (LAG-3, TIGIT, etc.) might further augment anti-tumor immunity in BTC. The rationale is that dual checkpoint inhibition could unleash complementary arms of the immune system, potentially converting a proportion of current non-responders into responders, though at the cost of higher toxicity, which will need careful assessment. BTCs often harbor actionable mutations (e.g., FGFR2 fusions, IDH1 mutations, HER2 amplifications) that are treated with targeted inhibitors in second-line settings. An open question is how to sequence or combine these with immunotherapy. The potential synergy between targeted therapies and immunotherapy remains an area of active investigation, and prospective combination trials are underway. For example, should a patient with an FGFR2 fusion receive immunochemotherapy first-line or go directly to an FGFR inhibitor? At present, immunotherapy is given to all-comers in the first line, and targeted agents are used on progression [16]. Future trials could explore personalized strategies, such as upfront targeted therapy in selected molecular subgroups with immunotherapy reserved for later, or conversely, adding targeted drugs to the chemoimmunotherapy backbone to see if synergistic efficacy results. Careful research is needed to determine the optimal sequencing of these therapies so that patients can derive maximum benefit over the course of their disease.

Future studies should specifically investigate the efficacy of combining chemoimmunotherapy with targeted agents (e.g., FGFR inhibitors or IDH1 inhibitors) and explore the integration of systemic chemoimmunotherapy with loco-regional treatments (e.g., radioembolization, hepatic arterial infusion chemotherapy) to enhance therapeutic responses and outcomes.

Furthermore, as chemoimmunotherapy becomes established in advanced disease, we should examine its role in earlier disease settings. Adjuvant or neoadjuvant trials are warranted in high-risk resectable BTC to see if adding immunotherapy around surgery can eradicate micrometastatic disease and prevent recurrence. Given the positive results in metastatic disease, it is rational to test similar combinations in the postoperative setting or as induction therapy before surgery for borderline resectable tumors. This could potentially increase cure rates for BTC if successful. Additionally, investigating maintenance strategies is important: in current practice, patients typically stop cisplatin after 6–8 cycles due to cumulative toxicity, but continue immunotherapy for a maximum of two years as per current trial protocols. Is there a role for maintenance single-agent immunotherapy beyond two years in those with ongoing response, or can we stop treatment earlier in certain cases? Prospective studies and long-term follow-up will inform how long to treat with immunotherapy to balance efficacy and toxicity/cost. Another area of interest is combining loco-regional therapies with immunotherapy. Techniques like radioembolization, ablation, or hepatic arterial infusion chemotherapy might provoke additional tumor antigen release

or alter immune contexture; their combination with systemic immunotherapy could be synergistic and is an intriguing frontier for clinical trials.

Finally, continued monitoring of patient outcomes and quality of life in the real-world adoption of chemoimmunotherapy will be essential. As more patients receive this combination outside of clinical trials, large registry studies or phase IV trials should collect data on efficacy, toxicity, and QoL to ensure the trial results translate to broader populations. Health economics analyses will also be important, given the high cost of immunotherapies; demonstrating a survival benefit is one aspect, but we must also show that this approach is cost-effective and accessible, especially in regions where BTC incidence is high but resources may be limited. In summary, the advent of chemoimmunotherapy has opened multiple research directions: refining patient selection through biomarkers, exploring new combinatorial regimens, moving immunotherapy into earlier stages, and addressing pragmatic issues of treatment duration and cost. Ultimately, prospective biomarker-driven and combination studies, along with real-world registry data on QoL and cost-effectiveness, will be critical to fully realize the potential of chemoimmunotherapy across BTC subtypes.

6. Conclusions

In conclusion, this meta-analysis of 1754 patients demonstrated that adding PD-1/L1 inhibitors to gemcitabine–cisplatin significantly reduced the risk of death by 17% (OS HR = 0.83; 95% CI 0.72–0.96) and the risk of progression or death by 20% (PFS HR = 0.80; 95% CI 0.67–0.96). These results support chemoimmunotherapy as a first-line option for advanced BTC. While further long-term and real-world data are needed to optimize patient selection and management, our findings align with pivotal trials that led to PD-1/L1 approval and mark a major advance in systemic BTC treatment [13].

Supplementary Materials: The following supporting information can be downloaded at: https://www.mdpi.com/article/10.3390/biomedicines13092099/s1, File S1: Supplementary Methodology and Sensitivity Analysis. Figure S1: Forest plot for overall survival (OS) sensitivity analysis. Figure S2: Forest plot for progression-free survival (PFS) sensitivity analysis. Figure S3: Forest plot for subgroup analysis (OS) based on immune checkpoint inhibitors. Figure S4: Forest plot for subgroup analysis (PFS) based on immune checkpoint inhibitors.

Author Contributions: Conceptualization: A.S. and A.T.; resources: A.T. and A.S.; methodology: A.T., O.M.Y. and R.M.O.; project administration: A.S. and A.T.; writing—original draft: A.T.; writing—review and editing: A.T., A.S., S.R. and I.H.S.; supervision: A.S.; validation: A.T.; visualization: A.T. All authors have read and agreed to the published version of the manuscript.

Funding: This research received no external funding.

Conflicts of Interest: Anwaar Saeed reports research grants (to institution) from AstraZeneca, Bristol Myers Squibb, Merck, Clovis, Exelixis, Actuate Therapeutics, Incyte Corporation, Daiichi Sankyo, Five Prime Therapeutics, Amgen, Innovent Biologics, Dragonfly Therapeutics, KAHR Medical, BioNTech, and advisory board fees from Merck, AstraZeneca, Bristol Myers Squibb, Exelixis, Taiho, and Pfizer. The remaining authors have no relevant financial interests to disclose.

References

1. Banales, J.M.; Marin, J.J.; Lamarca, A.; Rodrigues, P.M.; Khan, S.A.; Roberts, L.R.; Cardinale, V.; Carpino, G.; Andersen, J.B.; Braconi, C. Cholangiocarcinoma 2020: The next horizon in mechanisms and management. *Nat. Rev. Gastroenterol. Hepatol.* **2020**, *17*, 557–588. [CrossRef] [PubMed]
2. Blechacz, B.; Gores, G.J. Cholangiocarcinoma: Advances in pathogenesis, diagnosis, and treatment. *Hepatology* **2008**, *48*, 308–321. [CrossRef] [PubMed]
3. Valle, J.; Wasan, H.; Palmer, D.H.; Cunningham, D.; Anthoney, A.; Maraveyas, A.; Madhusudan, S.; Iveson, T.; Hughes, S.; Pereira, S.P.; et al. Cisplatin plus Gemcitabine versus Gemcitabine for Biliary Tract Cancer. *N. Engl. J. Med.* **2010**, *362*, 1273–1281. [CrossRef] [PubMed]

4. Ruggieri, A.N.; Yarchoan, M.; Goyal, S.; Liu, Y.; Sharon, E.; Chen, H.X.; Olson, B.M.; Paulos, C.M.; El-Rayes, B.F.; Maithel, S.K. Combined MEK/PD-L1 inhibition alters peripheral cytokines and lymphocyte populations correlating with improved clinical outcomes in advanced biliary tract cancer. *Clin. Cancer Res.* **2022**, *28*, 4336–4345. [CrossRef] [PubMed]
5. Kelley, R.K.; Ueno, M.; Yoo, C.; Finn, R.S.; Furuse, J.; Ren, Z.; Yau, T.; Klümpen, H.-J.; Chan, S.L.; Ozaka, M. Pembrolizumab in combination with gemcitabine and cisplatin compared with gemcitabine and cisplatin alone for patients with advanced biliary tract cancer (KEYNOTE-966): A randomised, double-blind, placebo-controlled, phase 3 trial. *Lancet* **2023**, *401*, 1853–1865. [CrossRef] [PubMed]
6. Oh, D.-Y.; He, A.R.; Bouattour, M.; Okusaka, T.; Qin, S.; Chen, L.-T.; Kitano, M.; Lee, C.-k.; Kim, J.W.; Chen, M.-H. Durvalumab or placebo plus gemcitabine and cisplatin in participants with advanced biliary tract cancer (TOPAZ-1): Updated overall survival from a randomised phase 3 study. *Lancet Gastroenterol. Hepatol.* **2024**, *9*, 694–704. [CrossRef]
7. Oh, D.Y.; Lee, K.H.; Lee, D.W.; Yoon, J.; Kim, T.Y.; Bang, J.H.; Nam, A.R.; Oh, K.S.; Kim, J.M.; Lee, Y.; et al. Gemcitabine and cisplatin plus durvalumab with or without tremelimumab in chemotherapy-naive patients with advanced biliary tract cancer: An open-label, single-centre, phase 2 study. *Lancet Gastroenterol. Hepatol.* **2022**, *7*, 522–532. [CrossRef] [PubMed]
8. Zhou, J.; Li, J.; Fan, Z.; Lv, G.; Wang, G. Clinical outcomes of immune checkpoint inhibitor combined with other targeted or immunological therapy regimens for the treatment of advanced bile tract cancer: A systematic review and meta-analysis. *Front. Immunol.* **2024**, *15*, 1378760. [CrossRef] [PubMed]
9. Benson, A.B.; D'Angelica, M.I.; Abrams, T.; Abbott, D.E.; Ahmed, A.; Anaya, D.A.; Anders, R.; Are, C.; Bachini, M.; Binder, D. NCCN guidelines® Insights: Biliary tract cancers, version 2.2023: Featured updates to the NCCN guidelines. *J. Natl. Compr. Cancer Netw.* **2023**, *21*, 694–704. [CrossRef] [PubMed]
10. Sterne, J.A.; Savović, J.; Page, M.J.; Elbers, R.G.; Blencowe, N.S.; Boutron, I.; Cates, C.J.; Cheng, H.-Y.; Corbett, M.S.; Eldridge, S.M. RoB 2: A revised tool for assessing risk of bias in randomised trials. *BMJ* **2019**, *366*, l4898. [CrossRef] [PubMed]
11. Monge, C.; Pehrsson, E.C.; Xie, C.; Duffy, A.G.; Mabry, D.; Wood, B.J.; Kleiner, D.E.; Steinberg, S.M.; Figg, W.D.; Redd, B. A phase II study of pembrolizumab in combination with capecitabine and oxaliplatin with molecular profiling in patients with advanced biliary tract carcinoma. *Oncologist* **2022**, *27*, e273–e285. [CrossRef] [PubMed]
12. Hack, S.P.; Verret, W.; Mulla, S.; Liu, B.; Wang, Y.; Macarulla, T.; Ren, Z.; El-Khoueiry, A.B.; Zhu, A.X. IMbrave 151: A randomized phase II trial of atezolizumab combined with bevacizumab and chemotherapy in patients with advanced biliary tract cancer. *Ther. Adv. Med. Oncol.* **2021**, *13*, 17588359211036544. [CrossRef] [PubMed]
13. Mauro, E.; Sanduzzi-Zamparelli, M.; Sauri, T.; Soler, A.; Iserte, G.; Fortuny, M.; Forner, A. Evaluation of Overall Survival by Restricted Mean Survival Time of Advanced Biliary Tract Cancer treated with Immunotherapy: A Systematic Review and Meta-Analysis. *Cancers* **2024**, *16*, 2077. [CrossRef] [PubMed]
14. Goodman, A. Immunotherapy/Chemotherapy Combination Prolongs Survival in Advanced Biliary Tract Cancers. ASCO Post. 2023. Available online: https://ascopost.com/issues/may-25-2023/immunotherapychemotherapy-combination-prolongs-survival-in-advanced-biliary-tract-cancers/ (accessed on 5 May 2025).
15. Wilbur, H.C.; Azad, N.S. Immunotherapy for the treatment of biliary tract cancer: An evolving landscape. *Ther. Adv. Med. Oncol.* **2024**, *16*, 17588359241235799. [CrossRef] [PubMed]
16. Vogel, A.; Ducreux, M. ESMO Clinical Practice Guideline interim update on the management of biliary tract cancer. *ESMO Open* **2025**, *10*, 104003. [CrossRef] [PubMed]
17. Bang, Y.; Doi, T.; De Braud, F.; Piha-Paul, S.; Hollebecque, A.; Razak, A.A.; Lin, C.; Ott, P.; He, A.; Yuan, S. 525 Safety and efficacy of pembrolizumab (MK-3475) in patients (pts) with advanced biliary tract cancer: Interim results of KEYNOTE-028. *Eur. J. Cancer* **2015**, *51*, S112. [CrossRef]

Disclaimer/Publisher's Note: The statements, opinions and data contained in all publications are solely those of the individual author(s) and contributor(s) and not of MDPI and/or the editor(s). MDPI and/or the editor(s) disclaim responsibility for any injury to people or property resulting from any ideas, methods, instructions or products referred to in the content.

MDPI AG
Grosspeteranlage 5
4052 Basel
Switzerland
Tel.: +41 61 683 77 34

Biomedicines Editorial Office
E-mail: biomedicines@mdpi.com
www.mdpi.com/journal/biomedicines



Disclaimer/Publisher's Note: The title and front matter of this reprint are at the discretion of the Guest Editors. The publisher is not responsible for their content or any associated concerns. The statements, opinions and data contained in all individual articles are solely those of the individual Editors and contributors and not of MDPI. MDPI disclaims responsibility for any injury to people or property resulting from any ideas, methods, instructions or products referred to in the content.





Academic Open
Access Publishing

mdpi.com

ISBN 978-3-7258-8728-6